

**Functional characterization of genetic polymorphisms in
the organic cation transporter OCT1 with a special focus
on the substrate-specific effects of the M420del
polymorphism**

Doctoral Thesis

In partial fulfillment of the requirements for the degree
“Doctor rerum naturalium (Dr. rer. nat.)”

in the Molecular Medicine Study Program
at the Georg-August University Göttingen

submitted by

Tina Seitz

born in Hoyerswerda

Göttingen, 2016

Members of the Thesis Committee:

Supervisor:

Name, Institute: **Prof. Dr. med. Jürgen Brockmüller**, Department of Clinical Pharmacology, University Medical Center, Georg-August University Göttingen

Second member of the thesis committee:

Name, Institute: **Prof. Dr. Gerhard Burckhardt**, Department of Vegetative Physiology and Pathophysiology, University Medical Center, Georg-August University Göttingen

Third member of the thesis committee:

Name, Institute: **Prof. Dr. Viacheslav O. Nikolaev**, Institute of Experimental Cardiovascular Research, University Medical Center Hamburg-Eppendorf

Advisor:

Name, Institute: **Dr. Mladen Tzvetkov**, Department of Clinical Pharmacology, University Medical Center, Georg-August University Göttingen

Date of Disputation:

AFFIDAVIT

Here I declare that my doctoral thesis entitled “*Functional characterization of genetic polymorphisms in the organic cation transporter OCT1 with a special focus on the substrate-specific effects of the M420del polymorphism*” has been written independently with no other sources and aids than quoted.

Tina Seitz

Göttingen, March 2016

2.8	Bacterial strain	37
2.9	Plasmids	37
2.10	Cell lines	40
2.11	Software and databases	42
3	Methods	43
3.1	Recombinant DNA techniques	43
3.1.1	Agarose gel electrophoresis	43
3.1.2	Extraction of DNA fragments from agarose gel	44
3.1.3	Capillary sequencing analysis	44
3.1.4	Single base primer extension (SNaPshot™)	47
3.1.5	Site-directed mutagenesis	49
3.1.6	Validation PCRs of stable transfected HEK293 cell lines	51
3.1.7	Isolation of total genomic DNA	55
3.1.8	Photometric quantification of nucleic acid	55
3.1.9	Analytical restriction digestion	56
3.1.10	Preparative restriction digest	57
3.1.11	Ligation	58
3.1.12	Dialysis	59
3.2	Quantification of mRNA expression	59
3.2.1	Isolation of total RNA	59
3.2.2	Reverse transcription reaction	60
3.2.3	Real-time PCR (qPCR) using TaqMan® Assay	60
3.3	Microbiological techniques used	62
3.3.1	Growth media and culturing conditions	62
3.3.2	Bacterial solid culturing	63
3.3.3	Bacteria liquid culture	63
3.3.4	Long time storage of bacterial strains	63

3.3.5	Transformation of bacteria by electroporation	64
3.3.6	Isolation of plasmid DNA by alkaline lysis	64
3.3.7	Isolation of high quality plasmid DNA by solid extraction (midi prep)	66
3.4	Mammalian cell culturing and transfection	66
3.4.1	Cell culturing conditions	67
3.4.2	Freezing mammalian cell lines	67
3.4.3	Thawing mammalian cell lines	67
3.4.4	Determination of cell count	68
3.4.5	Stable transfection of T-REx™ 293 cells	69
3.4.6	Transient transfection of T-REx™ 293 cells	70
3.4.7	Generation of stable transfected cell lines	71
3.5	Protein analyses	74
3.5.1	Determination of protein concentration	74
3.5.2	SDS polyacrylamide gel electrophoresis (SDS-PAGE)	75
3.5.3	Western Blot	77
3.5.4	Deglycosylation with <i>PNGase F</i> and <i>Endo H</i>	79
3.5.5	Immunostaining	80
3.6	Transport experiments	81
3.6.1	Scintillation counting	83
3.6.2	Fluorescence measurement	84
3.6.3	HPLC	85
3.6.4	LC-MS/MS	86
3.7	Statistics	88
4	Results	89
4.1	Functional characterization of genetic polymorphisms in the organic cation t ransporter <i>OCT1</i>	89
4.1.1	Generation and validation of cell lines used to analyze non-synonymous substitutions in OCT1	89

4.1.2	Functional characterization of <i>OCT1</i> allelic variants.....	94
4.1.3	Subcellular localization and differences in the glycosylation pattern of <i>OCT1</i> allelic variants.....	98
4.2	Prediction of the allele-specific effects on morphine and metformin uptake using model substrates	103
4.3	Interaction of M420del with other naturally occurring non-synonymous polymorphisms in OCT1	104
4.4	In-depth analysis of the effects of M420del on OCT1 function.....	110
4.4.1	Substrate-specific effects of the M420del variant.....	110
4.4.2	Reduction of the extracellular loop between the 9 th and the 10 th TMD cannot explain the effect of M420del	116
4.4.3	The observed substrate-specific effects of the M420del variant are caused by loss of the methionine side chain	122
5	Discussion	152
5.1	Strong variations in the effects of OCT1 allelic variants on transport activity ...	152
5.1.1	Complete loss of transport activity is caused by improper membrane localization	157
5.1.2	Evolutionary conservation as a predictor of loss of function.....	161
5.2	Strong worldwide variations in the frequency of loss of OCT1 activity.....	167
5.3	Model substrates are not sufficiently to predict allele-specific effects on morphine and metformin uptake.....	174
5.4	Prediction of multiple binding sites in OCT1.....	175
5.5	M420del caused highly substrate specific effects in OCT1 loss of function	177
5.5.1	Effects of M420del are caused by the specific loss of the methionine side chain	181
5.5.2	The D474E substitution in human OCT1 strongly affects substrate uptake	188
5.5.3	Species-specific differences in transport activity between human OCT1 and rodent orthologs for different substrates	194
5.6	The M408V and G414A polymorphism do not alter the effect of M420del.....	197

6	Summary and outlook	199
7	References	202
8	Curriculum Vitae	214

List of publications

Seitz T, Stalmann R, Dalila N, Chen J, Pojar S, Dos Santos Pereira JN, Krätzner R, Brockmüller J, Tzvetkov MV, Global genetic analyses reveal strong inter-ethnic variability in the loss of activity of the organic cation transporter OCT1. *Genome Medicine*, 7:56 (2015)

Tzvetkov MV, **Seitz T**, Bokelmann K, Mueller T, Brockmüller J, Koepsell H, Does the haplotype Met408-Del420, which was apparently predictive for imatinib efficacy, really exist and how strongly may it affect OCT1 activity? *Blood*, 123(9):1427-9 (2014)

Acknowledgments

I would like to express my gratitude to the following people who contributed to this thesis and supported me during my work.

I would like to sincerely thank Prof. Jürgen Brockmöller for the opportunity to work in the Department of Clinical Pharmacology and on this project, for his expert advice and supervision. Further, I would like to thank my thesis committee members, Prof. Gerhard Burckhardt and Prof. Viacheslav Nikolaev for their support and constructive discussions during our meetings that essentially contributed to this thesis.

I am indebted to my supervisor Dr. Mladen Tzvetkov for his excellent scientific education, for his support at any time and his committed guidance throughout my entire thesis. Without his help and advice this work would not have been possible.

Special thanks go to Prof. Hermann Koepsell and Prof. Thomas Mueller for their expertise in the field of transporters and their scientific support. Further I would like to thank Dr. Ralph Krätzner for his great support in protein modeling, Dr. Eva Wagner for her technical and methodical support concerning microscopy, and Prof. Beißbarth for performing the hierarchical clustering analyses. I would like to thank Sherin Pojar and Marleen Meyer for their collaboration and contribution to this thesis. Further, I would like to thank Dr. Kristin Bokelmann and Karoline Jobst for their technical assistance and supportive advice and experience throughout my work.

Further, I would like to thank my colleagues from the Department of Clinical Pharmacology and all my friends and study colleagues for having an intense and great time and for all the experiences throughout the years. Especially I would like to thank Stefanie Meyer-Roxlau, Claudia Lüske, and Andreas Schraut for being such good friends and for cheering me up at any time. Moreover, I need to thank Brian Golat for making me laugh so hard. Our tea times made my days. Special thanks go to Jaroslav Morozov for our long-lasting friendship and his odd sense of empathy that always cheers me up.

To my dear family: Words cannot express the gratefulness I need to owe you. Thanks to my grandparents and my brother. My deepest gratitude goes to my parents for their any time support and for always being there for me.

Abstract

The human organic cation transporter 1 (OCT1) is strongly expressed in the sinusoidal membrane of hepatocytes. OCT1 mediates the uptake of drugs and exogenous substances with cationic or weak basic structures into the liver. The OCT1 gene has high genetic variability with five common amino acid substitutions R61C, C88R, G401S, G465R and the deletion of M420del that are known to cause loss of OCT1. The loss of OCT1 function decreases the hepatic uptake of drugs like morphine, tropisetron, and O-desmethyltramadol (the active metabolite of tramadol) and increases their plasma concentrations. This may result in increased efficacy of these drugs, but also increases the risk of adverse effects. In Caucasians, 9 % of the individuals carry two inactive *OCT1* alleles and further 42 % carry only one inactive *OCT1* allele. Recent next-generation resequencing analyses of 53 global populations as well as the existing data of 14 populations of the 1000 Genomes project led to the identification of additional amino acid substitutions predicted to affect OCT1 function.

In the first part of this thesis, 19 amino acid variants in OCT1 (including the 5 common, 5 novel, and 9 population-specific) were functionally characterized using a broad spectrum of structurally diverse OCT1 substrates. The aim was to generate a world map of genetically-determined loss of OCT1 function. This world map might shed light on the potential role of *OCT1* polymorphisms in interethnic differences in drug therapy. Furthermore, the global distribution of loss of OCT1 function might point to a selection pressure for either retention or loss of OCT1 activity.

Targeted genomic integration was used to generate HEK293 cell lines overexpressing *OCT1* allelic variants. The cells were used to measure the effect of the variants on the uptake of the model substrates MPP⁺, TEA⁺, ASP⁺ as well as of the drugs morphine, metformin, tropisetron, debrisoquine, and O-desmethyltramadol. The subcellular localization of OCT1 was analyzed by western blot analysis and immunofluorescence staining detected by confocal microscopy.

Fifteen major *OCT1* alleles causing a more than 50 % decrease or increase of the wild type transport activity were identified. An additional 6 sub-alleles were identified that did not substantially affect the transport properties of the major allele. Four major alleles *OCT1**5

(G465R/M420del), *OCT1*6* (C88R/M420del), *OCT1*12* (S29L), and *OCT1*15* (E284K) showed complete substrate-wide loss of activity caused by improper membrane localization of the protein. Three alleles *OCT1*3* (R61C), *OCT1*4* (G401S), and *OCT1*14* (R206C/M420del) showed strong substrate-wide decrease in transport activity. Of these, *OCT1*3* and *OCT1*14* showed reduced plasma membrane localization. A substantial number of alleles (5 out of 19 tested) showed substrate-specific loss of activity: *OCT1*2* (M420del), *OCT1*7* (S14F), *OCT1*10* (S189L), *OCT1*11* (I449T), and *OCT1*13* (T245M). Two alleles *OCT1*8* (R488M) and *OCT1*9* (P117L) showed more than 50 % increase in activity for at least one substrate tested. A world map of genetically-determined loss of OCT1 function, which was generated based on these analyses, showed strong variability in the loss of OCT1 function among different world regions. Almost all individuals in East Asia and Oceania carry two active *OCT1* alleles. In contrast, more than 80 % of the Surui Indians, a Native American tribe in the Amazon, carried two loss-of-function alleles. These findings should be taken into consideration for recommendations of individualized adjustment of drug medication in specific populations.

This work provides functional analysis of existing *OCT1* allelic variants on a broad spectrum of structurally diverse substances revealing strong differences in the effect of these variants on transporter function. The high number of substrate-specific loss of function variants suggests that it is not sufficient to test single OCT1 substrates in order to predict the effect of OCT1 variants.

Among the substrate-specific loss-of-function alleles *OCT1*2* (M420del) was by far the most common one. It was ubiquitously observed across tested populations and was the only loss-of-function OCT1 variant observed in Surui Indians. In the second part of the thesis the structural mechanism underlying the highly substrate-specific effects of M420del was analyzed.

First, it could be shown that the substrate-specific effects of M420del are not caused by an unspecific reduction of the protein chain but rather due to the deletion of the amino acid at codon 420. The transport activity of the mutants L427del and H428del, which were expected to show transport activity similar to M420del, did not differ from wild type. The mutant insertion of alanine after proline₄₂₅ (A426ins) on M420del background, which was expected to restore wild type activity, showed the similar activity as M420del. Furthermore, the mutant M420A showed no differences in the uptake kinetics compared to

M420del using structurally different OCT1 substrates. Furthermore, neither isoleucine, nor threonine, nor cysteine at position 420 could restore wild type transport activity. This data confirmed that the effects of M420del are caused by a specific loss of the methionine side chain.

Finally, interactions of methionine₄₂₀ with amino acids in the 7th transmembrane domain (L364 and H367) were analyzed. An interaction between M420 and L364 or H367 could not be confirmed, as a mutation of these amino acids resulted in a general reduction of OCT1 uptake. Analyses of interactions between methionine₄₂₀ and amino acids known to be involved in substrate binding and translocation suggest complex interaction of M420del with D474, but not with W217 and F159.

Taken together, it could be shown that the substrate-specific effects of M420del are caused by the specific loss of the methionine side chain and indirect interactions with essential transport domains were suggested. Further experiments applying detailed homology modeling are needed to reveal the exact structural mechanism how M420del affects OCT1 function.

List of figures

Figure 1.1 Structure and function of OCT1	5
Figure 1.2 Haplotype combinations constituting 16 major and 14 sub-alleles of <i>OCT1</i>	14
Figure 1.3 Minor allele frequencies of 16 <i>OCT1</i> polymorphisms in 39 different populations worldwide	15
Figure 1.4 Localization and function of OCT1 in hepatocytes.	21
Figure 3.1 Schematical presentation of primer binding sites of validation PCR 1, PCR 2, and PCR 3.....	52
Figure 3.2 Schematical representation of the generation of stably transfected HEK293 cell lines	73
Figure 4.1 Validation of the correct integration of the constructs overexpressing different <i>OCT1</i> allelic variants into the genome of the HEK293 cells	92
Figure 4.2 Analysis for potential multiple tandem integration of the constructs overexpressing different <i>OCT1</i> allelic variants into the HEK293 genome.....	93
Figure 4.3 RT-qPCR demonstrating equal mRNA expression levels among the <i>OCT1</i> allelic variants.....	94
Figure 4.4 Differences in the uptake between HEK293 cells stably transfected with wild type <i>OCT1</i> and with the empty expression vector pcDNA5.....	95
Figure 4.5 Functional characterization of <i>OCT1</i> allelic variants	97
Figure 4.6 Analysis of the subcellular localization of <i>OCT1</i> allelic variants.....	101
Figure 4.7 Western blot analysis of <i>OCT1</i> allelic variants.....	102
Figure 4.8 Correlation between the effects of the substrate-specific loss-of-function <i>OCT1</i> allelic variants on the uptake of model substrates and the drugs morphine and metformin.	104
Figure 4.9 Western blot and immunocytochemical analysis of OCT1 variants carrying all four theoretically possible haplotype combinations of M420del-M408V	106
Figure 4.10 Comparison of the uptake activity of OCT1 variants carrying all theoretically possible M420del-M408V haplotypes.....	107
Figure 4.11 Combined effects of G414A and M420del on OCT1-mediated uptake	109
Figure 4.12 Substrate-specific effects of M420del.	111
Figure 4.13 Differences in K_m (upper part) and v_{max} (lower part) of the M420del in relation to wild type OCT1	114

Figure 4.14 Simultaneous uptake measurements of fenoterol and sumatriptan in wild type and M420del cells.	116
Figure 4.15 Secondary structure of OCT1 showing the mutations, which were used to analyze if the substrate-specific effects of M420del are caused by reduction of the protein chain resulting in shortening of the extracellular loop between transmembrane domains 9 and 10.....	117
Figure 4.16 Validation of HEK293 cells overexpressing the <i>OCT1</i> mutants L427del, H428del, A426ins/M420del.....	119
Figure 4.17 Effects of single amino acid deletions or insertion within the extracellular loop between TMD 9 and TMD 10 on OCT1-mediated uptake of MPP ⁺ , TEA ⁺ , and ASP ⁺	121
Figure 4.18 Secondary and 3D structure of OCT1 showing the mutations L364A and H367A as well as F159Y, W217Y, and D474E that were generated to test whether the substrate-specific effects of M420del are caused by sterical interactions with amino acids in TMD 7 or key amino acids involved in the substrate binding or translocation	124
Figure 4.19 Validation of HEK293 cells overexpressing the mutants <i>L364A</i> and <i>H367A</i> on M420del background	126
Figure 4.20 Analysis of the interaction of methionine ₄₂₀ with the amino acids L364 and H367 in TMD 7.....	127
Figure 4.21 Validation of HEK293 cells overexpressing the <i>OCT1</i> mutants M420A, M420I, M420I, and M420C.....	130
Figure 4.22 Comparative analysis of the uptake activity of M420del and the M420A mutant measured at single concentration of the substrate	131
Figure 4.23 Comparative analyses of the transport kinetics of M420del and M420A.	132
Figure 4.24 Comparative analyses of the effect of M420del, M420A, M420T, M420I, and M420C on the uptake of TEA ⁺ , MPP ⁺ , ASP ⁺ , morphine, and metformin.....	135
Figure 4.25 Comparative analyses of the effects of M420del, M420A, M420T, M420I, and M420C mutants on the uptake kinetics of TEA ⁺	136
Figure 4.26 Validation of HEK293 cells overexpressing the <i>OCT1</i> mutants D474E, W217Y, and F159Y on the wild type and M420del OCT1 background.....	139
Figure 4.27 Comparative analyses of the effect of D474E, W217Y, and F159Y mutations on transport activity of wild type or M420del OCT1	142

Figure 4.28 Comparative analyses of the combined effects of the M420del polymorphism and the D474E mutation on the uptake kinetics of TEA ⁺ , MPP ⁺ , ASP ⁺ , metformin, and sumatriptan	143
Figure 4.29 Comparative presentation of the differences in K _m (top panel) and v _{max} (lower panel) caused by the D474E mutation on the OCT1 wild type (left site, black bars) or M420del background (right site, blue bars).....	145
Figure 4.30 Graphical representation of the differences in K _m (upper part) and v _{max} (lower part) caused by the M420del polymorphisms on mutant D474E background	147
Figure 4.31 Differences between human OCT1 and mouse and rat orthologs in the uptake of MPP ⁺ , TEA ⁺ , ASP ⁺ , and morphine	149
Figure 4.32 Species-specific differences in the effects of D474E, W217Y, and F159Y mutants on substrate uptake	151
Figure 5.1 Processing of <i>N</i> -linked oligosaccharides of the glycosylated protein in the endoplasmic reticulum (ER) and in the Golgi apparatus	159
Figure 5.2 Evolutionary conservation of amino acids in OCT1 orthologs (upper part) and paralogs (lower part).	161
Figure 5.3 Localization of functional <i>OCT1</i> polymorphisms within the secondary structure of the OCT1 protein.	164
Figure 5.4 Predicted 3D model of the OCT1 protein showing the position and possible interactions of serine ₄₀₁	166
Figure 5.5 Map illustrating the global distribution of loss of function of OCT1 activity ..	167
Figure 5.6 Two-dimensional hierarchical clustering analysis.....	177
Figure 5.7 BLOSUM62 matrix.	184

List of tables

Table 1.1 Selected substrates and inhibitors of human OCT1	11
Table 2.1 Primer for site-directed mutagenesis.....	34
Table 2.2 SNaPshot™ primers	36
Table 2.3 Primers for validation PCRs.....	36
Table 2.4 Purchased plasmids	37
Table 2.5 pcDNA3.1 plasmids	38
Table 2.6 pcDNA5 plasmids	39
Table 3.1 Sequencing Primers used to detect single nucleotide exchanges leading to non-synonymous amino acid exchanges in OCT1	45
Table 3.2 Analytical restriction digest of pcDNA3.1::hOCT and pcDNA5::hOCT1 and expected fragment sizes	57
Table 3.3 Linear range of substrates used for uptake measurements.....	82
Table 3.4 Substrate-specific experimental conditions using LC-MS/MS.....	87
Table 3.5 MS detection parameters	88
Table 4.1 Generated pcDNA3.1 plasmids with point mutations in <i>OCT1</i> for the analysis of non-synonymous substitutions in OCT1.....	90
Table 4.2 HEK293 cell lines generated by targeted chromosomal integration for the analysis of non-synonymous substitutions in OCT1	91
Table 4.3 Kinetic parameters of wild type OCT1 and M420del HEK293 cells for different substrates.....	113
Table 4.4 Kinetic parameters of the M420A variant.....	133
Table 4.5 Kinetic parameters of M420A, M420T, M420I, and M420C mutants for TEA ⁺ uptake.....	137
Table 4.6 Kinetic parameters of D474E mutant on wild type and M420del background..	144
Table 5.1 Population genetic statistics for the OCT1 gene in different world regions.	170
Table 5.2 Uptake kinetic parameters of different substrates in different <i>in vitro</i> systems.	193

Abbreviations

4-Di-1-ASP, ASP ⁺	4-(4-(Dimethylamino)styryl) -N-Methylpyridinium
APS	Ammonium persulfate
bp	base pairs
cDNA	Complementary deoxyribonucleic acid
DAPI	4',6-Diamidino-2-Phenylindole, Dihydrochloride
ddH ₂ O	Aqua bidest
DMEM	Dulbecco's Modified Eagle's Medium
DNA	Deoxyribonucleic acid
DTT	Dithiothreitol
<i>E. coli</i>	<i>Escherichia coli</i>
EDTA	Ethylenediaminetetraacetic acid
<i>Endo H</i>	Endo-β-N-acetylglucosaminidase H
FRT	FLP recognition target
Flp	Flippase
h	Hour
HBSS	Hank's buffered salt solution
HCl	Hydrogen chloride
HEK293	Human embryonic kidney cells 293
HEPES	4-(2-hydroxyethyl)-1-piperazineethanesulfonic acid
Hi-Di™ Formamide	Highly de-ionized formamide
hOCT1	Human organic cation transporter 1
IS	Immunostaining
LB medium	lysogeny broth medium (Luria-Bertani medium)
MgSO ₄	Magnesium sulfate
min	minute
mOct1	Mouse organic cation transporter 1
MPP ⁺	1-methyl-4-phenylpyridinium

Na ⁺ /K ⁺ ATPase	Sodium-potassium adenosine triphosphatase
NaCl	Sodium chloride
NaH ₂ PO ₄	Sodium dihydrogen phosphate
OCT1	Organic cation transporter 1
PBS	Phosphate-buffered saline
PCR	Polymerase Chain Reaction
PMSF	Phenylmethanesulfonyl fluoride
<i>PNGase F</i>	Peptid-N-Glykosidase F
PVDF	Polyvinylidene difluoride
RIPA buffer	Radioimmunoprecipitation assay buffer
RNA	Ribonucleic acid
RNase	Ribonuclease
rOct1	Rat organic cation transporter 1
RT	Reverse transcriptase
SDS	Sodium dodecyl sulfate
SLC	Solute carrier
TBE buffer	Tris base, boric acid, EDTA buffer
TBP	TATA-binding protein
TBS	Tris-buffered saline
TBST	Tris-buffered saline with Tween 20
TEA ⁺	Tetraethylammonium
TEMED	Tetramethylethylenediamine
TMD	Transmembrane domain
U	Units
UV	Ultraviolet
WB	Western blot
w/o	without

Units

Quantity Name	Unit name	Symbol
Amount of substance	mole	M
Capacitance	farad	F
Celsius Temperature	degree Celsius	°C
Electric potential difference	volt	V
Electric resistance	ohm	Ω
Length	meter	m
Mass	kilogram	kg
Time	second	s
Volume	liter	l

Prefixes

Name	Symbol	Factor
kilo	k	10 ³
mili	m	10 ⁻³
mikro	μ	10 ⁻⁶
nano	n	10 ⁻⁹
pico	p	10 ⁻¹²

Amino acids

Name	3-Letter code	1-Letter code
Alanine	Ala	A
Arginine	Arg	R
Asparagine	Asn	N
Aspartic acid	Asp	D
Cysteine	Cys	C
Glutamic Acid	Glu	E
Glutamine	Gln	Q
Glycine	Gly	G
Histidine	His	H
Isoleucine	Ile	I
Leucine	Leu	L
Lysine	Lys	K
Methionine	Met	M
Phenylalanine	Phe	F
Proline	Pro	P
Serine	Ser	S
Threonine	Thr	T
Tryptophan	Trp	W
Tyrosine	Tyr	Y
Valine	Val	V

1 Introduction

1.1 OCT1 is an organic cation transporter from the SLC22 family

Four main steps, known as ADME, determinate the pharmacokinetics of drugs in the human body: absorption, distribution, metabolism, and excretion. During this process drugs pass through a number of membrane barriers and cell monolayers including epithelial cells, intestinal mucosa, and alveolar epithelium. Due to their low membrane permeability, hydrophilic and charged substances require carrier-mediated transport to penetrate cell membranes.

Increasing evidence underlines the importance of membrane transporters like OCT1 in drug disposition and response (Gong and Kim, 2013; Tzvetkov et al., 2016). The route of orally administered drugs through the body is influenced by various factors upon administration: transporters located in the intestine determine the reabsorption of a drug and its uptake in the circulation system. At this point pre-systemic elimination via bile excretion can already negatively influence the bioavailability of a drug (Sparreboom et al., 1997). Furthermore, transporters localized in the liver and kidneys mediate drug clearance. Transporters located in membranes of the blood-brain barrier or the blood-placental barrier, at so called immune-privileged sites, stringently restrict access of drugs to these special compartments (Kim et al., 1998; de Boer et al., 2003; Molsa et al., 2005; Vahakangas and Myllynen, 2009). Considering efflux pumps they decrease the intracellular concentration and may impair drug efficacy. Finally, co-administered drugs may affect pharmacokinetics as they can act as inhibitors of transporters (Shitara et al., 2003). Therefore, next to the expression profile of a transporter in various tissues and its substrate specificity, factors like genetic variability, cooperation with other transport systems as well as drug-drug interactions play a crucial role when analyzing the pharmacokinetics and pharmacodynamics of a drug.

The uptake and excretion of positively charged drugs and weak bases at physiological pH is mediated by members of the organic cation transporters of the SLC22 family (solute carrier family 22) as well as by members of the multidrug and toxin extrusion family SLC47 (recently reviewed in (Motohashi and Inui, 2016)).

The SLC22 family is part of the major facilitator superfamily (MFS), which is one of the largest families of membrane transporters, next to the ATP-binding cassette superfamily (ABC family). The MFS family comprises 74 families containing uniporters, symporters, and antiporters (Reddy et al., 2012). Members of the MFS are found in bacteria, archaea, and eukaryotes (Pao et al., 1998). In contrast to the ABC family, members of the MFS are single polypeptide secondary active transporters that only transport small molecules in response of a chemiosmotic ion gradient (Pao et al., 1998).

The SLC22 family of the MFS contains organic cation transporters (OCTs), organic zwitterionic and cationic transporters (OCTNs), and organic anion transporters (OATs) (for a recent overview see (Koepsell, 2013)). The organic cation transporters of the SLC22 family comprise three transporters: OCT1, OCT2, and OCT3. These three transporters are characterized by electrogenic, reversible, and Na^+ -independent transport (Gorboulev et al., 1997; Nagel et al., 1997; Koepsell and Endou, 2004). All three transporters OCT1, OCT2, and OCT3 are poly-specific. They are characterized by different but partially overlapping substrate specificities (Nies et al., 2011; Hendrickx et al., 2013; Sala-Rabanal et al., 2013; Ciarimboli, 2016). OCT1, OCT2, and OCT3 are tissue-specifically expressed: Whereas OCT1 is predominantly expressed in the sinusoidal membrane of hepatocytes (Figure 1.4), OCT2 is specifically expressed in the basolateral membrane of tubular epithelial cells (Zhang et al., 1997; Motohashi et al., 2002; Nies et al., 2009; Tzvetkov et al., 2009). In contrast, OCT3 transcripts are detectable in several tissues (Zhang et al., 1997; Wu et al., 2000; Motohashi et al., 2002; Nies et al., 2009).

OCT1 is a facilitated diffusion system whose transport mechanism is described with the help of the alternating access model (Figure 1.1) (Volk et al., 2009): This model suggests that the binding site of OCT1 is accessible from both sides of the membrane. For translocation of a substrate from the extracellular to the intracellular side, the substrate needs to be bound to the extracellular facing substrate binding site of the transporter. During translocation of the substrate across the plasma membrane the transporter passes through a state described as “occluded state”, in which the substrate is enclosed by the transporter. After the transporter achieved its inward-facing conformation the substrate is released to the intracellular side. Finally, the empty transporter flips back to its outward-facing conformation (Koepsell, 2011). While the transporter resides in the open outward or open inward conformation, the individual transmembrane domains are not bent. Instead,

the translocation process of a bound substrate, especially when concerning the occluded state, requires large structural changes of the transporter (Gorbunov et al., 2008; Egenberger et al., 2012).

There were no restrictions in vitality and fertility in Oct1^{-/-} knock out mice (Jonker et al., 2001), but differences in the pharmacokinetics of drugs, exogenous substances, and toxins were reported (Shu et al., 2007; Nies et al., 2008; Chen et al., 2014). Hence, although membrane transporters just seem to be a small part of the complex interplay of different factors that need to be considered when evaluating the profile of a drug, membrane transporters represent a key role as they mediate the first step of metabolism and excretion of a drug.

Figure 1.1 (previous page) Structure and function of OCT1. (A) The proposed secondary structure of OCT1. The OCT1 protein consists of 12 transmembrane helices with an intracellularly located N-terminal and C-terminal end. The big extracellular loop between the 1st and 2nd transmembrane domain contains putative glycosylation sites (ψ). The big intracellular loop between the 6th and 7th transmembrane domain contains putative phosphorylation sites (**P**). In rat Oct1 the amino acids F160, W218, Y222, T226, R440, L447, Q448, and D475 were reported to be located in the substrate binding region and to be involved in substrate binding and/or translocation (Gorboulev et al., 1999; Popp et al., 2005; Gorbunov et al., 2008; Volk et al., 2009). The corresponding amino acids in the human ortholog are indicated with green triangles. The corresponding amino acids in the human ortholog are: F159, W217, Y221, T225, R439, L446, I447, and D474. (B) Schematic representation of the alternating access model: During the outward open conformation a substrate binds at the binding cleft. This induces conformational changes leading to translocation of the substrate to the intracellular side and thereby the transporter passes through an occluded state. The substrate dissociates from the binding site and is released to the cytosol. The transporter flips back from its inward open conformation to the extracellular side. Based on (Koepsell and Keller, 2016). (C) Homology model of the outward and inward open conformation of rat Oct1. Outward open conformation of rat OCT1 from the side and from extracellular showing the substrate binding cleft. Inward open conformation of rat OCT1 from the side and from the intracellular showing the substrate binding cleft. The amino acids F160, W218, Y222, R440, L447, Q448, and D475, which are known to be involved in transport mechanism, are labeled in the substrate binding cleft shown from the extracellular and intracellular side. The transmembrane domains are colored as indicated. The 3D model of rat Oct1 is based on the crystal structure of LacY of *E.coli* (Popp et al., 2005; Gorbunov et al., 2008). The PDB file was kindly provided by Prof. Thomas Mueller from the University of Würzburg. Presentation and editing was made using Swiss Pdb Viewer v4.1

Rat Oct1 was the first gene of SLC22 transporters cloned and characterized in 1994 (Grundemann et al., 1994). The human OCT1 gene was cloned together with OCT2 in 1997 (Gorboulev et al., 1997; Zhang et al., 1997). The human OCT3 gene was cloned in 1998 (Grundemann et al., 1998). The human OCT1 protein shares 71 % and 50 % identical amino acids with the two other human paralogs OCT2 and OCT3, respectively (OCT1: NP_003048.1, OCT2: NP_003049.2, OCT3: NP_068812, protein alignment using <http://blast.ncbi.nlm.nih.gov>). The secondary structure of the OCT1 protein is characterized by 12 transmembrane helices with an intracellularly located amino and carboxyl terminus (Figure 1.1).

In human, the genes encoding OCT1, OCT2, and OCT3 are clustered together on the long arm of chromosome six (6q26-q27). Each gene comprises 10 introns and 11 exons. The OCT1 protein is characterized by a pseudosymmetric structure, which is common for all members of the MFS. Both, the N-terminal and C-terminal part, comprise six

transmembrane domains (Koepsell and Keller, 2016). There is a big extracellular loop between the first and second transmembrane helix in OCT1 containing putative glycosylation sites according to the motive N-X-S/T at position N71, N96, and N112 (X means any amino acid) (Zhang et al., 1997). The largest intracellular loop between the 6th and 7th transmembrane domain contains putative phosphorylation sites at position S285, S291, T327, T340, and T524 (Gorboulev et al., 1997; Zhang et al., 1997).

1.2 Structure-to-function relationships in OCT1

Intense mutagenesis analyses have been performed on rat Oct1 to investigate the structure-function relation. Because so far no crystal structure of OCT1 is available, structural properties underlying function of OCT1 are based on a model derived from the crystal structure of lactose permease LacY of *E. coli* (Figure 1.1) (Popp et al., 2005) or of a phosphate transporter of fungus *Piriformospora indica* (PiPT) (Pedersen et al., 2013). Between LacY and rat Oct1 12.4 % of the amino acids are identical and 28.8% were similar (Popp et al., 2005). The homology model was used in order to generate the inward open as well as the outward open conformation of rat Oct1 (Popp et al., 2005; Gorbunov et al., 2008). Recently, a 3D model of human OCT1 was derived from the crystal structure of a phosphate transporter of fungus *Piriformospora indica* (PiPT) (Pedersen et al., 2013). PiPT (accession number A8N031) and human OCT1 (accession number O15245) show 21 % amino acid identity (alignment using <http://blast.ncbi.nlm.nih.gov>). Both, LacY and PiPT are members of the MFS (Abramson et al., 2003; Pedersen et al., 2013).

The binding site of human OCT1 is suggested to rather have the shape of a pocket instead of a plane (Bednarczyk et al., 2003). In the outward open conformation of rat Oct1 the proposed binding cleft has a size of about 20 x 60 Å and is formed by the 1st, 2nd, 4th, 5th, 7th, 8th, 10th, and 11th transmembrane domain (Gorboulev et al., 2005; Popp et al., 2005). More than one molecule can bind to the binding cleft of rat Oct1 (Keller et al., 2011). The binding sites differ in their affinities: they are referred to as high and low affinity binding sites (Gorbunov et al., 2008). For the inhibitor substrate TBuA (tetrabutyl ammonium) three binding sites within the outward facing conformation of rat Oct1 were suggested. These binding sites differ in their affinity for TBuA as suggested by highly different dissociation constants (K_d = 0.3 μM, 0.4 μM, and 2 pM, respectively) (Gorbunov et al.,

2008). It is assumed that in order to initiate the translocation process, first a low affinity binding site needs to be occupied by the substrate (Gorbunov et al., 2008; Koepsell and Keller, 2016). The data of the study by Gorbunov *et al.* also suggested that F483 and F486 are involved in the conformational change during the translocation process. Furthermore, their predicted model of rat Oct1 suggests that F483 and/or F486 in the 11th transmembrane domain interact with W147 in the 2nd transmembrane domain in the inward facing, but not in the outward facing conformation (Gorbunov et al., 2008). The interaction of the 2nd and the 11th transmembrane domain seem to be important for the stabilization of rat Oct1 conformation. Hence, this interaction seems to be involved in conformational changes during the translocation process (Gorbunov et al., 2008).

Additionally, the 11th transmembrane domain contains a hinge domain containing glycine residues (C474-N475-L476-G477-G478), which is involved in conformational changes during the translocation process after substrate binding (Egenberger et al., 2012). As the hinge domain provides flexibility in a protein, it allows substrate occlusion during transport. So far it could be shown that at least three transmembrane domains (the 5th, 8th, and 11th) are involved in conformational changes during translocation. The 5th and the 8th transmembrane domain are suggested to be involved in structural changes depending on the transported substrate, whereas the 11th transmembrane domain is suggested to be involved in structural changes independent of the transported substrate (Egenberger et al., 2012; Koepsell and Keller, 2016). Site-directed mutagenesis experiments on rat Oct1 revealed that the amino acids F160 (TMD 2), W218 (TMD 4), Y222 (TMD 4), T226 (TMD 4), R440 (TMD 10), A443 (TMD 10), L447 (TMD 10), Q448 (TMD10), C451 (TMD10), and D475 (TMD 11) are involved in translocation (Gorboulev et al., 1999; Popp et al., 2005; Gorbunov et al., 2008; Volk et al., 2009). These amino acids are all located in the predicted binding cleft of rat Oct1 (Popp et al., 2005). Among them, F160, W218, and D475 were suggested to be directly involved in substrate binding (Gorboulev et al., 1999; Popp et al., 2005; Volk et al., 2009). Replacement of alanine₄₄₃, leucine₄₄₇ or glutamine₄₄₈ in rat Oct1 by the respective amino acid of rat Oct2 (isoleucine₄₄₃, tyrosine₄₄₇ or glutamate₄₄₈, respectively) increased the affinity for corticosterone in rat Oct1 (Gorboulev et al., 2005). The results indicated that the 10th transmembrane domain is involved in substrate binding. However, as indirect effects of these mutations on the binding site of the transporter cannot be excluded, the data do not provide clear evidence that the amino acids

alanine₄₄₃, leucine₄₄₇, and glutamine₄₄₈ are directly involved in binding of corticosterone (Koepsell and Keller, 2016).

When the amino acid aspartate₄₇₅, which is located in the 11th transmembrane domain, was mutated to glutamate, the K_m for TEA⁺ but not MPP⁺ was strongly decreased. Furthermore, the IC₅₀ values for TBuA (tetrabutyl ammonium), TPrA (tetrapropylammonium), and TPeA (tetrapentylammonium), which are inhibitors of rat Oct1, were also decreased. These findings indicated that aspartate₄₇₅ is involved in binding of TEA⁺, TBuA, TPrA, and TPeA (Gorboulev et al., 1999).

Further studies revealed that in the outward-facing conformation of rat Oct1, TEA⁺ and MPP⁺ share common binding domains (Popp et al., 2005). The K_m value for both substrates was reduced after tryptophan₂₁₈ and tyrosine₂₂₂ were mutated to tyrosine and leucine, respectively. In contrast, mutagenesis experiments revealed only a decreased K_m value for MPP⁺ when tyrosine₂₂₆ was mutated to alanine suggesting involvement of tyrosine₂₂₆ in MPP⁺ but not TEA⁺ transport (Popp et al., 2005). These findings suggested that different substrates do not have identical but rather overlapping binding sites allowing poly-specificity of rat Oct1.

The extracellular loop of OCT1 is involved in oligomerization of rOct1 (Keller et al., 2011). The oligomerization of the transporter is pivotal for its membrane localization. Disulfide bonds in the extracellular loop mediate its structural integrity and are essential for transporter oligomerization. However, oligomerization is not required for Oct1 function as no differences between oligomerized and non-oligomerized transporters in substrate affinity were observed (Keller et al., 2011). Moreover, each monomer of the oligomer complex seems to transport its bound substrate independent of the other one. The uptake for TEA⁺ was reduced when the extracellular domain of rat Oct1 was replaced by the extracellular domain of rat Oct2 or Oat1, underlining its importance for transport function (Keller et al., 2011). Also for hOCT2 the importance of cysteines in the extracellular loop in protein folding, oligomerization and hence correct plasma membrane localization was shown before (Brast et al., 2012).

Concerning short term regulation of OCT1 function, the big intracellular loop between the 6th and the 7th transmembrane domain comprises putative protein kinase C (PKC) phosphorylation sites suggesting protein kinase mediated regulation of OCT1 (Gorboulev

et al., 1997; Mehrens et al., 2000). In rat Oct1 the uptake of ASP^+ was stimulated by protein kinase C after phosphorylation of a serine residue in Oct1. Furthermore, the affinity of rat Oct 1 for TEA^+ increased after PKC stimulation (Mehrens et al., 2000). But as in the study of Mehrens *et al.* an antibody-specific for serine phosphorylation was used, it was not possible to specify the exact serine residue that was phosphorylated.

1.3 Polyspecificity of OCT1

OCT1 is predominantly expressed in the sinusoidal membrane of human hepatocytes (Zhang et al., 1997; Nies et al., 2009). This position may be essential for controlling the hepatic uptake and following detoxification of a number of drugs and other xenobiotics. OCT1 has been reported to mediate the uptake of structurally diverse organic substances that are completely or partially positively charged at physiological pH (Table 1.1) but with broadly varying structures. Therefore, OCT1 should be able to bind to a broad spectrum of chemically different structures but without changing its substrate selectivity. This polyspecificity is achieved by binding sites, which allow binding of more than one ligand and separate but partially overlapping binding sites (Gorboulev et al., 1999; Gorboulev et al., 2005; Popp et al., 2005). Polyspecific binding sites were suggested by mutagenesis analysis, in which the affinity for individual cations was changed, e.g. by mutation of glutamate₄₇₅ to aspartate the affinity for TEA^+ increased, whereas the affinity for MPP^+ was not changed (Gorboulev et al., 1999). This data indicate that D475 is important for substrate selectivity. Moreover, the mutation D475E did not only increase the affinity for the transported substrate TEA^+ but also for the non-competitive inhibitor TPeA (tetrapentylammonium) (Gorboulev et al., 1999).

OCT1 is a facilitative diffusion system that transports cations in both directions. Crucial factors are substrate concentration and membrane potential (Egenberger et al., 2012). The translocated substrates are mainly characterized by primary to tertiary or quaternary amine groups. Whereas the protonation of the primary to tertiary amine groups is dependent on their pK_a values and the pH of the medium, quaternary amines are permanently charged independent of the pH. Already 15 years ago polyspecificity of OCT1 was acknowledged and first attempts were made to classify different groups of substrates. For rat Oct1, organic cations have been classified as type I and type II (van Montfoort et al., 2001).

Organic cations type I are substrates of OCT1. They are characterized by high hydrophilicity and are mostly below 500 Da, e.g. TEA⁺ and MPP⁺. In contrast, type II organic cations are less hydrophilic and more bulky such as quinine and quinidine (van Montfoort et al., 2001). Type II organic cations are not translocated by rat Oct1 (Nagel et al., 1997).

Concerning the classification of drugs, Wu *et al.* developed the Biopharmaceutics Drug Disposition Classification System (BDDCS) in order to predict drug disposition and drug-drug-interaction in the intestine and the liver in humans (Wu and Benet, 2005). The BDDCS focuses on the elimination route of a drug: Drugs displaying high intestinal permeability are mainly eliminated via metabolism, whereas drugs with weak intestinal permeability are mainly eliminated as unchanged drug in the urine and the bile (Wu and Benet, 2005). The classification is a modification of the Biopharmaceutics Classification System (BCS), which is based on evaluating the permeability and solubility of a drug (Amidon et al., 1995). The classification of the BDDCS comprises 4 classes. According to the BDDCS drugs of the class 3, which are characterized by high solubility and poor metabolism such as ranitidine and metformin, are substrates of OCT1 (Bourdet et al., 2005; Wu and Benet, 2005; Shu et al., 2007).

Next to the intense study of the structure-function relationship of OCT1, also structural properties of substrates that inhibit OCT1 mediated transport were analyzed in detail. Ahlin *et al.* screened 191 structurally diverse compounds for their ability to inhibit OCT1 mediated transport of ASP⁺. Of these, 62 were OCT1 inhibitors and 47 of them were novel inhibitors (Ahlin et al., 2008). According to their analyses, good inhibitors are hydrophobic, lipophilic, and positively charged substances. Instead, polar compounds with many hydrogen bond donor and acceptor moieties did not inhibit OCT1 (Ahlin et al., 2008). It needs to be pointed out that Ahlin *et al.* did not define the inhibitory mechanism of the identified inhibitors such as competitive and non-competitive inhibitors. Furthermore, they did not analyze if the inhibitory compounds are themselves transported by OCT1. More recently Hendrix *et al.* have performed comparative high throughput analyses of substrates of OCT1 and OCT2 (Hendrickx et al., 2013). According to their study, molecular volume and positive charge determine if a substance is transported by OCT1. Molecules with a molecular weight not greater than 500 Da are considered as possible substrates of OCT1 (Hendrickx et al., 2013).

Table 1.1 Selected substrates and inhibitors of human OCT1

Substrates of human OCT1	PubChem CID ¹	Reference
Model substrates		
ASP ⁺	6438078	(Ahlin et al., 2011)
MPP ⁺	39484	(Zhang et al., 1997; Shu et al., 2003)
TEA ⁺	5413	(Sakata et al., 2004)
Drugs		
Acyclovir	2022	(Takeda et al., 2002)
Debrisoquine	2966	(Saadatmand et al., 2012)
Ganciclovir	3454	(Takeda et al., 2002)
Metformin	4091	(Shu et al., 2007; Tzvetkov et al., 2009; Yoon et al., 2013)
Morphine	5288826	(Tzvetkov et al., 2013)
O-desmethyltramadol	130829	(Tzvetkov et al., 2011)
Tropisetron	656665	(Tzvetkov et al., 2012)
Hormones		
Adrenaline	5816	(Breidert et al., 1998)
Prostaglandin E ₂	5280360	(Kimura et al., 2002)
Prostaglandin F _{2α}	5280363	(Kimura et al., 2002)
Neurotransmitter		
Acetylcholine	187	(Lips et al., 2005)
Dopamine	681	(Breidert et al., 1998)
Vitamins		
Thiamine	1130	(Chen et al., 2014)
Phytochemicals		
Atropine	174174	unpublished Data Chen <i>et al.</i>
Monocrotaline	9415	(Tu et al., 2013)
Others		
DAPI	2954	(Yasujima et al., 2011)
Tyramine	5610	(Breidert et al., 1998; Seitz et al., 2015)
Inhibitors of human OCT1		
Drugs		
Amitriptyline	2160	(Ahlin et al., 2011)
Codeine	5284371	(Tzvetkov et al., 2013)
Ondansetron	4595	(Tzvetkov et al., 2012)
Prazosin	4893	(Hayer-Zillgen et al., 2002)
Quinidine	441074	(Shu et al., 2007)
Verapamil	2520	(Zhang et al., 1998; Ahlin et al., 2011)
Hormones		
Corticosterone	5753	(Hayer-Zillgen et al., 2002)
β-estradiol	5757	(Ahlin et al., 2008)
Others		
Decynium D22	5484462	(Zhang et al., 1997)

¹ PubChem CID...Compound Identifier on <https://pubchem.ncbi.nlm.nih.gov/> for details about 2D structure

1.4 Genetic variability of OCT1

The OCT1 gene is highly genetically variable. In a study by Leabman *et al.*, genetic variants of OCT1 and further 23 membrane transporters of the SLC family as well as of the ABC family were analyzed. OCT1 had the highest genetic variability among the organic cation transporters of the SLC22 family with a non-synonymous nucleotide diversity of 5.11×10^{-4} and a ratio of non-synonymous to synonymous nucleotide diversity of 0.46 (Leabman *et al.*, 2003). Furthermore, analyses of the available 1000 genomes data showed that OCT1 has the highest genetic variability among the organic cation transporters of the SLC22 and SLC47 families (Tzvetkov *et al.*, 2016).

The first systematic studies on the genetic variability in OCT1 were performed more than 10 years ago by Kerb *et al.* (Kerb *et al.*, 2002) and Leabman *et al.* (Leabman *et al.*, 2003). Kerb *et al.* re-sequenced *OCT1* coding and promoter regions in 57 Caucasians and identified 25 genetic variations, which were analyzed regarding their population frequency (Kerb *et al.*, 2002). They further analyzed 190 Caucasians for 16 variants of which 8 were found in the coding region of *OCT1* leading to amino acid exchanges. The four amino substitutions R61C, C88R, F160L, G401S, and the deletion of methionine₄₂₀ were found to have an allele frequency of 9.1, 0.6, 22, 3.2, and 16 %, respectively. Among them, R61C, C88R, and G401S were found to affect OCT1 mediated uptake of MPP⁺ (Kerb *et al.*, 2002). Leabman *et al.* screened for genetic variants in the coding region of *OCT1* in 247 unrelated individuals containing 100 European Americans, 100 African Americans, 30 Asians, 10 Mexicans, and 7 Pacific Islanders. The group identified 15 non-synonymous variants in OCT1 from which five were found to strongly decrease or even to completely abolish OCT1 activity (R61C, G220V, P341L, G401S, and G465R) (Leabman *et al.*, 2003; Shu *et al.*, 2003).

Besides Caucasians, several studies analyzed the genetic variability of *OCT1* in Asians. There seem to be inter-ethnic differences in the frequency of loss of OCT1 activity as the amount as well as the frequency of genetic variants in *OCT1* was much lower in Asians than in Caucasian populations (Itoda *et al.*, 2004; Chen *et al.*, 2010; Yoon *et al.*, 2013). In 48 Japanese unrelated individuals, 29 single nucleotide polymorphisms have been identified in *OCT1*, of which three were found in the coding region of *OCT1* leading to non-synonymous substitutions (Saito *et al.*, 2002). Among the analyzed genetic variants, the genetic variants P283L and R287G were restricted to the Asian population (Saito *et al.*,

2002; Takeuchi et al., 2003; Sakata et al., 2004). In a study of Chen *et al.*, the group identified and functionally characterized loss-of function polymorphisms in *OCT1* in a sample set of 30 samples of Chinese in Beijing, 30 Japanese in Tokyo (both from the 1000 Genomes project) (Chen et al., 2010) and 66 Japanese patients (Shu et al., 2003). They identified the three non-synonymous substitutions Q97K, P117L, and R206C with a minor allele frequency of 0.017 and 0.02 for Q97K and P117L, respectively. The variant R206C was only found as a single individual in a heterozygous form (Chen et al., 2010).

Most of the population genetic data about loss-of function polymorphisms were limited to specific populations. Recently, our group analyzed the frequency of loss-of function polymorphisms on a global scale (Seitz et al., 2015). The functional characterization of these variants described in this thesis was part of this study. The complete coding sequence of the *OCT1* gene and its flanking regions was resequenced in 2171 unrelated individuals from 67 populations worldwide using semiconductor-based massively parallel sequencing. From 85 identified variants, 44 variants have been found in the coding region of *OCT1*. Of those, 29 variants caused amino acid substitutions (Figure 1.2).

Haplotype	Ser14Phe	Ser29Leu	Arg61Cys	Cys88Arg	Gln97Lys	Pro117Leu	Phe160Leu	Ser189Leu	Arg206Cys	Gly220Val	Thr245Met	Glu284Lys	Pro341Leu	Arg342His	Gly401Ser	Met408Val	Gly414Ala	Met420del	Ile449Thr	Gly465Arg	Arg486Met	N	
OCT1*1 A	Ser	Ser	Arg	Cys	Gln	Pro	Phe	Ser	Arg	Gly	Thr	Glu	Pro	Arg	Gly	Val	Gly	Met	Ile	Gly	Arg	2165	
1 B	Ser	Ser	Arg	Cys	Gln	Pro	Phe	Ser	Arg	Gly	Thr	Glu	Pro	Arg	Gly	Met	Gly	Met	Ile	Gly	Arg	736	
1 C	Ser	Ser	Arg	Cys	Gln	Pro	Leu	Ser	Arg	Gly	Thr	Glu	Pro	Arg	Gly	Met	Gly	Met	Ile	Gly	Arg	377	
1 D	Ser	Ser	Arg	Cys	Gln	Pro	Phe	Ser	Arg	Gly	Thr	Glu	Leu	Arg	Gly	Val	Gly	Met	Ile	Gly	Arg	246	
1 E	Ser	Ser	Arg	Cys	Gln	Pro	Leu	Ser	Arg	Gly	Thr	Glu	Pro	Arg	Gly	Val	Gly	Met	Ile	Gly	Arg	7	
1 F	Ser	Ser	Arg	Cys	Gln	Pro	Phe	Ser	Arg	Gly	Thr	Glu	Pro	His	Gly	Val	Gly	Met	Ile	Gly	Arg	1	
1 G	Ser	Ser	Arg	Cys	Gln	Pro	Phe	Ser	Arg	Gly	Thr	Glu	Leu	Arg	Gly	Met	Gly	Met	Ile	Gly	Arg	1	
OCT1*2 A	Ser	Ser	Arg	Cys	Gln	Pro	Phe	Ser	Arg	Gly	Thr	Glu	Pro	Arg	Gly	Val	Gly	del	Ile	Gly	Arg	515	
2 B	Ser	Ser	Arg	Cys	Gln	Pro	Leu	Ser	Arg	Gly	Thr	Glu	Pro	Arg	Gly	Val	Gly	del	Ile	Gly	Arg	1	
2 C	Ser	Ser	Arg	Cys	Gln	Pro	Phe	Ser	Arg	Gly	Thr	Glu	Pro	Arg	Gly	Val	Ala	del	Ile	Gly	Arg	2	
OCT1*3 A	Ser	Ser	Cys	Cys	Gln	Pro	Leu	Ser	Arg	Gly	Thr	Glu	Pro	Arg	Gly	Met	Gly	Met	Ile	Gly	Arg	122	
3 B	Ser	Ser	Cys	Cys	Gln	Pro	Phe	Ser	Arg	Gly	Thr	Glu	Pro	Arg	Gly	Val	Gly	Met	Ile	Gly	Arg	7	
OCT1*4 A	Ser	Ser	Arg	Cys	Gln	Pro	Leu	Ser	Arg	Gly	Thr	Glu	Pro	Arg	Ser	Met	Gly	Met	Ile	Gly	Arg	32	
4 B	Ser	Ser	Arg	Cys	Gln	Pro	Phe	Ser	Arg	Gly	Thr	Glu	Pro	Arg	Ser	Met	Gly	Met	Ile	Gly	Arg	2	
OCT1*5	Ser	Ser	Arg	Cys	Gln	Pro	Phe	Ser	Arg	Gly	Thr	Glu	Pro	Arg	Gly	Val	Gly	del	Ile	Arg	Arg	40	
OCT1*6	Ser	Ser	Arg	Arg	Gln	Pro	Phe	Ser	Arg	Gly	Thr	Glu	Pro	Arg	Gly	Val	Gly	del	Ile	Gly	Arg	8	
OCT1*7 A	Phe	Ser	Arg	Cys	Gln	Pro	Phe	Ser	Arg	Gly	Thr	Glu	Pro	His	Gly	Val	Gly	Met	Ile	Gly	Arg	18	
7 B	Phe	Ser	Arg	Cys	Gln	Pro	Phe	Ser	Arg	Gly	Thr	Glu	Pro	Arg	Gly	Val	Gly	Met	Ile	Gly	Arg	8	
7 C	Phe	Ser	Arg	Cys	Gln	Pro	Leu	Ser	Arg	Gly	Thr	Glu	Pro	Arg	Gly	Met	Gly	Met	Ile	Gly	Arg	1	
OCT1*8 A	Ser	Ser	Arg	Cys	Gln	Pro	Phe	Ser	Arg	Gly	Thr	Glu	Pro	Arg	Gly	Met	Gly	Met	Ile	Gly	Met	19	
8 B	Ser	Ser	Arg	Cys	Gln	Pro	Phe	Ser	Arg	Gly	Thr	Glu	Pro	Arg	Gly	Val	Gly	Met	Ile	Gly	Met	18	
8 C	Ser	Ser	Arg	Cys	Gln	Pro	Phe	Ser	Arg	Gly	Thr	Glu	Pro	His	Gly	Val	Gly	Met	Ile	Gly	Met	1	
OCT1*9	Ser	Ser	Arg	Cys	Gln	Pro	Leu	Leu	Ser	Arg	Gly	Thr	Glu	Pro	Arg	Gly	Met	Gly	Met	Ile	Gly	Arg	4
OCT1*10	Ser	Ser	Arg	Cys	Gln	Pro	Phe	Leu	Arg	Gly	Thr	Glu	Pro	Arg	Gly	Met	Gly	Met	Ile	Gly	Arg	3	
OCT1*11	Ser	Ser	Arg	Cys	Gln	Pro	Phe	Ser	Arg	Gly	Thr	Glu	Pro	Arg	Gly	Met	Gly	Met	Thr	Gly	Arg	2	
OCT1*12	Ser	Leu	Arg	Cys	Gln	Pro	Phe	Ser	Arg	Gly	Thr	Glu	Leu	Arg	Gly	Val	Gly	Met	Ile	Gly	Arg	2	
OCT1*13	Ser	Ser	Arg	Cys	Gln	Pro	Phe	Ser	Arg	Gly	Met	Glu	Pro	Arg	Gly	Val	Gly	Met	Ile	Gly	Arg	1	
OCT1*14	Ser	Ser	Arg	Cys	Gln	Pro	Phe	Ser	Cys	Gly	Thr	Glu	Pro	Arg	Gly	Val	Gly	del	Ile	Gly	Arg	1	
OCT1*15	Ser	Ser	Arg	Cys	Gln	Pro	Phe	Ser	Arg	Gly	Thr	Lys	Pro	Arg	Gly	Val	Gly	Met	Ile	Gly	Arg	1	
OCT1*16	Ser	Ser	Arg	Cys	Gln	Pro	Phe	Ser	Arg	Val	Thr	Glu	Pro	Arg	Gly	Val	Gly	Met	Ile	Gly	Arg	1	

Figure 1.2 Haplotype combinations constituting 16 major and 14 sub-alleles of *OCT1*. Amino acid substitutions (shown in yellow) that cause a more than 50 % decrease or increase of transport activity in comparison to the reference *OCT1*1* allele for at least one substrate tested were designated as major alleles. The sub-allele differs from the appropriate major allele by amino acid substitutions (shown in white) that do not affect OCT1 activity. From Seitz *et al.* (Seitz et al., 2015).

1.4.1 Impact of coding genetic polymorphisms on OCT1 function

The first effort to predict the effect of coding genetic variants on OCT1 function was the analysis using the amino acid scoring systems Grantham and BLOSUM62 (Leabman et al., 2003). Lower Grantham values indicate chemical similarity, whereas higher values indicate radical chemical changes (Grantham, 1974). A more negative BLOSUM62 value indicates an evolutionary unfavorable change (Cargill et al., 1999; Shu et al., 2003). Nevertheless, in order to definitely characterize the effect of genetic polymorphism in *OCT1*, functional studies of these variants are unavoidable. Out of the available studies about the genetic

variability in *OCT1* (Kerb et al., 2002; Shu et al., 2003; Shu et al., 2007; Tzvetkov et al., 2009), one deletion and four amino acid substitutions were of special interest as they were frequently observed and associated with reduced transport activity of OCT1: the deletion of methionine in codon 420 (M420del) and the substitutions R61C, C88R, G401S, and G465R.

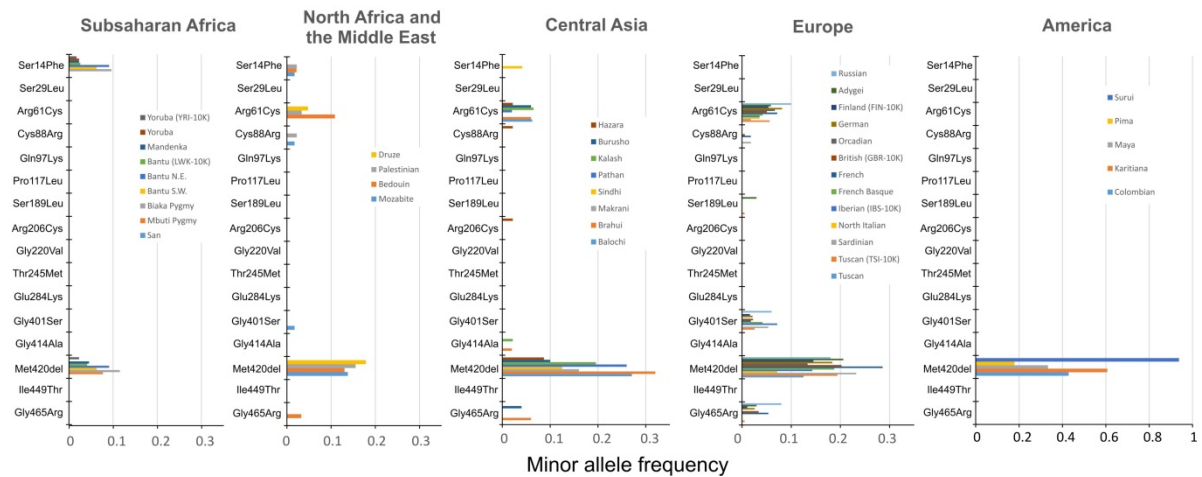


Figure 1.3 Minor allele frequencies of 16 *OCT1* polymorphisms in 39 different populations worldwide. Shown are 39 populations from Sub-Saharan Africa, North Africa and the Middle East, Central Asia, Europe, and America. The M420del variant was the most frequent and the only ubiquitously observed among the worldwide populations studied. From Seitz *et al.* (Seitz et al., 2015)

M420del

The deletion of methionine₄₂₀ is the most common and the only ubiquitously observed variant in *OCT1* (Figure 1.3), (Shu et al., 2003; Shu et al., 2007; Seitz et al., 2015). The affected methionine₄₂₀ is located in the 9th transmembrane domain of the *OCT1* protein and M420del apparently does not affect subcellular localization of *OCT1* (Ahlin et al., 2011). Recently, genetic analyses in humans revealed that the M420del only exists in combination with the M408V polymorphism (Tzvetkov et al., 2014).

In-vitro functional analyses revealed highly substrate-specific effects regarding loss of activity of the M420del variant: The uptake of the model substrates MPP^+ and ASP^+ did not significantly differ from wild type *OCT1* (Kerb et al., 2002; Shu et al., 2003; Ahlin et al., 2011). The transport of debrisoquine was slightly decreased due to reduced v_{max} . The K_m of debrisoquine was not affected (Saadatmand et al., 2012). In contrast, the M420del

variant significantly decreased the uptake of metformin and morphine uptake was decreased by more than 60 % (Shu et al., 2007; Tzvetkov et al., 2013). The uptake of tropisetron was reduced by more than 80 % (Tzvetkov et al., 2012). Moreover, the M420del variant showed complete lack of transport activity for the uptake of O-desmethyltramadol (Tzvetkov et al., 2011). Up to now, structural mechanisms underlying the substrate-specific effect of M420del are not known (Shu et al., 2007).

Although the uptake of ASP^+ did not significantly differ between the M420del variant and wild type OCT1, the M420del variant was shown to be more susceptible to inhibition of ASP^+ uptake, showing up to 14 times lower IC_{50} values than wild type OCT1 using different inhibitors of OCT1 (Ahlin et al., 2011). This finding indicates increased potency of some inhibitors to inhibit transport of M420del. Similar to this finding, the M420del variant was more susceptible to the inhibition of metformin uptake by verapamil (Ahlin et al., 2011). These findings suggest complex drug-drug interactions at the binding site of the M420del variant.

R61C

The amino acid substitution R61C is a common OCT1 variant observed in Caucasians, but not in Africans or Asians (Figure 1.3). The affected arginine₆₁ is located in the big extracellular loop between the 1st and the 2nd transmembrane domain. The R61C variant is less expressed on the plasma membrane displaying a more diffuse localization and cytosolic retention than reference wild type OCT1 (Shu et al., 2007; Ahlin et al., 2011). The R61C variant strongly decreased transport activity of OCT1 in *in-vitro* for all substrates tested: The uptake of the model substrates MPP^+ and ASP^+ was strongly reduced by more than 70 % and 60 %, respectively (Kerb et al., 2002; Shu et al., 2003; Ahlin et al., 2011). The uptake of morphine was reduced by 86 % and the uptake of tropisetron and O-desmethyltramadol was completely abolished (Tzvetkov et al., 2011; Tzvetkov et al., 2012; Tzvetkov et al., 2013). Comparable to M420del, the R61C variant was more susceptible to inhibition of ASP^+ transport. The IC_{50} values were up to 23 times lower than for wild type reference (Ahlin et al., 2011). The uptake of debrisoquine was strongly reduced although the K_m was not affected (Saadatmand et al., 2012). The uptake of metformin was decreased by up to 91 % due to reduced v_{max} (Ahlin et al., 2011).

C88R

The C88R substitution is one of the rarest OCT1 variants and is only observed in Caucasians (Figure 1.3). The variant was only detected in 8 individuals in a sample set of 1079 individuals (Seitz et al., 2015). Genetic analysis revealed that the C88R substitution is only observed in combination with the M420del variant (also known as *OCT1* allele *6) (Tzvetkov et al., 2012). The affected cysteine₈₈ is located in the big extracellular loop between the 1st and the 2nd transmembrane domain. Previously it was shown that the cysteines located in the extracellular loop of OCT1 are involved in formation of disulfide bonds, which are crucial for homo oligomerization and localization of the transporter in the plasma membrane (Keller et al., 2011). Mutation of cysteine₈₉ in human OCT2 (the analog of cysteine₈₈ in OCT1) to alanine was retained in the cortisol (Brast et al., 2012). The C88R variant showed lack of transport activity for the uptake of debrisoquine, tropisetron, and morphine (Saadatmand et al., 2012; Tzvetkov et al., 2012; Tzvetkov et al., 2013).

G401S

The amino acid substitution G401S is observed in Caucasians but not in African or Asian populations (Figure 1.3). The affected glycine₄₀₁ is located in the small intracellular loop between the 8th and the 9th transmembrane domain. Glycine₄₀₁ is conserved among the other two paralogs OCT2 and OCT3 (Shu et al., 2003). The variant G401S as well as the variants G220V and G465R change evolutionary conserved glycine residues and strongly reduce transport activity. Hence, it was suggested that evolutionary conserved glycine residues are important for OCT1 function and that substitution of these strongly affect OCT1 activity (Shu et al., 2003). *In-vitro* studies revealed that the G401S variant showed a strong reduction in the transport of all substances tested: The G401S variant almost completely lacked uptake of MPP⁺ and tropisetron (Shu et al., 2003; Tzvetkov et al., 2012). The uptake of debrisoquine, metformin, morphine, and O-desmethytramadol was strongly decreased (Shu et al., 2007; Tzvetkov et al., 2011; Saadatmand et al., 2012; Tzvetkov et al., 2013).

G465R

The amino acid substitution G465R is a variant, which is only observed in Caucasian population (Figure 1.3). The affected glycine₄₆₅ is located in the 11th transmembrane domain of the OCT1 protein. The affected glycine₄₆₅ is also present in OCT2, OCT3, OAT1-3 and also in OCTN2 and therefore may be of generally importance for transporter function (Shu et al., 2003). The G465R variant completely fails to localize in the plasma membrane (Shu et al., 2003). Therefore it causes complete lack of transport activity for all substrates previously tested: MPP⁺, metformin, debrisoquine, tropisetron, O-desmethyl-tramadol, and morphine (Shu et al., 2003; Shu et al., 2007; Tzvetkov et al., 2011; Saadatmand et al., 2012; Tzvetkov et al., 2012; Tzvetkov et al., 2013). Haplotype analyses suggested that G465R is inherited only in a combination with the M420del variant (referred also as *OCT1* allele *5) (Tzvetkov et al., 2012).

Further common OCT1 variants

The variant P341L was commonly observed in Asians (Saito et al., 2002; Shu et al., 2003; Itoda et al., 2004). The variant F160L was commonly observed in Caucasian and Asian populations (Shu et al., 2003; Sakata et al., 2004). Both variants were shown not do affect OCT1 activity: For P341L the uptake of TEA⁺, MPP⁺ and metformin was only slightly decreased, whereas F160L did not affect the uptake of these substrates (Shu et al., 2003; Takeuchi et al., 2003; Sakata et al., 2004; Shu et al., 2007). The P341L and F160L did not alter the subcellular localization of OCT1 (Sakata et al., 2004).

The *OCT1* allelic variant S14F was commonly observed in Africa (Figure 1.3). Also for S14F substrate-specific effects were reported: whereas the uptake of MPP⁺ was increased in relation to wild type reference, S14F significantly reduced the uptake of metformin (Shu et al., 2003; Shu et al., 2007).

Very rare OCT1 variants

A number of rare OCT1 variants have been functionally characterized *in vitro*. Takeuchi *et al.* demonstrated lack of TEA⁺ transport for the amino acid exchanges P283L and R287G although membrane localization of the transporter in these variants was not altered (Takeuchi *et al.*, 2003). A possible impact of these variants on transporter function was already hypothesized earlier, as the variants P283L and R287G were found to change conserved amino acids among the organic cation transporters (Saito *et al.*, 2002). The variants P283L and R287G were only observed in the Asian population (Saito *et al.*, 2002; Takeuchi *et al.*, 2003; Sakata *et al.*, 2004).

The variant P117L is a very rare variant that was identified in a sample set of 116 Japanese individuals for the first time (Itoda *et al.*, 2004). The affected proline₁₁₇ is conserved among the mammalian OCTs (Itoda *et al.*, 2004). The uptake of metformin was significantly reduced, although membrane localization was not altered (Chen *et al.*, 2010).

The variants R206C and Q97K were found in Japanese population (Chen *et al.*, 2010). The affected arginine₂₀₆ is highly conserved among mammalian OCTs, whereas glutamine₉₇ is only highly conserved among OCT1 orthologs and in OCT2. The uptake of metformin is significantly decreased in R206C and Q97K variants. The decrease in metformin uptake by R206C was due to reduced v_{\max} and by Q97K due to increased K_m . Analysis of the sub-cellular localization revealed decreased membrane localization and retention in the endoplasmic reticulum for the R206C variant, whereas the membrane localization of the Q97K variant was not affected (Chen *et al.*, 2010).

Other variants analyzed showed a substrate-specific decrease in transport activity: the variant S189L showed no differences in the uptake of MPP⁺ compared to the wild type reference, but a significant decrease in the uptake of metformin due to reduced v_{\max} (Shu *et al.*, 2003; Shu *et al.*, 2007). The variants S189L was only observed in Caucasians (Shu *et al.*, 2003; Tzvetkov *et al.*, 2014).

The variants R342H and R488M were observed in African populations and were shown not to affect the uptake of MPP⁺ and metformin (Shu *et al.*, 2003; Shu *et al.*, 2007; Seitz *et al.*, 2015).

1.4.2 Impact of genetic variation in OCT1 on drugs pharmacokinetics and response

Single nucleotide polymorphisms in *OCT1* affect transporter function (Figure 1.4). Therefore, they may cause inter-individual variations in drug response and may influence pharmacotherapy. Any of the polymorphisms R61C, C88R, G401S, G465R, or a deletion of methionine₄₂₀ (M420del) causes partial or complete loss of OCT1 function. In Caucasians the frequency of these variants have been reported to be on average 9.6 %, 0.6 %, 2.8 %, 1.8 %, and 15.4 %, respectively (Kerb et al., 2002; Tzvetkov et al., 2012). Individuals can be divided to carriers of zero, one, or two loss-of function alleles in *OCT1*. In Caucasians 42 % of the individuals carry one and further 9 % two loss-of-function *OCT1* alleles (Shu et al., 2007; Tzvetkov et al., 2012). Data is rapidly accumulating that this genetically-determined loss of OCT1 activity may affect the pharmacokinetics, efficacy, and toxicity of drugs that are metabolized or act in the liver. Affected are cationic and weak basic like the opioids morphine and tramadol, the antiemetics tropisetron and ondansetron, and the very commonly administrated oral antidiabetic metformin.

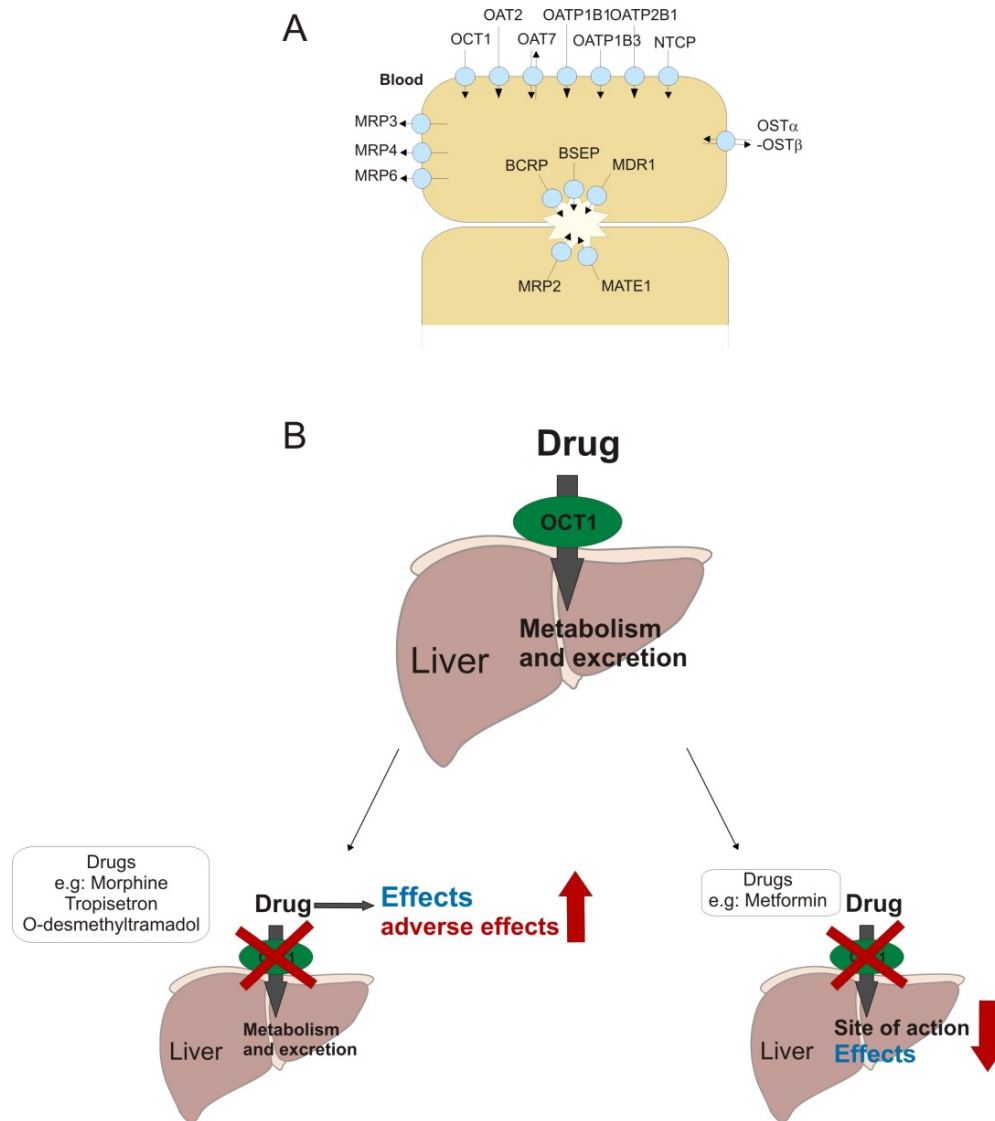


Figure 1.4 Localization and function of OCT1 in hepatocytes. (A) OCT1 is mainly expressed in the sinusoidal membrane of human hepatocytes. Next to OCT1, the following uptake transporters are expressed in the sinusoidal membrane: the organic anion transporter 2 (OAT2;SLC22A7) and 7 (OAT7; SLC22A9), three members of organic anion transport polypeptides (OATP1B1 (SLCO1B1), OATP1B3 (SLCO1B3), OATP2B1 (SLCO2B1), and the uptake transporter sodium/taurocholate co-transporting peptide (NTCP; SLC10A1). Transporters in the basolateral membrane are the efflux transporters multidrug resistance protein MRP3 (ABCC3), MRP4 (ABCC4), and MRP6 (ABCC6). Transporters in the canalicular membrane are the efflux pumps multidrug resistance 1 transporter (MDR1; ABCB1), the bile-salt export pump (BSEP; ABCB11), the breast cancer resistance protein (BCRP; ABCG2), MRP2 (ABCC2), and the multidrug and toxin extrusion protein 1 (MATE1; SLC47A1), the heteromeric organic solute transporter (OST α -OST β ; SLC51a/Slc51b) is located in the apical membrane. (B) OCT1 as a mediator of drugs as the first step of metabolism and excretion. For drugs that rely on OCT1 uptake, e.g. morphine, tropisetron, and O-desmethyltramadol, as the first step of metabolism and excretion, loss of OCT1 function lead to higher plasma levels of these drugs. This results in higher efficacy, but also increases the risk of adverse effects. Drugs like metformin rely on OCT1 uptake in order to reach their side of action. Loss of OCT1 function decreases metformin efficacy.

Morphine is a natural opioid analgesic, which directly acts on the central nervous system (Mayer and Price, 1976). Codeine is the pro-drug of morphine and needs to be metabolized to morphine by CYP2D6. Morphine and codeine are used for treatment of moderate to severe pain e.g. during surgery or cancer therapy (Hanks et al., 2001). Polymorphisms in the CYP2D6 gene were associated with increased risk of morphine adverse effects (Gasche et al., 2004; Kirchheiner et al., 2007; Crews et al., 2012). But polymorphisms in the CYP2D6 gene could only partially explain the high morphine plasma concentrations after treatment with codeine (Lotsch et al., 2009; Sistonen et al., 2012). Morphine is a hydrophilic, weak base that is positively charged at physiological pH ($pK_a = 7.4$). Morphine is a substrate of OCT1 whereas the uptake of the pro-drug codeine into hepatocytes is not OCT1 dependent (Tzvetkov et al., 2013). Codeine is highly membrane permeable and enters hepatocytes by passive diffusion. Moreover, codeine was shown to inhibit OCT1 transport activity (Tzvetkov et al., 2013). Recently, the increase in morphine plasma concentration was also related to higher sensibility to adverse effects in healthy volunteers (Tzvetkov et al., 2013). Therefore, the knowledge of individual OCT1 genotypes may help to adjust drug medication also in regard of adverse effects. Similar effects were also observed in patients. Children with loss of function alleles in *OCT1* showed increased morphine plasma concentrations after morphine administration. Moreover, it was shown that these patients had reduced levels of morphine 3-glucuronid, the main metabolite of morphine generated in hepatocytes (Fukuda et al., 2013).

Tramadol is a synthetic opioid analgesic used in the treatment of moderate pain. It is a prodrug that needs to be metabolized to its active metabolite O-desmethyltramadol, which binds with high affinity to the μ -opioid receptor (Sevcik et al., 1993). The reaction is catalyzed by CYP2D6 in hepatocytes (Paar et al., 1997). Polymorphisms in the CYP2D6 gene were shown to affect tramadol pharmacokinetics. But these polymorphisms could just partially explain inter-individual differences in subgroups defined as individuals with high, intermediate or low CYP2D6 activity (Stamer et al., 2003; Kirchheiner et al., 2008). Whereas tramadol can cross plasma membranes by carrier independent passive diffusion, the uptake of its hydrophilic metabolite O-desmethyltramadol into hepatocytes depends on OCT1 (Tzvetkov et al., 2011). After re-uptake of O-desmethyltramadol into hepatocytes it is bio-inactivated by glucuronidation by UGT2B7 (Lehtonen et al., 2010). Individuals carrying two loss-of-function *OCT1* alleles showed higher plasma levels of O-desmethyltramadol (Tzvetkov et al., 2011). In line with the increased plasma concentrations tramadol

induced miosis, which was used as an indicator of opioid effects, was stronger and prolonged in these individuals. Hence, the pharmacokinetic of tramadol is not only influenced by polymorphisms in the CYP2D6 gene but also by polymorphisms in the OCT1 gene as OCT1 is assumed as the rate limiting step of O-desmethyltramadol bioin-activation (Tzvetkov et al., 2011).

Tropisetron is a serotonin antagonist of the 5-hydroxytryptamine 3 receptor (5-HT₃ receptor) (Simpson et al., 2000). It is used as an antiemetic for the treatment of chemotherapy induced and postoperative nausea and vomiting (Simpson et al., 2000). The 5-HT₃ receptor mediates nausea and vomiting in the peripheral and central nervous system. Although tropisetron was shown to be effective in treatment of nausea, some patients still do not respond sufficiently to tropisetron therapy (Bruntsch et al., 1993; Adams et al., 1995; Mystakidou et al., 1998). Genetic polymorphisms in the metabolizing enzyme CYP2D6 are well known to strongly contribute, but could not completely explain the observed strong inter-individual differences in response to tropisetron (Kees et al., 2001; Kaiser et al., 2002; Kim et al., 2003; Pickering et al., 2012). More recently also genetically-determined loss of OCT1 activity was associated with a variation in the pharmacokinetics and activity of tropisetron and ondansetron (Tzvetkov et al., 2012). In a study of Tzvetkov *et al.* 253 patients were genotyped for five common amino acid substitutions that are associated with reduced activity of OCT1: R61C, C88R, G401S, M420del or G465R. Of these patients 12 % carried two loss-of-function *OCT1* alleles, further 38 % carried one. In patients carrying two loss-of-function alleles the plasma concentration of tropisetron after 3 and 6 hours of administration was higher than in patients with only one variant allele or two active *OCT1* alleles. Moreover, these patients showed greater therapeutic effect of tropisetron treatment as vomiting was less observed than in patients carrying two active *OCT1* alleles (Tzvetkov et al., 2012).

Next to opioids and antiemetics, metformin was also shown to be a substrate of OCT1 (Shu et al., 2007). Metformin is a hydrophilic cation with a biguanide structure, which is widely used for the treatment of diabetes type 2 (Tahrani et al., 2011). Metformin leads to decreased absorption of glucose in the intestine and reduces gluconeogenesis (Ikeda et al., 2000; Kim et al., 2008; Foretz et al., 2010). The exact molecular mechanism underlying metformin action remains partially understood (An and He, 2016). It is assumed that it acts via activation of AMP-activated protein kinase (AMPK), which inhibits enzymes

responsible for gluconeogenesis and leads to an increased uptake of glucose into muscle and liver cells (Sarabia et al., 1992; Abbud et al., 2000; Zhou et al., 2001; Zhang et al., 2009). Metformin is a substrate of OCT1 and genetic polymorphisms in *OCT1* were shown to affect metformin uptake *in vitro* (Shu et al., 2007). When performing an oral glucose tolerance test in healthy volunteers that were carriers of loss-of-function *OCT1* alleles, the plasma glucose level was significantly higher after 180 min of metformin administration than in carriers of the OCT1 wild type reference (Shu et al., 2007; Chen et al., 2010). In contrast, the variant P341L was not shown to influence metformin pharmacokinetics in healthy volunteers (Yoon et al., 2013). Metformin is primarily eliminated by renal excretion (Pentikainen et al., 1979). Although in much lower levels as in the liver, the human OCT1 protein was detected in apical membrane of proximal and distal renal tubules (Tzvetkov et al., 2009). It was shown in a study of healthy male Caucasians that metformin clearance significantly increased in carriers of loss of function *OCT1* alleles and account for 9.1 % of inter-individual variation in metformin clearance (Tzvetkov et al., 2009).

1.5 Aim of this work

One of the major problems in prediction of the effects of *OCT1* single nucleotide polymorphisms leading to non-synonymous amino acid exchanges in OCT1 on transporter function is the limited number of substrates analyzed. Most of the available functional *in vitro* studies on OCT1 transport activity were performed using either one or two model substrates (usually TEA⁺ or MPP⁺) or a single drug. Studies comparing the effect of single nucleotide polymorphism on OCT1 activity for a broad spectrum of substrates especially drugs are missing. So far, the OCT1 variants M420del, S14F, and S189L were reported to have highly substrate-specific effects on OCT1 activity, but so far, substrate-specific effects of single nucleotide polymorphisms in *OCT1* were not systematically analyzed and some highly substrate-specific effects may still be undetected.

The first aim of this thesis was to characterize in detail the substrate-specific and substrate overlapping effects of non-synonymous single nucleotide polymorphisms on OCT1 function. Comparative analyses were performed on all non-synonymous single nucleotide polymorphisms identified worldwide using a broad spectrum of OCT1 substrates. These results of this part of the work might give insight into population-specific differences in

loss of OCT1 function, which could be furthermore used for optimized dose administration in drug treatment.

The deletion of methionine₄₂₀ is one of the most common and the only ubiquitously observed variant in OCT1 (Figure 1.3) leading to substrate-specific loss of OCT1 activity. Hence, the second aim of this work was to identify possible mechanisms underlying M420del substrate-specific effects. Two main hypotheses were generated. First, we analyzed if the observed substrate-specific loss of function activity is due to the reduction of the protein chain caused by the deletion itself independent on the amino acid deleted. Second, we analyzed if the M420del effects are rather caused by the specific loss of the methionine side chain. In order to test the hypotheses, different mutants of *OCT1* overexpressing HEK293 cells were generated and analyzed regarding their transport activity and subcellular localization. This approach might help to understand the impact of M420del on transport function using multiple substrates. We hoped that these initial analyses may shed light on the mechanism enabling the poly-specificity of OCT1 and might identify specific structural properties of OCT1 substrates that are affected of by M420del.

2 Materials

2.1 Equipment

Equipment	Manufacturer
3130xl Genetic Analyzer	Applied Biosystems, Darmstadt, Germany
7900 HT Fast Real Time PCR System	Thermo Fisher Scientific, Darmstadt, Germany
API 4000 LC-MS/MS system	AB Sciex, Darmstadt Germany
Autoclave Laboklav 55-195	SHP Steriltechnik, Detzel Schloss, Germany
Balance BP210S	Sartorius, Göttingen, Germany
Balance M-Pact AX2202	Sartorius, Göttingen, Germany
Biological Safety Cabinet: CleanAir NSF 49	Cleanair, Woerden, Netherlands
BioPhotometer	Eppendorf, Hamburg, Germany
Brownlee SPP RP-Amide Column	PerkinElmer, Waltham, USA
Centrifuge 58010R	Eppendorf, Hamburg, Germany
Centrifuge Heraeus Fresco 17	Thermo Fisher Scientific, Darmstadt, Germany
Centrifuge J2-21 M/E	Beckman Coulter, Krefeld, Germany
Centrifuge JA-20 rotor	Beckman Coulter, Krefeld, Germany
CO ₂ incubator BBD6220	Thermo Fisher Scientific, Darmstadt, Germany
Degasser 310SP	ERC, Riemerling, Germany
Diaphragm pump MZ 2C	Vacuumbrand, Wertheim, Germany
Dri-Block [®] heater DB3	Techne, Stone, UK
Electrophoresis chamber	PeqLab, Erlangen, Germany
Electroporator Gene Pulser II	BioRad, Munich, Germany
Fluor-S TM Multi Imager	BioRad, Munich, Germany
Heating Plate OTS 40	Medite, Burgdorf, Germany
Heraeus Multifuge X3	Thermo Fisher Scientific, Darmstadt, Germany
Hybridization oven	Binder, Tuttlingen, Germany
Incubator Hood Incudrive H	Schütt, Göttingen, Germany
LaChrom fluorescence detector L-7400	Merck Hitachi, Darmstadt, Germany
LaChrom HPLC System: interface D-7000, pump L-7100, autosampler L-7200, degasser L-7614	Merck Hitachi, Darmstadt, Germany
LaChrom ultraviolet detector - L-7400	Merck Hitachi, Darmstadt, Germany

Laser Scanning Microscope LSM710	Carl Zeiss Microscopy GmbH, Oberkochen, Germany
LiChrospher 100 CN column	Merck, Darmstadt, Germany
LiChrospher 100 CN guard column	Merck, Darmstadt, Germany
LiChrospher 100 reverse phase-18e	Merck, Darmstadt, Germany
Magnetic stirrer	IKA, Staufen, Germany
Mastercycler gradient	Eppendorf, Hamburg, Germany
Microscope Axiovert 40 CFL	Carl Zeiss Microscopy GmbH, Oberkochen, Germany
Mini Laboratory Centrifuges Spectrafuge™	Labnet, Edison, USA
MS2 mini shaker	IKA, Staufen, Germany
MultiScreen Column Loader	Merck, Darmstadt, Germany
Nanodrop cuvette	Implen, Munich, Germany
Neubauer cell chamber	Carl Roth, Karlsruhe, Germany
Orbital shaker KS 260 basic	IKA, Staufen, Germany
Platform Shake Polymax 1040 -	Heidolph Instruments, Schwabach, Germany
PTC-200 Thermal Cycler	BioRad, Munich, Germany
QIAcube robot	Qiagen, Hilden, Germany
QIAvac 24 Plus vacuum manifold	Qiagen, Hilden, Germany
Sample Concentrator	Techne, Stone, UK
Scintillation Counter LS6500	Beckman Coulter, Krefeld, Germany
Semi-dry blotter Fastblot B43	Biometra, Göttingen, Germany
Sequence Detection System	Applied Biosystems, Darmstadt, Germany
Seurity Guard C18 pre-column	Phenomenex, Aschaffenburg, Germany
SpeedVac® Plus SC110A concentrator	Savant Instruments, Holbrook, USA
Standard Power Pack P25	Biometra, Göttingen, Germany
Tecan Ultra Microplate Reader	Tecan Group AG, Männedorf, Switzerland
Thermal Cycler DNA Engine®	BioRad, Munich, Germany
Thermomixer® Comfort	Eppendorf, Hamburg, Germany
Transilluminator TI 2	Biometra, Göttingen, Germany
Vertical Electrophoresis Chambers mighty small II	Amersham Biosciences, San Francisco, USA
Water Bath GFL 1083	Schütt, Göttingen, Germany

2.2 Consumables

Material	Manufacturer
384 well PCR plate	Thermo Fisher Scientific, Darmstadt, Germany
96 well filter plate MAHV N45 plate	Merck, Darmstadt, Germany
96 well PCR plate	Thermo Fisher Scientific, Darmstadt, Germany
Adhesive sealing sheets	Thermo Fisher Scientific, Darmstadt, Germany
Cell culture flask 25 cm ²	Sarstedt, Nümbrecht, Germany
Cell culture flask 75 cm ²	Greiner Bio-One, Frickenhausen, Germany
Cell scraper 25 cm	Sarstedt, Nümbrecht, Germany
Cell strainer, 40 µm	BD Biosciences, Heidelberg, Germany
Centrifuge tube 15 ml	Greiner Bio-One, Frickenhausen, Germany
Centrifuge tube 50 ml	Sarstedt, Nümbrecht, Germany
Combitips (500 µl, 2.5 ml, 5 ml)	Eppendorf, Hamburg, Germany
Corning® 96 well microplates, black	Corning, Wiesbaden, Germany
Cover slip	Gerhard Menzel, Braunschweig, Germany
Dialysis membrane filter 0.025 µm	Merck, Darmstadt, Germany
Electroporation cuvettes – 2mm	PeqLab, Erlangen, Germany
Filter Paper Nr. 2668	Schleicher und Schuell, Dassel, Germany
Filter Paper Nr. 2CHR	Schleicher und Schuell, Dassel, Germany
Filter pipette tip, sterile (1000, 100 and 10 µl)	Kisker, Steinfurt, Germany
Flat cap strips, 8er	Thermo Fisher Scientific, Darmstadt, Germany
FrameStar 384 PCR Plate	4titude, Wotton, UK
GelSaver II Spitzen 1-200µl	Kisker, Steinfurt, Germany
Glass Pasteur pipette 230 mm	Brand, Wertheim, Germany
Lab-Tek® II Chamber Slide	Thermo Fisher Scientific, Darmstadt, Germany
Minisart-plus, 0,2 µM	Sartorius, Göttingen, Germany
Nunc® CryoTubes® 1.8 ml	Thermo Fisher Scientific, Darmstadt, Germany
Nunclon™ Multidishes 6 and 12 wells	Thermo Fisher Scientific, Darmstadt, Germany
Optical clear adhesive seal	Thermo Fisher Scientific, Darmstadt, Germany
Petri dish for cell culture, 100 mm	BD Biosciences, Heidelberg, Germany
Petri dish, 100 mm	Sarstedt, Nümbrecht, Germany
Pipette tip (10, 100 and 1000 µl,)	Sarstedt, Nümbrecht, Germany
Pipette tip 2500 µl	Eppendorf, Hamburg, Germany
Plate retainer for sequencing	Applied Biosystems, Darmstadt, Germany
Imobilon-P Membrane, PVDF, 0.45 µM	Merck, Darmstadt, Germany

Reaction tubes (1.5 ml , 2 ml)	Sarstedt, Nümbrecht, Germany
Reaction tubes (5 ml)	Eppendorf, Hamburg, Germany
Screw-cap micro tube with skirted base 2ml	Sarstedt, Nümbrecht, Germany
Serological pipettes (5ml, 10 ml, 20 ml)	Sarstedt, Nümbrecht, Germany
Syringe Discardit II 20 ml	BD Biosciences, Heidelberg, Germany
TC Plate 96 well	Sarstedt, Nümbrecht, Germany

2.3 Chemicals, reagents and drugs used

Chemicals and Reagents	Manufacturer
2-Propanol \geq 99.9%	AppliChem, Darmstadt, Germany
2x Multiplex Master Mix	Qiagen, Hilden, Germany
4-Di-1-ASP	Thermo Fisher Scientific, Darmstadt, Germany
Acetonitril	LGC Promochem, Wesel, Germany
Acrylamide 4K - Solution (40 %)	AppliChem, Darmstadt, Germany
Agar Bacteriology grade	AppliChem, Darmstadt, Germany
Agarose ultrapure	Invitrogen, Darmstadt, Germany
Ammonium persulfate \geq 98%	Sigma-Aldrich, Taufkirchen, Germany
Ampicillin Sodium Salt	AppliChem, Darmstadt, Germany
Aquasafe 500 Plus liquid scintillator	Zinsser Analytics, Frankfurt am Main, Germany
Bicinchoninic Acid	Sigma-Aldrich, Taufkirchen, Germany
Big Dye [®] Sequencing Kit	Applied Biosystem, Darmstadt, Germany
Boric acid	Merck, Darmstadt, Germany
Bovine serum albumin	Sigma-Aldrich, Taufkirchen, Germany
Bromophenol blue sodium salt	Carl Roth, Karlsruhe, Germany
Chloroform	J.T. Baker, Phillipsburg, USA
Copper sulfate pentahydrate	Sigma-Aldrich, Taufkirchen, Germany
DAPI	Thermo Fisher Scientific, Darmstadt, Germany
Dimethylsulfoxid	AppliChem, Darmstadt, Germany
DMEM cell culture medium	Gibco, Darmstadt, Germany
DNA Ladder 100 bp	Thermo Fisher Scientific, Darmstadt, Germany
DNA Ladder 1kb	Thermo Fisher Scientific, Darmstadt, Germany
DNeasy blood and tissue kit	Qiagen, Hilden, Germany
dNTP Set (dATP, dCTP, dGTP and dTTP, 100 mM each)	Thermo Fisher Scientific, Darmstadt, Germany

DTT	Invitrogen, Darmstadt, Germany
EDTA Lösung, pH 8.0 (0.5 M)	AppliChem, Darmstadt, Germany
Ethanol	Merck, Darmstadt, Germany
Ethanol, denatured 99%	Central Pharmacy, Clinic Hospital Göttingen
Ethidium bromide	Merck, Darmstadt, Germany
Expand long template PCR system	Roche Diagnostics, Mannheim, Germany
Fetal Bovine Serum	Thermo Scientific, Darmstadt, Germany
Fluoromount-G™	Southern Biotech, Birmingham, USA
Formic acid	Merck, Darmstadt, Germany
FuGENE® 6 Transfection Reagent	Promega, Mannheim, Germany
GeneScan™ 120 LIZ™ dye Size Standard	Thermo Fisher Scientific, Darmstadt, Germany
Glycerol 85%	Central Pharmacy, Clinic Hospital Göttingen
Glycine	AppliChem, Darmstadt, Germany
Halt™ Protease Inhibitor Cocktail	Thermo Fisher Scientific, Darmstadt, Germany
HBSS	Thermo Fisher Scientific, Darmstadt, Germany
HEPES	Sigma-Aldrich, Taufkirchen, Germany
Hexanucleotide random Primer	Roche Diagnostics, Mannheim, Germany
Hi-Di™ Formamide	Thermo Fisher Scientific, Darmstadt, Germany
Hydrochloric acid 32%	Merck, Darmstadt, Germany
Hygromycin B	Invitrogen, Darmstadt, Germany
Isoamylalcohol 98%	Merck Schuchardt, Hohenbrunn, Germany
KOD Hot Start DNA Polymerase Kit	Merck, Darmstadt, Germany
Ligate-IT Rapid Ligation Kit	Affymetrix, Santa Clara, USA
Lipofectamine® 2000 Transfection Reagent	Thermo Fisher Scientific, Darmstadt, Germany
Magnesium sulfate ≥ 99,5%	Merck, Darmstadt, Germany
Methanol	LGC Promochem, Wesel, Germany
MPP dihydrochloride hydrate ≥97%	Sigma-Aldrich, Taufkirchen, Germany
MPP ⁺ , N-[methyl- ³ H], 80 Ci/mmol	Hartmann Analytic, Braunschweig, Germany
Nonidet®P40 Substitute (Nonylphenylethylenglycol)	Fluka/ Sigma-Aldrich, Taufkirchen, Germany
PBS buffer (10-fold Dulbecco's), powder	AppliChem, Darmstadt, Germany
Penicillin – Streptomycin solution	Thermo Fisher Scientific, Darmstadt, Germany
Phenylmethanesulfonyl fluoride	Sigma-Aldrich, Taufkirchen, Germany
Plasmid midi prep Kit	Qiagen, Hilden, Germany
Poly D-lysine hydrobromide, 1000-4000 g/mol	Sigma-Aldrich, Taufkirchen, Germany
Ponceau S solution (0.2 %)	Serva Electrophoresis, Heidelberg, Germany

QIAquick Gel Extraction Kit	Qiagen, Hilden, Germany
qPCR Master Mix	Primer Design, Southampton, UK
Q-solution	Qiagen, Hilden, Germany
RNase A	AppliChem, Darmstadt, Germany
Rnase Inhibitor	Affymetrix, Santa Clara, USA
RNaseZAP™	Sigma-Aldrich, Taufkirchen, Germany
RNeasy Plus Mini Kit	Qiagen, Hilden, Germany
Roti®-Block (10x)	Carl Roth, Karlsruhe, Germany
Roti®-Histofix 4 %, phosphate-buffered formaldehyde solution	Carl Roth, Karlsruhe, Germany
SeeBlue Plus2 Prestained Protein Standard	Thermo Fisher Scientific, Darmstadt, Germany
Sephadex G50 Superfine	GE Healthcare, Solingen, Germany
Skim milk powder	Milupa, Bad Homburg, Germany
SNaPshot™ Multiplex Kit	Applied Biosystems, Darmstadt, Germany
Sodium chloride	Merck, Darmstadt, Germany
Sodium deoxycholate	Sigma-Aldrich, Taufkirchen, Germany
Sodium dihydrogen phosphate	Merck, Darmstadt, Germany
SDS	AppliChem, Darmstadt, Germany
Sodium hydrogen phosphate	Merck, Darmstadt, Germany
Sodium hydroxide	Merck, Darmstadt, Germany
SuperScript® II Reverse Transcriptase Kit	Thermo Fisher Scientific, Darmstadt, Germany
SuperSignal West Femto Substrate Trial Kit	Thermo Fisher Scientific, Darmstadt, Germany
SuperSignal West Pico Substrate Trial Kit	Thermo Fisher Scientific, Darmstadt, Germany
TEMED ≥ 99%	Sigma-Aldrich, Taufkirchen, Germany
TEA [ethyl-1-14C], 55 mCi/mol	Hartmann Analytic, Braunschweig, Germany
Tetraethylammonium chloride ≥99.0%	Sigma-Aldrich, Taufkirchen, Germany
Tris base	Carl Roth, Karlsruhe, Germany
Triton-X-100	Carl Roth, Karlsruhe, Germany
Trypan Blue solution, 0.4 %	Sigma-Aldrich, Taufkirchen, Germany
TrypLE™ Express	Thermo Fisher Scientific, Darmstadt, Germany
Tryptone	AppliChem, Darmstadt, Germany
Tween 20 (Polyoxyethylen-Sorbit-Monolaurat)	BioRad, Munich, Germany
Yeast extract	AppliChem, Darmstadt, Germany
β - Mercaptoethanol	Sigma-Aldrich, Taufkirchen, Germany

Drug	Manufacturer
Atropine	Sigma-Aldrich, Taufkirchen, Germany
Buformine hydrochloride	Wako Chemicals, Neuss, Germany
Chlorguanide-d6 hydrochloride (Proguanil-d6)	Biozol Diagnostica, Eching, Germany
Debrisoquine sulfate	Sigma-Aldrich, Taufkirchen, Germany
Fenoterol	Sigma-Aldrich, Taufkirchen, Germany
Metformin hydrochloride	Sigma-Aldrich, Taufkirchen, Germany
Metformin hydrochloride, [biguanidine- ¹⁴ C], 90 mCi/mmol	Hartmann Analytic, Braunschweig, Germany
Morphine, [N-methyl- ¹⁴ C], 55 mC/mmol	Hartmann Analytic, Braunschweig, Germany
Ondansetron hydrochloride dihydrate	Sigma-Aldrich, Taufkirchen, Germany
Proguanil hydrochloride	Sigma-Aldrich, Taufkirchen, Germany
Sumatriptan-d6	Santa Cruz Biotechnology, Heidelberg, Germany
Sumatriptan succinate	Sigma-Aldrich, Taufkirchen, Germany
Tropisetron monohydrochloride	Sigma-Aldrich, Taufkirchen, Germany
Tyramine [8- ¹⁴ C] hydrochloride, 55 mCi/mmol	Hartmann Analytic, Braunschweig, Germany
Venlafaxine hydrochloride	Sigma-Aldrich, Taufkirchen, Germany

2.4 Enzymes

Enzyme	Manufacturer
<i>DpnI</i>	New England Biolabs, Frankfurt am Main, Germany
<i>EcoRI</i>	Thermo Fisher Scientific, Darmstadt, Germany
<i>EcoRV</i>	Thermo Fisher Scientific, Darmstadt, Germany
<i>Endo H</i>	New England Biolabs, Frankfurt am Main, Germany
<i>ExoI</i>	Thermo Fisher Scientific, Darmstadt, Germany
FastAP (alkaline phosphatase)	Thermo Fisher Scientific, Darmstadt, Germany
<i>HindIII</i>	Thermo Fisher Scientific, Darmstadt, Germany
<i>PNGase F</i>	New England Biolabs, Frankfurt am Main, Germany
<i>PstI</i>	Thermo Fisher Scientific, Darmstadt, Germany
<i>SalI</i>	Thermo Fisher Scientific, Darmstadt, Germany
Shrimp Alkaline Phosphatase (SAP)	Affymetrix, Santa Clara, USA

2.5 Antibodies

Primary antibody	Manufacturer	Dilution	
		WB	IS
Monoclonal mouse anti - human GAPDH (6C5)	Zytomed Systems, Berlin, Germany	1:10 000	-
Monoclonal mouse anti - human OCT1 (2C5) (range of immunogen used: 284 – 347 amino acid)	Novus Biologicals, Abingdon, UK	1:500	1:500
Monoclonal rabbit anti - Na ⁺ /K ⁺ ATPase (EP1845Y)	Abcam, Cambridge, UK	-	1:200
Polyclonal rabbit anti - Calnexin	Abcam, Cambridge, UK	-	1:1000
Secondary antibody	Manufacturer	Dilution	
		WB	IS
Peroxidase-conjugated rabbit anti-mouse (pAb), polyclonal	Dianova, Hamburg, Germany	1: 10 000	-
Alexa Fluor [®] 546 goat anti - rabbit IgG (H+L), polyclonal	Thermo Fisher Scientific, Darmstadt, Germany	-	1:400
Alexa Fluor [®] 488 goat anti - mouse IgG (H+L), polyclonal	Thermo Fisher Scientific, Darmstadt, Germany	-	1:400

2.6 Primers

All Primers used were obtained from Eurofins Genomics, Ebersberg, Germany. The primers were delivered as lyophilisates and were solved in ddH₂O to reach a concentration of 100 µM.

Table 2.1 Primer for site-directed mutagenesis

Name		Sequence* (5' → 3')	°C**
S29L	forward	ATCTTATGCCTGCTG <u>TTGG</u> CTGCCTTTGCGCCC	58 °C
	reverse	GGGCGCAAAGGCAGCCAACAGCAGGCATAAGAT	
F159Y	forward	CCTGTTTGAATGCGGGCT <u>ACT</u> TCTTTGGCTCTCTCGG	68 °C
	reverse	CCGAGAGAGCCAAAGAAGTAGCCCGCATTCAAACAGG	
R206C	forward	ACATGTCCATGCTGCTCTT <u>TGC</u> CTGCTGCAGGGCCTGGTC	68 °C
	reverse	GACCAGGCCCTGCAGCAGGCAGAAGAGCAGCATGGACATGT	
W217Y	forward	CTGGTCAGCAAGGGCAACT <u>AT</u> ATGGCTGGCTACACCCTAA	60 °C
	reverse	TTAGGGTGTAGCCAGCCATATAGTTGCCCTTGCTGACCAG	
T245M	forward	TACCAGATGGCCTT <u>CAT</u> GGTGGGGCTGGTGGCG	60 °C
	reverse	CGCCACCAGCCCCACCATGAAGGCCATCTGGTA	
E284K	forward	CTACTGGTGTGTGCCG <u>AAG</u> TCCCCTCGGTGGCT	60 °C
	reverse	AGCCACCGAGGGGACT <u>TCCG</u> CACACACCAGTAG	
R342H	forward	CCTGTCCGCACGCCG <u>CAC</u> CTGAGGAAGCGCACCT	58 °C
	reverse	AGGTGCGCTTCCTCAGGTGCGGCGTGCGGAACAGG	
L364A	forward	TGTGCTCTATCAGGGG <u>GCC</u> ATCCTGCACATGGGC	54 °C
	reverse	GCCCATGTGCAGGATG <u>GCCCC</u> CTGATAGAGCACA	
H367A	forward	ATCAGGGGCTCATCCTG <u>GCC</u> ATGGGCGCCACCAGCG	56 °C
	reverse	CGCTGGTGGCGCCCATG <u>GCC</u> AGGATGAGCCCCTGAT	
M408V	forward	CATCTACCCCATGGCC <u>GTG</u> TCAAATTTGTTGGC	58 °C
	reverse	GCCAACAAATTTGACACG <u>GCC</u> ATGGGGTAGATG	
G414A	forward	TCAAATTTGTTGGCG <u>GCG</u> CAGCCTGCCTCGTC	68 °C
	reverse	GACGAGGCAGGCTGCCG <u>CCG</u> CCAACAAATTTGA	
M420A	forward	CAGCCTGCCTCGTC <u>GCG</u> ATTTTATCTCACCTG	68 °C
	reverse	CAGGTGAGATAAAAATC <u>GCG</u> ACGAGGCAGGCTG	
M420I	forward	CAGCCTGCCTCGTC <u>ATC</u> ATTTTATCTCACCTG	58 °C
	reverse	CAGGTGAGATAAAAATGATGACGAGGCAGGCTG	

M420del	forward	GGGCAGCCTGCCTCGTCATTTTTATCTCACCTGA	58 °C
	reverse	TCAGGTGAGATAAAAAATGACGAGGCAGGCTGCCC	
A426ins	forward	GTCATTTTTATCTCACCT <u>GCC</u> GACCTGCACTGGTTAAAC	56 °C
	reverse	GTTTAACCAGTGCAGGT CGGC AGGTGAGATAAAAAATGAC	
L427del	forward	ATTTTTATCTCACCTGACCACTGGTTAAACATCATA	54 °C
	reverse	TATGATGTTTAACCAGTGGTCAGGTGAGATAAAAAAT	
H428del	forward	TTTATCTCACCTGACCTGTGGTTAAACATCATAATC	54 °C
	reverse	GATTATGATGTTTAACCAACAGGTCAGGTGAGATAAAA	
I449T	forward	ATTGCAATACAAATG <u>ACCT</u> GCCTGGTGAATGCT	60 °C
	reverse	AGCATTCACCAGGCAGGTCATTTGTATTGCAAT	
D474E	forward	GTGTGTTCCCTCCCTGTGT <u>GAA</u> ATAGGTGGGATAATCACC	70 °C
	reverse	GGTGATTATCCACCTATTT CACAC AGGGAGGAACACAC	

* Affected codons are underlined and mutated bases are highlighted in bold

** Annealing temperature used for side-directed mutagenesis PCR (chapter 3.1.5)

Table 2.2 SNaPshot™ primers

Name	Sequence* (5' → 3')	Length [bp]	100 µl Master Mix
Mix A			87 µl ddH ₂ O
S14F	gaTCTGGAGCAGGTTGGGGAGT	22	1 µl
S189L	gagatcAGAAGGCCATGAGCACGCC	26	1 µl
T245M	gatcgatcgatcgTAAGCGCCACCAGCCCCACC	33	2 µl
P117L	gatcgatcgatcgatcgCACCAACAGGAGCCACCTGC	37	3 µl
I449T	gatcgatcgatcgatcgatcGCTCAGCATTACCAGGCAG	40	6 µl
M420del	gatcgatcgatcgatcgatcgatcgatcGCGGGGGCAGCCTGCCTCGTCAT	50	2 µl
Mix B			87 µl ddH ₂ O
E284K	gatcgatcgaTAACAGCCACCRAGGGGACT	30	2 µl
G414A	gatcgatATGGCCRTGTCAAATTTGTTGGCRG	32	6 µl
R206C	gatcgatcgatcgatcgatcGACCAGGCCCTGCAGCAGGC	40	1 µl
M420del	gatcgatcgatcgatcgatcgatcgatcGCGGGGGCAGCCTGCCTCGTCAT	50	2 µl

* Small letters indicate the sequence-unspecific part of the SNaPshot™ primer. Degenerate bases used at positions known to be polymorphic are highlighted in bold.

Table 2.3 Primers for validation PCRs

Reaction	Name	Sequence (5' → 3')	Amplicon [bp]
PCR 1	P _{SV40}	AGCTGTGGAATGTGTGTCAGTTAGG	519
	Hyg _{r2}	ACGCCCTCCTACATCGAAGCTGAAA	
PCR 2	P _{CMV}	CCATGGTGATGCGGTTTTGGCAGTA	3137
	LacZ	CCTTCCTGTAGCCAGCTTTCATCAA	
PCR 3	PFRT _f	AATCGGGGGCTCCCTTTAGGGTTCC	214
	PHyr _r	CTTCGCCCTCCGAGAGCTGCATCAG	

2.7 Gene expression assays

Gene of interest	Assay ID	Assay information: Exon boundary	Fluorescent dye	Manufacturer
SLC22A1	Hs00427552_m1	6-7	FAM™	Applied Biosystems
SLC22A1_new	Hs00427550_m1	4-5	FAM™	Applied Biosystems
Internal control	Accession Number	Ordering number	Fluorescent dye	Manufacturer
Hu TBP	M55654.1	4326322E	VIC	Applied Biosystems

2.8 Bacterial strain

Bacterial strain	Origin	Feature	Manufacturer
TOP10 (One Shot® TOP10 <i>E. coli</i>)	<i>Escherichia coli</i>	Electro-competent	Thermo Fisher Scientific

2.9 Plasmids

Table 2.4 Purchased plasmids

Plasmids	Obtained from
pOG44	Thermo Fisher Scientific
pcDNA5/FRT	Thermo Fisher Scientific

Table 2.5 pcDNA3.1 plasmids

pcDNA3.1 plasmids	Obtained from
pcDNA3.1::hOCT1	Hermann Koepsell, Institute of Anatomy and Cell Biology, University Würzburg
pcDNA3.1::hOCT1-S14F-R342H-M408V	pcDNA3.1::hOCT1-R342H-M408V
pcDNA3.1::hOCT1-S29L	pcDNA3.1::hOCT1 ¹
pcDNA3.1::hOCT1-F159Y-M408V	pcDNA3.1::hOCT1-M408V
pcDNA3.1::hOCT1-F159Y-M408V-M420del	pcDNA3.1::hOCT1-M408V-M420del
pcDNA3.1::hOCT1-R206C	pcDNA3.1::hOCT1 ¹
pcDNA3.1::hOCT1-W217Y-M408V	pcDNA3.1::hOCT1-M408V
pcDNA3.1::hOCT1-W217Y-M408V-M420del	pcDNA3.1::hOCT1-M408V-M420del
pcDNA3.1::hOCT1-T245M	pcDNA3.1::hOCT1 ¹
pcDNA3.1::hOCT1-L364A-M408V	pcDNA3.1::hOCT1-M408V
pcDNA3.1::hOCT1-L364A-M408V-M420del	pcDNA3.1::hOCT1-M408V-M420del
pcDNA3.1::hOCT1-H367A-M408V	pcDNA3.1::hOCT1-M408V
pcDNA3.1::hOCT1-H367A-M408V-M420del	pcDNA3.1::hOCT1-M408V-M420del
pcDNA3.1::hOCT1-E284K	pcDNA3.1::hOCT1 ¹
pcDNA3.1::hOCT1- M408V	pcDNA3.1::hOCT1 ¹
pcDNA3.1::hOCT1-M408V-M420del	pcDNA3.1::hOCT1-M420del ²
pcDNA3.1::hOCT1- G414A	pcDNA3.1::hOCT1 ¹
pcDNA3.1::hOCT1- G414A-M408V-M420del	pcDNA3.1::hOCT1-M408V-M420del
pcDNA3.1::hOCT1-M420A-M408V	pcDNA3.1::hOCT1-M408V
pcDNA3.1::hOCT1-M420C-M408V	pcDNA3.1::hOCT1-M408V
pcDNA3.1::hOCT1-A426ins-M408V-M420del	pcDNA3.1::hOCT1-M408V-M420del
pcDNA3.1::hOCT1-L427del-M408V	pcDNA3.1::hOCT1-M408V
pcDNA3.1::hOCT1-H428del-M408V	pcDNA3.1::hOCT1-M408V
pcDNA3.1::hOCT1-I449T	pcDNA3.1::hOCT1 ¹
pcDNA3.1::hOCT1-D474E-M408V	pcDNA3.1::hOCT1-M408V
pcDNA3.1::hOCT1-D474E-M408V-M420del	pcDNA3.1::hOCT1-M408V-M420del

¹ provided by Hermann Koepsell, University of Würzburg² generated by Ali Reza Saadatmand as previously described (Saadatmand et al., 2012)

Table 2.6 pcDNA5 plasmids

pcDNA5 plasmids	Obtained from
pcDNA5::hOCT1-S14F	Ali Reza Saadatmand ¹
pcDNA5::hOCT1-S14F-R342H-M408V	Generated in this work
pcDNA5::hOCT1-S29L	
pcDNA5::hOCT1-P117L	Ali Reza Saadatmand ¹
pcDNA5::hOCT1-S189L	
pcDNA5::hOCT1-R206C-M408V-M420del	
pcDNA5::hOCT1-T245M	
pcDNA5::hOCT1-E284K	
pcDNA5::hOCT1-M408V	Generated in this work
pcDNA5::hOCT1-M408V-M420del	
pcDNA5::hOCT1-G414A	
pcDNA5::hOCT1-G414A-M408V-M420del	
pcDNA5::hOCT1-M420del	Ali Reza Saadatmand ²
pcDNA5::hOCT1-I449T	
pcDNA5::hOCT1-F159Y	
pcDNA5::hOCT1-F159Y-M408V-M420del	
pcDNA5::hOCT1-W217Y	
pcDNA5::hOCT1-W217Y-M408V-M420del	
pcDNA5::hOCT1-L364A	Generated in this work
pcDNA5::hOCT1-L364A-M408V-M420del	
pcDNA5::hOCT1-H367A	
pcDNA5::hOCT1-H367A-M408V-M420del	
pcDNA5::hOCT1-M420A	
pcDNA5::hOCT1-M420C	
pcDNA5::hOCT1-M420I	Marleen Meyer ³
pcDNA5::hOCT1-M420T	

pcDNA5::hOCT1-A426ins-M408V-M420del

pcDNA5::hOCT1-L427del

pcDNA5::hOCT1-H428del

Generated in this work

pcDNA5::hOCT1-D474E

pcDNA5::hOCT1-D474E-M408V-M420del

¹ generated by Ali Reza Saadatmand, Institute of Clinical Pharmacology, University Medical Center Göttingen

² generated by Ali Reza Saadatmand, Institute of Clinical Pharmacology, University Medical Center, as previously described (Saadatmand et al., 2012)

³ in close collaboration with Marleen Meyer, Institute of Clinical Pharmacology, University Medical Center, Göttingen

2.10 Cell lines

Cell line	Obtained from
Flp-In™ T-REx™ 293 ¹ (further referred to as HEK293)	Thermo Fisher Scientific
HEK293 - pcDNA5	Ali Reza Saadatmand ²
HEK293 - hOCT1	
HEK293 - hOCT1-S14F	
HEK293 - hOCT1-S29L	Generated in this work
HEK293 - hOCT1-R61C	Ali Reza Saadatmand ^{2*}
HEK293 - hOCT1-C88R-M420del	
HEK293 - hOCT1-P117L	Generated in this work
HEK293 - hOCT1-F159Y-M408V	
HEK293 - hOCT1-F159Y-M408V-M420del	
HEK293 - hOCT1-F160L	Sherin Pojar ³
HEK293 - hOCT1-S189L	Generated in this work
HEK293 - hOCT1-R206C-M408V-M420del	
HEK293 - hOCT1-W217Y-M408V	
HEK293 - hOCT1-W217Y-M408V-M420del	
HEK293 - hOCT1-T245M	

HEK293 - hOCT1-E284K	Generated in this work
HEK293 - hOCT1-P341L-M408V	Sherin Pojar ³
HEK293 - hOCT1-L364A-M408V-M420del	Generated in this work
HEK293 - hOCT1-H367A-M408V-M420del	
HEK293 - hOCT1-G401S	Ali Reeza Saadatmand ²
HEK293 - hOCT1-M420del	
HEK293 - hOCT1-M408V	
HEK293 - hOCT1-M408V-M420del	
HEK293 - hOCT1-G414A	
HEK293 - hOCT1-G414A-M408V-M420del	
HEK293 - hOCT1- M420A-M408V	Generated in this work
HEK293 - hOCT1- M420I-M408V	
HEK293 - hOCT1-A426ins-M408V-M420del	
HEK293 - hOCT1- L427del-M408V	
HEK293 - hOCT1- H428del-M408V	
HEK293 - hOCT1-I449T	
HEK293 - hOCT1-R488M	Sherin Pojar ³
HEK293 - hOCT1-R488M-M408V	
HEK293 - hOCT1-G465R-M420del	Ali Reeza Saadatmand ²
HEK293 - hOCT1-D474E-M408V	Generated in this work
HEK293 - hOCT1-D474E-M408V-M420del	
HEK293 - mOct1	
HEK293 - mOct1-F160Y	
HEK293 - mOct1-W218Y	Helen Massy ⁴
HEK293 - mOct1-D475E	
HEK293 – rOct1	

¹ human embryonic kidney cells 293 containing a Flp Recombination Target site (FRT site) for stable transfection, only cell line used in this study

² Ali Reeza Saadatmand; Institute of Clinical Pharmacology, University Medical Center Göttingen, ^{2*} cell lines generated as previously described (Saadatmand et al., 2012)

³ Sherin Pojar, Institute of Clinical Pharmacology, University Medical Center Göttingen (Pojar, 2015)

⁴ in close collaboration with Helen Massy, Institute of Clinical Pharmacology, University Medical Center Göttingen

2.11 Software and databases

Software	Company
3130xl Data Collection Software v3.0	Applied Biosystems, Darmstadt, Germany
Adobe Photoshop CS2 v9.0	Adobe Systems GmbH, Munich, Germany
Clone Manager 6, v6.0	Sci Ed Central
CorelDraw X3, v13	Corel Corporation, Munich, Germany
EndNote X7	Thomson Reuters, New York, USA
Eppendorf BioPhotometer Online v1.01	Eppendorf, Hamburg, Germany
GeneMapper Software v3.7	Applied Biosystems, Darmstadt, Germany
Graph Pad Prism, v5.01	GraphPad Software, San Diego California, USA
ImageJ v1.46r	National Institute of Health, Bethesda, USA
Microsoft Office 2007	Microsoft Corporation, Redmond, USA
Quantity One v4.2.3 and v4.6.7	BioRad, Munich, Germany
Sequencing. Analysis Software v5.2	Applied Biosystems, Darmstadt, Germany
SigmaPlot, v12.5	Systat Software, San Jose, California,US
Staden Package	SourceForge.ne
Swiss Pdb Viewer v4.1	Swiss Institute of Bioinformatics, Switzerland
XFluor4 v4.40	Tecan Group AG, Männedorf, Switzerland
ZEN 2012 (black edition) v8.0	Carl Zeiss Microscopy GmbH, Oberkochen, Germany

Database	URL
National Center for Biotechnology Information	http://www.ncbi.nlm.nih.gov/
NetPhos 2.0	http://www.cbs.dtu.dk/services/NetPhos/
Pubchem	https://pubchem.ncbi.nlm.nih.gov/
Pubmed	http://www.ncbi.nlm.nih.gov/pubmed

3 Methods

3.1 Recombinant DNA techniques

3.1.1 Agarose gel electrophoresis

1 x TBE buffer (pH 8.3)

Substance	Concentration [mM]
Tris	100
Boric acid	100
EDTA	3

5 x Loading buffer

Substance	Concentration
Glycerol	30 % (v/v)
EDTA	50 mM
Bromophenol blue	0,25 %(v/v)

Using gel electrophoresis, DNA samples were separated according to their size using an agarose gel. The DNA with its negatively charged backbone moves in an electric field towards the anode. According to the expected DNA fragment size a concentration of 0.8 % to 1.5 % agarose in TBE buffer was used. The agarose gel was made by adding the appropriate amount of agarose to 70 ml of 1 x TBE buffer: 560 mg for a 0.8 %, 700 mg for 1% or 1005 mg for a 1.5 % gel. The agarose was dissolved in 1 x TBE buffer by heating up the solution in a microwave until boiling. After the solution cooled down at room temperature for 10 min, 5 μ l of ethidium bromide was added. The solution was cooled down for an additional 10 min and then poured in a gel tray with gel combs. As soon as the agarose gel became solid the gel combs were removed and the tray was placed in an electrophoresis gel chamber filled with 1 x TBE buffer supplemented with 0.5 % ethidium bromide (v/v). DNA samples were mixed with 5 x loading buffer and applied on the gel. The electrophoresis was carried out at 120 V until the dye front reached the bottom of the gel. The ethidium bromide-stained DNA was visualized under UV light using the Fluor-STM Multi Imager with the Quantity One v4.2.3 software.

3.1.2 Extraction of DNA fragments from agarose gel

For extraction of DNA from an agarose gel the QIAquick Gel Extraction Kit (Qiagen) was used according to the manufacturer's instructions. Briefly, the agarose gel slice containing the desired DNA fragment was cut under UV light using the Transilluminator TI 2 and was placed in a 2 ml reaction tube. The DNA was extracted from the agarose gel using the QIAcube robot (Qiagen) and eluted with 50 µl elution buffer.

3.1.3 Capillary sequencing analysis

The order of nucleotides in a DNA sequence can be analyzed by capillary sequencing. The principle of capillary sequencing is based on the dideoxy sequencing method developed by Sanger and Coulson (Sanger et al., 1977). During DNA replication the DNA polymerase catalyzes the formation of a phosphodiester bond between the 3' - hydroxyl group of a nucleotide with the 5' - phosphate group of a newly added nucleotide. By applying dideoxy sequencing, the reaction contains both dNTPs and dideoxynucleotides (ddNTPs), which can be incorporated by the DNA polymerase but due to the missing 3' – hydroxyl group in the ddNTPs no further nucleotide can be added. This leads to termination of DNA synthesis. Because the ddNTPs are incorporated randomly, different DNA fragment sizes are generated, which can be separated by capillary electrophoresis according to their size. In this work the Big Dye[®] Sequencing Kit (Applied Biosystems) was used, which contains different florescent labeled ddNTPs that were used to detect different DNA fragments.

In this work capillary sequencing was applied to verify the correctness of *OCT1* variants either from overexpressing plasmids or from total genomic DNA. The primers used are summarized in Table 3.1. In case of genomic DNA, *OCT1* was amplified before sequencing by performing PCR 2 as described in chapter 3.1.6. For capillary sequencing the 3130xl Genetic Analyzer (Applied Biosystems) was used.

In order to sequence the complete coding region of *OCT1* the following primers, which were also used for site-directed mutagenesis, were used: S29L forward, C88R forward, C88R reverse, T245M forward, T245M reverse, L364A forward, L364A reverse, M408V reverse, G465R forward. For primer sequences see Table 2.1.

Table 3.1 Sequencing Primers used to detect single nucleotide exchanges leading to non-synonymous amino acid exchanges in OCT1

Mutation	Sequencing primer	
	Name	Sequence (5' → 3')
S14F	C88R reverse	ACTTCATAGCGCCTG <u>CGCT</u> TGGCCAAGGAAGGCC
S29L		
P117L	T245M reverse	CGCCACCAGCCCCACCATGAAGGCCATCTGGTA
F159L		
S189L		
R206C		
W217Y		
T245M		
E284K	L364A reverse	GCCCATGTGCAGGATGGCCCCCTGATAGAGCACA
L364A		
H367A	E284K forward	CTACTGGTGTGTGCCG <u>AAGT</u> CCCCCTCGGTGGCT
M408V		
G414A	L364A forward	TGTGCTCTATCAGGGGG <u>GCC</u> ATCCTGCACATGGGC
M420del		
M420A		
M420I		
M420T		
M420C		
A426ins		
L427del		
H428del		
I449T		
D474E		

Reaction mixture for capillary sequencing

Reagent	Volume [μ l]
ddH ₂ O	2.25
DMSO	0.25
Sequencing primer (10 μ M)	0.5
Big Dye [®]	1
DNA	1
Total volume	5

Reaction conditions for capillary sequencing

Phase	Temperature	Time
Initial denaturation	94 °C	2 min
Denaturation	96 °C	15 sec
Annealing	56.5 °C	15 sec
Elongation	60 °C	4 min
Final elongation	72 °C	7 min

x 25

The sequencing reaction product was purified from unincorporated nucleotides and salts from the reaction buffer via size exclusion chromatography. For preparation of the Sephadex column, 35 mg of Sephadex G50 Superfine (the Sephadex was portioned with the help of a multiscreen column loader) was applied on a 96 well filter plate (MAHV N45). Three hundred μ l ddH₂O was added and incubated for 3 h. The water was removed by centrifugation at 700 g for 5 min and 150 μ l ddH₂O was added to the Sephadex and was incubated for further 30 min. The water was removed by centrifugation at 700 g for 5 min. The sequencing reaction product was diluted in 35 μ l ddH₂O and applied on the Sephadex column. By centrifugation at 700 g for 5 min the purified sequencing reaction product was collected in a new 96 well plate. The plate was loaded onto a plate retainer and sequencing analysis was performed using the 3130xl Genetic Analyzer. The sequencing data was analyzed using Sequencing Analysis Software v5.2 followed by Staden Package on Clone Manager 6.

3.1.4 Single base primer extension (SNaPshot™)

The SNaPshot™ Multiplex Kit (Applied Biosystems) is based on the single base primer extension method. Its principle is based on the incorporation of fluorescence labeled ddNTPs, which lead to termination of DNA elongation. In contrast to capillary sequencing described in chapter 3.1.3, the reaction mixture contains only ddNTPs and no dNTPs. As a result the reaction terminates after the addition of a single ddNTP. Special SNaPshot™ primers were designed (Table 2.2), which ends one nucleotide upstream of the expected nucleotide exchange. The reaction mixture can contain several primers so that different nucleotide exchanges can be analyzed at ones (Primer Mix A or B as shown in Table 2.2). These primers differ in their length so that they can be separated by capillary sequencing according to their size.

SNaPshot™ was used in this work to validate the presence of single nucleotide polymorphisms in *OCT1*.

Prior to the SNaPshot™ reaction the OCT1 gene was amplified with PCR 2 and the PCR product was enzymatically purified as described in chapter 3.1.6. After purification, 2 μ l was added to 3 μ l of the following SNaPshot™ reaction mixture:

Reagent	Volume [μ l]
ddH ₂ O	1
2x SNaPshot™ Reaction Mix	1.5
10x SNaPshot™ Primer Mix	0.5
Total volume	3

The reaction was run under the following conditions:

Phase	Temperature	Time
Initial denaturation	96 °C	2 min
Denaturation	96 °C	10 sec
Annealing	50 °C	5 sec
Elongation	60 °C	30 sec

25 x

The SNaPshot™ reaction was purified from unincorporated nucleotides prior to capillary electrophoresis. Therefore, 1 µl of the following purification mixture was added to the SNaPshot™ reaction and incubated for one hour at 37 °C:

Purification mixture

Reagent	Volume [µl]
FastAP buffer	0.5
FastAP	0.5
<hr/>	
Total volume	1

The reaction was stopped by heat inactivation at 80 °C for 15 min.

Finally, the sample was prepared for analysis by adding 10 µl of the following loading solution:

Reagent	Volume [µl]
Hi-Di™ Formamide	10
GeneScan-120LIZ®	0.2
(Molecular size standard)	
<hr/>	
Total volume	10.2

The sample was incubated at 95 °C for 5 min to denature the DNA. Following incubation, the sample was immediately stored on ice for 10 min.

The sample was analyzed via capillary electrophoresis using the 3130xl Genetic Analyzer with 50 cm capillaries and data was analyzed using the GeneMapper Software v3.7.

3.1.5 Site-directed mutagenesis

Using site-directed mutagenesis PCR, single nucleotide exchanges were introduced into pcDNA3.1::hOCT1 and pcDNA3.1::hOCT1-M420del plasmids using site-directed mutagenesis primer (Table 2.1). The amplification of the whole plasmid was carried out using the KOD Hot Start DNA polymerase, which is a high fidelity polymerase with 3'→5' exonuclease activity. The template plasmids used were obtained from dam⁺ *E.coli* strain TOP10 (chapter 2.8). This bacteria strain shows a specific methylation pattern due to the expression of the dam methylase encoded by the dam gene. The dam methylase specifically transfers a methyl group from S-adenosylmethionine to an adenosine residue in the sequence GATC. Using the methylation sensitive endonuclease *DpnI*, which only cuts methylated adenosine residues, the template plasmid can be degraded after PCR.

In order to determine the optimal annealing temperature of each primer pair a gradient PCR was performed. Different annealing temperatures in a range of 50 °C to 70 °C degree (50 °C, 53.2 °C, 58.4 °C, 64.6 °C and 70 °C) were tested. Primers and the optimal annealing temperatures used are summarized in (Table 2.1).

Site-directed mutagenesis PCR mixture:

Reagent	Volume [μ l]
ddH ₂ O	11.2
Q-solution (Qiagen)	5
10 x KOD Buffer	2.5
dNTPs (2mM)	2.5
MgSO ₄	1
Forward primer (10 μ M)	0.65
Reverse primer (10 μ M)	0.65
Template DNA (50 ng/ μ l)	1
Hot Start KOD Polymerase	0.5
Total volume	20

Site-directed mutagenesis PCR conditions:

Phase	Temperature	Time
Initial denaturation	95 °C	3 min
Denaturation	95 °C	30 sec
Annealing	50-70 °C	30 sec
Elongation	72 °C	4 min

x 19

The PCR resulted in an amplification product of about 7193 bp. After amplification, the plasmid template was digested with *DpnI*. Therefore, 2 μ l of *DpnI* was added to the PCR product and incubated for 1 h at 37 °C. Following initial digestion, an additional 1 μ l *DpnI* was added and the reaction was incubated for another hour at 37 °C. Alternatively an overnight incubation at 37 °C with 3 μ l *DpnI* was performed.

The successful amplification was proven using agarose gel electrophoresis. Therefore, 10 μ l of the reaction was run on a 0.8 % agarose gel together using a 1 kb DNA ladder as a molecular size marker (see chapter 3.1.1).

3.1.6 Validation PCRs of stable transfected HEK293 cell lines

The successful integration of the expression plasmid pcDNA5 containing the gene of interest into the genome of T-REx™ 293 cells after stable transfection was confirmed by three integration-specific PCRs. For this propose total genomic DNA was extracted from untransfected T-REx™ 293 cells, T-REx™ 293 cells stably transfected with the empty expression vector pcDNA5 or transfected with pcDNA5 containing *OCT1* (chapter 2.9). The genomic DNA of untransfected T-REx™ 293 cells was used as a negative control. The first PCR reaction verified the integration of pcDNA5 into the genome of T-REx™ 293 cells and resulted in an amplification product of 518 bp. The second PCR detected the gene of interest within the integration site and resulted in amplification products of 1376 bp and of about 3140 bp for T-REx™ 293 cells stably transfected with the empty expression vector pcDNA5 and for T-REx™ 293 cells stably transfected with pcDNA5 containing *OCT1*, respectively. The binding sites of primer pairs of both PCR reactions are schematically shown in (Figure 3.1). The third PCR was performed in order to identify possible multiple tandem integration of the expression vector pcDNA5 containing *OCT1* into the genome of T-REx™ 293 cells. In case of multiple tandem integration the PCR3 resulted in an amplification product of 214 bp (Figure 3.1). The primer sequences of validation PCRs are listed in Table 2.3.

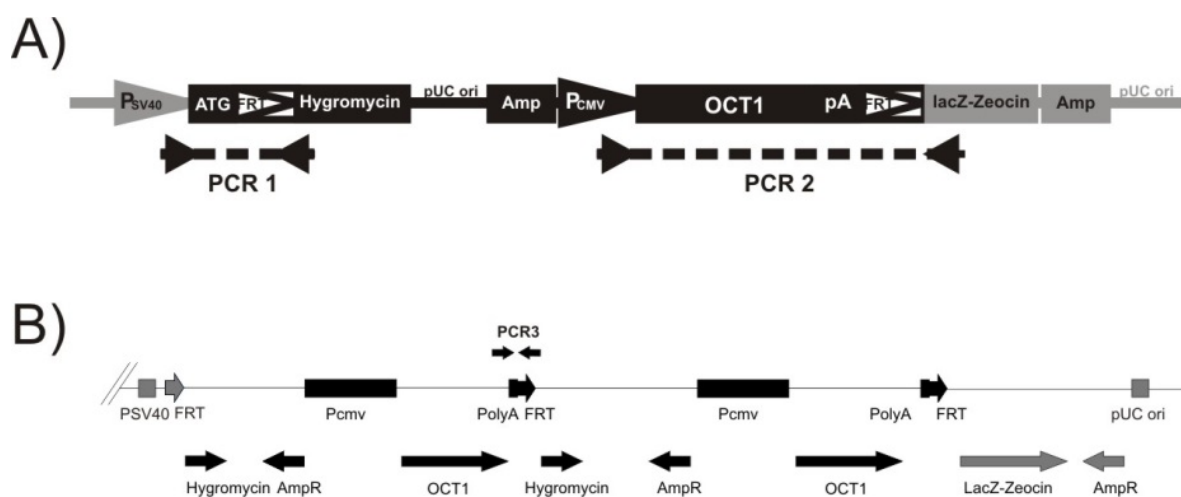


Figure 3.1 (previous page) Schematical presentation of primer binding sites of validation PCR 1, PCR 2, and PCR 3. (A) Schematic presentation of the expression plasmid pcDNA5 (black) integrated into the pFRT/lacZeo site of the genome of HEK293 cells (gray). The positions of the primers of PCR 1 and PCR 2 are indicated. PCR 1 resulted in an amplification product of 519 bp and PCR 2 resulted in an amplification product of 1376 bp (empty pcDNA5 vector) or about 3140 bp (pcDNA5 containing *OCT1* or its allelic variants). Taken from (Seitz et al., 2015). (B) Schematic presentation of PCR 3 that was performed to identify clones with multiple tandem integration of the expression plasmid pcDNA5. Shown are two expression plasmids pcDNA5::OCT1 (dark and light blue) integrated at the FRT site of T-REx™ 293 cells (black). Annealing positions of the primers (PFRT_f and PHyr_r) are indicated. Amplification resulted in a 214 bp product.

The PCR reactions were performed as follows:

PCR 1: reaction mixture

Reagent	Volume [μl]
ddH ₂ O	8.8
Q-solution	4.4
10 x KOD Buffer	2.2
dNTPs (2mM)	2.2
MgSO ₄	0.9
Primer P _{SV40} (100 μM)	0.5
Primer Hyg_r2 (100 μM)	0.5
Genomic DNA	2
Hot Start KOD Polymerase	0.5
Total volume	22

PCR 1: reaction conditions

Phase	Temperature	Time
Initial denaturation	95 °C	2 min
Denaturation	95 °C	30 sec
Annealing	64 °C	30 sec
Elongation	72 °C	1 min
Final elongation	72 °C	10 min

x 34

PCR 2: reaction mixture

Reagent	Volume [μ l]
ddH ₂ O	9.8
Q-solution	5.6
10 x Expand long Buffer	2.8
dNTPs (2mM)	4.5
MgSO ₄	1
Primer P _{CMV} (100 μ M)	0.5
Primer LacZ (100 μ M)	0.5
Genomic DNA	3
Expand Long Polymerase Mix	0.3
Total volume	28

PCR 2: reaction conditions

Phase	Temperature	Time
Initial denaturation	94 °C	2 min
Denaturation	96 °C	30 sec
Annealing and Elongation	68 °C	4 min
Final elongation	68 °C	10 min

x 35

The successful amplification of both PCRs was confirmed using 10 μ l of each sample, which was analyzed on a 0.8 % agarose gel using a 1 kb DNA ladder as a molecular size marker (chapter 3.1.1).

The PCR product of the second PCR was further used in downstream applications like capillary sequencing (chapter 3.1.3) and SNaPshotTM (chapter 3.1.4). To this end, the PCR product needed to be enzymatically purified using *ExoI* and SAP. Exonuclease I (*ExoI*) degrades single-stranded DNA in 3' → 5' direction removing unincorporated primers and any remaining single-stranded DNA. The shrimp alkaline phosphatase (SAP) removes remaining dNTPs from the reaction mixture of the former PCR that would interfere with downstream analyses. To 18 μ l of PCR product 3 μ l of the following mix was added to enzymatically purify the PCR product:

Reagent	Volume [μ l]
SAP	2
<i>ExoI</i>	0.3
10 x SAP buffer	0.7
Total volume	3

The reaction mixture was added to 18 μ l of the PCR product of PCR 2 and the reaction was incubated for one hour at 37 °C. The reaction was terminated by incubation at 80 °C for 15 min.

PCR 3: reaction mixture

Reagent	Volume [μ l]
2 x Multiplex Master Mix	5.5
Q-solution	2.2
10 x Primer mix (2 μ M PFRT_f and 2 μ M PHyr_r)	1.1
H ₂ O	1.2
Genomic DNA	1
Total Volume	11

The 10 x Primer Mix containing 2 μ M of PFRT_f and 2 μ M of PHyr_r (for primer sequences see Table 2.3) was made by diluting the primer stock of each primer with a concentration of 100 μ M 1:50 in ddH₂O. Therefore, 5 μ l of each primer was added to 240 μ l of ddH₂O.

PCR 3: reaction conditions

Phase	Temperature	Time
Initial denaturation	95 °C	15 min
Denaturation	94 °C	30 sec
Annealing	58 °C	1 min 30 sec
Elongation	72 °C	2 min
Final elongation	72 °C	10 min

x 30

The successful amplification of the third PCR was analyzed on a 1.5 % agarose gel together with a 100 bp DNA ladder (see chapter 3.1.1).

3.1.7 Isolation of total genomic DNA

For isolation of total genomic DNA the DNeasy blood and tissue kit (Qiagen) was used following the manufacturer's instructions. One to two million HEK293 cells were harvested in a 2 ml screw-cap micro tube and centrifuged for 4 min at 500 g. The cell pellet was dissolved in 100 μ l PBS buffer. The total genomic DNA was automatically extracted using the QIAcube robot (Qiagen) and eluted in 100 μ l elution buffer. Typically concentrations between 100 and 200 ng/ μ l were obtained.

3.1.8 Photometric quantification of nucleic acid

Photometrical determination of nucleic acid concentration was performed by applying 3 μ l sample of DNA or RNA solution on a Nanodrop cuvette (Implen) and absorption at 260 nm was measured using the Biophotometer (Eppendorf). The absorption was calculated using the BioPhotometer Online v1.01 software according to the Lambert-Beer law and the concentration of nucleic acid was then calculated according to the formula:

$c [\mu\text{g/ml}] = \text{OD}_{260} \times F \times \text{DF}$ where OD_{260} is the absorption at 260 nm, DF is the dilution factor and F is the conversion factor. The conversion factor is the concentration of nucleic acid, which results in an absorption of 1 (50 $\mu\text{g/ml}$ for double stranded DNA and 40 $\mu\text{g/ml}$ for RNA).

The purity of the nucleic acid sample can be evaluated by analyzing the ratio 260/280. Proteins have an absorption maximum at a wavelength of 280 nm. While nucleic acids have an absorption maximum at 260 nm, but also have a substantial absorption at 280 nm, the absorption ratio between 260 nm/280 nm for pure DNA is 1.8 and for RNA is 2.0. A ratio smaller than 1.8 for DNA and 2.0 for RNA indicates protein contamination. Samples with such ratios were not used in further analyses. Another ratio, which can be used to evaluate the purity of nucleic acid preparation, is the ratio 260/230. A ratio of 2.0 to 2.2 indicates pure nucleic acid preparation. A higher value indicates contamination with

substances that absorb at 230 nm like EDTA and phenol that can occur from extraction procedures.

3.1.9 Analytical restriction digestion

An analytical restriction digestion was performed in order to validate DNA preparations based on their specific restriction fragments after restriction digest using endonucleases. The reaction mixture was made as follows:

Reagent	Volume [μ l]
Buffer	1
Restriction enzyme	1
DNA	1
H ₂ O	7
Total volume	10

The buffers were enzyme-specific and supplied together with the enzyme. The reaction was incubated for one hour at 37 °C. Afterwards the DNA fragments were analyzed on an agarose gel (see chapter 3.1.1).

After ligation reaction (chapter 3.1.11), successful ligation of the insert into pcDNA5 was validated using the restriction enzymes *EcoRV* and *HindIII*, as well as *PstI*, *SalI*, and *EcoRI*. The double digest using *EcoRV* and *HindIII* was performed in order to proof insertion of the insert into the vector. *PstI*, *SalI*, and *EcoRI* were used in order to distinguish between pcDNA3.1::hOCT1 and pcDNA5::hOCT1 due to different restriction fragments (see Table 3.2).

Table 3.2 Analytical restriction digest of pcDNA3.1::hOCT and pcDNA5::hoCT1 and expected fragment sizes

Restriction enzyme	Buffer*	Fragment sizes [bp]	
		pcDNA3.1::hOCT1	pcDNA5::hOCT1
<i>EcoRV</i> and <i>HindIII</i>	10x Buffer R	1814, 5379	1814, 5017
<i>PstI</i>	10x Buffer O	68, 168, 929, 1385, 4649	68, 168, 929, 964, 4702
<i>SalI</i>	10x Buffer R	34, 2188, 4977	2188, 4643
<i>EcoRI</i>	10x Buffer EcoRI	7193	879, 5952

* purchased together with the respective enzyme from Thermo Scientific™

3.1.10 Preparative restriction digest

To prepare plasmids or DNA fragments for cloning procedures a preparative restriction digest was performed. For this work a double restriction digest with the endonucleases *EcoRV* and *HindIII* was performed as follows:

Reagent	Volume [µl]
Buffer	5
<i>EcoRV</i>	3
<i>HindIII</i>	3
DNA	39
Total volume	50

The restriction digest was incubated for 2 h at 37 °C. Afterwards additional 2 µl of each enzyme was added and the reaction was incubated for another hour. The complete reaction was applied on a 1 % agarose gel (see chapter 3.1.1). The agarose gel with the desired DNA fragment was extracted from the agarose gel using the QIAquick Gel Extraction Kit (see chapter 3.1.2).

3.1.11 Ligation

During a ligation reaction DNA fragments with complementary ends are covalently bound (ligated). The reaction is catalyzed by enzymes called ligases (e.g. T4 ligase), which catalyze the formation of a phosphodiester bond between the 3' hydroxyl end of one and the 5' phosphate end of another DNA fragment. This method is used to ligate a DNA fragment (insert) into a linearized vector. Because the reaction needs complementary DNA ends of the insert and the vector used, both are digested with restriction enzymes producing blunt or sticky ends. Therefore both, the DNA fragment (insert) and the vector were prepared by preparative restriction digest (chapter 3.1.10)

Prior to ligation, the DNA was concentrated using vacuum centrifugation. The reaction tube containing the DNA eluate was placed opened in the SpeedVac[®] Plus SC110A vacuum centrifuge pre-warmed (setting: high) for 10 min. The samples were centrifuged for about 10 min under vacuum until approximately 14 μ l were left. Afterwards the samples were immediately placed on ice. The condensed water made the DNA pellet visible. With 2 μ l of ddH₂O the DNA was washed from the wall of the reaction tube and added to the remaining solution. If necessary the volume was adjusted with ddH₂O to 14 μ l. For the ligation reaction the Ligate-IT Rapid Ligation Kit (Affymetrix) was used. The following reaction mix was prepared:

Reagent	Volume [μ l]
DNA fragment (insert)	14
Linearized vector	1
5x Ligase Buffer	4
T4 Ligase	1
Total volume	20

As a negative control for ligation reaction 14 μ l ddH₂O was used instead of the DNA fragment. The negative control was used to analyze the amount of self-ligated vector molecules. The ligation reaction was incubated for 10 min at room temperature and the

samples were immediately stored on ice. After dialysis (chapter 3.1.12), samples could be used for transformation into *E.coli* (chapter 3.3.5).

3.1.12 Dialysis

The technique described here is called “drop dialysis”. Samples were applied on top of a dialysis membrane filter (0.025 µM, Merck) that floated in a vessel filled with ddH₂O. The samples were dialyzed for 30 min at room temperature. The diluted DNA was carefully removed from the membrane and transferred to a reaction tube.

3.2 Quantification of mRNA expression

While working with RNA it was very important to avoid RNase contamination that would lead to RNA degradation. Hence, the working place and all pipettes used were cleaned with RNaseZAP™, a RNase decontamination solution. All working steps were carried out under the hood that was provided only for work that dealt with RNA. Furthermore gloves should be worn at any time and while working with RNA samples, RNase free water and RNase free materials should be used.

3.2.1 Isolation of total RNA

Total RNA was isolated using the RNeasy Plus Mini Kit (Qiagen) according to the manufacturer’s instructions. A cell suspension of 1 to 2 x10⁶ HEK293 cells was harvested in a 2 ml reaction tube and centrifuged at 500 g for 4 min. The supernatant was discarded and 350 µl of the lysis buffer RLT buffer supplemented with 1 % β-mercaptoethanol (v/v) (further referred to as RLT buffer plus) was added to the cell pellet and resuspended by vortexing. The RLT buffer stabilized and protected RNA from degradation. The pellet dissolved in RLT buffer plus was immediately used for RNA isolation or stored at -20 °C. During extraction, genomic DNA was removed with the help of a genomic DNA eliminator spin column provided by the kit. The isolation was automatically performed using the QIAcube robot (Qiagen) and RNA was eluted in 50 µl of RNase free ddH₂O.

3.2.2 Reverse transcription reaction

A reverse transcription reaction is used for the synthesis of complementary DNA (cDNA) from a RNA template. The reaction is catalyzed by the enzyme reverse transcriptase, a RNA dependent DNA polymerase. This method is used for mRNA expression analysis in downstream applications like real-time PCR (chapter 3.2.3). For cDNA synthesis the SuperScript® II Reverse Transcriptase Kit (Thermo Fisher Scientific) and the RNase Inhibitor (Affymetrix) was used. One µg of RNA was diluted in a final volume of 17.75 µl of RNase free ddH₂O and 1 µl of random hexamer nucleotide primers was added. The reaction mixture was incubated at 70 °C for 10 min. During this step RNA was denatured and hexamer nucleotide primers annealed to RNA molecules. For cDNA synthesis, 11.25 µl of the following reaction mixture was added to each sample:

Reagent	Volume [µl]
5 x RT buffer	6
DTT (0.1 M)	3.5
dNTPs (10 mM)	1
RNase Inhibitor	0.5
Super Script II Reverse Transcriptase	0.25
Total volume	11.25

The reverse transcription reaction was incubated for one hour at 42 °C. The cDNA samples were diluted in 70 µl of ddH₂O. Samples were stored at -20 °C.

3.2.3 Real-time PCR (qPCR) using TaqMan® Assay

Real Time PCR is used to analyze mRNA expression. During real-time PCR it was possible to detect incremental PCR products over time using florescent labeled probes. To detect the gene of interest the TaqMan® assays as listed in chapter 2.7 were used. The expression assay Hs00427552_m1, which detects a sequence located in the exon border of exon 6 and exon 7 of *OCT1*, was used for the expression analysis of *OCT1* allelic variants

presented in chapter 4.1.1. The *OCT1* expression of mutants, which were analyzed in chapter 4.4, was analyzed using the expression assay Hs00427550_m1 (SLC22A1_new). This probe detects a sequence located in the exon border of exon 4 and exon 5. The former assay could not be used, as one of the introduced mutations in *OCT1* (leading to the amino acid exchange H367A) interfered with assay binding. The expression of TBP was used as an internal control.

The TaqMan[®] gene expression assay probes consisted of a fluorescent dye at their 5' terminal end and a quencher dye at their 3' terminal end, which quenches the fluorescent signal. The probes are complementary to a specific sequence of the gene of interest and are within the amplicon. During PCR the 5' → 3' nuclease activity of the DNA polymerase cleaves the 5' end of the probe and releases the fluorescent dye which leads to a fluorescent signal as it is not further suppressed by the quencher dye. The increase of fluorescent signal is proportional to the increase of PCR product.

The real-time PCR reaction was carried out in a 384 well PCR plate. The PCR reaction was set up as follows:

Reagent	Volume [μl]
2 x qPCR Master Mix	9
20 x Gene expression assay Mix	0.9
cDNA	3
ddH ₂ O	5.1
Total volume	15

The qPCR Master Mix used contained the thermostable Taq polymerase, buffer, MgCl₂ and dNTPs and was obtained ready to use from PrimerDesign. All samples were measured in triplicates. The 384 well plate was covered with an optical clear adhesive seal and the real-time PCR was performed using the 7900 HT Fast Real Time PCR System (Thermo Fisher Scientific) with the following conditions:

Phase	Temperature	Time	
Initial denaturation and Taq-polymerase activation	95 °C	10 min	
Denaturation	95 °C	15 sec	40 x
Primer annealing and elongation	60 °C	1 min	

For this work the expression of *OCT1* was relatively quantified using TBP as an internal control according to the $\Delta\Delta C_T$ method as described by Livak and Schmittgen (Livak and Schmittgen, 2001) and was calculated with the following equation:

$$\text{Relative expression} = 2^{-[Ct(OCT1) - Ct(TBP)] - [Ct(\text{control}) - Ct(TBP)]}$$

The value for C_T gives the number of amplification cycles needed to reach a fluorescent signal greater than a certain threshold. As control cDNA samples from T-REx™ 293 cells transfected with the empty expression vector pcDNA5 were used.

3.3 Microbiological techniques used

3.3.1 Growth media and culturing conditions

In this work One Shot® TOP10 Electrocomp™ *E. coli* (Thermo Fisher) were used for transformation via electroporation. The TOP10 *E.coli* were used for high transformation efficiency and allowed stable replication of a high number of plasmids.

For cultivation of TOP10 *E. coli* LB medium was made as follows:

LB-Medium

Substance	Amount
Tryptone	10 g
Yeast extract	5 g
NaCl	5 g
ddH ₂ O	Add 1000 ml

The substances were dissolved in 1000 ml ddH₂O and immediately autoclaved. The liquid LB medium was stored at 4 °C.

For agar plates 14 g of agarose was added to 1 l of LB media before autoclaving. The solution was autoclaved and after cooling down to at least 55°C ampicillin as the selective antibiotic was added to a final concentration of 100 µg/ml.

3.3.2 Bacterial solid culturing

Streaking the bacteria on an agar plate, a glass Pasteur pipette was formed into a Drigalski spatula above a flame. Before use the heated spatula need to be cooled to room temperature in order to not risk killing the bacteria. Different volumes (50 µl, 100 µl, and 200 µl) of a bacterial solution were pipetted on the plate and equally spread by moving the Drigalski spatula back and forth while simultaneously rotating the agar plate. The bacteria were grown over night at 37 °C. Bacterial colonies grown on LB agar plates could be stored up to 4 weeks at 4 °C.

3.3.3 Bacteria liquid culture

In order to prepare a liquid culture of bacteria, ampicillin was added to 5 ml of LB medium in a 15 ml centrifugation tube to a final concentration of 100 µg/ml. A single bacteria colony, picked from an LB agar plate using a sterile pipette tip, was resuspended in the LB medium. The bacterial suspension was grown under shaking and sufficient oxygen supply over night at 37 °C.

3.3.4 Long time storage of bacterial strains

Bacterial glycerol stock solutions were made for long time storage of generated plasmids. Stock solutions were prepared by mixing 600 µl of fresh bacterial overnight culture with 600 µl of sterile 50 % glycerol and were immediately stored at -80 °C.

3.3.5 Transformation of bacteria by electroporation

Transformation of plasmids into bacteria was performed by electroporation using electro-competent One Shot[®] TOP10 *E. coli* cells (Thermo Fisher Scientific). Prior to electroporation, plasmids, bacteria, and the electroporation cuvette were kept on ice. One aliquot of TOP10 *E. coli* consisted of 40 μ l bacterial solution and was diluted 1:4 by adding 120 μ l ddH₂O. From this dilution, 40 μ l was pipetted into an electroporation cuvette and 1 μ l of plasmid was added. The plasmid sample was dialyzed prior to transformation in order to remove salts from upstream applications. Electroporation was performed using the Electroporator Gene Pulser II (BioRad) with the following parameters: voltage: 2.5 kV, capacitance: 25 μ F, resistance 200 Ω .

Immediately after the electroporation, 800 μ l of pre-warmed LB medium (37°C) was added to the suspension. The suspension was incubated for one hour at 37°C to allow bacteria to recover from electroporation and to express the plasmid encoded ampicillin resistance gene *bla*. Afterwards 50 μ l, 100 μ l, and 200 μ l of bacterial suspension were streaked on agar plates containing ampicillin. Ampicillin was used as the selective antibiotics. The plates were incubated over night at 37°C. On the next day ampicillin resistant bacterial colonies were used for preparation of an overnight liquid culture (chapter 3.3.3) in order to isolate plasmids from bacteria via chloroform extraction (see chapter 3.3.6; mini-preparation/mini-prep).

3.3.6 Isolation of plasmid DNA by alkaline lysis

Small-scale isolation of plasmid DNA from bacteria was performed using alkaline lysis followed by chloroform extraction. The following buffers were used:

Resuspension buffer

Substance	Concentration
Tris-HCl, pH 8.0	50 mM
EDTA	10 mM
RNase A	100 μ g/ml

RNase A was added after the resuspension buffer was autoclaved.

Lysis buffer

Substance	Concentration
NaOH	200 mM
SDS	1 % (w/v)

Neutralization buffer

Substance	Concentration
Potassium acetate, pH 7.5	3 M

Chloroform/ isoamyl alcohol (24:1)

Substance	Volume
Chloroform	96 ml
Isoamyl alcohol	4 ml

Plasmid DNA was extracted from 5 ml of fresh overnight bacterial culture. After overnight cultivation, 5 µl of bacterial suspension was plated on a LB agar plate (chapter 3.3.2) to save bacteria. The remaining bacterial suspension was centrifuged at 4000 rpm for 10 min at room temperature. The supernatant was discarded and the pellet was resuspended in 250 µl of resuspension buffer. The solution was transferred into a 1.5 ml reaction tube and 250 µl of lysis buffer consisting of SDS and NaOH was added. The SDS in the lysis buffer acts as a detergent disrupting membranes. The sodium hydroxide in the lysis buffer denatures both, chromosomal and plasmid DNA. However, plasmid DNA remains stable. The solution was mixed by inverting the tube up to 8 times. Afterwards 350 µl of neutralization buffer was added to neutralize the basic pH so that DNA is able to renature. Due to its size this is not possible for chromosomal DNA. The potassium acetate precipitates the SDS along with lipids, proteins, and chromosomal DNA, whereas the plasmid DNA stays in solution.

The mixture was kept on ice for about 5 min and was afterwards centrifuged at 13.000 g for 10 min at 4°C. The supernatant was carefully transferred into a new 1.5 ml reaction tube taking care not to transfer any precipitate. Five hundred µl of chloroform/ isoamyl alcohol mixture (24:1) was added. The solution was mixed by inverting the tube 10 times. The solution was centrifuged at 13 000 g for 5 min at 4 °C. This liquid-liquid extraction led to the generation of two liquid phases and an interphase. The upper aqueous phase

contained the plasmid DNA, whereas remaining proteins were in the interphase. The aqueous phase was transferred into a new 1.5 ml reaction tube. The plasmid DNA was precipitated by adding 650 μ l ice-cold 2-propanol. After mixing the solution by repeatedly inverting the tube, the solution was centrifuged at 13.000 g for 15 min at 4 °C. The supernatant was discarded. The plasmid DNA pellet was washed two times by adding 800 μ l of 70 % ethanol and inverting the tube until the pellet “floated” in the solution. The tube was centrifuged at 13.000 g for 5 min at 4°C. The ethanol was carefully removed. The plasmid DNA pellet was air-dried, and finally dissolved in 50 μ l ddH₂O. An analytical restriction digestion was performed to analyze the correctness and for semi-quantification of the obtained plasmid (chapter 3.1.9).

3.3.7 Isolation of high quality plasmid DNA by solid extraction (midi prep)

For plasmid preparation of high purity and concentration a plasmid midi-preparation (midi-prep) was performed. A 5 ml liquid pre-culture of bacteria was prepared as described in chapter 3.3.3 and was shaken for 8 hours at 37°C. Thirty μ l of bacteria pre-culture was added to 30 ml of LB medium supplemented with 100 μ g/ml ampicillin. The bacteria were cultured over night at 37 °C on a shaking platform at 200 rpm. On the next day, the midi-prep was performed using the Plasmid Plus Midi Kit (Qiagen) following the manufacturer’s instruction. After isolation, the DNA plasmid concentration was photometrically determined as described in chapter 3.1.8. The plasmid DNA of midi-prep quality was used for transient and stable transfection (see chapter 3.4.6 and 3.4.5).

3.4 Mammalian cell culturing and transfection

All work with mammalian cells was performed under sterile conditions using a biosafety cabinet. Surfaces and pipettes were cleaned with 70 % ethanol. According to S1 laboratory guidelines the complete waste was collected and sterilized prior disposal. Solid waste was autoclaved and liquid trash from cell culturing was treated with the disinfectant Helipur[®] (Braun) by collecting liquid waste after aspiration in a vessel filled with Helipur[®].

3.4.1 Cell culturing conditions

T-REx™ HEK293 cells and all stably transfected cell lines derived from them were cultured in DMEM supplemented with 10 % fetal bovine serum (FBS) and 1 % penicillin/streptomycin solution (v/v) under 5 % CO₂ and 95 % humidity at 37°C in a CO₂ incubator BBD6220 (Thermo Fisher Scientific). When cells reached 80 % to 90 % confluence they were split and sub-cultured at a concentration of 1:6 in a new flask. To do so, the old medium was removed from the cells and the cells were resuspended in 12 ml medium from which 2 ml of cell suspension was pipetted into the new flask containing 15 ml of pre-warmed (37 °C) medium. Cells with a passage 30 or lower were used in the experiments.

3.4.2 Freezing mammalian cell lines

For preservation of T-REx™ HEK293 cells and generated cell lines, cells were frozen and stored in liquid nitrogen at -170 °C. Cryo-medium consisting of FBS supplemented with 10 % DMSO was prepared and pre-cooled to 4°C on ice. DMSO acts as a cryo-protective agent preventing formation of ice crystals, which would destroy cell membranes.

Cells from a T75 cell culture flask with 80 % to 90 % confluence were resuspended in the medium contained in the flask. The cell suspension was transferred into a 50 ml centrifugation tube and centrifuged at 300 g for 3 min at room temperature. The supernatant was removed and the cell pellet was carefully resuspended in 7.2 ml ice-cold cryo-medium and aliquoted into four cryo-tubes each containing 1.8 ml of cell suspension. Cryo-tubes were placed on an ice-water vessel containing ice, water, and sodium chloride for one hour. Afterwards, cells were stored at -80 °C for a week before they were transferred to a liquid nitrogen tank for long time preservation.

3.4.3 Thawing mammalian cell lines

To thaw cells that are stored in liquid nitrogen, a cryo- tube containing the cells was slewed for 2 min in a water bath (37 °C). Because DMSO is toxic to the cells the thawed cell suspension was immediately diluted in 10 ml of pre-warmed cell culture medium. The cell suspension was centrifuged at 300 g for 3 min at room temperature. The supernatant was

discarded and the cell pellet was carefully resuspended with 6 ml of pre-warmed cell culture medium. The cell suspension was transferred into a T25 cell culture flask. After one day of culturing, the cell culture medium was changed. To do so, the old medium was aspirated and 6 ml of fresh pre-warmed cell culture medium was carefully pipetted to the cells. As soon as the cells reached up to 80 % confluence, they were transferred into a T75 cell culture flask.

3.4.4 Determination of cell count

For plating the exact number of cells for chapter 3.4.5, 3.4.6, 3.5.5, and 3.6, the cell count was determined using the Neubauer chamber. The medium from a cell culture flask was removed and 3.5 ml of trypsin (TrypLE™ Express) was added and the flask was incubated for 4 min in the CO₂ incubator. The reaction was stopped by adding 10 ml of medium and the cell suspension was transferred to a 50 ml centrifugation tube, which was centrifuged at 300 g for 3 min at room temperature. The supernatant was discarded and the cell pellet was resuspended in 12 ml medium. For cell counting, 20 µl of cell suspension was mixed with 40 µl of 0.4 % trypan blue solution and 20 µl medium in a 1.5 ml reaction tube and 10 µl of this suspension was applied on a Neubauer chamber. After counting the cells in four big squares, the cell concentration was determined as follows:

$$\text{Number of cells/ml} = \frac{\text{total number of cells counted} \times \text{dilution factor} \times \text{chamber factor}}{4}$$

The chamber factor for the Neubauer chamber used was 10⁴ (each square has an area of 0.01 cm² and a depth of 0.1 mm, which results in a volume per square of 0.1 µl). The dilution factor for the procedure described above was 4.

3.4.5 Stable transfection of T-REx™ 293 cells

Stable transfection of T-REx™ 293 cells was achieved through targeted chromosomal integration of the expression plasmid pcDNA5. For this purpose, the Flp/FRT recombination site specific system was used and FuGENE® 6 (Promega) was used as the transfection agent.

The genetically modified T-REx™ 293 cells carry a FRT site in their genome. The FRT site is also present in the expression vector pcDNA5. These artificially introduced FRT sites are the target sequences for the Flp recombinase, which is encoded by the helper plasmid pOG44. The Flp recombinase mediates the DNA recombination and therefore leads to the integration of pcDNA5 into the genome of T-REx™ 293 cells. Figure 3.2 schematically shows the principle of the integration of pcDNA5 into the genome of T-REx™ 293 cells.

The stable transfection was carried out as follows: 1×10^6 T-REx™ 293 cells were plated per well on a 6 well plate. The plate should not be pre-coated with poly D-lysine. The cells were incubated for 24 hours. On the day of transfection, 100 μ l of DMEM w/o supplements was added to a 1.5 ml reaction tube and 400 ng of plasmid DNA and 3.6 μ g of the helper plasmid pOG44 (both in midi-prep quality) was added. In another 1.5 ml reaction tube containing 100 μ l pure DMEM and 12 μ l FuGENE® 6 were added. After 5 min pre-incubation at room temperature the content of both tubes was mixed with each other by pipetting up and down five times. The mixture was incubated for 15 min at room temperature. Meanwhile the cells were washed once with 2 ml DMEM containing 10 % FBS (v/v) and 2 ml DMEM with 10 % FBS (v/v) was pipetted to the cells and they were placed back in the CO₂ incubator. After 15 min incubation was over, 200 μ l of the DNA - FuGENE® 6 - reaction mixture was pipetted dropwise to the cells and the cells were incubated overnight in the CO₂ incubator. One day after transfection, the medium was changed to DMEM medium with 10 % FBS (v/v) and 1 % penicillin/ streptomycin (v/v).

Two days after transfection, cells were transferred from the 6 well plate to a 100 mm Petri dish. Therefore the medium from the 6 well plate was removed and the cells were detached from the plate with 2 ml cell culture medium and transferred to a 100 mm Petri dish containing 18 ml cell culture medium. The cells were distributed by gently shaking the Petri dish left to right, back and forth. The cells were incubated overnight in the CO₂

incubator. On the third day after transfection, 120 µl of 50 mg/ml hygromycin B solution (final concentration 300 µg/ml) was added to the cells dropwise. Hygromycin B acted as the selective antibiotic as just successfully stable transfected T-REx™ 293 cells expressed the hygromycin B resistance gene, which was encoded by the expression plasmid pcDNA5. The DMEM medium with 10 % FBS (v/v), 1 % penicillin/ streptomycin (v/v), and 300 µg/ml hygromycin B was renewed four days after adding hygromycin B for the first time. Ten days after adding hygromycin B for the first time, single cell colonies appeared. Up to 24 colonies were selected and transferred to a 12 well plate containing 2 ml of DMEM medium with 10 % FBS (v/v), 1 % penicillin/ streptomycin (v/v), and 100 µg/ml hygromycin B per well. Cells were grown in the 12 well plate until they reached 80 % to 90 % confluence and were then transferred to a 6 well plate. Cells were grown in a 6 well plate until they reached 80 % to 90 % confluence and were then transferred to a T25 cell culture flask.

As soon as the cells needed to be passaged for the first time to a new T25 cell culture flask, samples for DNA and RNA isolation were taken as described in chapter 3.1.7 and 3.2.1. These samples were used for validation of the generated stable transfected T-REx™ 293 cells (for details see chapter 3.1.6, 3.2.2, and 3.2.3). Eight to 10 clones were used for validation.

3.4.6 Transient transfection of T-REx™ 293 cells

Transient transfection introduces plasmid DNA into T-REx™ 293 cells without integration into the genome of the cells. Hence, the genetic information is not passed to the next generation after cell division and the plasmid molecules are diluted out. In contrast to the generation of stable transfected T-REx™ 293 cells (chapter 3.4.5.), transient transfection is a time sparing method to overexpress a gene of interest in T-REx™ 293 cells and to analyze its function.

For transient transfection the Lipofectamine® 2000 (Thermo Fisher Scientific) reagent was used. The principle of this reagent is that it consists of lipids, which form liposomes and thereby include the plasmid DNA. The liposomes fuse with the plasma membrane of T-REx™ 293 cells and thereby release the plasmid DNA into the cytosol of the cells. For transient transfection plasmid DNA of midi-prep quality was used (chapter 3.3.7).

Five hundred thousand cells per well were plated on poly D-lysine pre-coated 12 well plates. For coating the plates, 500 μ l of 0.2 % poly D-lysine solution was pipetted into each well and incubated for 30 min at 37 °C in a CO₂ incubator. Afterwards the poly D-lysine was removed and the plates were dried under the biosafety cabinet. The cells were plated and grown over night.

For transient transfection, the reaction per well was performed as follows: 100 μ l of DMEM medium (without serum and antibiotics) was mixed with 5 μ l Lipofectamine[®] 2000 reagent. The mixture was incubated for 5 min at room temperature. Afterwards, 2 μ g of plasmid DNA was added and the mixture was incubated for 20 min at room temperature. Meanwhile the cells were washed with 1 ml DMEM medium containing 10 % FBS (v/v). After washing the cells, 900 μ l of DMEM medium containing 10 % FBS (v/v) was added to the cells and the cells were placed back in the CO₂ incubator until the end of incubation time. After 20 min, 100 μ l of DMEM- Lipofectamine[®] 2000-DNA mixture was added dropwise to the cells. After 6 h the medium was changed to DMEM supplemented with 10 % FBS (v/v) and 1 % penicillin/ streptomycin solution (v/v).

The cells were cultured for 48 h before to be used for transport experiments (chapter 3.4.6).

3.4.7 Generation of stable transfected cell lines

For the generation of HEK293 cells stably or transiently transfected to overexpress *OCT1* variants, point mutations were introduced into pcDNA3.1 plasmids by site-directed mutagenesis (chapter 3.1.5). After site-directed mutagenesis, PCR products were digested with *DpnI*, dialyzed (chapter 3.1.12), and transformed into *E.coli* by electroporation (chapter 3.3.5). After plasmids were isolated from bacteria by alkaline lysis (chapter 3.3.6), an analytical restriction digest was performed with *EcoRV* and *HindIII* (chapter 3.1.9) in order to verify plasmid preparation. The correctness of *OCT1* variants from overexpressing plasmids was verified with capillary sequencing (chapter 3.1.3). According to this procedure, pcDNA3.1 plasmids have been generated as listed in Table 2.5.

The mutated *OCT1* genes were re-cloned into pcDNA5 (chapter 3.1.11). Therefore a preparative restriction digestion (chapter 3.1.10) was performed using *EcoRV* and *HindIII* and cutting both, the mutated pcDNA3.1 plasmid carrying *OCT1* and the pcDNA5

plasmid. The DNA fragments were separated on a gel by electrophoresis (chapter 3.1.1) and the respective DNA fragments were extracted from the gel (chapter 3.1.2). The mutated OCT1 genes were re-cloned in pcDNA5 (chapter 3.1.11). After ligation the plasmids were dialyzed (chapter 3.1.12). Finally, the generated pcDNA5 plasmids were transformed into *E.coli* by electroporation (chapter 3.3.5). Plasmids were isolated from bacteria by alkaline lysis followed by chloroform extraction (chapter 3.3.6). In order to verify successful re-cloning analytical restriction digests were performed with *Pst*I, *Eco*RI, *Sal*I, or *Eco*RV in combination *Hind*III (chapter 3.1.9). The correctness of *OCT1* variants from overexpressing plasmids was verified with capillary sequencing (chapter 3.1.3). According to this procedure, pcDNA5 plasmids were generated as listed in Table 2.6 and used for transfection (chapter 3.4.5 and 3.4.6). For transfection, pcDNA5 plasmids of high quality preparation (midi prep, chapter 3.3.7) were used. According to this procedure, HEK293 cell lines were generated as listed in chapter 2.10. From each generated mutation, two clones have been saved and the validation of the respective clone, which was used for analyses, is presented in chapter 4.1.1, 4.4.2, and 4.4.3.

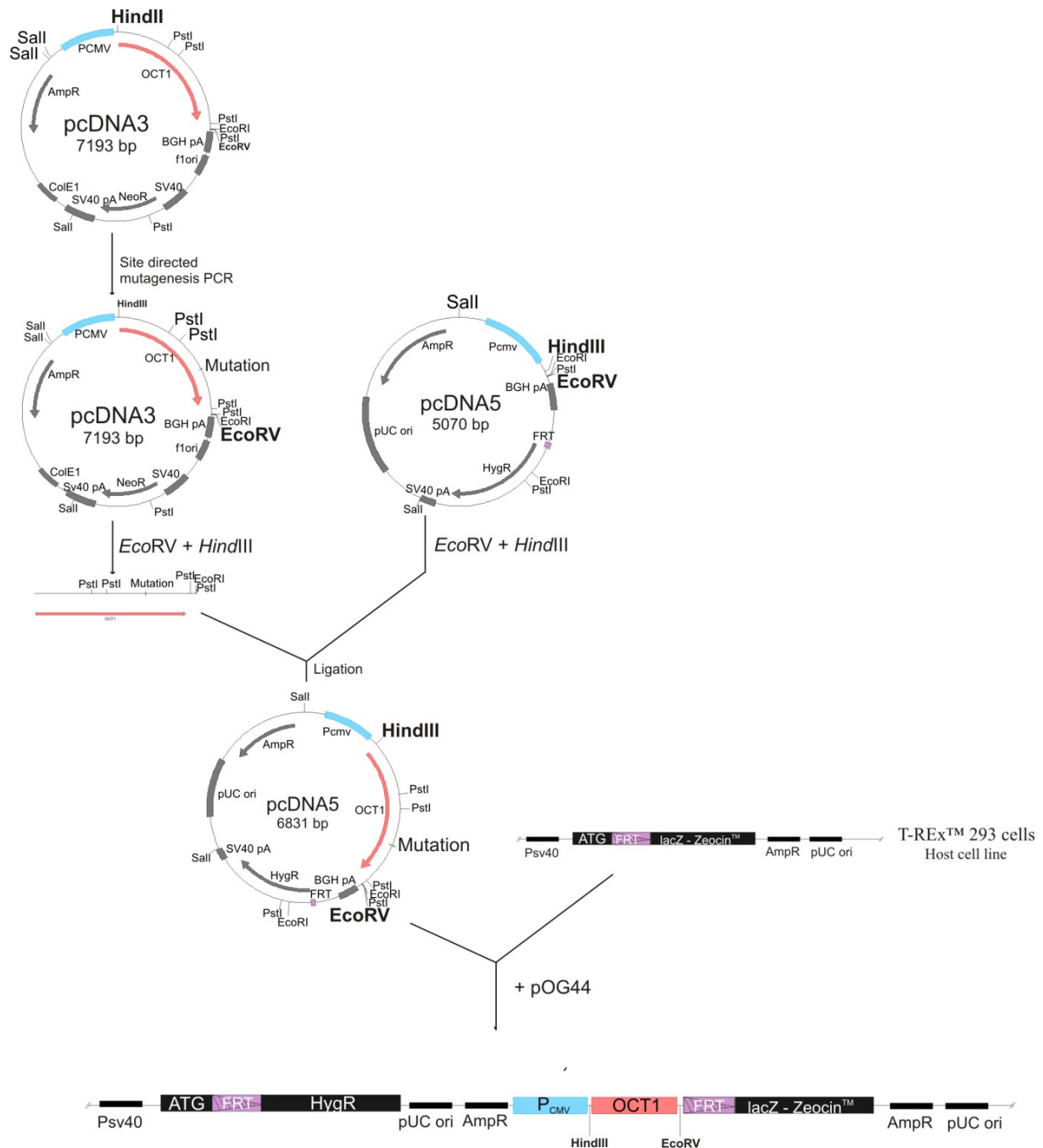


Figure 3.2 Schematic representation of the generation of stably transfected HEK293 cell lines. Using site-directed mutagenesis PCR, single nucleotide exchanges were introduced in *OCT1* leading to non-synonymous amino acid exchanges (mutation indicated in green). After preparative restriction digest of pcDNA3.1::hOCT1 and pcDNA5 using *EcoRV* and *HindIII*, the fragment of *OCT1* was re-cloned into the expression plasmid pcDNA5. For integration of pDNA5 in the genome of HEK293 at the FRT site, the Flp recombinase was used, which is encoded by the helper plasmid pOG44. The Flp recombinase recognizes the FRT site, which is present in the expression plasmid pcDNA5 and in the genome of T-REx™ 293 cells (shown in dark blue). Via DNA recombination the expression plasmid is stably integrated at the FRT site of the host cell line.

3.5 Protein analyses

3.5.1 Determination of protein concentration

The bicinchoninic acid (BCA) assay was performed to determine the protein concentration of cell lysates. This colorimetric method was first described by Smith *et al.* (Smith et al., 1985). It is based on the reduction of Cu^{2+} ions to Cu^+ by peptide bonds. This reaction is proportional to the amount of protein in the sample. After reduction, two molecules of bicinchoninic acid chelate a Cu^+ ion and form a purple-colored product whose absorption can be measured at a wavelength of 570 nm.

To obtain whole cell protein lysates, cells were lysed in RIPA buffer. Cell debris were removed by centrifugation at 16500 g for 10 min and the supernatant was transferred to a new 1.5 ml reaction tube. If necessary, protein samples were diluted in ddH₂O. The linear range of the assay was between 1 μg and 15 μg protein.

RIPA buffer

Substance	Concentration
Tris HCl pH 7.4	50 mM
NaCl	150 mM
EDTA	1 mM
NP-40	1 % (v/v)
Sodium deoxycholate	0.25 % (w/v)
SDS	0.1 % (w/v)

BCA reaction solution

Substance	Amount
BCA	50 parts
4 % copper sulfate pentahydrate	1 part

The BCA assay was performed in a 96 well plate. Five μl of protein sample was pipetted in triplicates into separate wells. To determine protein concentration a standard curve with increasing amounts of BSA (0 μg , 1 μg , 3 μg , 5 μg , 10 μg , and 15 μg) was used. A standard BCA solution with a concentration of 1 mg/ml BSA dissolved in water was used. Two hundred μl of a BCA reaction solution was added to each. The BCA reaction solution was prepared by adding 1 part of a 4% copper sulfate pentahydrate solution (v/v) to 50 parts of BCA.

The reaction was incubated for 30 min at 37 °C. The absorbance at 570 nm was measured using the Tecan Ultra Microplate Reader.

3.5.2 SDS polyacrylamide gel electrophoresis (SDS-PAGE)

The separation of proteins in an electric field using a discontinuous polyacrylamide gel and SDS as a denaturing agent is called SDS-PAGE. SDS provides the denatured proteins with a constantly negative charge so that they are moving towards the anode only depending on the difference in their size but not in their charge. The discontinuous gel is made of a stacking gel, a low concentrated gel, which concentrates the loaded protein sample to a tight band, and a resolution gel a higher concentrated gel, which separates the proteins according to their size. Bigger proteins move slower in the polyacrylamide gel matrix than smaller proteins.

The stacking gel and the resolution gel were made as follows:

Stacking gel, 4 %

Substance	Volume [μl]
ddH ₂ O	1625
1.5 M Tris HCl, pH 8.8	625
10 % SDS	25
40 % Acrylamide	250
10 % APS	12.5
TEMED	2.5

Resolution gel, 12 %

Substance	Volume [μ l]
ddH ₂ O	2180
1.5 M Tris HCl, pH 8.8	1250
10 % SDS	50
40 % Acrylamide	1500
10 % APS	25
TEMED	2.5

4 x Sample buffer*

Substance	Concentration
Tris HCl, pH 6.8	240 mM
DTT	400 mM
Bromphenol blue	0.008 % (w/v)
Glycerol	28 % (v/v)
SDS	8 % (w/v)
ddH ₂ O	Add 25 ml*

*make 1 ml aliquots and store at -20 °C

Running buffer

Substance	Concentration
Tris HCl, pH 8.4	25 mM
Glycine	19.2 mM
SDS	0.1 % (w/v)
ddH ₂ O	Add 1 l

Transfer buffer

Substance	Concentration
Tris HCl, pH 8.3	25 mM
Glycine	192 mM
Methanol	10 % (v/v)
ddH ₂ O	Add 1 l

Blocking buffer

Substance	Volume
Roti [®] -Block (10x)	5 ml
ddH ₂ O	45 ml

Total cell lysates were analyzed. Approximately 2 mio cells were lysed in RIPA buffer supplemented with 1 mM phenylmethanesulfonylfluoride (PMSF) and Halt[™] Protease Inhibitor Cocktail (Thermo Fisher Scientific).

The cells were lysed by incubation on ice for 30 min with pulse-vortexing every 5 min. Cellular debris were removed by centrifugation at 13 000 g for 10 min at 4 °C and the supernatant containing the proteins was transferred to a new 1.5 ml reaction tube. The protein concentration of cell lysates was determined using BCA assay (chapter 3.5).

Protein samples were prepared for SDS-PAGE by adding 5 µl of 4 x sample buffer to 15 µl of protein sample. The proteins were denatured by incubating the samples at 95 °C for 5 min. Afterwards, protein samples were immediately stored on ice. For analysis, 10 µg of total protein was applied to the gel and 5 µl of SeeBlue[®] Plus2 Prestained Protein Standard (Thermo Fisher) was used as a molecular weight marker.

Electrophoresis was performed using the Vertical Electrophoresis Chambers mighty small II (Amersham) filled with running buffer. The gel was run at an electric current of 20 A until the dye front reached the boarder of the stacking gel. Then the electric current was increased to 35 A. The gel was run until the dye front reached the bottom of the gel. The gel was used for western blot analysis (chapter 3.5.3).

3.5.3 Western Blot

Western blot analysis was performed following SDS-PAGE in order to transfer electrophoretically separated proteins to a membrane and to identify single proteins using specific antibodies. The blot was constructed as follows:

Cathode

3 Layers of thick filter paper (Nr. 2CHR)

1 Layer of thin filter paper (Nr. 2668)

Gel

PVDF membrane

1 Layer of thin filter paper

3 Layers of thick filter paper

Anode

For western blot analysis a PVDF membrane (Imobilon-P, Merck) was used, which was soaked for 1 min in methanol in order to activate the hydrophobic membrane. The methanol was removed by washing the membrane with water. Afterwards, all filters and the PVDF membrane were equilibrated for 10 min in transfer buffer and the blot was constructed as indicated above. A semi-dry blot was performed using the Fastblot B43 (Biometra). The membrane was blotted for 1.5 h with an electric current of 50 A.

Successful protein transfer to the membrane was verified by unspecific staining of protein on the membrane with Ponceau S solution. The membrane was incubated in Ponceau S solution for 10 min on a shaking platform. Afterwards the Ponceau S solution was removed by washing the membrane with water.

To block the membrane, it was incubated in blocking buffer for 1 h at room temperature on a shaking platform. The primary antibodies (see chapter 2.5) were diluted in TBST supplemented with 5 % non-fat dry milk. The antibodies were diluted 1:400 and 1:10 000 for anti-OCT1 and anti-GAPDH, respectively. The membrane was incubated with the primary antibody overnight at 4 °C. On the next day the membrane was washed with TBST three times for 5 min at room temperature on a shaking platform. The membranes were incubated for 1 h with the secondary antibody (see chapter 2.5) diluted in TBST supplemented with 0.5 % non-fat dry milk. The secondary antibody was a horseradish peroxidase-conjugated anti-mouse antibody, which was diluted 1:10 000. Afterwards the membrane was washed with TBST three times for 5 min at room temperature on a shaking platform. A final washing step was performed with TBS for 5 min at room temperature on a shaking platform.

Horseradish peroxidase activity was detected by chemiluminescence using SuperSignal[®] West Pico Kit for detecting GAPDH or SuperSignal[®] West Femto Kit for OCT1 (both Thermo Fisher Scientific) for detecting OCT1 according to the manufacturer's instructions. The signal was visualized using the VersaDoc[™] imaging system with Quantity One software v4.6.7 (BioRad).

10 x TBS*

Substance	Concentration
Tris HCl, pH 7.6	200 mM
NaCl	1.5 M
ddH ₂ O	Add 1 l

*to get 1 x TBS dilute 1:10 in ddH₂O

1 x TBST

Substance	Concentration
Tris HCl, pH 7.6	20 mM
NaCl	150 mM
Tween 20	0.1 % (v/v)
ddH ₂ O	Add 1 l

3.5.4 Deglycosylation with *PNGase F* and *Endo H*

The glycosidases Peptid-N-Glykosidase F (*PNGaseF*) and Endo- β -N-acetylglucosaminidase H (*Endo H*, both New England Biolabs) were to identify and analyze glycosylation of proteins. *PNGaseF* cleaves between the innermost N-acetylglucosamine and asparagine residues of high mannose and complex oligosaccharides from N-linked glycoproteins. *Endo H* cleaves within the chitobiose core of high mannose and some hybrid oligosaccharides from N-linked glycoproteins (reviewed in (Maley et al., 1989)).

Protein samples prepared as described in chapter 3.5.2 were glycosylated following the manufacturer's instructions of New England Biolabs. Briefly, 22 μ g of total protein was denatured by incubation for 5 min at 95 °C in sample buffer for SDS PAGE (chapter 3.5.2). For deglycosylation with *Endo H*, 1250 units *Endo H* and sodium citrate to a final

concentration of 50 mM were added. For deglycosylation with *PNGase F*, 500 units *PNGaseF*, NP-40 and sodium citrate were added to a final concentration of 1 % and 50 mM, respectively. The reactions were incubated for 1 hour at 37 °C. The deglycosylated samples were directly applied to SDS-PAGE and were analyzed by western blotting (see chapter 3.5.2 and 3.5.3).

3.5.5 Immunostaining

10 x Blocking buffer

Substance	Concentration
FBS	5 % (v/v)
BSA	1% (w/v)
Triton X-100	0.5 % (v/v)
PBS	Add 50 ml

Immunostaining using fluorescent labeled secondary antibodies was performed followed by visualization with confocal microscopy. The method was used to analyze cellular localization of the protein of interest in detail.

For immunostaining 0.2×10^6 cells were plated on a poly D-lysine pre-coated chamber slide (Lab-Tek®II Chamber Slide, Thermo Fisher). To do so, the cells were trypsinized and counted. The cells were passed through a 40 µm strainer (BD Falcon), plated and cultured overnight in a CO₂ incubator.

The staining was performed as follows: Cells were washed once with 1 ml sterile PBS. Afterwards 1 ml of Roti®-Histofix, a 4 % formaldehyde solution, was added and incubated for 20 min at room temperature to fix the cells. The fixed cells were washed twice with PBS and permeabilized with 1 ml of 1 x blocking buffer (10 x blocking buffer diluted 1:10 with PBS) for 15 min at room temperature.

The blocking buffer was removed and the cells were incubated with the primary antibody. The primary antibodies and dilution factors used are listed in chapter 2.5. Dilution was performed with 1x blocking buffer. Calnexin was used as a marker for the endoplasmic

reticulum and Na^+/K^+ ATPase was used as marker for the plasma membrane. The cells were incubated with 200 μl of primary antibody dilution for 1 h at room temperature on a shaking platform. Afterwards, cells were washed three times with 1 ml of 1 x blocking buffer for 5 min at room temperature on a shaking platform. After that, the cells were incubated with the secondary antibodies Alexa Fluor[®] 488 goat anti-mouse, or Alexa Fluor[®] 546 goat anti-rabbit IgG, both diluted 1:500 in 1 x blocking buffer. The cells were simultaneously stained with DAPI, a fluorescent DNA-binding dye, which was used to stain the cell nucleus. DAPI was diluted 1:2000 in 1x blocking buffer. The cells were incubated with 200 μl of secondary antibody dilution and DAPI dilution for 1 h at room temperature on a shaking platform protected from light. Afterwards, the cells were washed three times with 1 ml of 1 x blocking buffer for 5 min at room temperature on a shaking platform. A final washing step was performed with 1 ml PBS for 5 min at room temperature on a shaking platform. In order to avoid fading of the fluorescent dyes, the samples were protected from light during all washing steps. Finally the cells were mounted with Fluoromount-G[™].

The samples were analyzed using the laser scanning microscope LSM 710 and images were processed using ImageJ software v. 1.47 for additional contrast adjustment for each channel.

3.6 Transport experiments

To analyze transport activity of OCT1 and its variants, uptake measurements were performed using the OCT1 model substrates MPP^+ , TEA^+ , and ASP^+ , the drugs morphine, metformin, tropisetron, O-desmethyltramadol, debrisoquine, sumatriptan, fenoterol, and proguanil, and the exogenous substance tyramine. The intracellular accumulation of the substrates was quantified using scintillation counting (MPP^+ , TEA^+ , morphine, metformin, tyramine), fluorescence measurement (ASP^+), HPLC (debrisoquine, O-desmethyltramadol), or LC-MS/MS (sumatriptan, proguanil, fenoterol, metformin). Details about the different quantification methods are described in the chapter 3.6.1, 3.6.2, 3.6.3, and 3.6.4. For data analysis a standard curve was run in the same experiment (see Table 3.3) and the intracellularly accumulated substrate was normalized to the total amount of protein as determined by BCA assay (chapter 3.5). Using concentration dependent uptake

measurements, the K_m and v_{max} values of substrates were calculated by non-linear regression and Michaelis Menten equation using Graph Pad Prism v5.01.

Table 3.3 Linear range of substrates used for uptake measurements

Substrate	Detection method	Linear range
Debrisoquine	HPLC	0.03 μM – 2.825 μM
Fenoterol	LC-MS/MS	$2 \cdot 10^{-4}$ μM – 2 μM
Metformin	Scintillation counting	$5 \cdot 10^{-5}$ μM – 0.5 μM
Metformin	LC-MS/MS	0.2 μM – 30 μM
Morphine	Scintillation counting	10^{-5} μM – 1 μM
MPP ⁺	Scintillation counting	10^{-4} μM – 1 μM
O-Desmethytramadol	LC-MS/MS	0.002 μM – 0.3 μM
Proguanil	LC-MS/MS	0.001 μM – 1 μM
Sumatriptan	LC-MS/MS	0.01 μM – 5 μM
TEA ⁺	Scintillation counting	10^{-5} μM – 0.5 μM
Tropisetron	HPLC	0.07 μM – 3.515 μM

To this end, 0.6×10^6 cells or 9×10^6 cells were plated per well of a 12 well plates or on a Petri dish, respectively. The plates and Petri dishes have been pre-coated with poly D-lysine. For coating the plates, 500 μl or 4 ml of 0.2% poly D-lysine solution was pipetted into each well of a 12 well plat or a Petri dish, respectively. The poly D-lysine was incubated for 30 min at 37 °C in a CO₂ incubator. Afterwards the poly D-lysine was removed and the plates were dried under the biosafety cabinet. Cells were trypsinized and counted as described in chapter 3.4.4. The plated cells were cultured in a CO₂ incubator for 48 h prior to transport experiments. For transport experiments, HBSS supplemented with 10 mM HEPES (pH 7.4, further referred to as HBSS⁺) was used for washing steps and substrate dilutions. The pH of HBSS⁺ was adjusted to 7.4-7.6 with HCl individually before the transport experiment.

For uptake measurements performed in 12 well plates, the experiment was performed as follows: The 12 well plates was placed on a heating plate (37° C). Starting the experiment, the medium was removed and the cells were washed once with 2 ml pre-warmed HBSS⁺ (37° C). The uptake reaction was started by adding 400 μl of substrate solution and the substrate solution was incubated for 2 min (MPP⁺, TEA⁺, morphine, metformin, tyramine,

sumatriptan, proguanil, fenoterol) or 1 min (O-desmethytramadol). The uptake was stopped after 2 min or 1 min by adding 2 ml of ice-cold HBSS⁺ (4°C) and taking the plate off the heating plate. The cells were washed twice with 2 ml ice-cold HBSS⁺. For scintillation counting, the cells were lysed in 500 µl of 0.1 N NaOH containing 0.1 % SDS. For fluorescent measurement, cells were lysed with 500 µl of RIPA buffer (chapter 3.5). For LC-MS/MS detection, the samples for protein quantification were lysed in 500 µl of RIPA buffer and the samples for LC-MS/MS detection were lysed in lysis buffer containing 80 % acetonitrile and the respective internal standard (see chapter 3.6.4).

For uptake measurements performed in Petri dishes, the experiment was performed as follows: Starting the experiment, the medium was removed from the plates and the cells were washed with 10 ml pre-warmed HBSS⁺ (37 °C). The uptake reaction was started by adding 5 ml of substrate diluted in HBSS⁺ (37 °C). The reaction was stopped by adding 20 ml ice-cold HBSS⁺ (4 °C) after 3 min for tropisetron and after 1 min for debrisoquine. The cells were washed once with 20 ml of ice-cold HBSS⁺. Afterwards, 2 ml of ice-cold HBSS⁺ was added to the plates. With a cell scraper the cells were scraped into solution and transferred to a 2 ml reaction tube. The sample of this tube was used for HPLC analysis. From the 2 ml cell suspension, 500 µl were transferred to a 1.5 ml reaction tube. This aliquot was used to determine the protein concentration of the sample. Both tubes were centrifuged at 300 g for 10 min at 4 °C. The supernatant was discarded. The cell pellet of the 1.5 ml reaction tube used for protein quantification was lysed in 500 µl of 0.1 N NaOH containing 0.1 % SDS and protein concentration was determined using BCA assay as described in chapter 3.5. The cell pellet of the 2 ml reaction tube containing the sample for HPLC analysis was lysed in 1 ml of lysis buffer for HPLC analysis (see chapter 3.6.3)

3.6.1 Scintillation counting

The intracellular accumulation of MPP⁺ and TEA⁺ as well as of morphine, metformin, and tyramine was quantified using scintillation counting. The substrates were either labeled with ³H (MPP⁺) or with ¹⁴C (TEA⁺, morphine, metformin, and tyramine).

The transport experiments were performed using 12 well plates as described above. Finally, 400 µl of the cell lysate was transferred to a 20 ml poly-vial and mixed with 9 ml

Aquasafe 500+ liquid scintillator. The intracellular accumulated substrate was quantified using a liquid scintillation counter (LS6500).

3.6.2 Fluorescence measurement

The amount of intracellular accumulated ASP⁺ was determined by measuring the fluorescence. The transport experiments were performed using 12 well plates as described above. Finally, cells were lysed in RIPA buffer and were incubated for 10 min at room temperature on a shaking platform at 50 rpm. The plate was centrifuged at 700 rpm for 10 min at room temperature. The supernatant was used for fluorescence measurement and to determine protein concentration. For fluorescent measurements, 200 µl of the sample was transferred to a well of a black 96 well microplate (Corning[®]). Each sample was measured in duplicates. The fluorescence was measured using the Tecan Ultra Microplate Reader with the following parameter settings:

- Excitation wavelength: 485 nm
- Emission wavelength: 612 nm
- Gain: 50¹ or 45²
- Number of flashes: 10
- Lag time: 0
- Integration time: 40
- Mirror selection: Automatic
- Plate definition file: COS96fb.pdf
- Multiple Reads per well: 2 x 2
- Z-position³: e.g. 7165 µm

¹...Gain of 50 was used for samples of uptake measurements performed at single concentrations

²... Gain of 45 was used for samples from concentration dependent uptake measurements

³...Needed to be manually adjusted for every measurement

3.6.3 HPLC

Lysis buffer for tropisetron

Substance	Volume
Acetonitrile	40 ml
50 mM NaH ₂ PO ₄ , pH 5	10 ml
Internal standard : 1 ng/μl ondansetron	500 μl

Mobile phase for tropisetron

Substance	Concentration
Acetonitrile	20 %
50 mM NaH ₂ PO ₄ , pH 5	80 %

Lysis buffer for debrisoquine

Substance	Volume
Acetonitrile	40 ml
50 mM Sodium acetate, pH 5	10 ml
Internal standard: 1 ng/μl venlafaxine	500 μl

Mobile phase for debrisoquine

Substance	Concentration
Acetonitrile	5 %
50 mM Sodium acetate, pH 5	95 %

The amount of intracellularly accumulated tropisetron and debrisoquine was quantified using HPLC as described previously (Saadatmand et al., 2012; Tzvetkov et al., 2012). The experiments were performed using poly D-lysine pre-coated 100 mm Petri dishes with 9×10^6 plated cells cultured for 48 h. The experiment was performed as described above.

Finally, the cell lysate was centrifuged at 13 000 rpm for 10 min at 4 °C to remove cell debris. The supernatant was transferred into a 10 ml glass tube and evaporated to dryness under nitrogen stream at 40 °C. The pellet was reconstituted in 200 μl of mobile phase and

the amount of intracellular accumulated substrate was analyzed using HPLC (Saadatmand et al., 2012; Tzvetkov et al., 2012). Briefly, the LaChrome HPLC system with interface D-7000, pump L-7100, autosampler L-7200, degasser L-7614, an ultraviolet detector - L-7400 and fluorescence detector L-7400 were used for tropisetron and debrisoquine detection. Tropisetron was detected by ultraviolet detection at 284 nm. Fluorescence detection for debrisoquine was performed using an excitation wavelength of 210 nm and emission wavelength of 290 nm. The retention times of the substrate peaks and peaks of the internal standard are listed below. The area under the peak was used for quantification using external standardization.

Retention times

Substance	Retention Times [min]
Tropisetron	10
Ondansetron	13
Debrisoquine	9
Venlafaxine	16

3.6.4 LC-MS/MS

The intracellular accumulation of O-desmethyltramadol, proguanil, sumatriptan, and metformin was quantified using LC-MS/MS analysis. The uptake of O-desmethyltramadol was measured for 1 min, and the uptake of proguanil, sumatriptan, and metformin was measured for 2 min.

The transport experiment was performed in 12 well plates as described above. Finally, samples for LC-MS/MS detection were lysed in 500 µl of lysis buffer containing 80 % acetonitrile with the appropriate internal standard (see Table 3.4). Cell debris were removed by centrifugation at 16 500 g for 15 min and 400 µl of the supernatant was transferred to a new 1.5 ml reaction tube. Samples for detection of metformin, sumatriptan, and fenoterol were diluted 1:200, 1:10, and 1:8 in 0.1 % of formic acid, respectively. Samples for detection of O-desmethyltramadol and proguanil were evaporated as follows:

300 µl of lysate was transferred to a 10 ml glass tube and evaporated to dryness under nitrogen flow at 40 °C. The pellets for detection of O-desmethyltramadol or proguanil were reconstituted in 150 µl and 300 µl of 0.1 % formic acid, respectively.

Ten µl of the samples were used for analysis. HPLC was performed using a High Pressure Liquid Chromatographer Series 200 (Perkin Elmer, Rodgau, Germany) coupled with an API 4000 tandem mass spectrometer (Life Technology). For separation a Brownlee SPP RP-Amide column (4.6 x 100 mm inner dimension, 2.7 µm particle size; Perkin Elmer) with a SecurityGuard C18pre-column (4x2mm; Phenomenex) was used. Substrate peaks were detected using substrate-specific mass transitions and retention times (see Table 3.4). The area under the peak was used for quantification using a standard curve run in the same experiment.

Table 3.4 Substrate-specific experimental conditions using LC-MS/MS

Substance	Mass [Da]	RT [min]	Internal Standard (IS)		Mass (IS) [Da]	RT(IS) [min]	Mobile phase
			Name	Concentration			
Metformin	130.0 >71.0	2.8	Burformin	10	158.0 >60.0	4.0	3 % organic (ACN:Methanol 6:1)
Proguanil	254.2 >170.2	6.2	Proguanil-d6	10	260.31 >170.2	6.0	20 % organic (ACN:Methanol 6:1)
Sumatriptan	296.2 >58.2	5.9	Sumatriptan-d6	10	302.2 >64.2	5.9	8 % organic (ACN:Methanol 6:1)
O-desmethyl-tramadol	250.2 >58.1	4.2	Atropine	10	290.2 >142.2	4.8	15 % organic (ACN:Methanol 6:1)
Fenoterol	304.1 >107.1	4.9	Fenoterol-d6	5	310.3 >141.0	4.9	12 % organic (ACN:Methanol 6:1)

Table 3.5 MS detection parameters

Substance	Mass [Da]	DP	CE	CXP	CAD	CUR	GAS 1	GAS 2	Temp	IS
Metformin	130.0>71.0	40.0	35.0	10.0	12.0	30.0	50.0	60.0	450.0	5500.0
Burformin	158.0>60.0	40.0	35.0	10.0	12.0	30.0	50.0	60.0	450.0	5500.0
Proguanil	254.2>170.2	75.0	24.0	3.0	8.0	34.0	55.0	60.0	500.0	5500.0
Proguanil-d6	260.31>170.2	75.0	25.0	10.0	8.0	34.0	55.0	60.0	500.0	5500.0
Sumatriptan	296.2>58.2	50.0	30.0	12.0	9.0	25.0	50.0	50.0	450.0	5500.0
Sumatriptan-d6	302.2>64.2	70.0	30.0	12.0	9.0	25.0	50.0	50.0	450.0	5500.0
O-desme- thyltramadol	250.20>58.1	120.0	25.0	10.0	10.0	25.0	50.0	50.0	450.0	5500.0
Atropine	290.2>142.2	100.0	45.0	12.0	10.0	25.0	50.0	50.0	450.0	5500.0
Fenoterol	304.1>107.1	70.0	44.0	12.0	4.0	25.0	50.0	50.0	450.0	5500.0
Fenoterol-d6	310.3>141.0	70.0	26.0	12.0	4.0	25.0	50.0	50.0	450.0	5500.0

3.7 Statistics

Statistical analyses were performed using Graph Pad Prism v5.01 and SigmaPlot v12.5. Analysis of variance (ANOVA) was applied for multi-group comparisons. In order to test two groups among the multiple-group the ANOVA testing was followed by post hoc analysis using Tukey's Honestly Significant Difference (HSD) test. P-values < 0.05 were regarded as significant.

4 Results

4.1 Functional characterization of genetic polymorphisms in the organic cation transporter *OCT1*

OCT1 is highly genetically variable. More than 10 years ago a number of common variants in OCT1 were identified and data was collected over the years how these variants affect the uptake of different OCT1 substrates (Kerb et al., 2002; Shu et al., 2003; Tzvetkov et al., 2016). However, those were different studies from different laboratories with partially contradictory results analyzing only a limited number of substrates (Shu et al., 2003; Gorboulev et al., 1997; Kerb et al., 2002; Tzvetkov et al., 2013). As it is known that OCT1 is a polyspecific transporter, which binds a broad range of structurally different substances, substrate-specific differences of different OCT1 variants could be kept undetected. Furthermore, using high-throughput massive parallel sequencing of 1079 worldwide DNA samples, our group recently identified common and rare single nucleotide polymorphisms that lead to a change in the amino acid sequence of OCT1 (Figure 1.2) (Seitz et al., 2015). The aim of this part of the thesis was the systematic functional characterization of these variants on a broad spectrum of known structurally diverse OCT1 substrates that enables comparison of their effects.

4.1.1 Generation and validation of cell lines used to analyze non-synonymous substitutions in OCT1

To this end, HEK293 cells were stably transfected to overexpress the following OCT1 variants: S14F, S29L, P117L, S189L, R206C/M408V/M420del, T245M, E284K, M408V, G414A, G414A/M408V/M420del, M408V/M420del, and I449T. We used these cells together with the eight existing cell lines (overexpressing the variants R61C, C88R/M420del, F160L, P341L/M408V, G401S, G465R/M420del, R488M, and R488M/M408V) to measure the uptake of eight OCT1 substrates and to determine their subcellular localization.

In order to generate the HEK293 cells overexpressing different allelic variants of *OCT1*, point mutations were introduced via site-directed mutagenesis. Ten mutated pcDNA3.1 plasmid constructs have been generated (Table 4.1).

Table 4.1 Generated pcDNA3.1 plasmids with point mutations in *OCT1* for the analysis of non-synonymous substitutions in *OCT1*

Plasmid name	Generated from
pcDNA3.1::hOCT1-S14F-R342H	pcDNA3.1::hOCT1-S14F ¹
pcDNA3.1::hOCT1-S29L	pcDNA3.1::hOCT1 ²
pcDNA3.1::hOCT1-R206C-M408V-M420del	pcDNA3.1::hOCT1-M408V-M420del
pcDNA3.1::hOCT1-T245M	pcDNA3.1::hOCT1 ²
pcDNA3.1::hOCT1-E284K	pcDNA3.1::hOCT1 ²
pcDNA3.1::hOCT1-M408V	pcDNA3.1::hOCT1 ²
pcDNA3.1::hOCT1-G414A	pcDNA3.1::hOCT1 ²
pcDNA3.1::hOCT1-G414A-M408V-M420del	pcDNA3.1::hOCT1-M408V-M420del
pcDNA3.1::hOCT1-M408V-M420del	pcDNA3.1::hOCT1-M420del ³
pcDNA3.1::hOCT1-I449T	pcDNA3.1::hOCT1 ²

¹ generated by Ali Reza Saadatmand, Institute of Clinical Pharmacology, University Medical Center Göttingen

² provided by Hermann Koepsell, University of Würzburg

³ generated by Ali Reza Saadatmand, Institute of Clinical Pharmacology, University Medical Center Göttingen as described elsewhere (Tzvetkov et al., 2012)

Together with the plasmids pcDNA3.1::hOCT1-S14F, pcDNA3.1::hOCT1-P117L, and pcDNA3.1::hOCT1-S189L that were previously generated in our lab (Table 2.5), the mutated OCT1 genes were re-cloned in pcDNA5. The generated pcDNA5 plasmids (Table 2.6) were used for stable transfection into HEK293 cells (Table 4.2).

Table 4.2 HEK293 cell lines generated by targeted chromosomal integration for the analysis of non-synonymous substitutions in OCT1

Cell line
HEK293-OCT1-S14F
HEK293-OCT1-S29L
HEK293-OCT1-P117L
HEK293-OCT1-S189L
HEK293-OCT1-R206C-M408V-M420del
HEK293-OCT1-T245M
HEK293-OCT1-E284K
HEK293-OCT1-M408V
HEK293-OCT1-G414A-M408V-M420del
HEK293-OCT1-G414A
HEK293-OCT1-M408V-M420del
HEK293-OCT1-I449T

In order to validate the generated cell lines three integration-specific PCRs were performed (chapter 3.1.6). Therefore, eight to ten clones of each variant were selected for testing. Of those, two positive clones were saved. PCR 1 and PCR 2 were performed to verify integration of pcDNA5 into the genome of HEK293 cells and to detect the gene of interest within the integration site. Figure 4.1 shows the results of PCR 1 and PCR 2 of the clone that was used for further analyses. PCR 1 resulted in an amplification product of 519 bp. PCR 2 resulted in an amplification product of 1376 bp for the empty pcDNA5 vector and of 3137 bp for pcDNA5 containing *OCT1* or its variants, respectively.

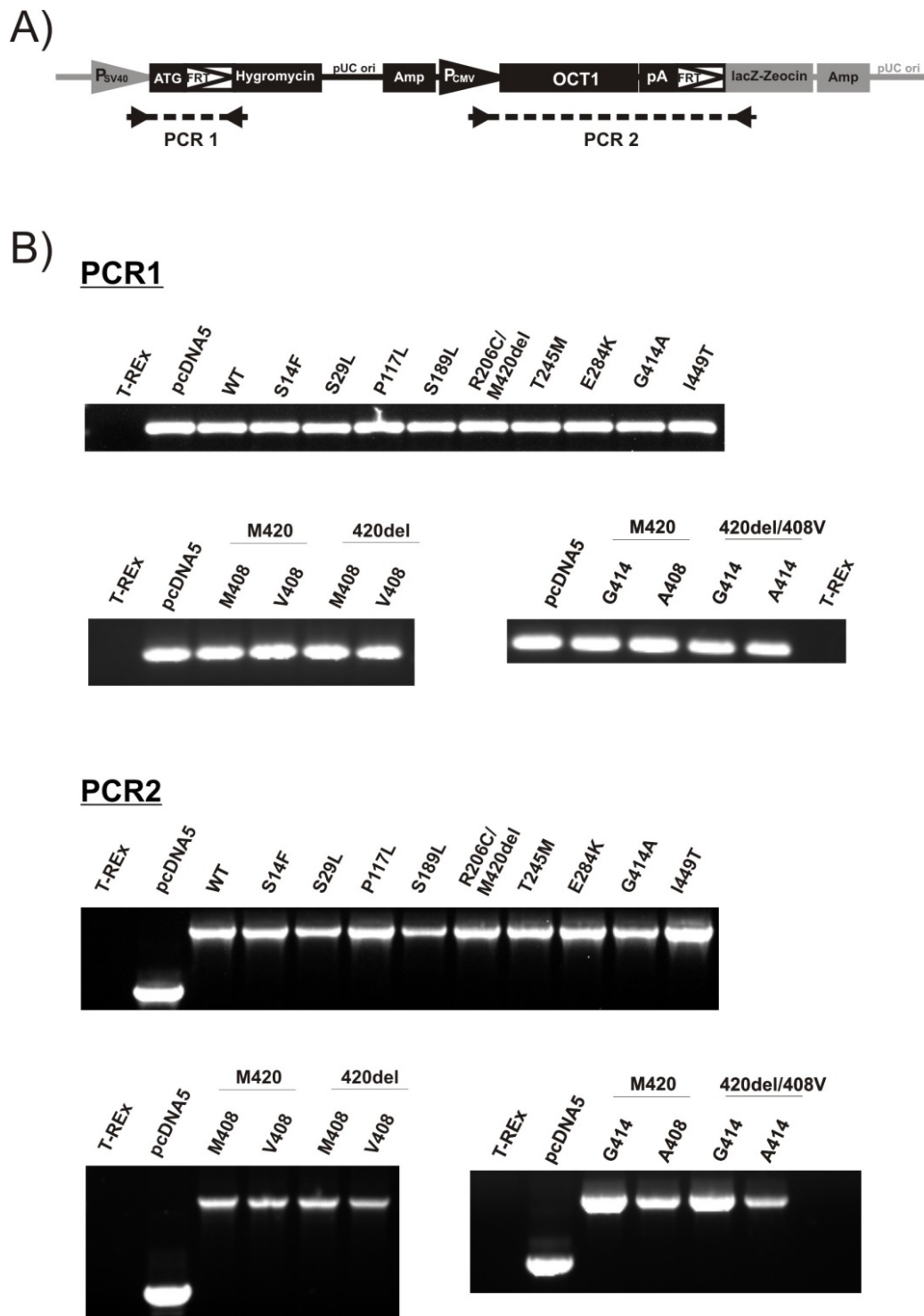


Figure 4.1 Validation of the correct integration of the constructs overexpressing different *OCT1* allelic variants into the genome of the HEK293 cells. (A) Schematic presentation of the expression plasmid pcDNA5 (black) integrated into the pFRT/lacZeo site of the genome of HEK293 cells (gray). The positions of the primers used in PCR 1 and PCR 2 are indicated. (B) PCR 1 resulted in an amplification product of 519 bp and PCR 2 resulted in an amplification product of about 3137 bp (wild type *OCT1* or its allelic variants) or 1376 bp (empty pcDNA5 vector). This figure was presented in a slightly modified form in Seitz *et al.* 2015 (Seitz *et al.*, 2015):

PCR 3 was performed in order to identify multiple tandem integration of the expression vector pcDNA5 containing *OCT1* into the genome of HEK293 cells. All of the variants tested, except the variants C88R/M420del and T245M, were confirmed as single integrands, as no amplification product was obtained (Figure 4.2). The variant C88R/M420del was generated previously (Tzvetkov et al., 2012).

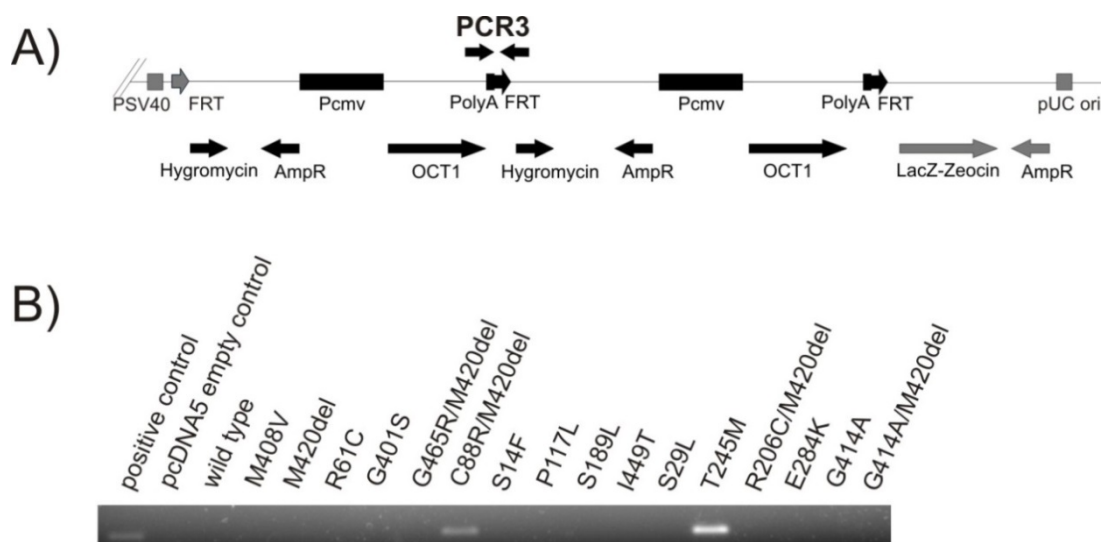


Figure 4.2 Analysis for potential multiple tandem integration of the constructs overexpressing different *OCT1* allelic variants into the HEK293 genome. (A) Schematic representation of double tandem integration of the *OCT1* overexpressing pcDNA5 plasmid (black) into the pFRT/lacZeo site in the HEK293 genome (gray). Annealing positions of the primers (PFRT_f and PHyr_r) are indicated. (B) In case of multiple integrands PCR 3 resulted in an amplification product of 214 bp. All variants, except C88R/M420del and T245M, were tested negative for multiple tandem integration. However, there were no obvious differences in expression levels in these clones (Figure 4.3).

The correctness of *OCT1* allelic variants was validated by SNaPshotTM and capillary sequencing. To this end, the PCR product of PCR 2 was purified and subjected either to SNaPshotTM genotyping or to re-sequencing. DNA samples of the following *OCT1* allelic variants have been analyzed using SNaPshotTM genotyping: S14F, S29L, P117L, S189L, R206C/M408V/M420del, T245M, E284K, M408V, M420del/M408V, G414A, and I449T. The variant G414/M408V/M420del was validated using capillary re-sequencing analysis. In order to confirm equal expression levels of *OCT1* and its variants in stable transfected HEK293 cells, a real-time PCR was performed (Figure 4.3). HEK293 cells overexpressing

OCT1 showed 100 % higher expression than HEK293 transfected with the empty control vector pcDNA5. The selected clones did not differ more than 10 % in their mRNA level compared to wild type OCT1.

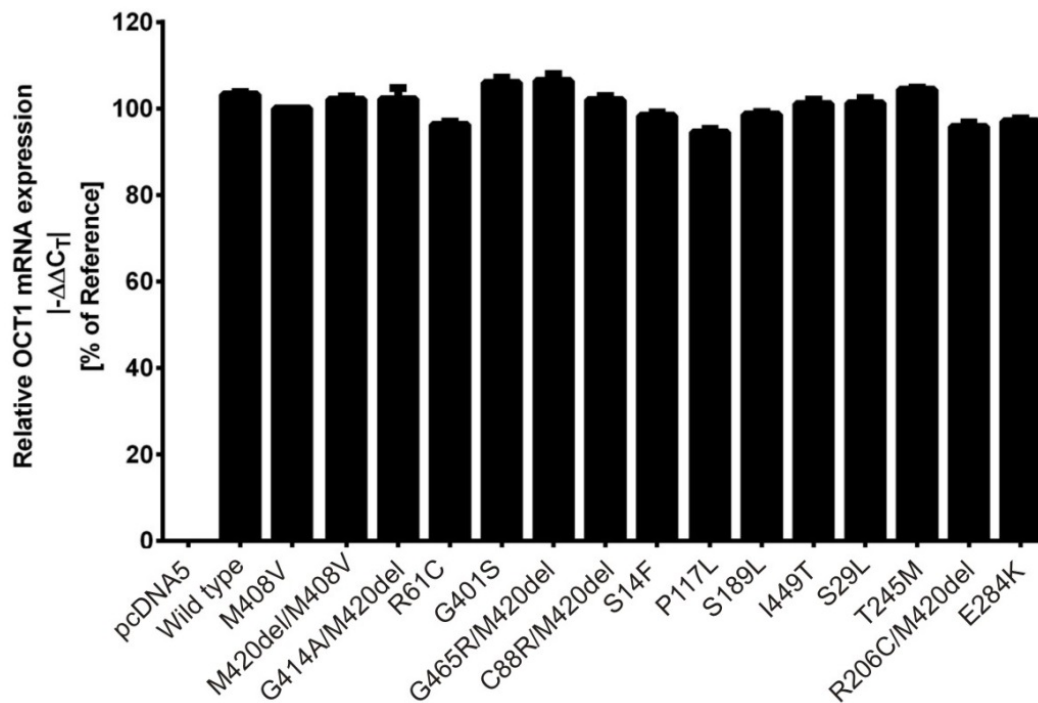


Figure 4.3 RT-qPCR demonstrating equal mRNA expression levels among the *OCT1* allelic variants. The mRNA level of HEK293 cells stably transfected with *OCT1* allelic variants are shown in relation to the levels in HEK293 cells stably transfected with wild type *OCT1*. The results are based on relative quantification using the $\Delta\Delta C_T$ method. The mRNA expression was normalized to the expression of TBP and RNA samples. Shown is the mean and error of the mean of three independent RNA extractions. This figure was presented in a slightly modified form in Seitz *et al.* 2015 (Seitz *et al.*, 2015).

4.1.2 Functional characterization of *OCT1* allelic variants

In order to characterize allelic variants of *OCT1*, the transport activity of the 15 major and 6 minor *OCT1* allelic variants was measured using 8 different substances: the model substrates MPP⁺, TEA⁺, ASP⁺, and the drugs morphine, metformin, tropisetron, O-desmethyltramadol, and debrisoquine. The intracellular accumulation of MPP⁺, TEA⁺, morphine, and metformin was analyzed using scintillation counting, of ASP⁺ using fluorescence measurement and of tropisetron and debrisoquine using HPLC analysis. The

uptake of O-desmethyltramadol was analyzed using the LC-MS/MS method. Analyzed were single concentrations that were either already reported, in order to compare uptake activities with previous studies, or concentrations that were far below or close to the reported K_m of the substance (Zhang et al., 1997; Takeuchi et al., 2003; Shu et al., 2007; Ahlin et al., 2011; Tzvetkov et al., 2011; Saadatmand et al., 2012; Tzvetkov et al., 2012; Tzvetkov et al., 2013; Nies et al., 2009). For details about transport measurements see chapter 3.6. For all substances tested the uptake was at least 1.9-fold higher in the cells overexpressing the wild type *OCT1*1* allele compared to the control cells transfected with the empty vector pcDNA5 (Figure 4.4).

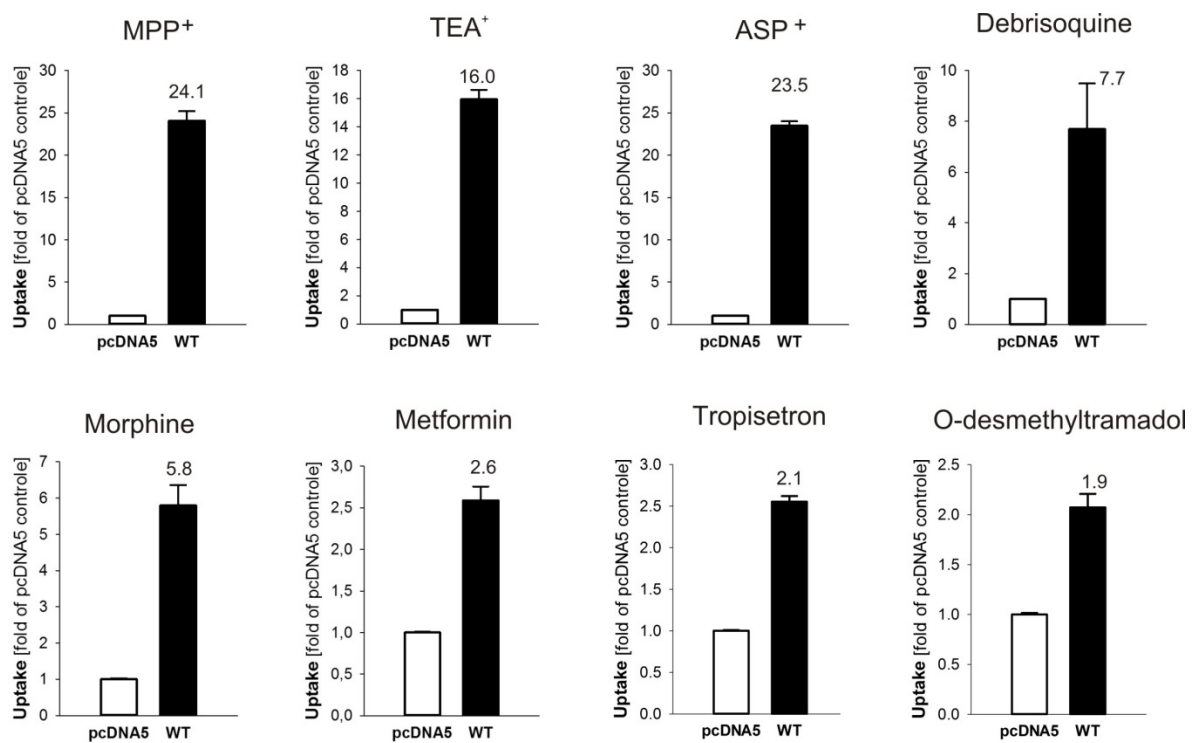


Figure 4.4 Differences in the uptake between HEK293 cells stably transfected with wild type *OCT1* and with the empty expression vector pcDNA5. Uptake is represented as fold increase of OCT1 wild type in comparison to pcDNA5 transfected cells. Shown is the mean and standard error of the mean of at least three independent experiments. This figure was presented in a slightly modified form in Seitz *et al.* 2015 (Seitz *et al.*, 2015).

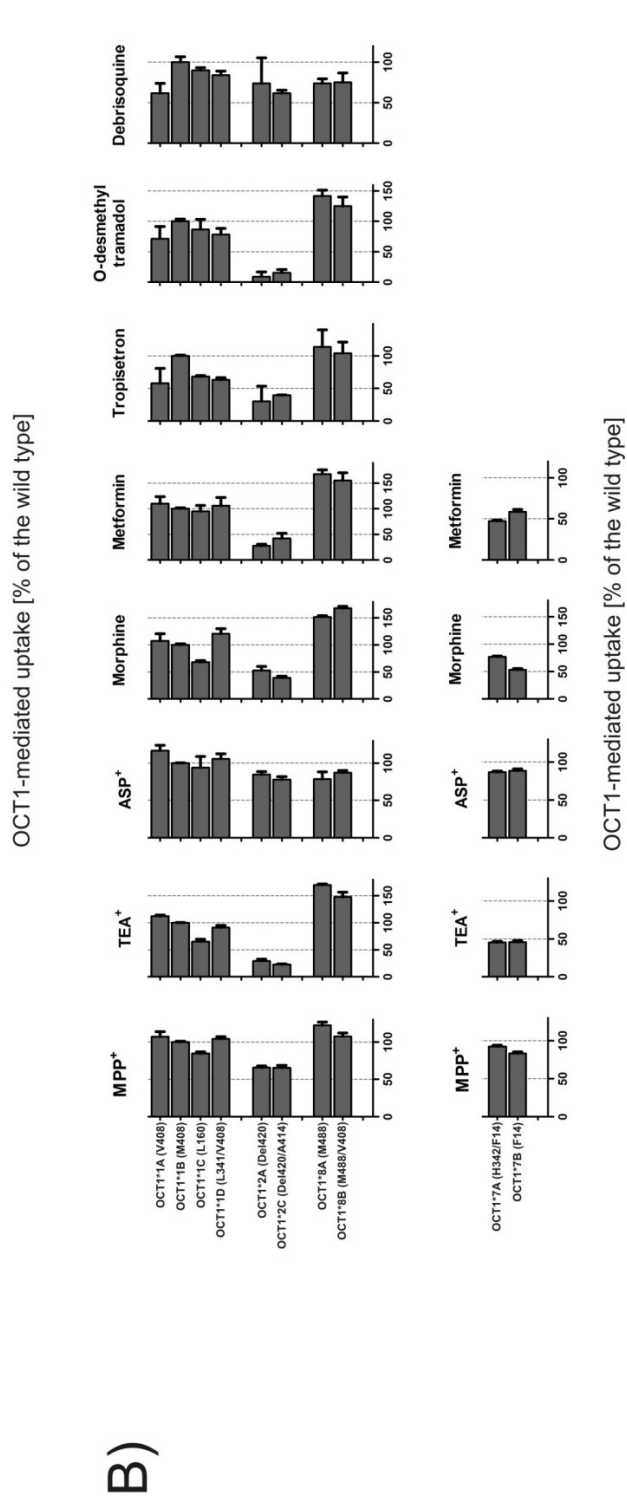
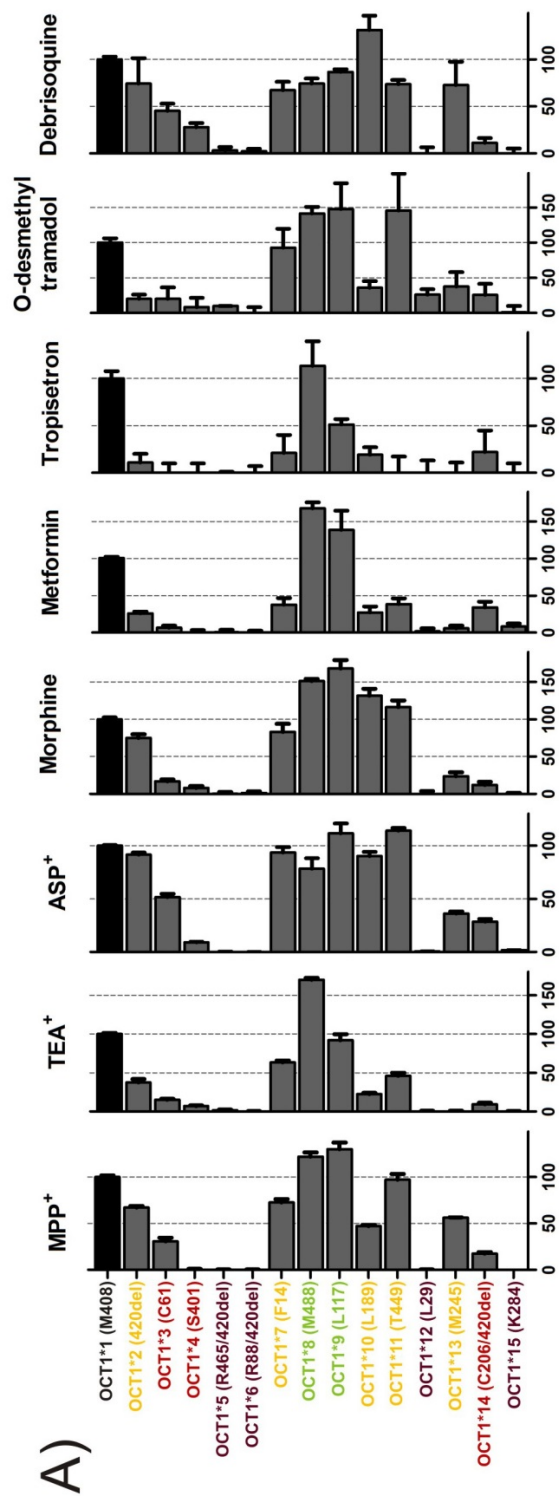


Figure 4.5 (previous page) Functional characterization of *OCT1* allelic variants. The effects of non-synonymous substitutions in OCT1 on transport activity were analyzed measuring the uptake of MPP⁺, TEA⁺, ASP⁺, morphine, metformin, tropisetron, O-desmethyltramadol, and debrisoquine. HEK293 cells transfected to overexpress *OCT1* allelic variants were incubated for 2 min with 10 μM MPP⁺, 5 μM TEA⁺, 5 μM ASP⁺, 1 μM morphine, or 5 μM metformin, or for 1 min with 1 μM debrisoquine or 1 μM O-desmethyltramadol, or for 3 min with 1 μM tropisetron. The OCT1-mediated uptake was calculated by subtracting the uptake of HEK293 cells transfected with the empty expression vector pcDNA5 from HEK293 cells overexpressing *OCT1* allelic variants. The results are shown as a percent of the uptake in wild type OCT1 cells (shown in black). Shown is the mean and error of the mean of at least three independent experiments. (A) Shows the uptake of the eight substrates by the 15 major *OCT1* alleles (designed as *OCT1*1B*, *OCT1*2A-3A*, *OCT1*4B*, *OCT1*5A-6A*, *OCT1*7B*, *OCT1*8* -**15* in Figure 1.2). The results shown for the alleles *OCT1*3*, *OCT1*4*, *OCT1*5*, and *OCT1*6* for the uptake of morphine and tropisetron are from previously published studies of our lab (Tzvetkov et al., 2011; Tzvetkov et al., 2013) and are shown here to enable direct comparison. The effect of allelic variants on transport activity is indicated in colors: gain of function variants are shown in green, variants with substrate-specific loss of activity in yellow, variants with strong substrate-wide decrease in light red, and variants with complete substrate-wide loss of activity in dark red. (B) Shows the uptake of the eight substrates by the six most common sub-alleles. The comparison of transport activity between the variants *OCT1*7A* and *OCT1*7B* (subfigure B) was made after transient transfection. All the remaining experiments were performed using stably transfected HEK293 cell lines. Shown is the mean and standard error of the mean of at least three independent experiments. A modified version of this figure has been presented by Seitz *et al.* (Seitz et al., 2015).

The functional analyses identified two gain-of-function OCT1 variants: the alleles *OCT1*8* (R488M) and *OCT1*9* (P117L) showed more than 50 % increase in the uptake of at least one substrate tested: the allele *OCT1*8* showed 70 %, 52 %, and 68 % increase in the uptake of TEA⁺, morphine, and metformin, respectively. The *OCT1*9* allele showed 68 % increase in the uptake of morphine. Most of the remaining variants tested showed loss of activity in OCT1 transport. These variants could be divided into three groups depending on their extent of loss of function: the alleles *OCT1*5* (G465R/M420del), *OCT1*6* (C88R/M420del), *OCT1*12* (S29L), and *OCT1*15* (E284K) showed complete loss of activity for all substrates tested. The alleles *OCT1*3* (R61C), *OCT1*4* (G401S), and *OCT1*14* (R206C/M420del) showed strong, but not complete loss of activity for all substrates tested. The alleles *OCT1*2* (M420del), *OCT1*7* (S14F), *OCT1*10* (S189L), *OCT1*11* (I449T), and *OCT1*13* (T245M) showed substrate-specific loss of activity. For example the *OCT1*2* allele strongly decreased the uptake of TEA⁺, metformin, tropisetron, and O-desmethyltramadol by 62 %, 74 %, 89 %, and 80 %, respectively. In contrast, the

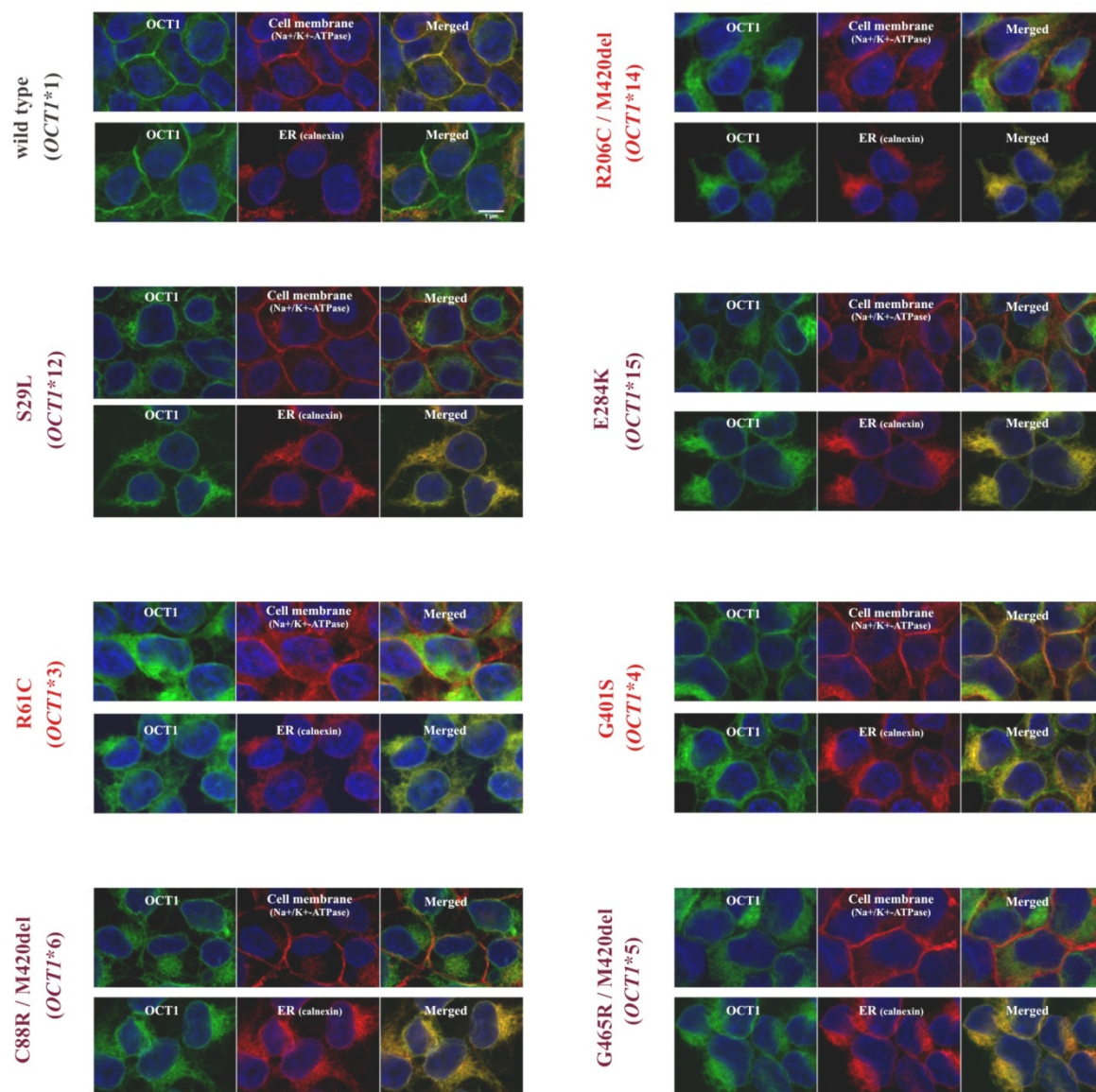
uptake of MPP⁺, morphine, and debrisoquine was only slightly decreased by 33 %, 25 %, and 26 %, respectively. For the uptake of ASP⁺, *OCT1**2 decreased the uptake only by 8 %.

The *OCT1* variants F160L, P341L, R342H, M408V, and G414A did not cause a more than 50 % decrease or increase in *OCT1* activity with any of the substrates tested (Figure 4.5 B). Therefore the haplotypes carrying these variants were designated as sub-alleles.

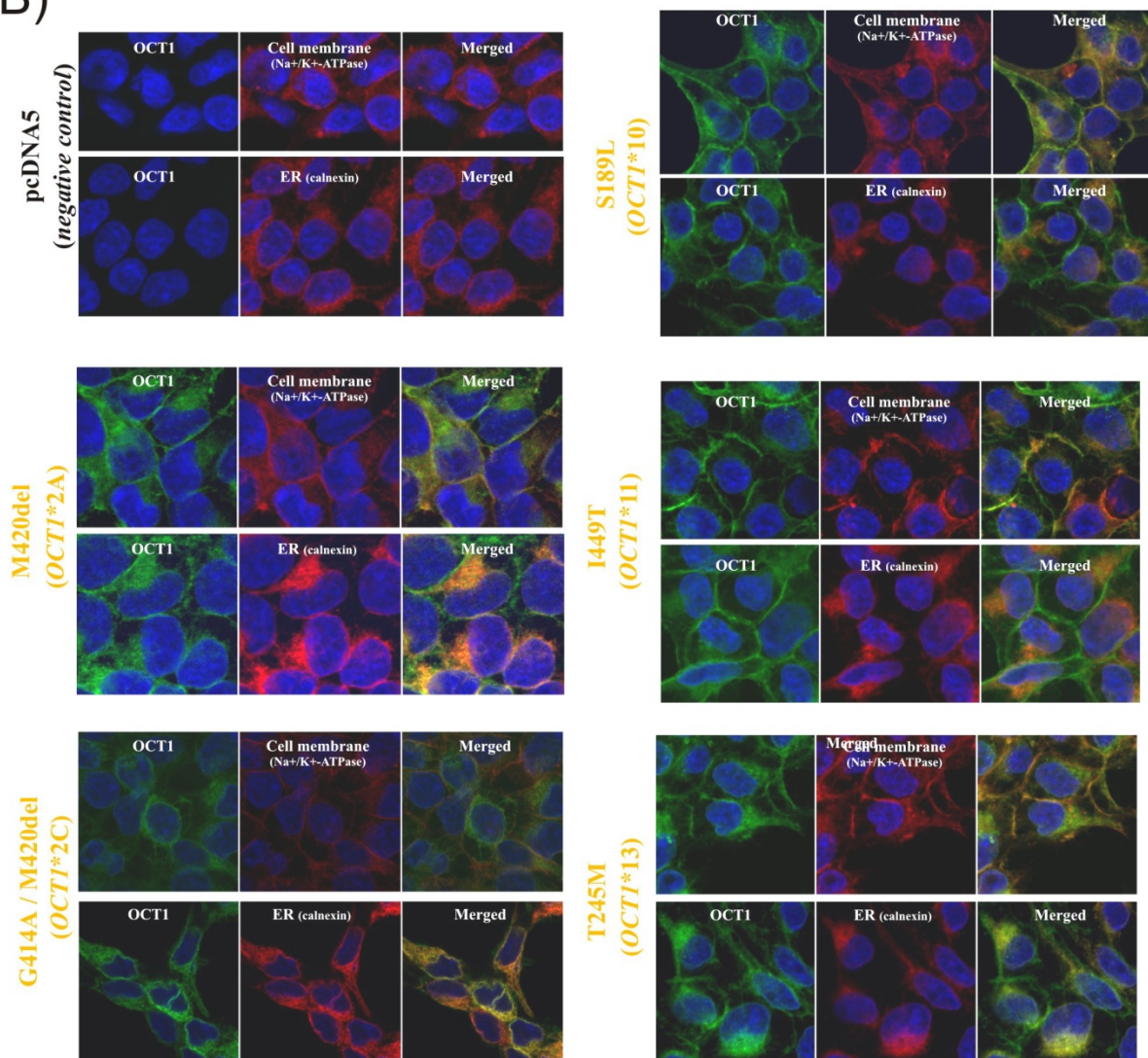
4.1.3 Subcellular localization and differences in the glycosylation pattern of *OCT1* allelic variants

In order to find a potential reason for substrate-wide loss of activity, the subcellular localization of *OCT1* allelic variants was analyzed. The subcellular localization was analyzed using immunofluorescence staining with confocal microscopy detection (Figure 4.6). In contrast to the control pcDNA5 cells, strong *OCT1* signals were detected in all cells overexpressing different *OCT1* allelic variants. However, the subcellular localization of the signals strongly varied among the different allelic variants. For the alleles *OCT1**5, *OCT1**6, *OCT1**12 and *OCT1**15, which caused complete loss of activity for all substrates tested (Figure 4.5), the *OCT1* protein was not located in the plasma membrane (Figure 4.6 A). This was evidenced by a missing co-staining with a Na⁺/K⁺ ATPase, which was used as a plasma membrane marker. For these allelic variants the *OCT1* protein was detected in the endoplasmic reticulum. This was demonstrated by co-staining of calnexin; a marker for the endoplasmic reticulum. In contrast, allelic variants that caused a strong but not complete (*OCT1**3, *OCT1**4, and *OCT1**14) or a substrate-specific (*OCT1**2, *OCT1**7, *OCT1**10, *OCT1**11, and *OCT1**13) loss of activity could be detected in the plasma membrane (Figure 4.6 B, C). However, for the allelic variants *OCT1**3 and *OCT1**14 the amount of *OCT1* seemed to be less on the plasma membrane than for wild type *OCT1* cells when directly comparing the staining for *OCT1* between these two allelic variants and *OCT1* wild type. The gain-of function variants *OCT1**8 and *OCT1**9 as well as the sub alleles *OCT1**1C and *OCT1**1D, which were shown not to affect transport activity (Figure 4.5 B), did not differ in membrane localization compared to wild type (Figure 4.5 B). Taken together, it could be concluded that the major reason for substrate-wide loss of activity was improper membrane localization of the *OCT1* protein due to its retention in the endoplasmic reticulum.

A)



B)



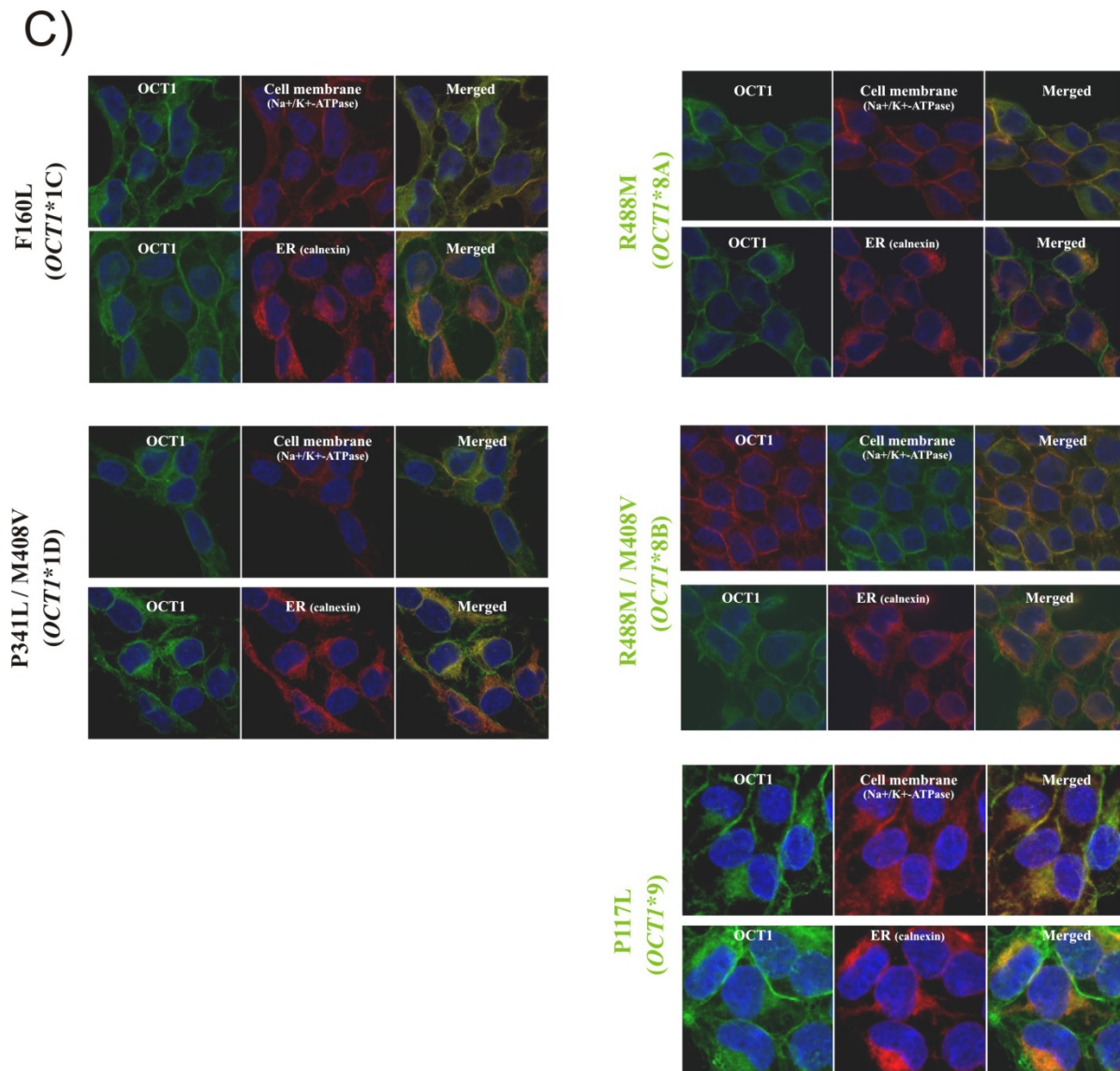


Figure 4.6 Analysis of the subcellular localization of *OCT1* allelic variants. The subcellular localization was analyzed using confocal microscopy after immunocytochemical staining for OCT1 (green). The exact subcellular localization of OCT1 was analyzed using co-staining with Na^+/K^+ ATPase as a marker for the plasma membrane (red, upper part) and calnexin as a marker for the endoplasmic reticulum (red, lower part). (A) Shown are the HEK293 cells overexpressing *OCT1* allelic variants with complete loss of activity (labeled in dark red) and substrate-wide strong decrease in transport activity (labeled in light red). The allelic variants with complete loss of activity *OCT1*5*, *OCT1*6*, *OCT1*12* and *OCT1*15* lack membrane localization. Comparison of the staining intensity suggests that *OCT1*3* and *OCT1*14* have partially impaired localization on the plasma membrane. HEK293 cells overexpressing wild type *OCT1* are shown as a reference. (B) The membrane localization of *OCT1* allelic variants that showed substrate-specific loss of activity was not altered (labeled in orange). Control pcDNA5 cells were negative for OCT1 staining. (C) Allelic variants that caused gain of OCT1 function are shown in green and variants that did not affect OCT1 activity are shown in black. This figure was presented in a slightly modified form in Seitz *et al.* 2015 (Seitz *et al.*, 2015).

OCT1 allelic variants were further characterized by western blot analysis of total cellular lysates. The *OCT1*-specific antibody (chapter 2.5) used for western blot analysis revealed two bands at 50 kDa and 70 kDa (Figure 4.7). Both bands were sensitive to deglycosylation (Figure 4.7). The band at 50 kDa was sensitive to both *EndoH* and *PNGase F* deglycosylation, while the 70 kDa band was sensitive to *PNGase F* only. The allelic variants *OCT1*5*, *OCT1*6*, *OCT1*12*, and *OCT1*15* showed a different glycosylation pattern compared to the wild type as just the 50 kDa band could be detected by western blot analysis. All these allelic variants showed substrate-wide loss of *OCT1* activity (Figure 4.5) and lacked plasma membrane localization (Figure 4.6 A).

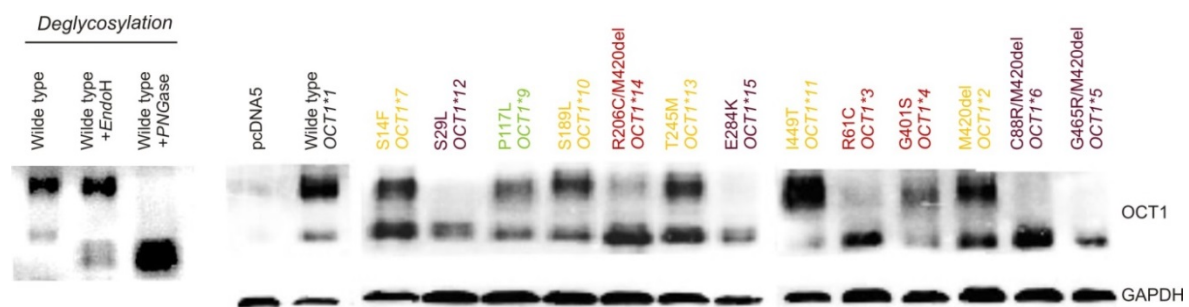


Figure 4.7 Western blot analysis of *OCT1* allelic variants. Western blot analysis of 10 μ g total cellular protein illustrates differences between the glycosylation patterns of *OCT1* variants retained in the endoplasmic reticulum (*OCT1*5*, *OCT1*6*, *OCT1*12*, and *OCT1*15*) and those correctly localized in the plasma membrane (the rest). *OCT1* was detected using a mouse monoclonal *OCT1*-specific antibody (2C5) and was detected as a double signal of a 70 kDa *PNGaseF*-sensitive and *EndoH*-resistant protein and a 50 kDa *EndoH*-sensitive glycosylated protein. As a loading control GAPDH was stained using a mouse monoclonal GAPDH-specific (6C5) antibody. This figure was presented in a slightly modified form in Seitz *et al.* 2015 (Seitz *et al.*, 2015).

Taken together, we observed strong variability in the effects of *OCT1* allelic variants on transport activity. Four out of 19 allelic variants tested showed complete loss of transport activity due to improper membrane localization. These variants also revealed a different glycosylation pattern in western blot analysis. Three allelic variants led to a strong decrease in activity independent from the substrate tested. These allelic variants seemed to have no aberrant membrane localization although reduced membrane localization could be assumed for single variants. A substantial number of allelic variants, five out of 19, showed substrate-specific loss of activity. Two allelic variants could be characterized as gain of

function alleles, as they show a more than 50 % increase in the uptake of at least one substrate tested.

4.2 Prediction of the allele-specific effects on morphine and metformin uptake using model substrates

The allelic variants *OCT1*2*, *OCT1*7*, *OCT1*10*, *OCT1*11*, and *OCT1*13* showing substrate-specific loss of activity were further characterized regarding the possibility to predict the effect of these variants on the transport of clinically relevant drugs like morphine and metformin using model substrates. To this end, the ability of these allelic variants to transport the model substrates MPP⁺, TEA⁺, and ASP⁺ was correlated to the ability to transport morphine and metformin (Figure 4.8). None of the model substrates tested could reflect the effect of these variants on both drugs. The uptake of morphine showed the strongest correlation with the uptake of ASP⁺ ($r^2= 0.7$, $P=0.036$). In contrast, the uptake of metformin correlated better with the uptake of TEA⁺ ($r^2=0.84$, $P=0.0058$). These results underline again the substrate-specific effects of the number of loss of function alleles including the most common one, *OCT1*2*. The generalized prediction of the effects of these variants is not possible and a better understanding of the mechanisms of the substrate-specificity of these allelic variants is required.

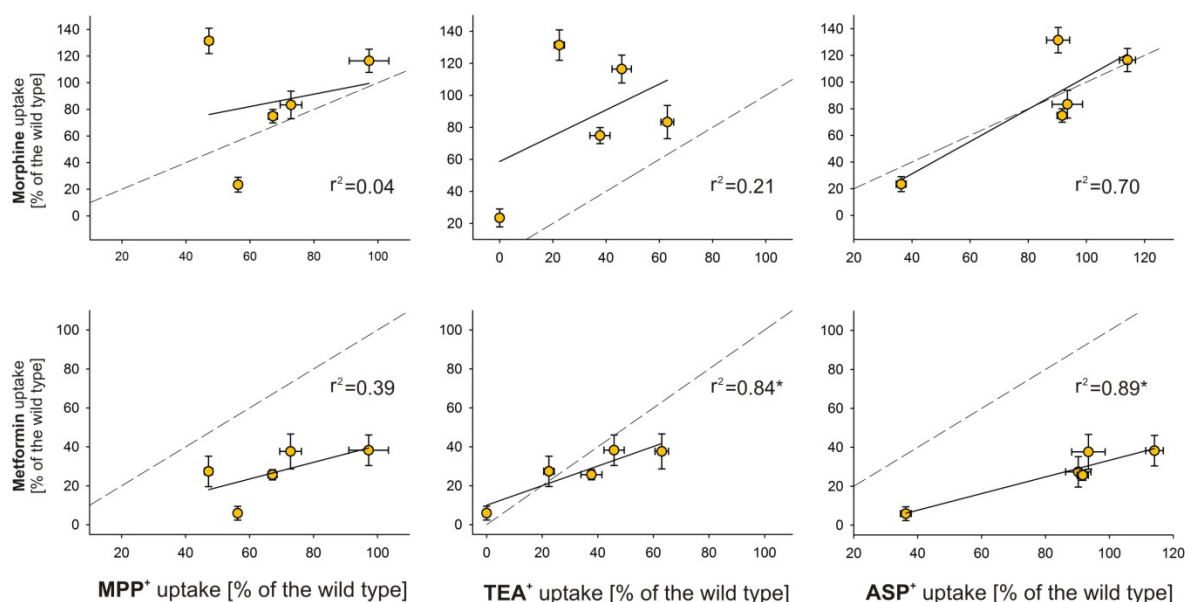


Figure 4.8 Correlation between the effects of the substrate-specific loss-of-function *OCT1* allelic variants on the uptake of model substrates and the drugs morphine and metformin. The effect of the alleles *OCT1**2, *OCT1**7, *OCT1**10, *OCT1**11, and *OCT1**13 on the transport of the model substrates MPP⁺, TEA⁺, and ASP⁺ was correlated to the effect on the transport of morphine and metformin. Shown are mean and standard error of the mean of at least three independent uptake measurements. Solid lines represent calculated linear regression curves; dashed lines represent an optimal theoretical correlation with identical effects of the allelic variants on the model substrates and drugs. * denotes significant correlation ($P < 0.05$). This figure was presented in a slightly modified form in Seitz *et al.* 2015 (Seitz *et al.*, 2015).

4.3 Interaction of M420del with other naturally occurring non-synonymous polymorphisms in OCT1

Recently, the M420del-M408 haplotype was associated with increased risk of imatinib treatment failure in 336 newly-diagnosed chronic phase patients suffering from chronic myeloid leukemia due to decreased imatinib uptake (Giannoudis *et al.*, 2013). In contrast, the haplotype M420del-V408 was shown to not affect the uptake of imatinib *in vitro* (Giannoudis *et al.*, 2013). However, PHASE and next-generation sequencing analyses by our research group revealed that the M420del only exists in combination with V408 (Tzvetkov *et al.*, 2014). None of the 371 individuals analyzed carried the haplotype M420del-M408. This was also true for further 1092 individuals from the 1000 genomes project. It was shown that the M420del exists exclusively together with valine₄₀₈ (Figure 1.2). However, for the purposes of this PhD project it was of interest, if there are possible

interactions between both amino acids in all theoretically possible haplotype combinations. Therefore, HEK293 cells were generated by stable transfection to overexpress all theoretically possible haplotype combinations: M420-M408, M420-V408, M420del-M408, and M420del-V408. Western blot analysis revealed equal protein expression of all four theoretically possible haplotypes (Figure 4.9 A). The subcellular localization of OCT1 was analyzed using immunofluorescence confocal microscopy. The OCT1 protein of all analyzed haplotype combinations was located in the plasma membrane as suggested by co-localization with Na^+/K^+ ATPase (Figure 4.9 B).

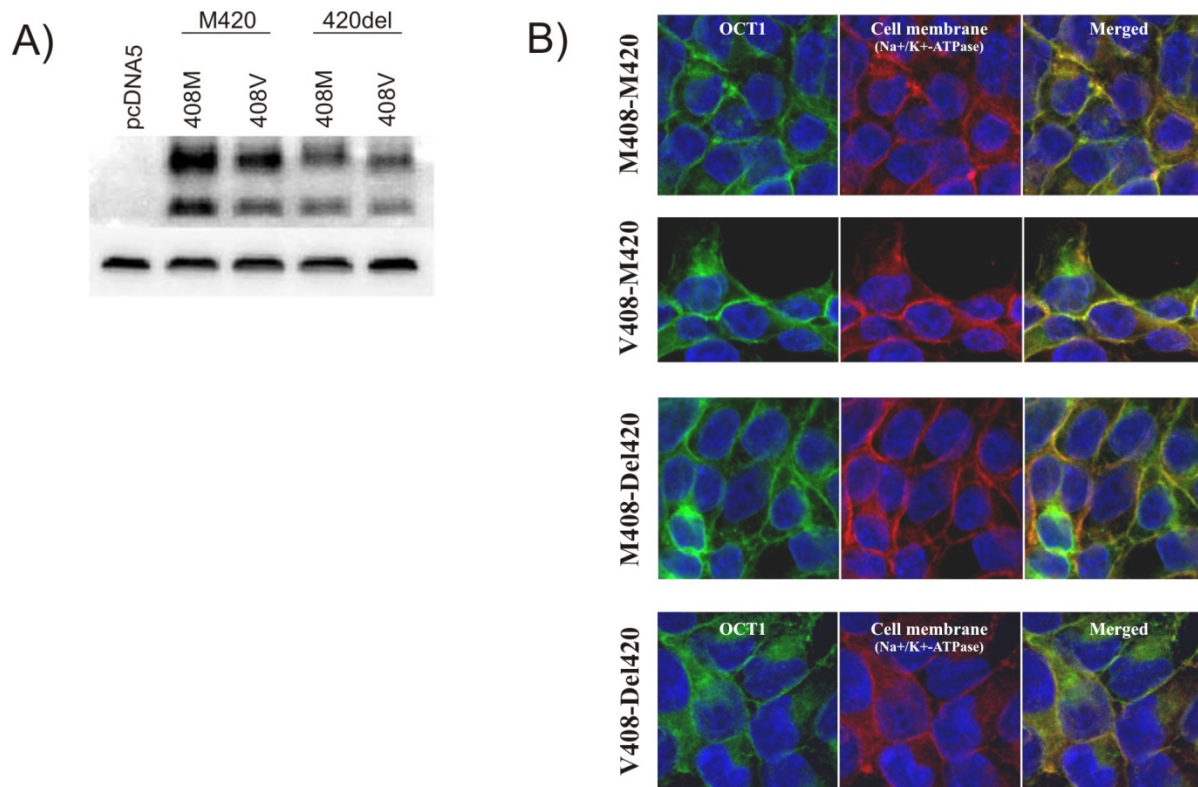


Figure 4.9 (previous page) Western blot and immunocytochemical analysis of OCT1 variants carrying all four theoretically possible haplotype combinations of M420del-M408V. (A) Western blot analysis was performed using 10 μg of total cellular protein lysates. OCT1 was detected using a mouse monoclonal OCT1-specific antibody (2C5). As a loading control GAPDH was stained using a mouse monoclonal GAPDH-specific (6C5) antibody. No apparent differences in protein amount could be detected between all four theoretically possible haplotype combinations. (B) Subcellular localization of OCT1 in HEK293 cells overexpressing all four theoretically possible M420del-M408V haplotypes was analyzed by immunostaining coupled to confocal microscopy. The OCT1 protein (green) was stained with a mouse monoclonal OCT1-specific antibody (2C5). Na^+/K^+ ATPase (red, the upper part) was stained using a Na^+/K^+ ATPase-specific rabbit monoclonal antibody (EP1845Y) as a plasma membrane marker and calnexin (red, the lower part) was stained with a calnexin-specific rabbit polyclonal antibody, which was used as a marker for the endoplasmic reticulum. The co-staining revealed membrane localization of all four haplotypes. Part of this figure was presented in Tzvetkov *et al.* 2014 and Seitz *et al.* 2015 (Tzvetkov *et al.*, 2014; Seitz *et al.*, 2015)

The cell lines overexpressing all four theoretically possible haplotype combinations of M420del-M408V were used to measure the uptake of MPP^+ , TEA^+ , ASP^+ , metformin, morphine, and debrisoquine (Figure 4.10). The M420del caused a substrate-specific loss of OCT1 transport activity independent of its combination with methionine₄₀₈ or valine₄₀₈. The M420del did not affect the uptake of MPP^+ and debrisoquine, neither in combination with methionine₄₀₈ nor valine₄₀₈. The M420del significantly decreased the uptake of TEA^+ by more than 60 %. The decrease was only slightly higher when M420del was in combination with M408 than with V408 (77 % and 62 %, respectively). However, also without the deletion of M420, V408 showed a slightly higher activity than M408, increasing TEA^+ uptake by 12 %. Similar effects were observed for morphine and metformin. Morphine uptake was decreased by 65 % and 25 % in M420del combined with methionine₄₀₈ or valine₄₀₈, respectively. As for TEA^+ the decrease was less strong in M420del cells in combination with V408 than with M408. However, also without deletion of M420, V408 slightly increased morphine uptake by 33 %. The uptake of metformin was reduced by 82 % and 75 % in M420del cells in combination with methionine₄₀₈ or valine₄₀₈, respectively.

In summary, M420deletion showed highly substrate-specific effects that were not affected by another naturally occurring polymorphism M408V.

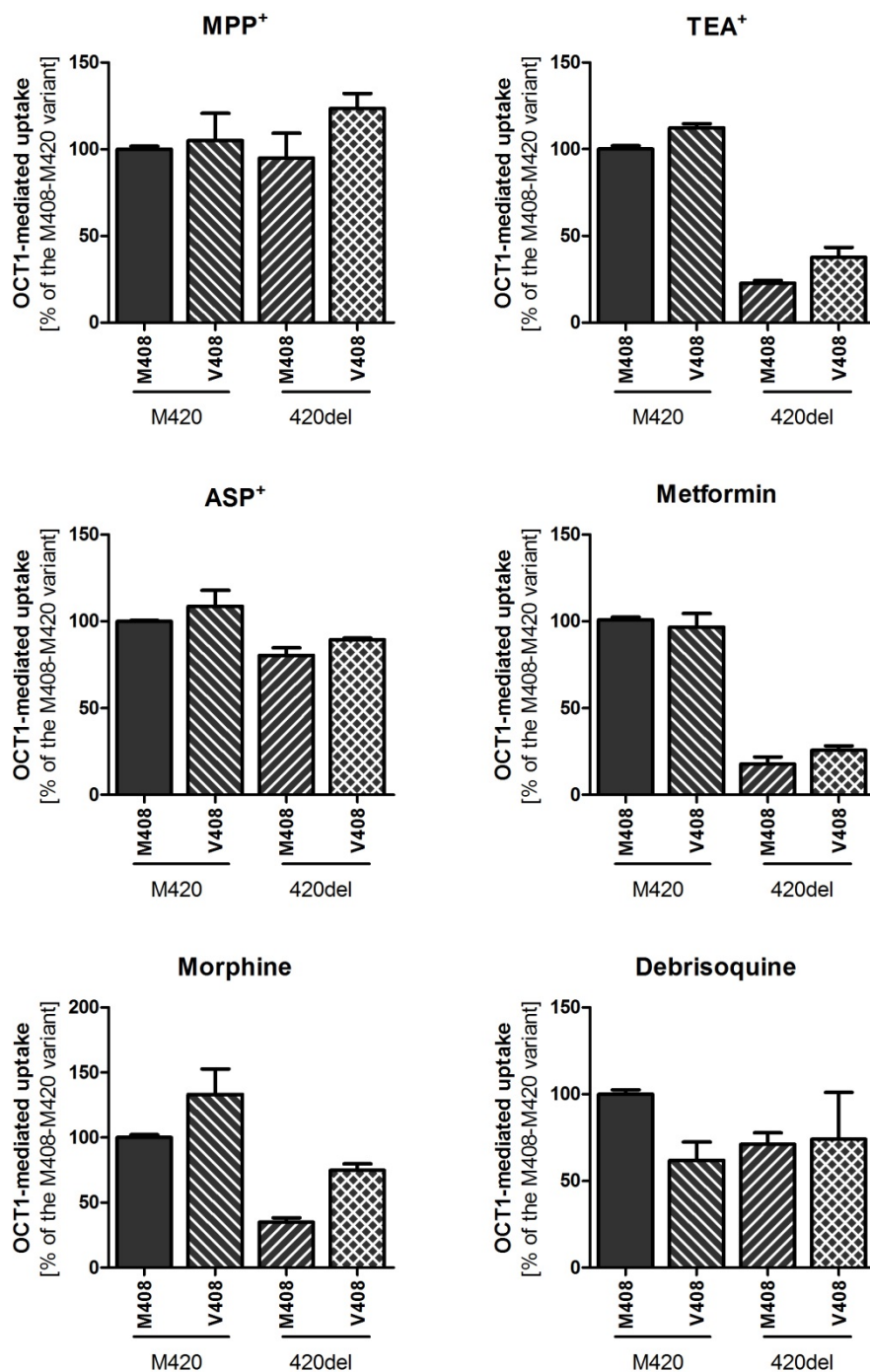


Figure 4.10 Comparison of the uptake activity of OCT1 variants carrying all theoretically possible M420del-M408V haplotypes. HEK293 cells stably transfected to overexpress all four possible combinations of the M420del-M408V genotypes were incubated for 2 min with 10 μ M MPP⁺, 5 μ M TEA⁺, 5 μ M ASP⁺, 1 μ M morphine, or 5 μ M metformin, or for 1 min with 1 μ M debrisoquine. The OCT1 mediated uptake was calculated by subtracting the uptake of the control cells (HEK293 cells transfected with the empty vector pcDNA5) from the uptake of the HEK293 overexpressing the indicated variants. Shown is the mean and error of the mean of at least three independent experiments. Part of these data was presented in Tzvetkov *et al.* 2014 (Tzvetkov *et al.*, 2014) and part in Seitz *et al.* 2015 (Seitz *et al.*, 2015).

Furthermore, the impact of other natural existing amino acid substitutions on the effect of M420del on OCT1 function was analyzed. Therefore, it was analyzed how the glycine to alanine substitution at codon 414 (G414A) modified the effects of M420del on transport activity of the OCT1 variants. Also in this case only the haplotype combinations G414-M420 (*OCT1*1B*), G414-420del (*OCT1*2A*), and A414-420del (*OCT1*2C*), but not A414-M420, were identified in the worldwide population genetic analysis of OCT1 and was characterized as a substrate-specific loss of function variant (Figure 4.5, (Seitz et al., 2015)).

However, also in this case for the purposes of this PhD project it was of interest, if there are possible interactions between both amino acids in all theoretically possible haplotype combinations. Therefore, HEK293 cells stably transfected by chromosomal integration were generated to overexpress the following haplotypes: G414-M420, G414-420del, A414-M420, A414-420del. Due to the findings presented in the previous paragraph, cell lines carrying a deletion of methionine₄₂₀ were generated in combination with valine₄₀₈. The cell lines were used to measure the uptake of MPP⁺, TEA⁺, ASP⁺, morphine, and metformin (Figure 4.11). The combination A414-M420 displayed the same transport activity as the wild type cells (M420-G414). In contrast, cells carrying the deletion of methionine₄₂₀ showed a substrate-specific loss of activity. The effect was independent of glycine₄₁₄ or its substitution to alanine₄₁₄. The M420del decreased the uptake of MPP⁺ by 35% and 30 % when combined with glycine₄₁₄ or alanine₄₁₄, respectively. The uptake of ASP⁺ was only slightly decreased by 25 % and 22 % when M420del was combined with glycine₄₁₄ or alanine₄₁₄, respectively. In contrast, the uptake of TEA⁺ was strongly decreased by 82 % and 77 % when M420del was combined with glycine₄₁₄ or alanine₄₁₄, respectively.

In summary, these data indicate that M420del determinates the effects of OCT1 transport activity both in combination with G414A and M408V. However, as M420del was observed only on V408 background all further experiments were performed using constructs containing valine and not methionine at position 408.

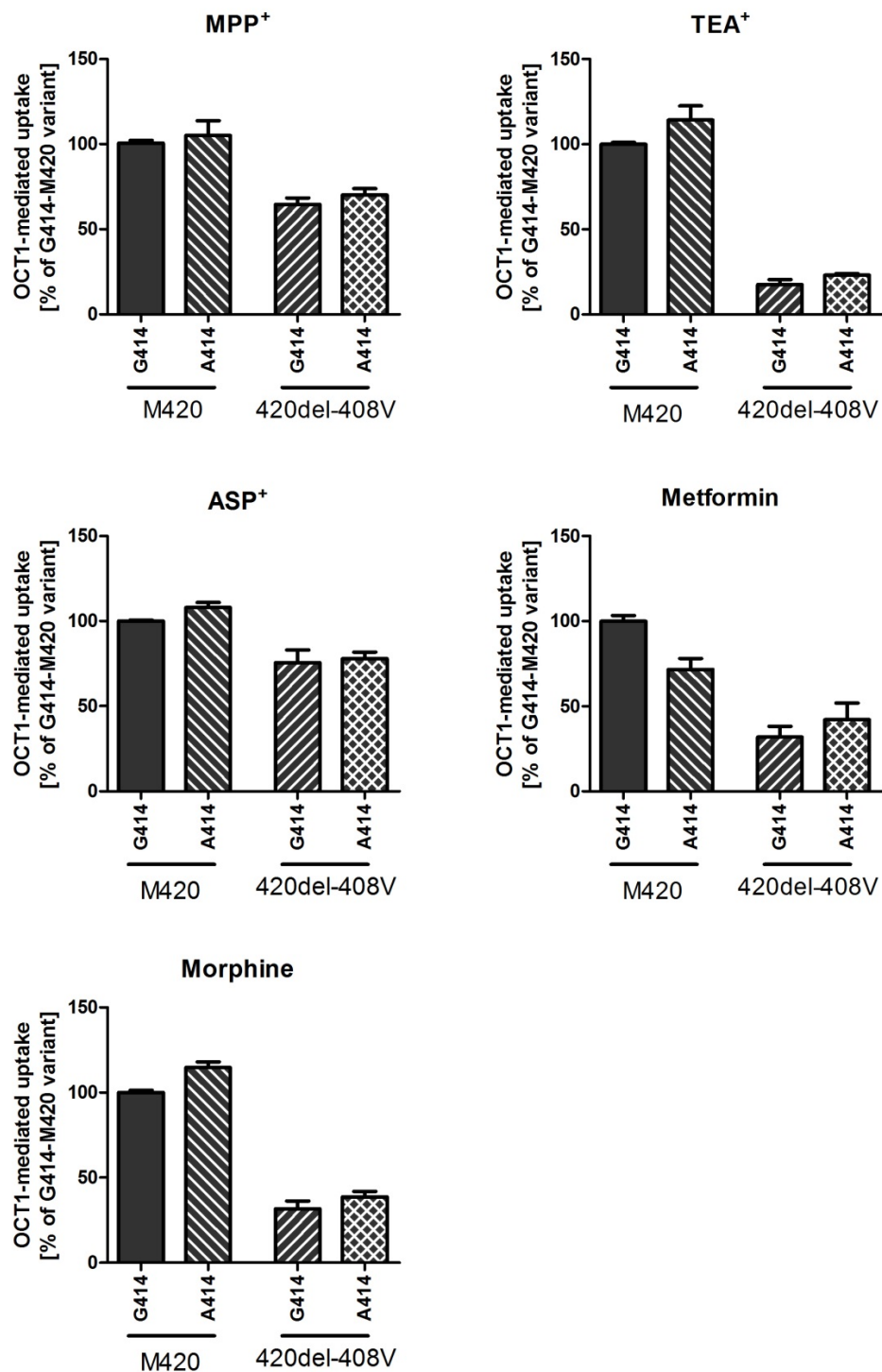


Figure 4.11 Combined effects of G414A and M420del on OCT1-mediated uptake. HEK293 cells stably transfected to overexpress all four theoretically possible M420del-G414A haplotypes were incubated for 2 min with 10 μ M MPP⁺, 5 μ M TEA⁺, 5 μ M ASP⁺, 1 μ M morphine, or 5 μ M metformin. The OCT1-mediated uptake was calculated by subtracting the uptake of the control HEK293 cells stably transfected with the empty vector pcDNA5 from HEK293 cells overexpressing the indicated OCT1 variants. Shown is the mean and error of the mean of at least three independent experiments.

4.4 In-depth analysis of the effects of M420del on OCT1 function

The M420del is the most frequent and the only ubiquitously observed loss of function polymorphism in OCT1 (Figure 1.3; (Kerb et al., 2002; Shu et al., 2003; Seitz et al., 2015). The affected methionine₄₂₀ is located in the 9th transmembrane domain of the protein (Figure 1.1). Up to now it is not reported that the 9th transmembrane domain is involved in substrate binding or in the transport mechanism of OCT1. However, our substrate-wide analyses of OCT1 transport activity revealed highly substrate-specific effects ranging from limited reduction in the uptake of ASP⁺ (92% of the reference *OCT1*1* allele) to close to complete loss of transport of O-desmethyltramadol and tropisetron (20 % and 11 % of the reference allele, respectively, Figure 4.5). The aim of this part of the thesis was the in-depth analysis of the effects of the deletion of methionine₄₂₀ on OCT1 activity.

4.4.1 Substrate-specific effects of the M420del variant

The substrate-wide analysis revealed highly substrate-specific effects of the M420del variant (Figure 4.5). Here these substrate-specific effects were analyzed in-depth by determining the effects of M420del variant on the uptake kinetics of different OCT1 substrates. Determined were K_m and v_{max} of TEA⁺, MPP⁺, ASP⁺, metformin, sumatriptan, and proguanil transport. Ranitidine was analyzed by Marleen Meyer and fenoterol was analyzed by Sherin Pojar, colleagues from our working group, but the data was also included in the comparative analyses made in this work (Pojar, 2015).

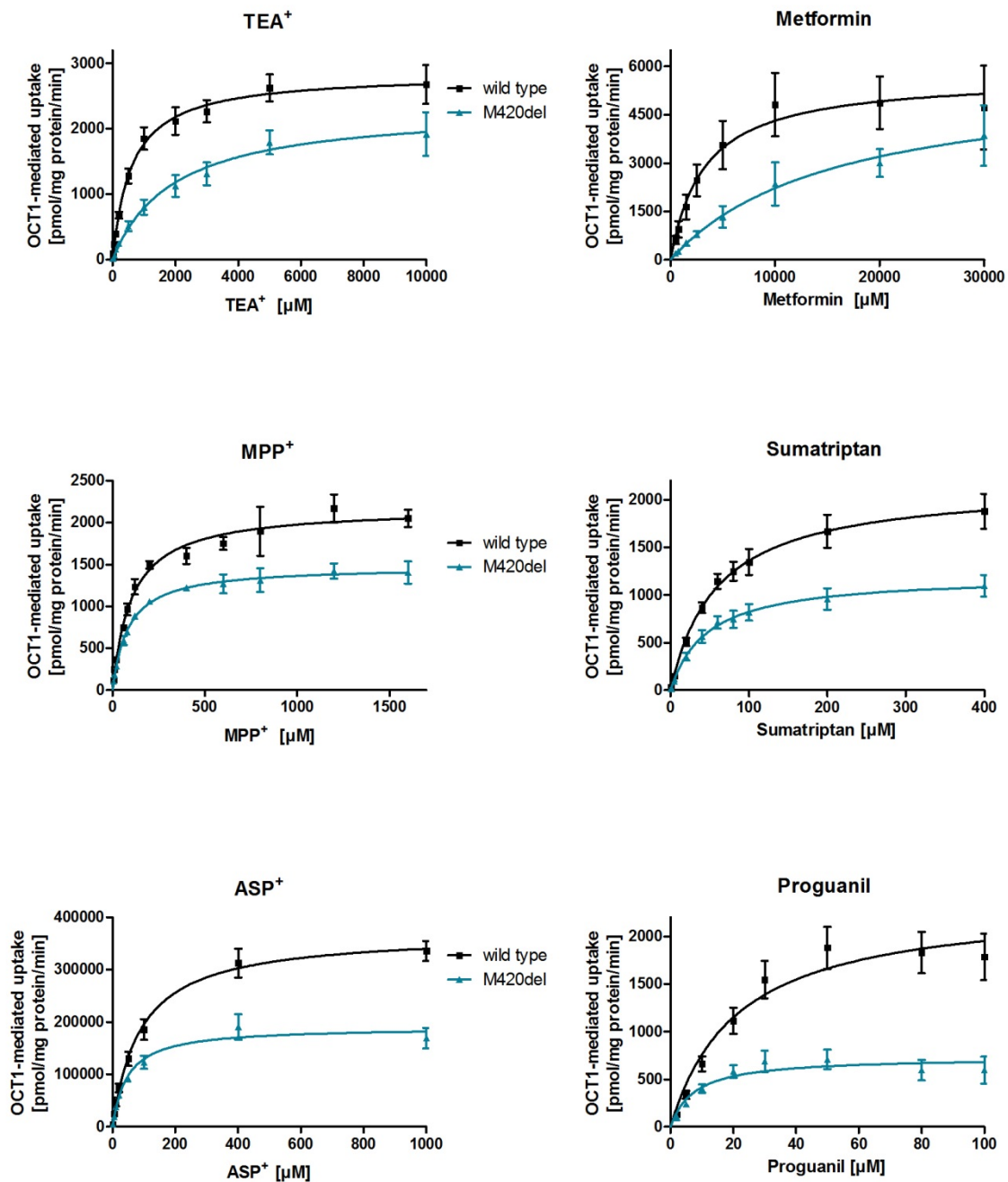


Figure 4.12 Substrate-specific effects of M420del. HEK293 cells stably transfected to overexpress wild type *OCT1* (*OCT1*1A*) or the M420del allelic variant (*OCT1*2*) were incubated for 2 min with increasing concentrations of TEA⁺, MPP⁺, ASP⁺, metformin, sumatriptan, or proguanil. The OCT1-mediated uptake was calculated by subtracting the uptake of cells stably transfected with the control vector pcDNA5 from wild type and M420del cells. Shown is the mean and error of the mean of at least three independent experiments.

The concentration dependence of the uptake for the different substrates was measured and the K_m and v_{max} values were calculated in comparison between wild type OCT1 (reference allele *OCT1*1A*) and OCT1 variant carrying M420del (*OCT1*2A*). M420del showed saturable uptake kinetics for all substrates tested. However, as expected from the single concentration measurements (chapter 4.1.2, Figure 4.5), M420del variant showed strong substrate-specific differences in the uptake. The v_{max} was reduced for all substrates tested, except for metformin, in M420del cells in comparison to wild type OCT1. The degree of decrease was also strongly substrate-specific. The v_{max} was reduced by 30 % for TEA⁺ and by 85 % for fenoterol in M420del cells (Figure 4.13). For metformin the apparent v_{max} was similar between M420del and wild type cells (5671 pmol/mg protein/min and 6240 pmol/mg protein/min, respectively). In relation to wild type, the K_m for MPP⁺, ASP⁺, sumatriptan, proguanil as well as for fenoterol and ranitidine is reduced in M420del cells. The decrease in K_m ranges from 17 % for MPP⁺ up to 65% for proguanil (Figure 4.13). In contrast, the K_m for TEA⁺ and metformin increased in M420del cells by 200 % and 400 %, respectively, compared to wild type (Figure 4.13). This demonstrates a highly substrate-specific decrease in the affinity of the Met420del variant for TEA⁺ and metformin.

Table 4.3 Kinetic parameters of wild type OCT1 and M420del HEK293 cells for different substrates

		Km [μ M]						
Variant	MPP ⁺	TEA ⁺	ASP ⁺	Sumatriptan	Proguanil	Metformin	Fenoterol ¹	Ranitidine ²
Wild type	108.6 \pm 17.4	589.5 \pm 44.0	93.4 \pm 19.3	58.9 \pm 5.1	21.7 \pm 3.3	3402.0 \pm 537.6	2.3 \pm 0.2	54.5 \pm 7.2
M420del	86.5 \pm 12.0	1778.4 \pm 164.5	46.4 \pm 8.7	46.3 \pm 0.6	7.9 \pm 2.1	17047.8 \pm 1127.5	1.0 \pm 0.2	52.2 \pm 8.4
		v _{max} [pmol/mg protein/min]						
Variant	MPP ⁺	TEA ⁺	ASP ⁺²	Sumatriptan	Proguanil	Metformin	Fenoterol ¹	Ranitidin ²
Wild type	2263.7 \pm 184.2	2848.7 \pm 207.6	372678.0 \pm 29568.8	2167.3 \pm 243.5	2385.7 \pm 306.5	5670.5 \pm 991.4	80.8 \pm 4.0	1047.1 \pm 123.4
M420del	1484.0 \pm 107.1	2114.8 \pm 206.8	185575.0 \pm 19693.1	1203.8 \pm 128.8	744.2 \pm 132.7	6239.8 \pm 915.5	12.4 \pm 0.9	402.0 \pm 51.2

¹ Data generated by Sherin Pojar and ² in tight collaboration with Marleen Meyer

² [RFU/mg protein/min]

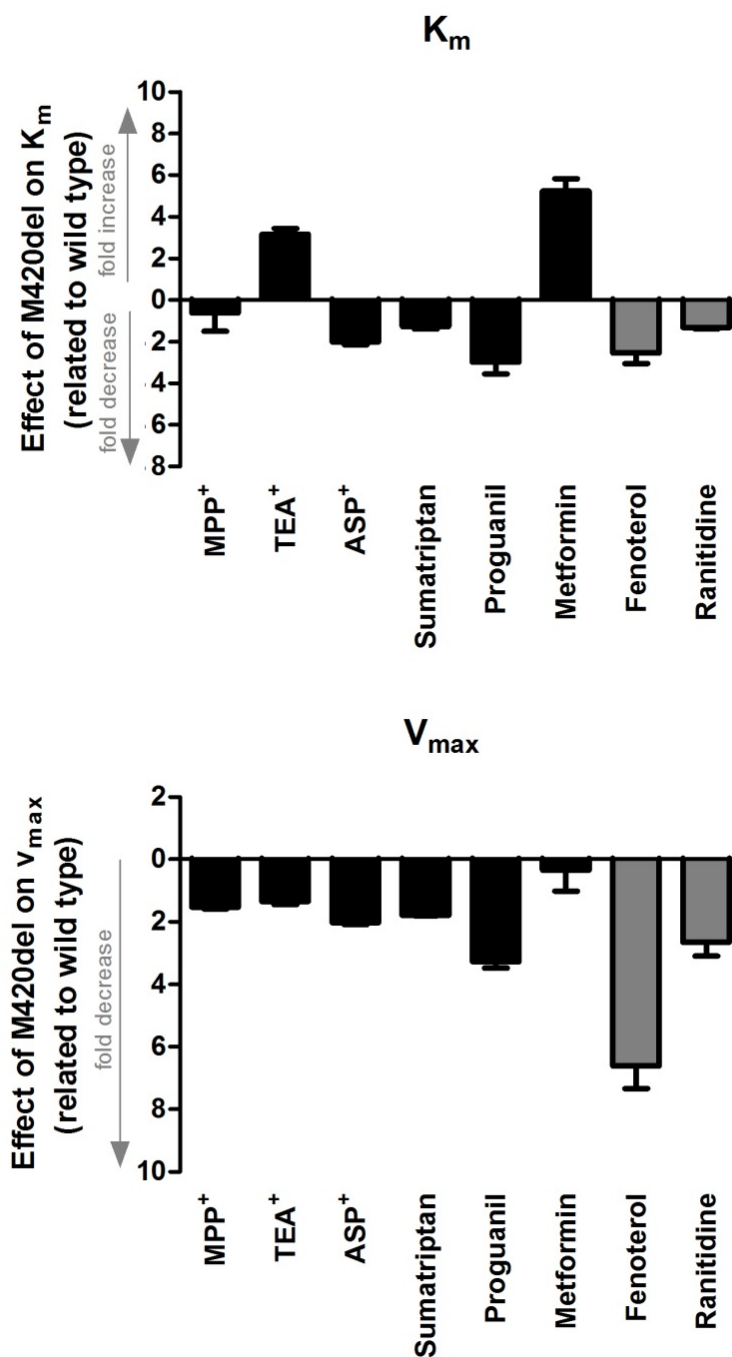


Figure 4.13 Differences in K_m (upper part) and v_{max} (lower part) of the M420del in relation to wild type OCT1. Shown is the mean and error of the mean of the differences between M420del and wild type from at least three independent experiments. K_m and v_{max} are based on results shown in Figure 4.12. Fenoterol values were obtained from the work of Sherin Pojar (Pojar, 2015). Ranitidine results were obtained in close collaboration with Marleen Meyer from our working group.

In order to ensure that inter-day differences like different cell passages did not affect the extent of the observed substrate-specific loss of activity of the M420del variant, simultaneous uptake measurements with fenoterol and sumatriptan were performed. The two drugs were chosen as fenoterol was strongly affected and sumatriptan was weakly affected by M420del. The uptake at three different concentrations (below K_m , close to K_m , and close to v_{max}) on the same day using identical cell passages was measured. The effect of M420del on the uptake of fenoterol and sumatriptan did not differ in three independent experiments (Figure 4.14). The M420del variant decreased the uptake of fenoterol and sumatriptan at the lowest concentration tested (0.1 μM for fenoterol and 1 μM for sumatriptan) by 41.2 % and 3.6 %, respectively. For the uptake of 1 μM sumatriptan, clear variability for the impact of M420del on sumatriptan uptake due to experimental conditions was observed: in two of three experiments the M420del decreased the uptake of 1 μM sumatriptan by 9.3 % and 3.9 %. In one experiment the M420del increased the uptake by 2.7 %. However, the data fluctuate around zero, indicating that the M420del does not affect the uptake of 1 μM sumatriptan. The M420del variant decreased the uptake of 2 μM and 25 μM fenoterol on average by 70.4 % and 71.3 %, respectively. The M420del variant decreased the uptake of 60 μM and 400 μM sumatriptan on average by 41.2 % and 47.2 %, respectively. The values observed were in line with the ones measured for sumatriptan and fenoterol in the early experiments (Figure 4.12 and (Pojar, 2015)). This experiment confirmed that the observed highly substrate-specific effects of M420del on OCT1 activity were not an artefact due to inter-day variability in the measurements.

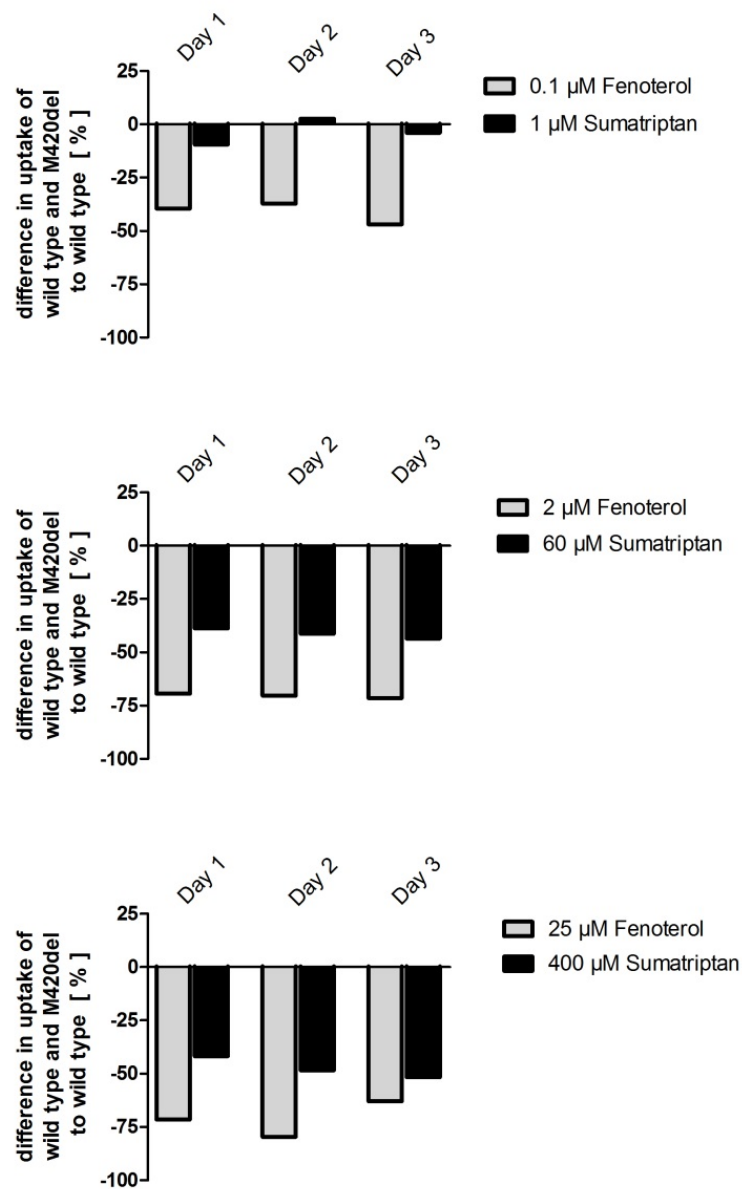


Figure 4.14 Simultaneous uptake measurements of fenoterol and sumatriptan in wild type and M420del cells. In order to exclude inter-day differences, the uptake of sumatriptan and fenoterol was measured at three different concentrations (below K_m , close to K_m , and close to v_{max}) on the same day using identical cell passages.

4.4.2 Reduction of the extracellular loop between the 9th and the 10th TMD cannot explain the effect of M420del

The *M420del* polymorphism is a deletion of a single amino acid. One hypothesis to explain the effects of the M420del variant is that not the methionine₄₂₀ specifically, but the deletion itself causes the effects. A deletion of an amino acid at this position causes a reduction of

the extracellular protein chain between the 9th and the 10th transmembrane domain. This may change the positions of amino acids in the 10th transmembrane domain. The amino acids A443, L447, Q448, and C451 in the 10th transmembrane domain were suggested to be involved in formation of the substrate binding cleft (Gorboulev et al., 2005; Sturm et al., 2007). Hence, changes of amino acid positions in the 10th transmembrane domain may affect substrate binding and affinities. To test this hypothesis, two artificial mutations, L427del and H428del, were generated on wild type background (Figure 4.15). These two amino acids are located directly in the loop between the 9th and the 10th transmembrane domain. Additionally, an insertion mutant was generated on M420del background: An insertion of alanine after proline₄₂₅ (A426ins), which should restore the length of the loop between the 9th and the 10th transmembrane. In case that the observed effect of the M420del is due to the shortening of the extracellular protein chain, *OCT1* L427del or H428del should cause the same effect on transport activity as M420del. In contrast, the insertion of alanine₄₂₆ on M420del background should restore transport activity to the levels of the wild type.

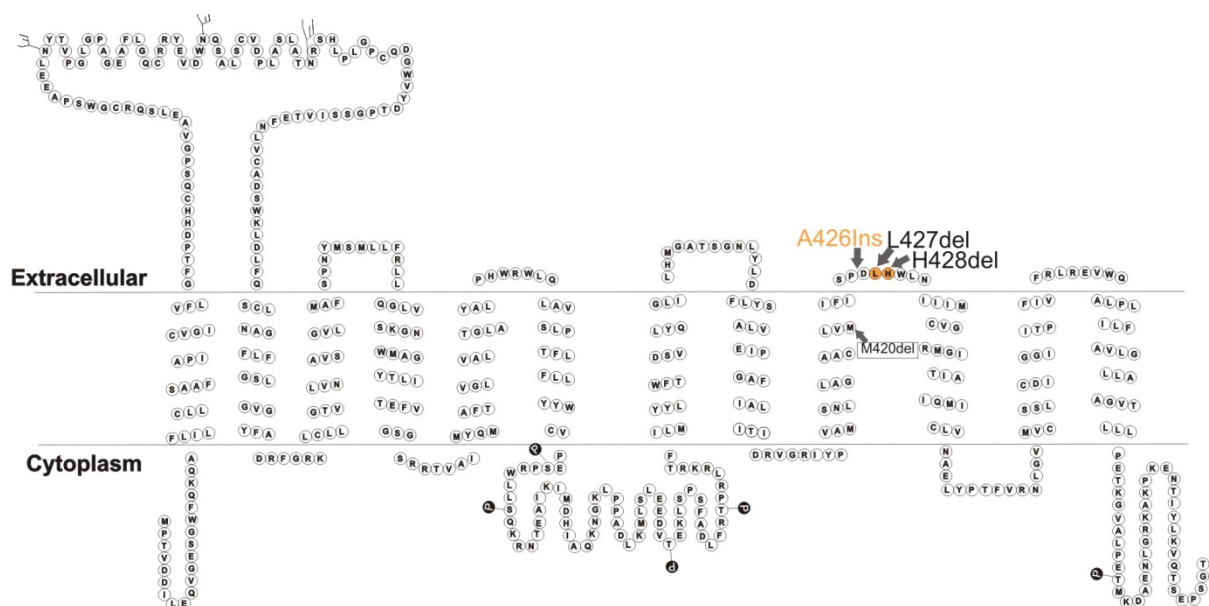


Figure 4.15 Secondary structure of OCT1 showing the mutations, which were used to analyze if the substrate-specific effects of M420del are caused by reduction of the protein chain resulting in shortening of the extracellular loop between transmembrane domains 9 and 10.

The artificially mutated constructs were generated and stably transfected in HEK293 cells. Briefly, point mutations were introduced into pcDNA3.1::hOCT1 using site-directed mutagenesis PCR (Table 2.5). The mutated OCT1 gene was re-cloned into the pcDNA5 expression vector. The generated pcDNA5 plasmids (Table 2.6) were used for stable transfection into HEK293 cells.

In order to validate the generated cell lines three integration-specific PCRs were performed (chapter 3.1.6). PCR 1 and PCR 2 were performed to verify integration of pcDNA5 into the genome of HEK293 cells and to detect the gene of interest within the integration site. Figure 4.16 shows results of PCR 1 and PCR 2 of the clone that was used for further analyses. PCR 1 resulted in an amplification product of 519 bp. PCR 2 resulted in an amplification product of 1376 bp for the empty pcDNA5 vector and of 3137 bp for pcDNA5 containing *OCT1* or its variants, respectively. PCR 3 was performed in order to identify possible multiple tandem integration of the expression vector pcDNA5 containing OCT1 into the genome of HEK293 cells. All of the variants tested were confirmed as single integrands, as no amplification product was obtained (data not shown). The strong and homogenous mRNA expression of the clones was confirmed by real-time qPCR (Figure 4.16 C)

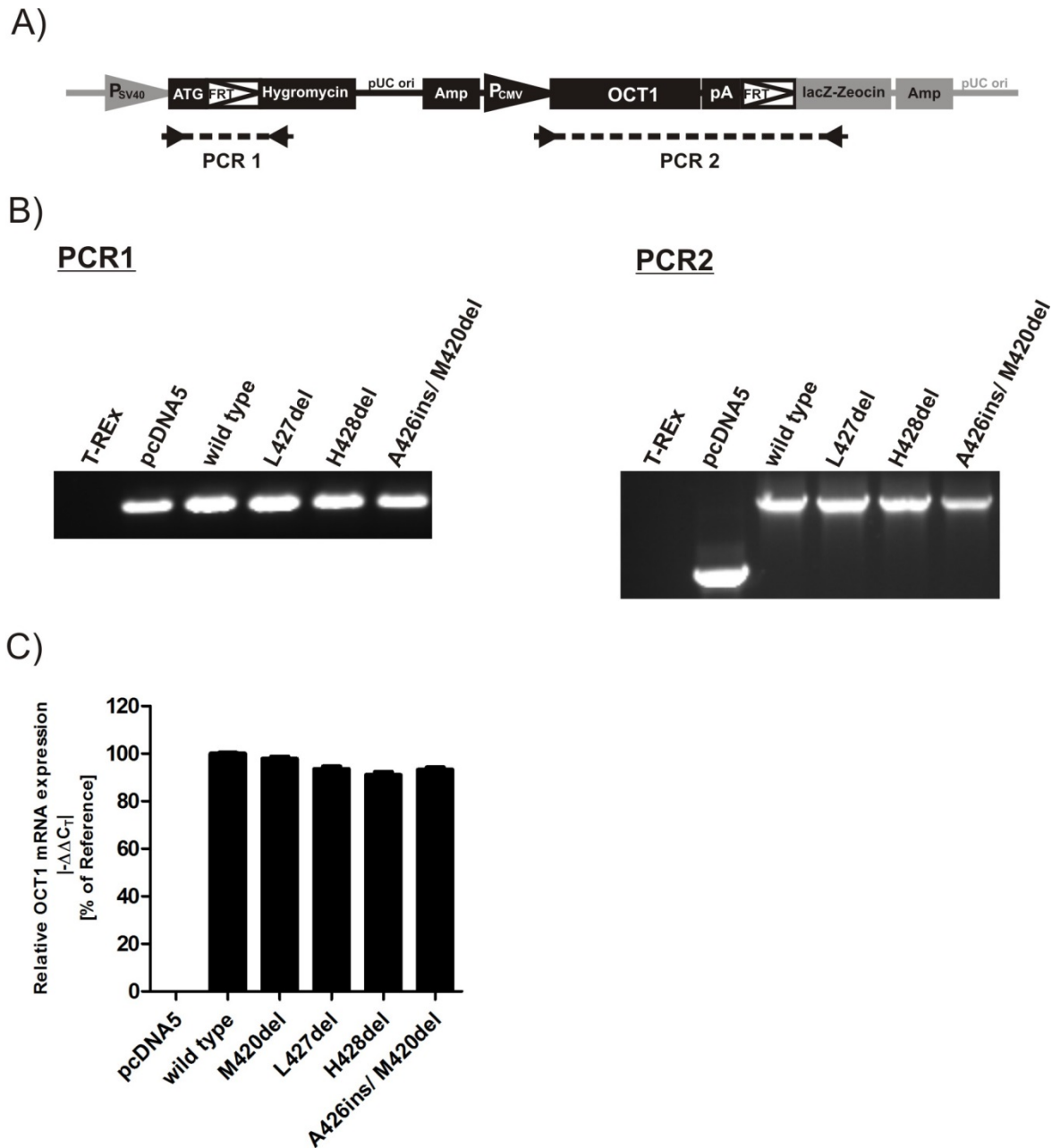


Figure 4.16 Validation of HEK293 cells overexpressing the *OCT1* mutants L427del, H428del, A426ins/M420del (A) Schematic representation of the expression plasmid pcDNA5 (black) integrated into the pFRT/lacZeo site of the genome of HEK293 cells (gray) as represented in Seitz *et al.* (Seitz *et al.*, 2015). The positions of the primers and the amplicons of PCR 1 and PCR 2 are indicated. (B) PCR 1 resulted in an amplification product of 519 bp and PCR 2 resulted in an amplification product of 1376 bp (for the control cells transfected with the empty pcDNA5 vector) or 3137 bp (transfected with pcDNA5 containing *OCT1*). (C) Relative mRNA expression using real-time qPCRs demonstrating high and equal *OCT1* mRNA levels among wild type *OCT1* and the generated mutants. Shown is the mean and error of the mean of three independent RNA extractions.

The OCT1 mutants were compared with M420del and wild type variants in their ability to transport TEA⁺, MPP⁺, and ASP⁺ at single concentration (Figure 4.17). Neither L427del and H428del on wild type background caused a decrease in TEA⁺ uptake that could be compared to those observed by M420del, nor A426ins increased the uptake of the M420del variant (Figure 4.17 A). The uptake in the L427del mutant was not significantly different to wild type cells. The uptake of TEA⁺ in H428del cells was decreased by 39 %, but this decrease was not statistically significant. More importantly, the TEA⁺ uptake of A426ins on M420del background did not differ from the M420del uptake (4.33 and 4.32 pmol/min/mg protein, respectively). No significant differences in the uptake of MPP⁺ and ASP⁺ were observed between wild type and M420del cells: M420del decreased the uptake of MPP⁺ by 22 % (Figure 4.17 B); the uptake of ASP⁺ did not differ from wild type cells (Figure 4.17 C). Therefore these substrates were only of limited use in this experiment.

The mutants L427del, H428del as well as A426ins did not show significant differences in the uptake of MPP⁺ and ASP⁺ compared to wild type and M420del cells, respectively, indicating that these mutations did not have an impact on MPP⁺ and ASP⁺ uptake themselves. These results suggest that the substrate-specific effects observed for the M420del are not caused by unspecific effects of the amino acid deletion but rather by the deletion of the methionine at this position.

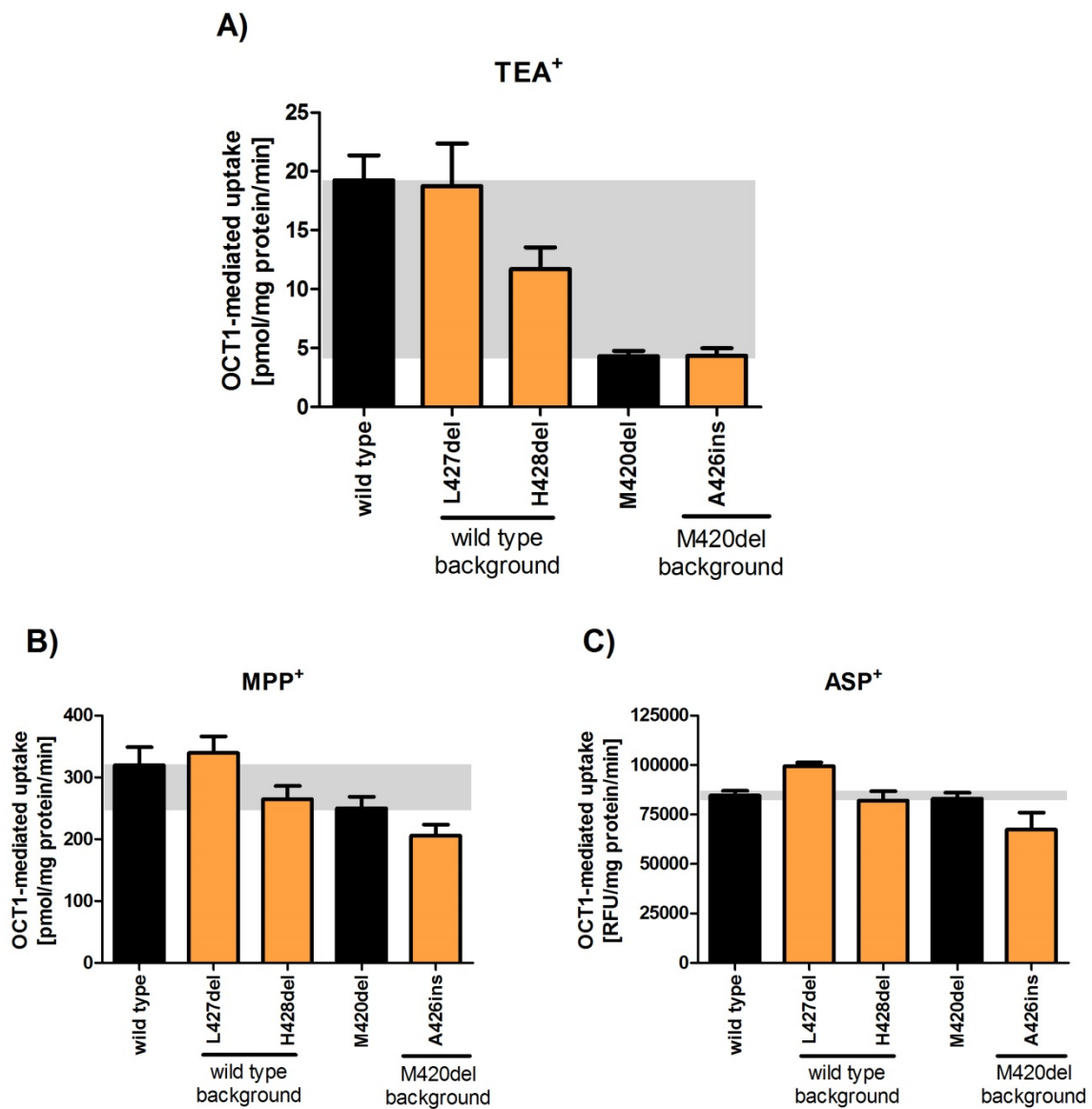


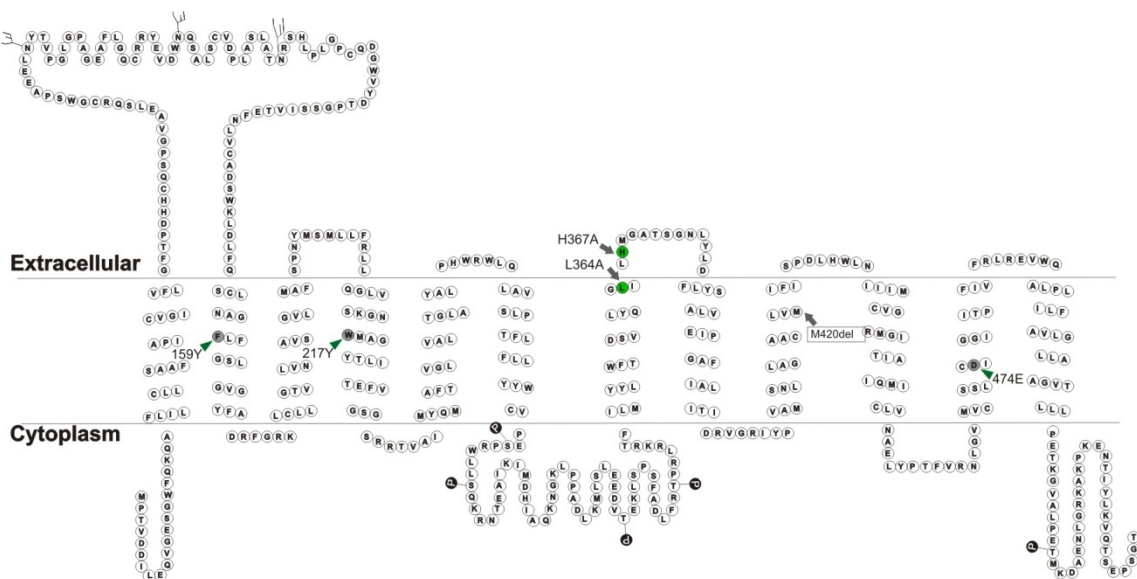
Figure 4.17 Effects of single amino acid deletions or insertion within the extracellular loop between TMD 9 and TMD 10 on OCT1-mediated uptake of MPP⁺, TEA⁺, and ASP⁺. HEK293 cells stably transfected to overexpress the wild type, the M420del variant as well as the mutants L247del, H428del, and A426ins were incubated for 2 min with 5 μ M TEA⁺(A), 10 μ M MPP⁺ (B), or 5 μ M ASP⁺ (C). The OCT1-mediated uptake was calculated by subtracting the uptake of the control cells stably transfected with the empty expression vector pcDNA5. The gray area highlights the difference in the uptake between the wild type and the M420del OCT1 variant. Shown is the mean and error of the mean of three independent experiments.

4.4.3 The observed substrate-specific effects of the M420del variant are caused by loss of the methionine side chain

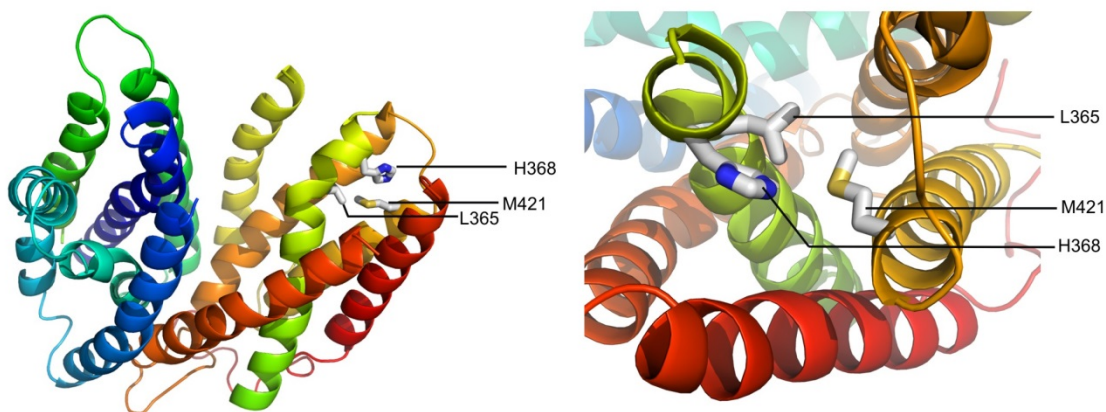
After it could be excluded that the effects of M420del are caused by simple reduction of the protein chain, the interaction of methionine₄₂₀ with other amino acids and the methionine side chain properties were analyzed in detail.

First, the interaction of methionine₄₂₀ with amino acids in the 7th transmembrane was analyzed. Based on the homology model of rat Oct1, it was suggested that due to protein folding the 9th and the 7th transmembrane domain are in close contact (Figure 4.18). The 7th transmembrane is known to be involved in substrate binding (Popp et al., 2005). By deletion of methionine₄₂₀ the more bulky amino acid isoleucine₄₂₁ is suggested to be roped into the membrane. This may change the interaction and position of amino acids in the 7th transmembrane domain. Especially, based on the model (Figure 4.18) a potential steric conflict was suggested between I420 and the amino acids L364 and H367. To test this hypothesis, mutants of *OCT1* were generated leading to substitution of leucine₃₆₄ or histidine₃₆₇ against alanine on M420del background, respectively. As alanine has a very short side chain, the suggested steric interference should be avoided in these mutants. If this is the case, the mutants L364A and H367A on M420del background should display the same transport activity as wild type OCT1.

A)



B)



C)

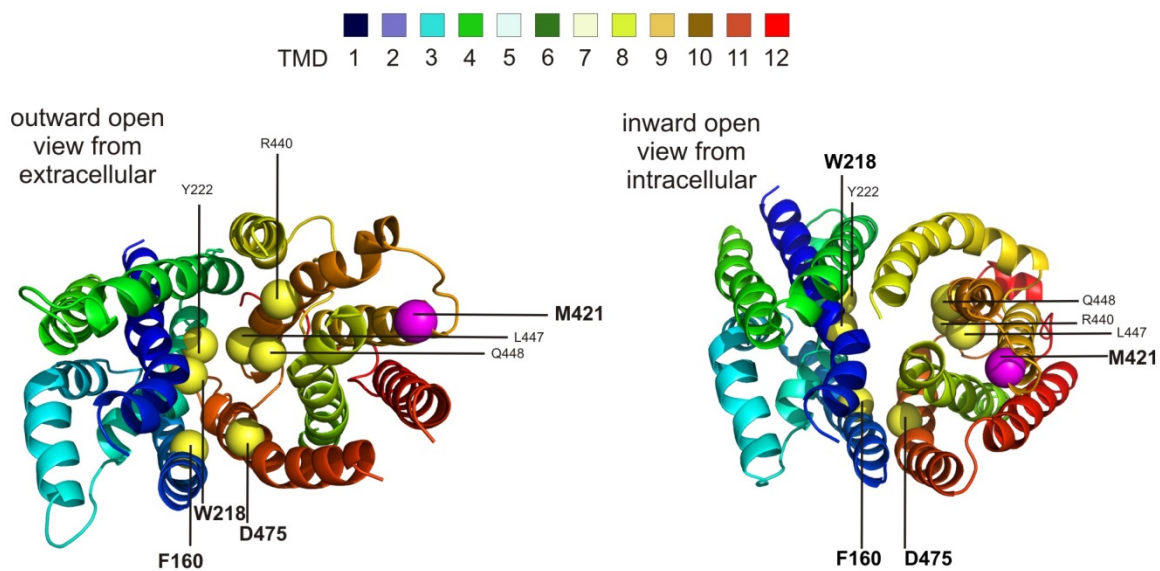
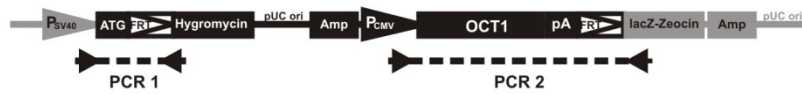


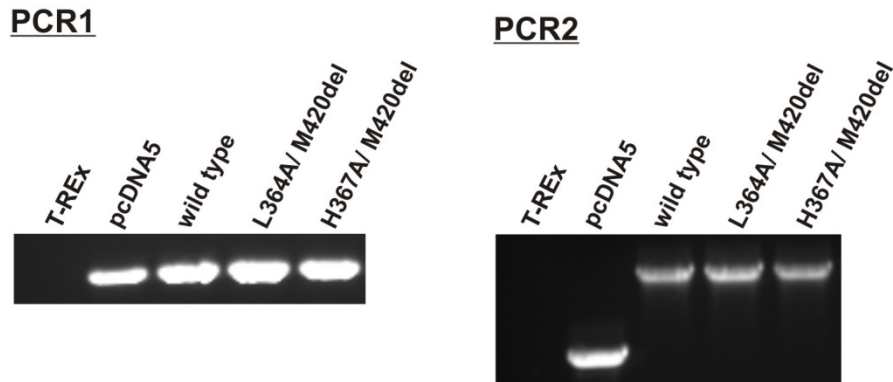
Figure 4.18 (previous page) Secondary and 3D structure of OCT1 showing the mutations L364A and H367A as well as F159Y, W217Y, and D474E that were generated to test whether the substrate-specific effects of M420del are caused by sterical interactions with amino acids in TMD 7 or key amino acids involved in the substrate binding or translocation. A) Secondary structure of human OCT1. Mutations that were generated to test if M420del interacts with amino acids in the 7th transmembrane domains are shown in orange. Mutations that were generated in order to analyze possible interactions of M420del with amino acids previously reported to be involved in the transport mechanism of rat Oct1 are shown in grey. B) Homology model of the outward open conformation of rat Oct1. The amino acids L365 and H368 (nitrogen shown in blue) in the 7th transmembrane domain and M421 (sulfur shown in yellow) in the 9th transmembrane domain are indicated. C) Homology model of open outward (left) and open inward (right) conformation of rat Oct1. The amino acids F160, W218, Y222, R440, L447, Q448, and D475, which are known to be involved in transport mechanism, are presented as spheres in the substrate binding cleft and are shown from the extracellular and intracellular side. Possible interactions between the amino acids F160, W218, and D475 and M421 (shown in bold) were analyzed. The transmembrane domains are colored as indicated. The 3D model of rat Oct1 is based on the crystal structure of LacY of *E.coli* (Popp et al., 2005; Gorbunov et al., 2008). The PDB file was kindly provided by Thomas Mueller from the University of Würzburg. Presentation and editing was made using PyMOL with kind support of Ralph Krätzner from the Department of Pediatrics and Adolescent Medicine, University Medical Center Göttingen

HEK293 cells were generated by targeted chromosomal integration to overexpress the mutants *L364A* and *H367A* on M420del background. The correct integration of the expression plasmid into the genome of HEK293 cells, the strong and homogenous mRNA expression and the correct membrane localization of the clones were confirmed (Figure 4.19).

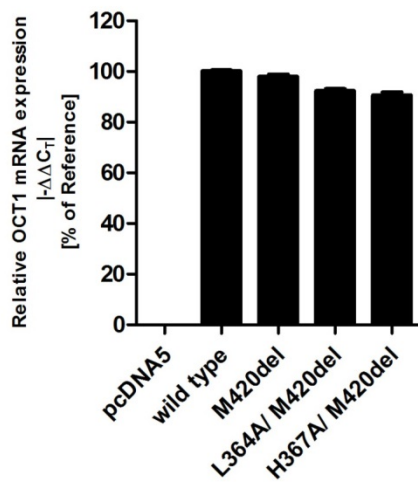
A)



B)



C)



D)

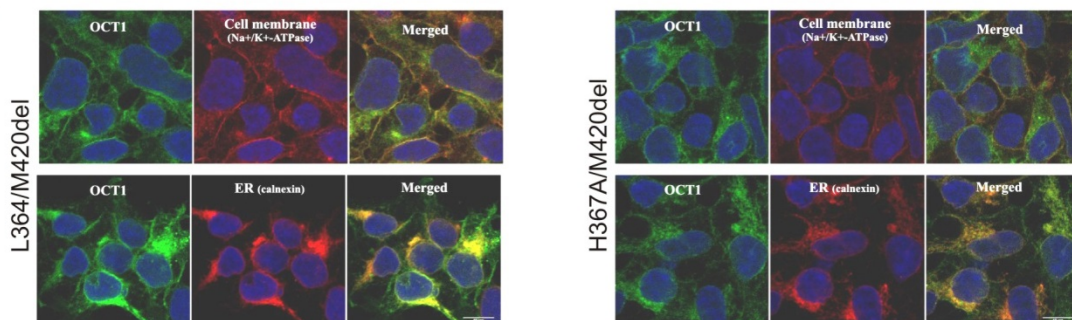


Figure 4.19 (previous page) Validation of HEK293 cells overexpressing the mutants *L364A* and *H367A* on M420del background (A) Schematic presentation of the expression plasmid pcDNA5 (black) integrated into the pFRT/lacZeo site of the genome of HEK293 cells (gray) as represented in Seitz *et al.* (Seitz *et al.*, 2015). The positions of the primers and the amplicons of PCR 1 and PCR 2 are indicated. (B) PCR 1 resulted in an amplification product of 519 bp and PCR 2 resulted in an amplification product of 1376 bp (for the control cells transfected with the empty pcDNA5 vector) or 3137 bp (transfected with pcDNA5 containing *OCT1*). (C) Relative mRNA expression using real-time qPCRs demonstrating high and equal *OCT1* mRNA levels among wild type *OCT1* and the generated mutants. Shown is the mean and error of the mean of three independent RNA extractions. (D) Immunocytochemical staining of *OCT1* (green) co-stained with Na^+/K^+ ATPase (red, upper part) as a plasma membrane marker, or calnexine (red, lower part) as a marker of endoplasmic reticulum.

The *OCT1* mutants were compared with M420del and wild type variants for their ability to transport TEA^+ , MPP^+ , and ASP^+ at single concentrations (Figure 4.20). The M420del did not significantly affect the uptake of MPP^+ and ASP^+ compared to wild type *OCT1* (Figure 4.20 A). In contrast, the mutants *L364A* and *H3647A* significantly decreased the uptake of MPP^+ ($P \leq 0.01$ and $P \leq 0.001$, respectively) and ASP^+ ($P \leq 0.01$ and $P \leq 0.001$, respectively) compared to wild type *OCT1*. *L364A* and *H367A* decreased the uptake of MPP^+ by 53 % and 82 %, respectively, and the uptake of ASP^+ was decreased by 16 % and 62 %, respectively. The results suggested involvement of *L364* and *H367* in transport of MPP^+ and *H367* in transport of ASP^+ .

To test whether the observed effect of *L364A* and *H367A* mutants is independent of wild type or M420del background, the amino acid substitution leucine₃₆₄ and histidine₃₆₇ against alanine were introduced on both backgrounds. The mutants were overexpressed in HEK293 cells by transient transfection. The uptake of TEA^+ was measured (Figure 4.20 B). M420del significantly decreased the uptake of TEA^+ by 70.3 % ($P \leq 0.01$). The mutants *L364A* and *H367A* strongly decreased the uptake of TEA^+ independent of the background tested. *L364A* and *H367A* significantly decreased TEA^+ uptake to the level of M420del cells showing a decreased by 73.5 % and 73.3 %, respectively. When *L364A* and *H367A* were expressed on M420del background, the mutation *L364A* and *H367A* decreased the uptake by 87 % and 68 % compared to M420del cells, respectively.

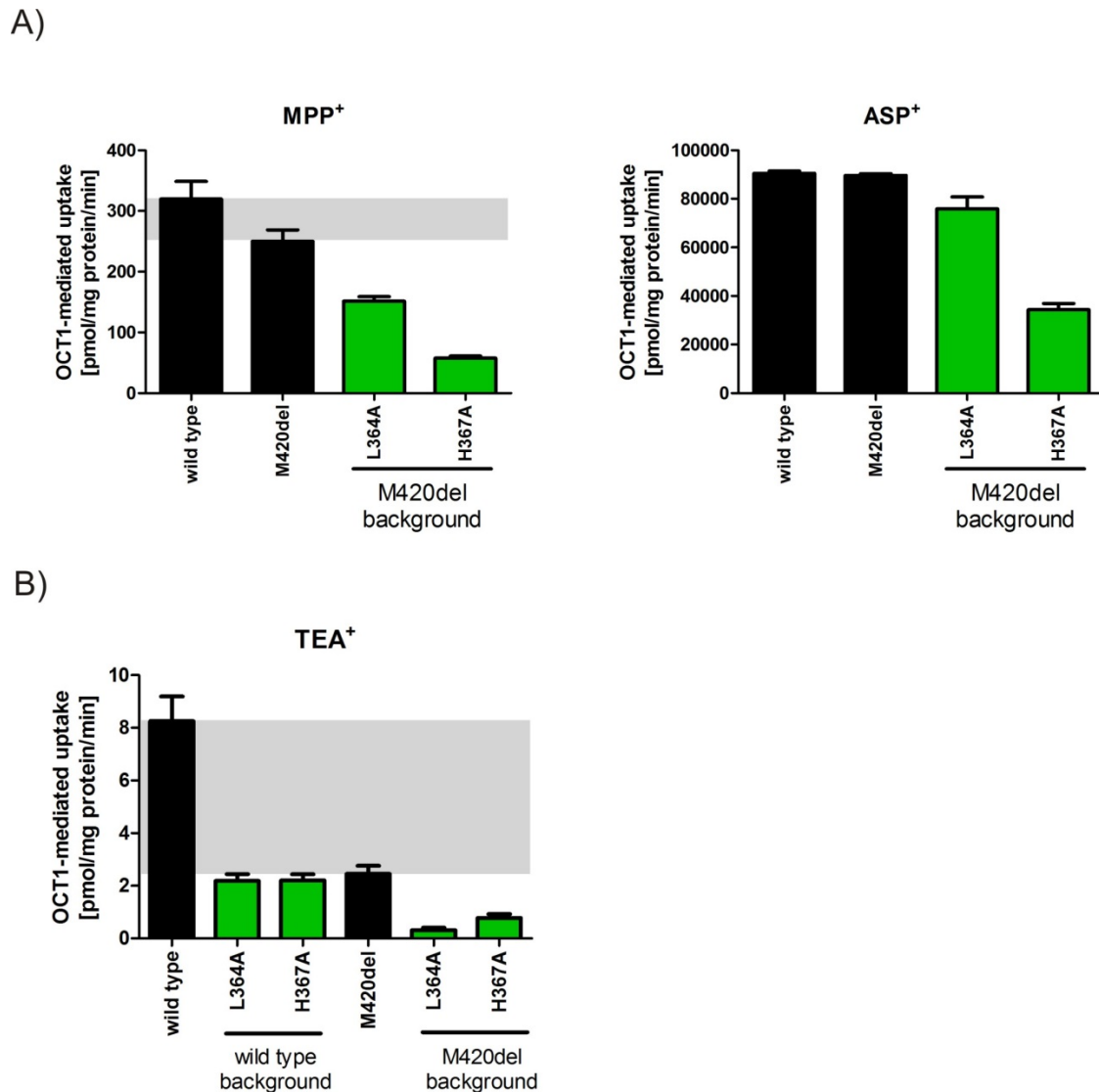


Figure 4.20 Analysis of the interaction of methionine₄₂₀ with the amino acids L364 and H367 in TMD 7. (A) HEK293 cells stably transfected to overexpress wild type *OCT1* and the *M420del* variant as well as the mutants *L364A* and *H367A* on *M420del* background were incubated with 10 μ M MPP⁺ and 5 μ M ASP⁺ for 2 min. (B) HEK293 cells transiently transfected with the expression plasmid pcDNA5 containing *OCT1* wild type, *M420del*, and *L364A* and *H367A* on both backgrounds were incubated with 5 μ M TEA⁺ for 2 min. The OCT-mediated uptake was calculated by subtracting the uptake of control cells transfected with the empty expression vector pcDNA5 from the uptake in the cells transfected with the wild type or variant *OCT1*. Shown is the mean and error of the mean of three independent experiments. The gray area highlights the difference in the uptake between the wild type *OCT1* and the *M420del* variant.

Due to the very strong decrease of OCT1 activity especially for the H367A mutant, the correct membrane localization of these mutants was analyzed by immunostaining and analysis by confocal microscopy was performed (Figure 4.19 D). L364A and H367A

mutants did not affect membrane localization of OCT1 in M420del cells suggesting that the observed strong decrease in the activity is not due to improper membrane localization.

In summary, the results indicate that L364 and H367 themselves are important for the transport of TEA⁺, MPP⁺, and ASP⁺. Therefore, with this experiment we were not able to correctly address the hypothesis of sterical interaction with these two variants as a reason for the substrate-specific effects of M420del.

Next, the importance of the methionine side chain properties for the substrate-specific effects of the M420del variant was analyzed. Therefore, HEK293 cells were generated by targeted chromosomal integration to overexpress mutants characterized by substitution of methionine₄₂₀ against alanine, threonine, isoleucine, or cysteine (M420A, M420T, M420I and M420C, respectively). The correct integration of the clones, the strong and homogenous mRNA expression and the correct membrane localization of the clones were confirmed (Figure 4.21).

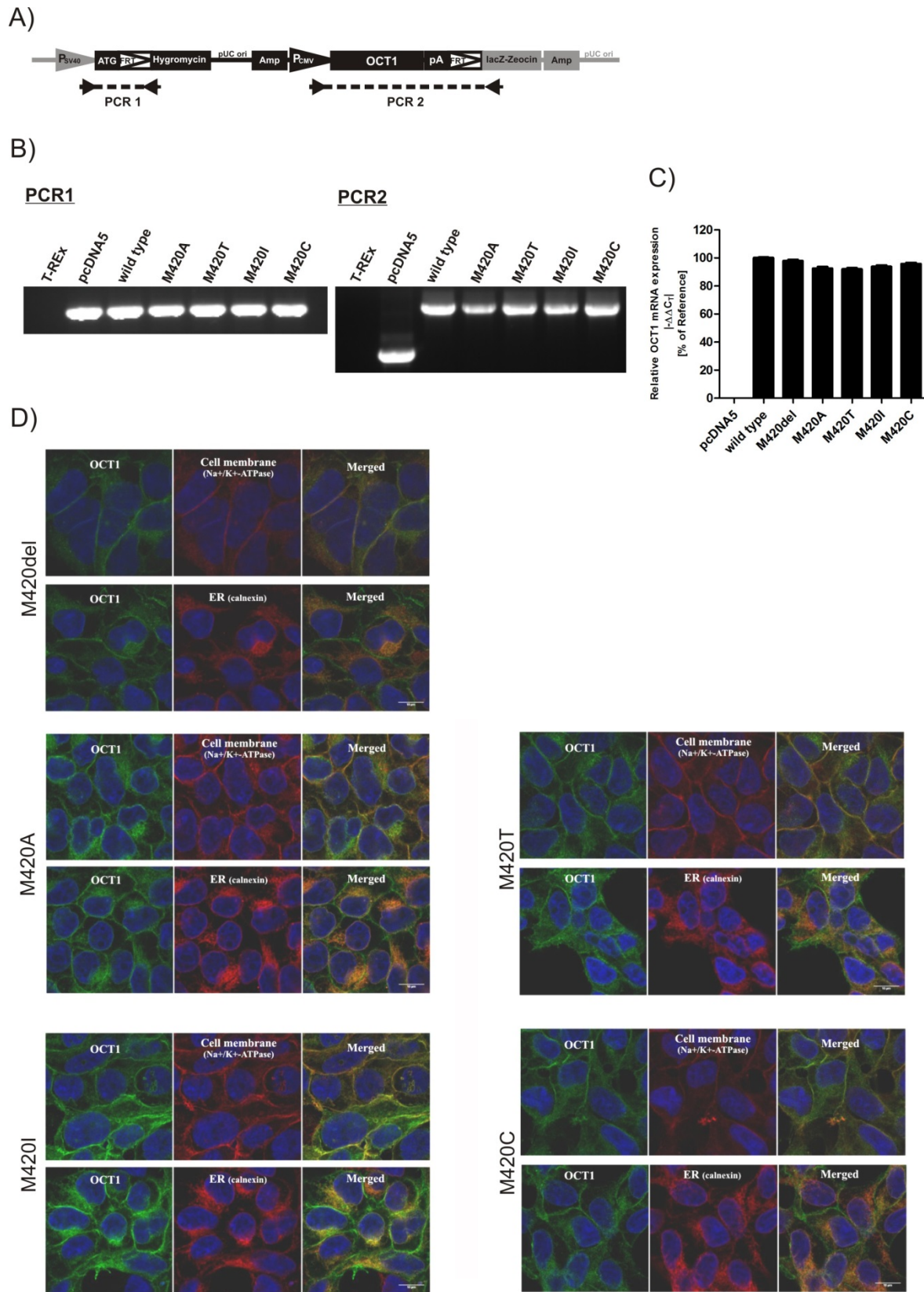


Figure 4.21 (previous page) Validation of HEK293 cells overexpressing the *OCT1* mutants M420A, M420I, M420I, and M420C. (A) Schematic presentation of the expression plasmid pcDNA5 (black) integrated into the pFRT/lacZeo site of the genome of HEK293 cells (gray) as represented in Seitz *et al.* (Seitz *et al.*, 2015). The positions of the primers and the amplicons of PCR 1 and PCR 2 are indicated. (B) PCR 1 resulted in an amplification product of 519 bp and PCR 2 resulted in an amplification product of 1376 bp (for the control cells transfected with the empty pcDNA5 vector) or 3137 bp (transfected with pcDNA5 containing *OCT1*). (C) Relative mRNA expression using real-time qPCRs demonstrating high and equal *OCT1* mRNA levels among wild type *OCT1* and the generated mutants. Shown is the mean and error of the mean of three independent RNA extractions. (D) Immunocytochemical staining of *OCT1* (green) co-stained with Na⁺/K⁺ ATPase (red, upper part) as a plasma membrane marker, or calnexine (red, lower part) as a marker of endoplasmic reticulum.

As alanine has next to glycine the shortest side chain among the proteinogenic amino acids, substitution of methionine₄₂₀ to alanine should not affect the position of adjacent amino acids, but represents a complete lack of the active amino acid side chain. If not the methionine itself, but the shortage of the amino acid chain or an unspecific steric interaction were the reasons for the M420del effects, then the M420A mutant should have transport activities similar to the wild type. However, the M420A mutant showed no significant differences to M420del in respect to uptake the of MPP⁺, TEA⁺, ASP⁺, morphine, metformin, tyramine, and proguanil (Figure 4.22).

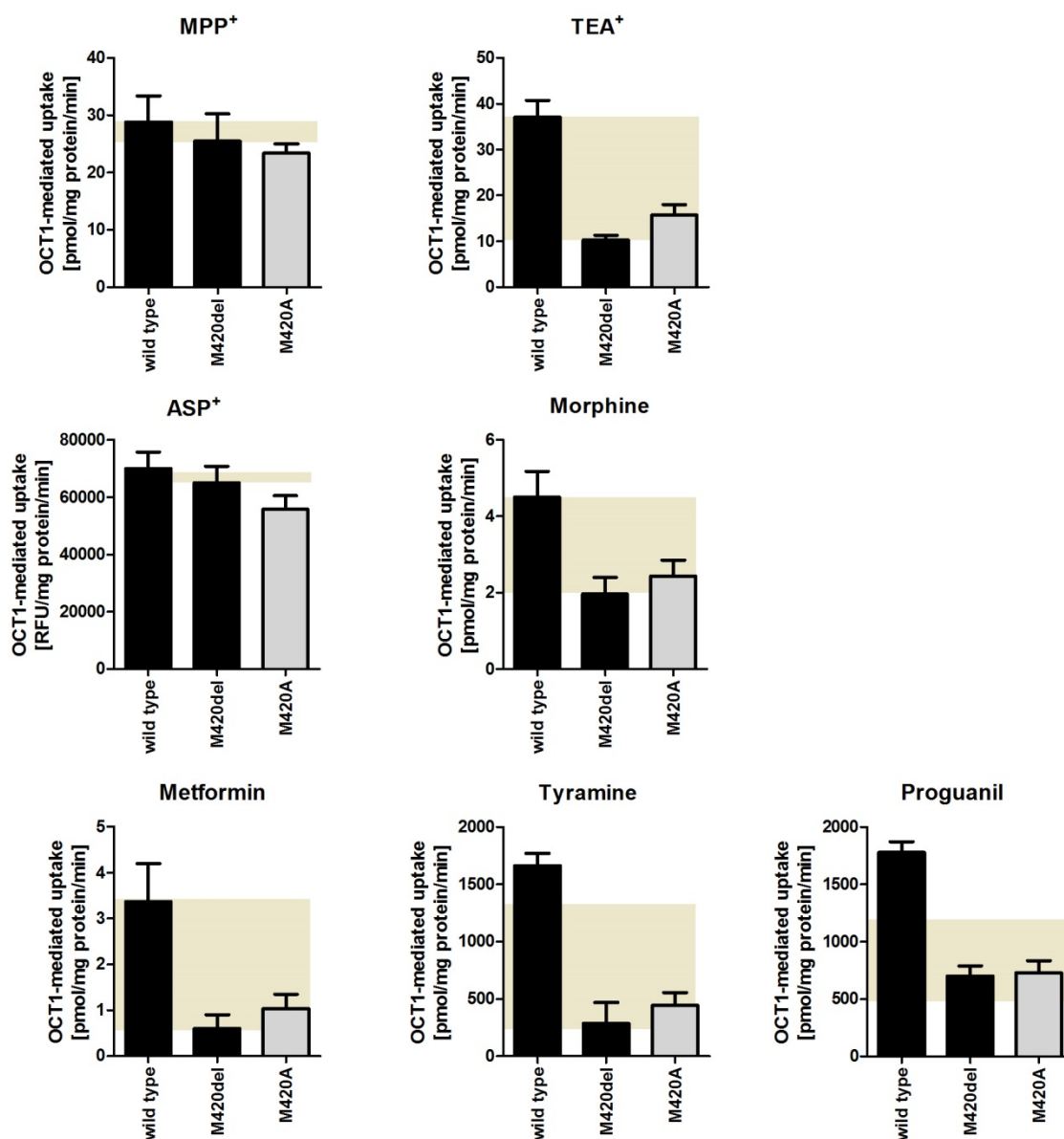


Figure 4.22 Comparative analysis of the uptake activity of M420del and the M420A mutant measured at single concentration of the substrate. HEK293 cells stably transfected to overexpress wild type *OCT1*, the *M420del* variant, as well as the *M420A* mutant were incubated for 2 min with 1 μM MPP⁺, 5 μM TEA⁺, 5 μM ASP⁺, 1 μM morphine, 5 μM metformin, 10 μM tyramine, or 80 μM proguanil. The OCT1-mediated uptake was calculated by subtracting the uptake of the control cells stably transfected with the empty control vector pcDNA5 from the cells overexpressing *OCT1* and its variants. Shown is the mean and error of the mean of at least three independent experiments. The gray area highlights the difference in the uptake between wild type *OCT1* and the M420del variant.

Furthermore, also detailed transport kinetic analyses showed no significant differences in uptake rates between the M420del and M420A mutants (Figure 4.23 and Table 4.4). TEA⁺ was the only substrate for which the K_m significantly differed between M420del and M420A. However, the difference was marginally significant with $P=0.028$.

Taken together, these results indicate that the side chain at position 420 is responsible for the observed substrate-specific effects of M420del.

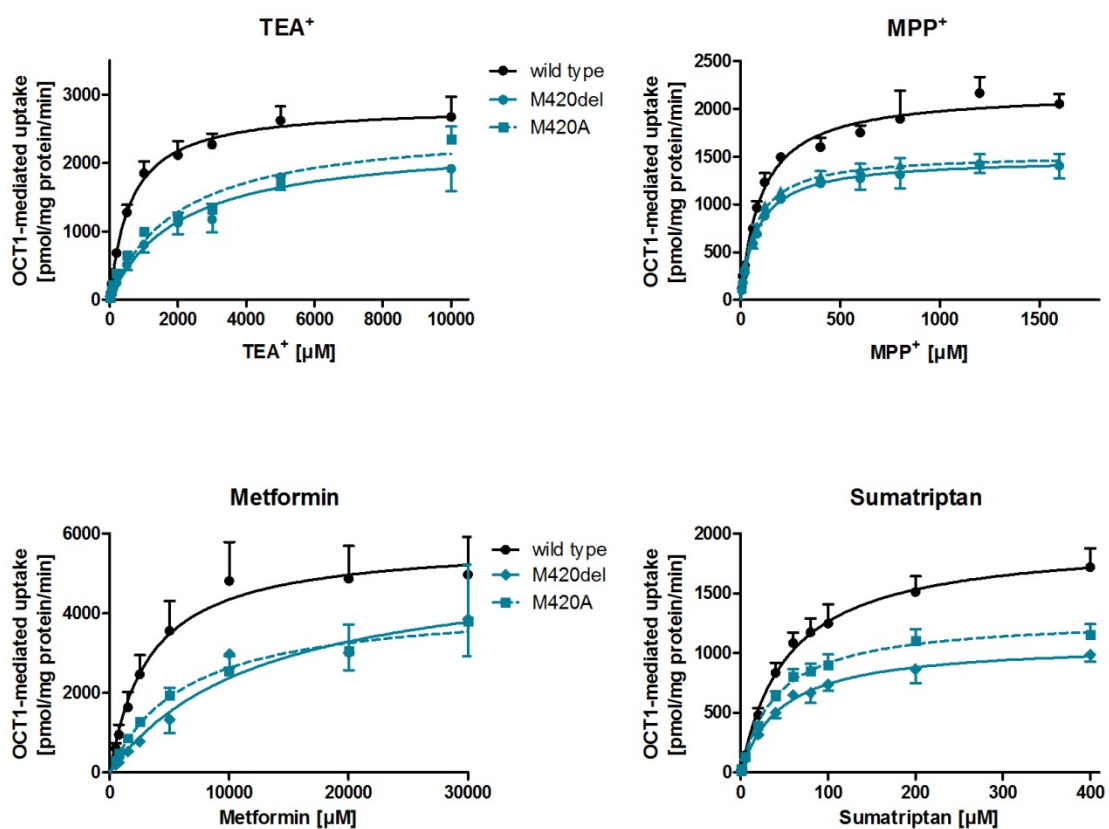


Figure 4.23 Comparative analyses of the transport kinetics of M420del and M420A. HEK293 cells stably transfected to overexpress wild type *OCT1*, *M420del*, or *M420A* were incubated for 2 min with increasing concentrations of TEA⁺, MPP⁺, metformin, and sumatriptan. The OCT1-mediated uptake was calculated by subtracting the uptake of control cells stably transfected with the empty control vector pcDNA5 from the uptake of the cells overexpressing wild type or variant *OCT1*. Shown is the mean and error of the mean of at least three independent experiments.

Table 4.4 Kinetic parameters of the M420A variant

Variant	MPP ⁺		TEA ⁺		Sumatriptan		Metformin	
	K _m [μM]	V _{max} [pmol/mg protein/ min]						
Wild type	108.6	2263.7	589.5	2848.7	58.9	2167.3	3402.0	5670.5
	±	±	±	±	±	±	±	±
	17.4	184.2	44.0	207.6	5.1	243.5	537.6	991.4
M420del	86.5	1484.0	1778.4	2114.8	46.3	1203.8	17047.8	6239.8
	±	±	±	±	±	±	±	±
	12.0	107.1	164.5	206.8	0.6	128.8	1127.5	915.5
M420A	73.8	1516.7	1063.9	2013.1	41.6	1299.7	18515.3	7396.3
	±	±	±	±	±	±	±	±
	8.3	61.8	53.3	138.7	2.1	112.8	11999.9	3232.5

Next, the specific structural properties of the methionine side chain were analyzed. Therefore, it was analyzed whether alanine, threonine, isoleucine, or cysteine may mimic the function of methionine at position 420. Threonine has a relatively short side chain, but possesses a polar although uncharged hydroxyl group. Isoleucine like methionine is a nonpolar, uncharged amino acid and has an almost comparable side chain length to methionine. Cysteine possesses a thiol group and therefore contains a sulfur atom like methionine. Due to its highly reactive thiol group, the mutation of methionine₄₂₀ to cysteine was expected to lead to the formation of untypical disulfide bonds and to lead to miss folding of the protein and improper membrane localization. However, using immunofluorescence confocal microscopy, the M420C mutant was shown to be correctly localized in the plasma membrane (Figure 4.21).

Similar to M420A, the mutants M420T, M420I, and M420C did not differ from M420del in their ability to transport TEA⁺, MPP⁺, ASP⁺, morphine, and metformin. No significant difference in the uptake between the M420del variant and the mutants could be detected for all substrates tested (Figure 4.24). For the uptake of MPP⁺ and ASP⁺ no significant difference between wild type, the M420del and the mutants was observed. The M420del

and the mutants significantly decreased the uptake of TEA⁺ at least by more than 54 % ($P \leq 0.01$). M420del significantly decreased morphine uptake by 49 % ($P \leq 0.05$). The decrease in morphine uptake was not significant for the mutants 420A, 420T, 420I, and 420C. The M420del significantly decreased metformin uptake by 68 % ($P \leq 0.01$). The mutants showed different effects on metformin uptake: the mutants 420A and 420I did not significantly decrease the uptake of metformin compared to wild type cells ($P = 0.1026$ and $P = 0.2187$ for 420A and 420I, respectively). Although for the 420A mutation metformin uptake was only decreased by 43 % compared to a decrease by 68 % for M420del at single concentration, analysis of metformin uptake kinetics revealed no difference between M420A and M420del (Figure 4.23). The mutants M420T and M420C significantly decreased metformin uptake by 65 % and 55 %, respectively. However, none of the mutants tested showed significant differences in substrate uptake compared to M420del and could completely restore wild type transport activity.

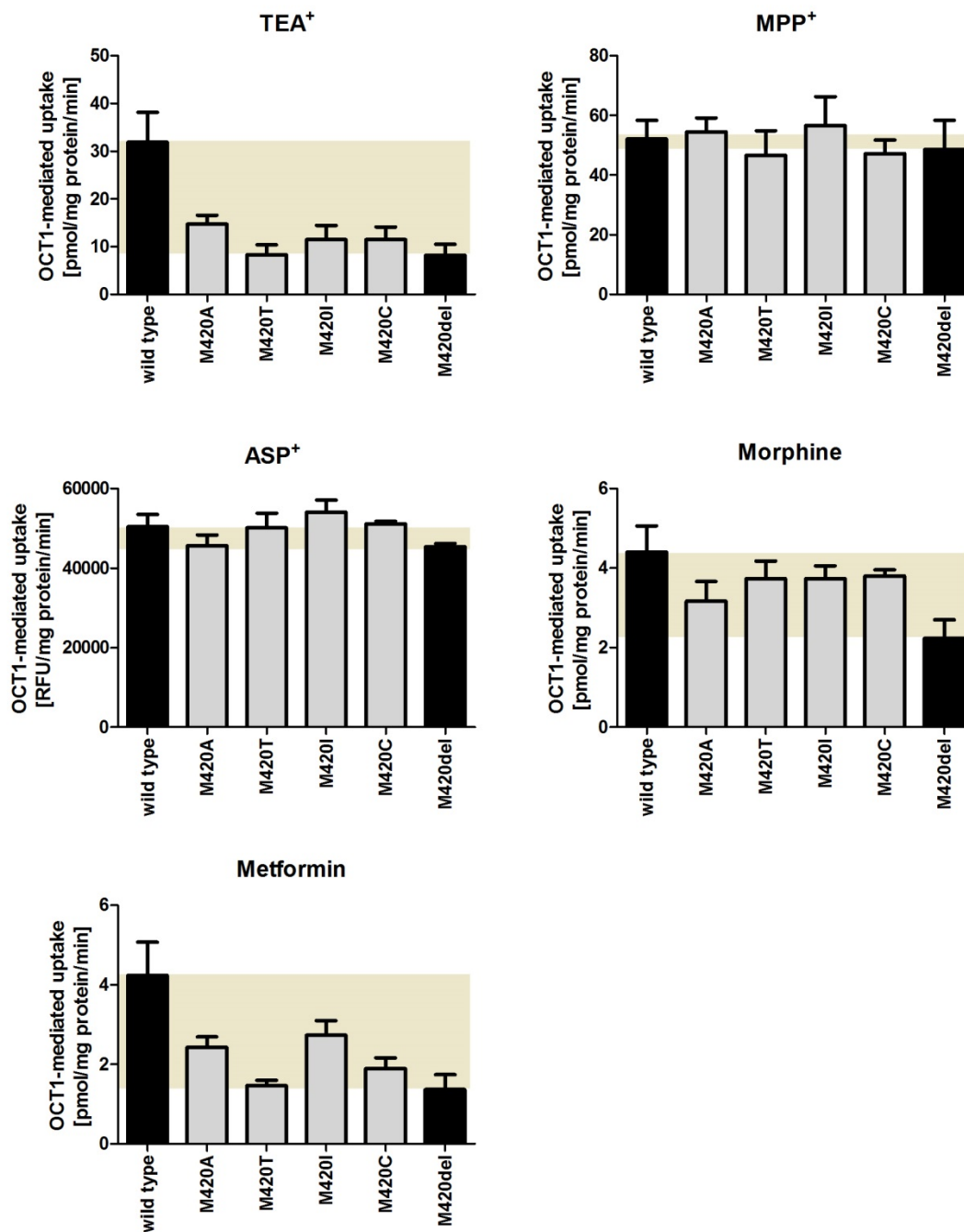


Figure 4.24 Comparative analyses of the effect of M420del, M420A, M420T, M420I, and M420C on the uptake of TEA⁺, MPP⁺, ASP⁺, morphine, and metformin. HEK293 cells stably transfected to overexpress wild type *OCT1*, the *M420del* variant as well as the mutants *M420A*, *M420T*, *M420I*, and *M420C* were incubated for 2 min with 5 μ M TEA⁺, 1 μ M MPP⁺, 5 μ M ASP⁺, 1 μ M morphine, and 5 μ M metformin. The OCT1-mediated uptake was calculated by subtracting the uptake of control cells stably transfected with the empty control vector pcDNA5 from the cells overexpressing the wild type or variant *OCT1*. Shown is the mean and error of the mean of three independent experiments. The light brown area highlights the difference in the uptake between wild type *OCT1* and the M420del variant.

Furthermore, the mutants M420T, M420I, and M420C showed a concentration-dependent uptake of TEA⁺ similar to M420del and not to the wild type (Figure 4.25, Table 4.5). M420del did not significantly decrease v_{\max} of TEA⁺ uptake compared to wild type cells. Equally, none of the mutants significantly affected the v_{\max} for TEA⁺ uptake, except 420A. The v_{\max} was significantly decreased ($v_{\max} = 2848 \pm 208$ pmol/mg protein/min and $v_{\max} = 2013 \pm 139$ pmol/mg protein/min uptake for wild type and 420A, respectively; $P = 0.008$). However, the focus was on the strong effect of M420del on K_m of TEA⁺ showing a significant increase compared to wild type cells. All the mutants tested showed similar K_m values as M420del, except M420A. As shown before, 420A showed a slightly significant decrease in K_m compared to M420del cells ($K_m = 1064 \pm 53$ for 420A and $K_m = 1778 \pm 165$ μ M for M420del; $P = 0.028$).

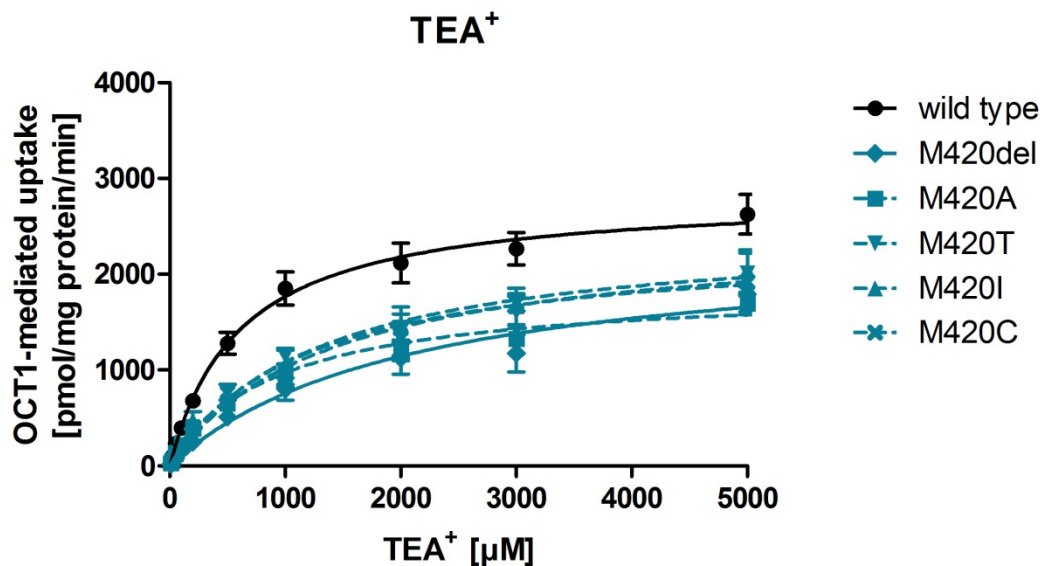


Figure 4.25 Comparative analyses of the effects of M420del, M420A, M420T, M420I, and M420C mutants on the uptake kinetics of TEA⁺. HEK293 cells stably transfected to overexpress wild type *OCT1*, the *M420del* variant, or the mutants *M420A*, *M420T*, *M420I*, or *M420C* were incubated for 2 min with increasing concentrations of TEA⁺. The OCT1-mediated uptake was calculated by subtracting the uptake of control cells stably transfected with the empty expression control vector pcDNA5 from the uptake in the cells overexpressing wild type or variant *OCT1*. Shown is the mean and error of the mean of three independent experiments.

Table 4.5 Kinetic parameters of M420A, M420T, M420I, and M420C mutants for TEA⁺ uptake

Variant	TEA ⁺	
	K _m [μM]	V _{max} [pmol/mg protein/min]
Wild type	589.5 ± 44.0	2848.7 ± 207.6
M420del	1778.4 ± 164.5	2114.8 ± 206.8
420A	1063.9 ± 53.3	2013.1 ± 138.7
420T	1420.2 ± 268.7	2480.7 ± 330.1
420I	1587.0 ± 48.4	2707.3 ± 284.0
420C	1160.9 ± 233.4	2259.7 ± 99.7

In conclusion, none of the amino acids with different functional properties in their side chain could restore wild type transport activity for the uptake of TEA⁺, MPP⁺, ASP⁺, morphine, and metformin. For TEA⁺ uptake, M420del caused a significant increase in K_m that was not significantly changed in the mutants M420T, M420I, and M420C. Indeed, in respect to TEA⁺ uptake the substitution M420A did not behave as M420del. The K_m value of M420A was 1064 ± 53 μM which is between the K_m values of the M420del and the wild type. However, this effect was not observed for other substrates and especially for metformin for which M420del also caused a strong variation in K_m (Figure 4.13, Table 4.3). The other substitutions on position 420 tested also did not significantly differ to M420del in their ability to transport TEA⁺. The data indicates that the side chain of methionine₄₂₀ is essential for the observed effects of the M420del mutant. Hence, with the analyzed mutants the substrate-specific effects caused by the loss of the methionine side chain at position 420 could not be explained.

Finally, the interactions between M420del and amino acids known to play an important role in substrate binding and translocation were analyzed. Based on the homology model no direct interaction could be suggested between methionine₄₂₀ and any of the amino acids in the substrate binding cleft of OCT1 (Figure 1.1). However, at this point possible indirect (functional) interactions with the amino acids D474, W217, and F159 were analyzed. These amino acids were chosen as in rat Oct1 the respective amino acids D475, W218, and F160 were shown to be involved in substrate binding and in transport of TEA⁺ and binding

of corticosterone (Gorboulev et al., 1999; Gorboulev et al., 2005; Popp et al., 2005; Gorbunov et al., 2008; Volk et al., 2009). The mutants D474E, W217Y, and F159Y were generated on wild type and M420del background of human OCT1. The mutants were overexpressed in HEK293 cells stably transfected by targeted chromosomal integration of the expression plasmid and validated as described in chapters 3.1.6, 3.1.3, and 3.2.3. The correct chromosomal integration was confirmed by PCR and capillary sequencing, the overexpression by real-time qPCR (Figure 4.26).

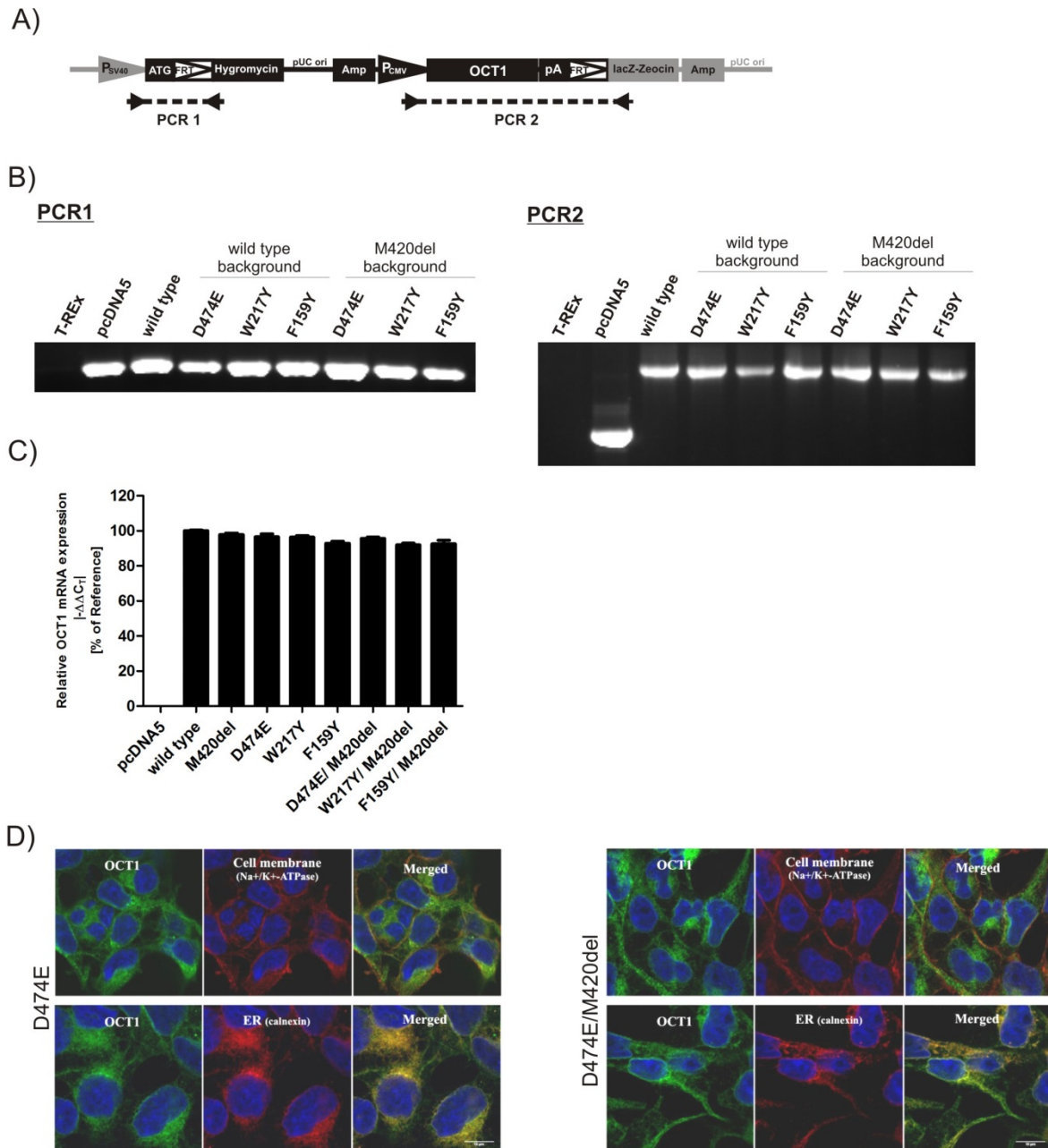


Figure 4.26 Validation of HEK293 cells overexpressing the *OCT1* mutants D474E, W217Y, and F159Y on the wild type and M420del *OCT1* background (A) Schematic presentation of the expression plasmid pcDNA5 (black) integrated into the pFRT/lacZeo site of the genome of HEK293 cells (gray) as represented in Seitz *et al.* (Seitz *et al.*, 2015). The positions of the primers and the amplicons of PCR 1 and PCR 2 are indicated. (B) PCR 1 resulted in an amplification product of 519 bp and PCR 2 resulted in an amplification product of 1376 bp (for the control cells transfected with the empty pcDNA5 vector) or 3137 bp (transfected with pcDNA5 containing *OCT1*). (C) Relative mRNA expression using real-time qPCRs demonstrating high and equal *OCT1* mRNA levels among wild type *OCT1* and the generated mutants. Shown is the mean and error of the mean of three independent RNA extractions. (D) Immunocytochemical staining of *OCT1* (green) co-stained with Na⁺/K⁺ ATPase (red, upper part) as a plasma membrane marker, or calnexine (red, lower part) as a marker of endoplasmic reticulum.

The mutants were characterized regarding their transport activity for the uptake of ASP⁺, MPP⁺, TEA⁺, morphine, metformin, tyramine, and proguanil at single concentrations. The mutations W217Y and F159Y did not significantly affect the uptake of ASP⁺, MPP⁺, TEA⁺, morphine, metformin, and tyramine neither on wild type nor on M420del background. F159Y in wild type OCT1 cells only slightly insignificantly decreased the uptake of TEA⁺ and tyramine by 26 % and 25.7 %, respectively (Figure 4.27). The mutation W217Y increased the uptake of proguanil by 23 % and 33 % in wild type and M420del cells, respectively. The increase was significant in wild type cells ($P \leq 0.05$), but not in M420del cells.

In contrast, the mutation D474E had strong effects on the uptake of all substances tested. On wild type background, D474E significantly decreased the uptake of all substrates tested by between 31 % and 76 % ($P \leq 0.01$). On M420del background, D474E significantly decreased the uptake of ASP⁺, MPP⁺, and proguanil by 79 % to 93 % ($P \leq 0.05$). However, also the uptake of TEA⁺, morphine, tyramine, and metformin was strongly decreased in D474E mutants by at least 73 %. More importantly, interaction between the mutation D474E and M420del was observed for some of the substrates: even though M420del cells without the D474E mutation showed only limited decrease in the uptake of ASP⁺ and MPP⁺, in combination with the D474E mutation much stronger effects of the M420del were observed. Without the mutation D474E, M420del showed only 7 % and 12 % decrease in the uptake of ASP⁺ and MPP⁺, respectively. In the presence of the D474E mutation, the M420del uptake was decreased by 65 % and 93 % for ASP⁺ and MPP⁺, respectively.

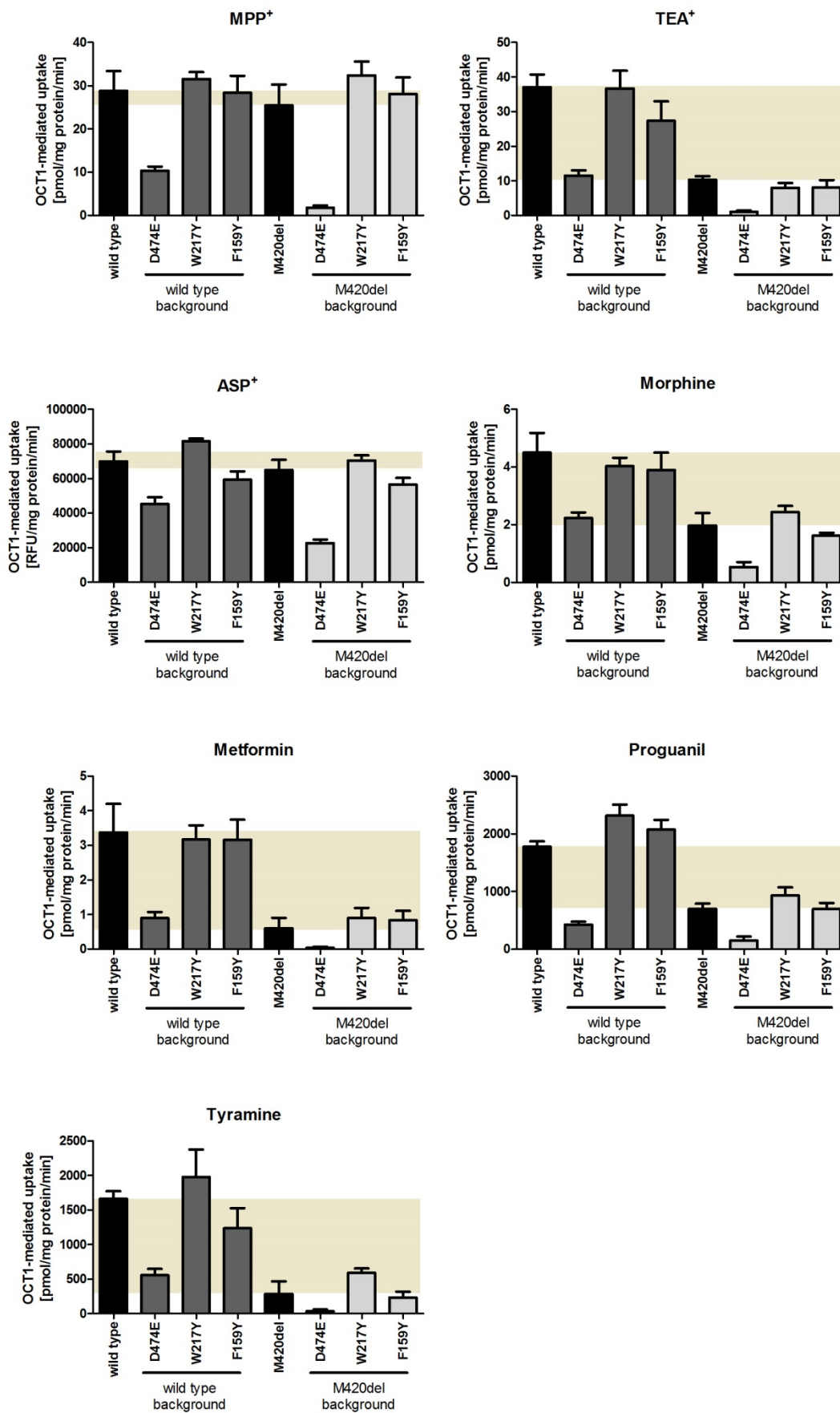


Figure 4.27 (previous page) Comparative analyses of the effect of D474E, W217Y, and F159Y mutations on transport activity of wild type or M420del OCT1. HEK293 cells stably transfected to overexpress wild type *OCT1*, the *M420del* variant as well *D474E*, *W217Y*, and *F159Y* mutants on wild type and M420del background were incubated for 2 min with 5 μM ASP^+ , 1 μM MPP^+ , 5 μM TEA^+ , 1 μM morphine, 80 μM proguanil, 10 μM tyramine, or 5 μM metformin. The OCT1-mediated uptake was calculated by subtracting the uptake of control cells stably transfected with the empty control vector pcDNA5 from the uptake of the cells overexpressing wild type or different variant *OCT1*. Shown is the mean and error of the mean of at least three independent experiments. The light brown area highlights the difference in the uptake between wild type OCT1 and the M420del variant.

Concentration-dependent uptake measurements were performed to determine K_m and v_{\max} for the uptake of TEA^+ , MPP^+ , ASP^+ , metformin, and sumatriptan for the D474E mutants on wild type and M420del background (Figure 4.28 and Table 4.6). The mutation D474E decreased v_{\max} in comparison to the respective background (wild type or M420del) (Figure 4.28).

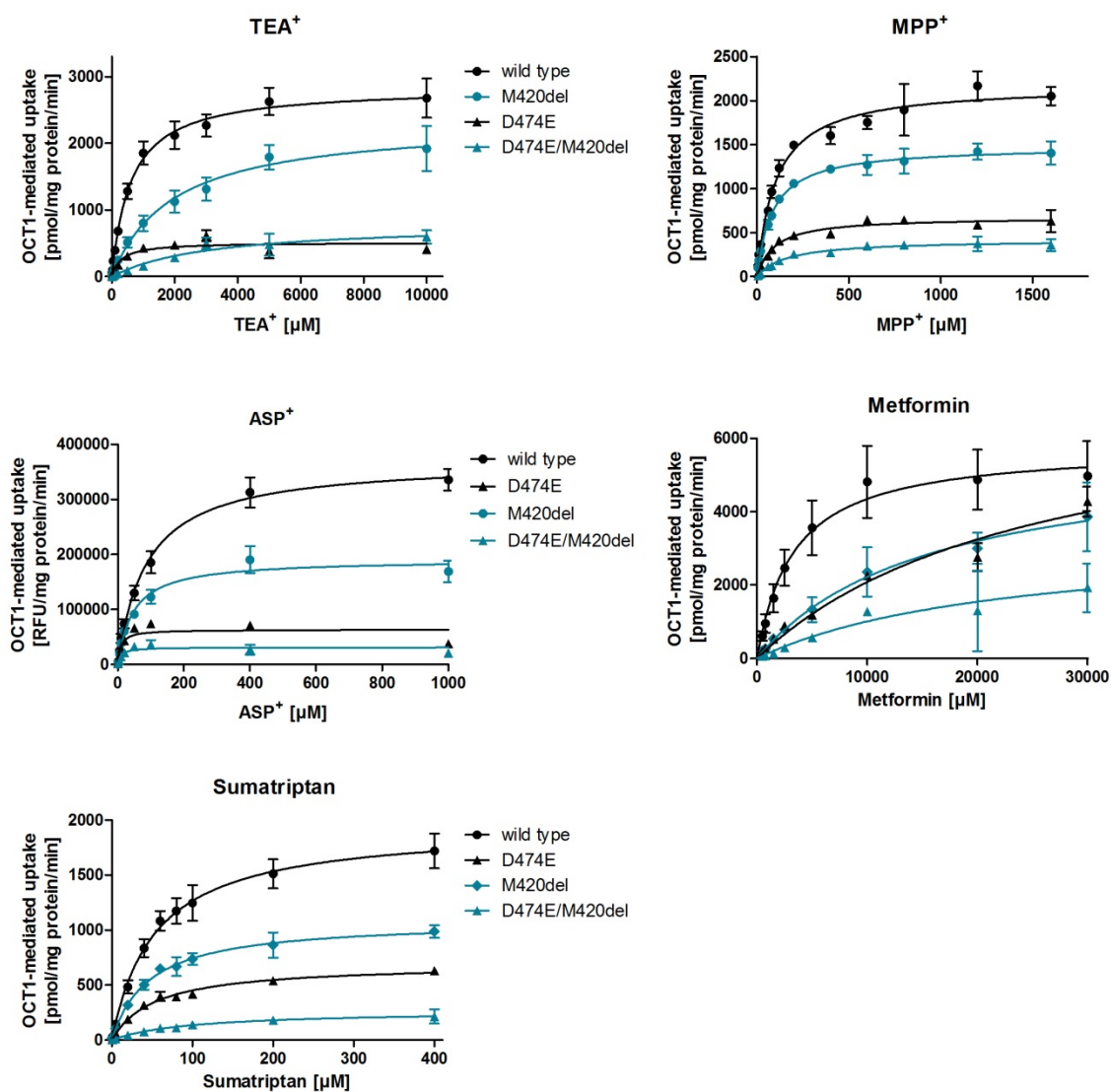


Figure 4.28 Comparative analyses of the combined effects of the M420del polymorphism and the D474E mutation on the uptake kinetics of TEA⁺, MPP⁺, ASP⁺, metformin, and sumatriptan. HEK293 cells stably transfected to overexpress wild type *OCT1*, the M420del variant, and the D474E mutant on wild type and M420del background were incubated for 2 min with increasing concentrations of TEA⁺, MPP⁺, ASP⁺, metformin, and sumatriptan. The OCT1-mediated uptake was calculated by subtracting the uptake of control cells stably transfected with the empty expression control vector pcDNA5 from the uptake cells overexpressing wild type or variant *OCT1*. Shown is the mean and error of the mean of at least three independent experiments.

Table 4.6 Kinetic parameters of D474E mutant on wild type and M420del background.

Variant	MPP ⁺		TEA ⁺		ASP ⁺		Sumatriptan		Metformin	
	K _m [μM]	V _{max} [pmol/mg protein/ min]	K _m [μM]	V _{max} [pmol/mg protein/ min]	K _m [μM]	V _{max} [RFU/mg protein/ min]	K _m [μM]	V _{max} [pmol/mg protein/ min]	K _m [μM]	V _{max} [pmol/mg protein/ min]
Wild type	108.6	2263.7	589.5	2848.7	93.4	372678.0	58.9	2167.3	3402.0	5670.5
	±	±	±	±	±	±	±	±	±	±
	17.4	184.2	44.0	207.6	19.3	29568.8	5.1	243.5	537.6	991.4
D4754E	120.5	740.5	344.1	541.7	17.7	84299.7	54.3	724.3	30233.0	8286.3
	±	±	±	±	±	±	±	±	±	±
	13.8	13.5	31.8	41.5	3.8	7437.2	3.0	34.1	9845.1	1782.9
M420del	86.5	1484.0	1778.4	2114.8	46.4	185575.0	46.3	1203.8	17047.8	6239.8
	±	±	±	±	±	±	±	±	±	±
	12.0	107.1	164.5	206.8	8.67	19693.1	0.6	128.8	1127.5	915.5
D474E/ M420del	171.1	420.5	2097.8	650.0	14.7	37976.3	94.5	295.2	42370.8	5709.4
	±	±	±	±	±	±	±	±	±	±
	53.4	70.2	381.5	152.8	2.3	6201.8	11.5	56.7	16802.7	2559.7

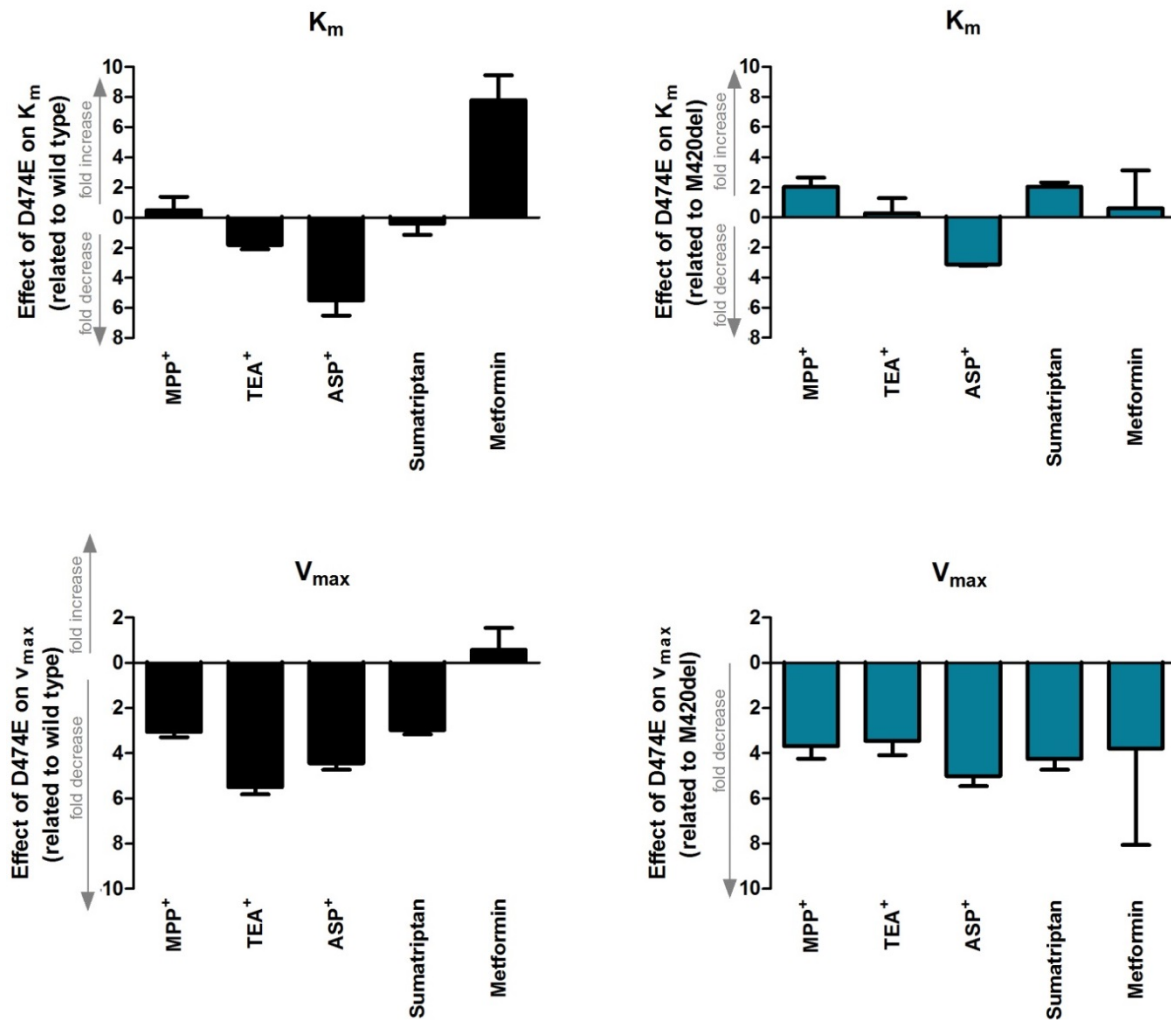


Figure 4.29 Comparative presentation of the differences in K_m (top panel) and v_{max} (lower panel) caused by the D474E mutation on the OCT1 wild type (left site, black bars) or M420del background (right site, blue bars). Shown is the mean and error of the mean of the differences between D474 and E474 from at least three independent experiments. K_m and v_{max} are based on results shown in Figure 4.28.

The graphs shown in Figure 4.29 illustrate the effect of D474E on K_m and v_{max} of OCT1 wild type or M420del.

On wild type background the D474E mutation decreased v_{max} at least by 66 % for all substrates tested, except for metformin. For metformin, v_{max} was slightly but insignificantly increased by 27 %. On M420del background, the D474E mutant strongly decreased the v_{max} by between 68 % and 79 % compared to M420del alone, with exception of metformin. For metformin uptake, the D474E mutation did not significantly change the v_{max} in M420del cells (Figure 4.29). Therefore, it could be concluded that there were strong, but

also substrate-specific effects of D474E on the transport capacity of human OCT1 and these effects were not dependent on M420del.

The effects of the D474E mutation on K_m were more complex and dependent on the M420del: D474E decreased the K_m for ASP^+ by 68 %. The decrease was similar to the effect of D474E on wild type background (K_m decreased by 81 %). In contrast, on the M420del background, D474E increased the K_m for MPP^+ , TEA^+ , and sumatriptan, by 41 %, 34 %, and 105 %, respectively. The increased K_m suggested a decrease in affinity for these substances. In comparison, on wild type background, D474E did not change or even caused a decrease of the K_m (by 41 % for TEA^+ and by 81 % for ASP^+) (Figure 4.29). For metformin, the D474E mutation caused a strong increase of the K_m . This increase, however, was much stronger on the wild type (679 %) than on M420del background (133 %). Because the effects of D474E on the affinity for the substrates (besides for metformin) were observed only together with M420del, one may speculate about interactions between D474E and M420del in the uptake of TEA^+ , MPP^+ , and sumatriptan. Regarding the effect on K_m of metformin, the effect of D474E and M420del does not seem to be additive as M420del and D474E increased the K_m by 424 % (Figure 4.13) and 679 % (Figure 4.29) in wild type cells, respectively, but D474E increased the K_m only by 133 % together with M420del (Figure 4.29). The data more likely indicate that the effect of D474E on the K_m of metformin is dominant to the effect of M420del.

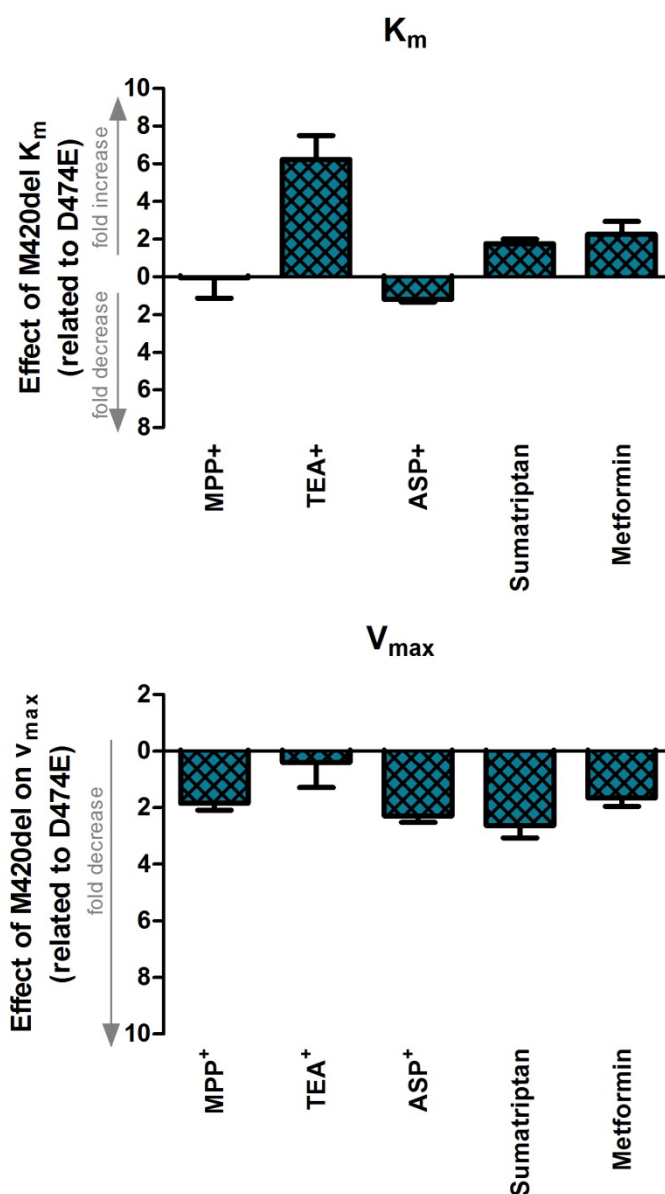


Figure 4.30 Graphical representation of the differences in K_m (upper part) and v_{max} (lower part) caused by the M420del polymorphisms on mutant D474E background. Shown is the mean and error of the mean of the differences between the M420 and 420deletion alleles on E474 background from at least three independent experiments. K_m and v_{max} are based on results shown in Figure 4.28.

Next, it was analyzed how M420del affects K_m and v_{max} in the presence of the D474E mutation (Figure 4.30). M420del caused a strong decrease of v_{max} (by between 43 % and 60 %) for all substrates tested, except for TEA⁺. The v_{max} of TEA⁺ was not affected.

M420del did not affect the K_m values of MPP⁺ and ASP⁺ in the D474E mutants. In contrast, the K_m of sumatriptan increased in the presence of M420del on D474E

background by 76 %. The increase was even stronger for the K_m of TEA^+ , which showed an increase of 523 % when M420del was present together with D474E. This effect was comparable with the effect of M420del on wild type background (217 % increase, Figure 4.13). This is in line with the lack of effects of D474E itself on the K_m for TEA^+ (Figure 4.29).

The effects of the mutations D474E, W217Y, and F159Y observed here in human OCT1 differed from the ones previously reported for the rat ortholog. The amino acids D475, W218, and F160 are known to have strong effects on MPP^+ and TEA^+ uptake in rat Oct1 (Gorboulev et al., 1999; Popp et al., 2005; Volk et al., 2009). However, in human OCT1 D474E strongly decreased the uptake of MPP^+ and TEA^+ and other substrates tested, but no effects were observed for W217Y and F159Y (Figure 4.27 and Figure 4.28). Therefore, the species-specific differences in the uptake of TEA^+ , MPP^+ , ASP^+ , and morphine between human OCT1 and its orthologs in mouse and rat were analyzed in more details. Second, differences in the effects of the mutations D475E, W218Y, and F160Y on the activity in mouse and human OCT1 orthologs were analyzed.

There were no significant differences in the uptake between mouse and rat Oct1 for any of the substrates tested (Figure 4.31). In contrast, there were strong differences in the uptake of TEA^+ and ASP^+ between human OCT1 and its rodent orthologs (Figure 4.31). TEA^+ uptake was 2.3-fold higher in rodent compared to human OCT1 ($P \leq 0.05$). In contrast, the ASP^+ uptake was decreased by 2.7-fold ($P \leq 0.01$) and 3.6-fold ($P \leq 0.01$) in mouse and rat Oct1, respectively.

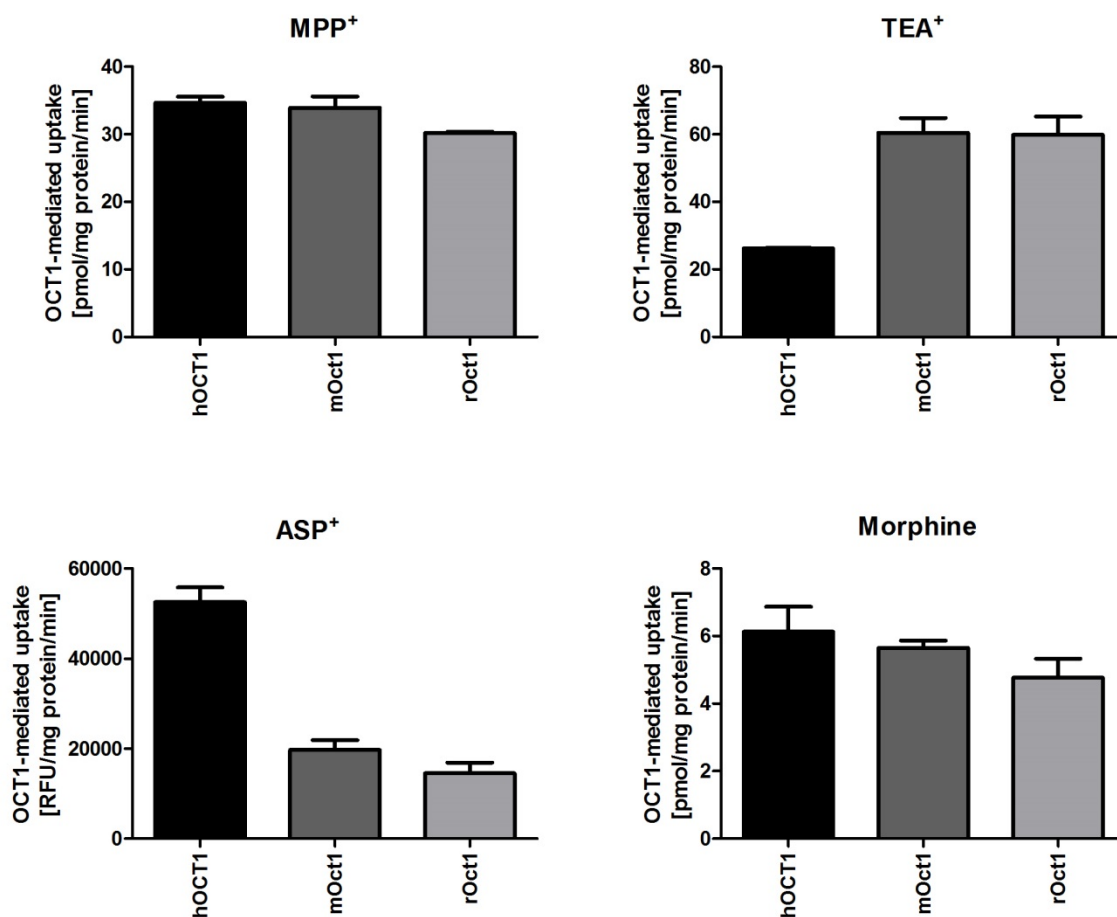


Figure 4.31 Differences between human OCT1 and mouse and rat orthologs in the uptake of MPP⁺, TEA⁺, ASP⁺, and morphine. HEK293 cells stably transfected to overexpress human *OCT1* or its rodent orthologs were incubated for 2 min with 1 μ M MPP⁺, 5 μ M TEA⁺, 5 μ M ASP⁺, and 1 μ M morphine. The OCT1-mediated uptake was calculated by subtracting the uptake of control cells stably transfected with the empty control vector pcDNA5 from the cells overexpressing human *OCT1* or its orthologs. Shown is the mean and error of the mean of three independent experiments.

Next, the effect of the mutants D475E, W218Y, and F160Y on transport activity for the uptake of TEA⁺, MPP⁺, ASP⁺, and morphine in mouse and human OCT1 ortholog was analyzed. The D475E mutation in mouse Oct1 significantly decreased the uptake of ASP⁺ and morphine by 78 % and 42 %, respectively (Figure 4.32). The decrease in ASP⁺ uptake was stronger in mouse Oct1 than in the human ortholog, in which ASP⁺ uptake was decreased by 31 %. In contrast to human OCT1, in mouse Oct1 D475E did not significantly affect the uptake of TEA⁺ and MPP⁺. Hence, in humans the mutation D474E seems to have stronger effects on the uptake of TEA⁺, MPP⁺, and morphine than the

mutation in mouse ortholog. In contrast, the uptake of ASP^+ seemed to be more strongly affected by the mutation in mouse Oct1.

In human OCT1 the mutations W217Y and F159Y did not affect substrate uptake. In contrast, in mouse Oct1, the uptake of ASP^+ and morphine was strongly affected by W218Y and F160Y. The ASP^+ uptake was significantly decreased in these mutants. For morphine uptake, W218Y significantly increased the uptake by 121 %, whereas F160Y significantly decreased the uptake by 37 %. In line with human OCT1, the uptake of TEA^+ and MPP^+ was not significantly affected by W218Y and F160Y in mouse Oct1.

In summary, next to species-specific differences between human OCT1 and rodent orthologs in the uptake of TEA^+ , MPP^+ , ASP^+ , and morphine, also the amino acids D474, W217, F159 in human OCT1 and their mouse orthologs have different impact on the uptake of the substances tested.

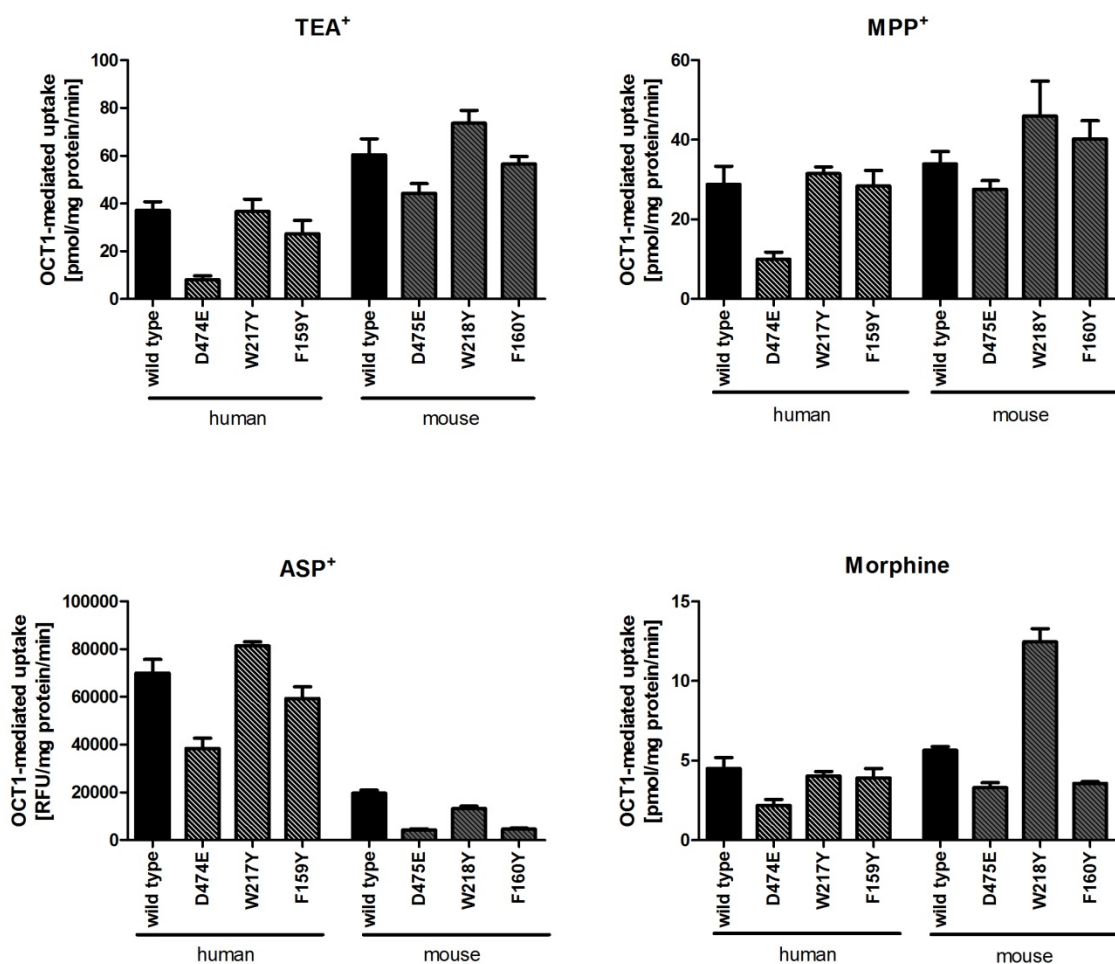


Figure 4.32 Species-specific differences in the effects of D474E, W217Y, and F159Y mutants on substrate uptake. HEK293 cells stably transfected to overexpress wild type and *D474E*, *W217Y*, and *F159Y* mutated human and mouse *OCT1* were incubated for 2 min with 5 μM TEA⁺, 1 μM MPP⁺, 5 μM ASP⁺, or 1 μM morphine. The OCT1-mediated uptake was calculated by subtracting the uptake of the control cells stably transfected with the empty control vector pcDNA5 from the uptake of the cells overexpressing the wild type and mutant human and mouse *OCT1*. Shown is the mean and error of the mean of three independent experiments.

5 Discussion

This work describes, in detail, a functional analysis of globally existing genetic variants of OCT1. Genetic analyses revealed strong variation in the frequency of loss of OCT1 activity worldwide. In this work, a comparative analysis of the genetic variants on a broad spectrum of structurally diverse substrates was performed. With this data, a substantial number of genetic variants that caused substrate-specific loss of OCT1 function were identified. This reflects the polyspecificity of the OCT1 transporter and suggests different substrate binding sites and transport mechanisms for different OCT1 substrates. Furthermore, it could be shown that the reason for complete substrate-wide loss of transport activity was improper membrane localization.

The most frequent and only ubiquitous loss-of function variant, M420del, was analyzed in detail. The M420del variant caused highly substrate-specific effects regarding loss of OCT1 function. Using targeted mutagenesis it could be shown that these effects were not caused by reduction of the protein chain due to deletion of methionine, but rather were caused by loss of the methionine side chain. OCT1 activity could not be restored by inserting threonine, isoleucine, or cysteine at the position of missing methionine₄₂₀. Complex interactions between methionine₄₂₀ and aspartate₄₇₄, an amino acid known to be involved in substrate binding in rat Oct1, were also observed.

5.1 Strong variations in the effects of OCT1 allelic variants on transport activity

In this work, a detailed functional characterization of 21 OCT1 allelic variants, which were previously reported or predicted to strongly affect OCT1 activity, was performed. Of the 21 allelic variants analyzed in this study, 16 major alleles were found to strongly affect OCT1 activity, whereas the 5 most common sub alleles did not affect transport activity of OCT1 (Figure 4.5). The 16 major alleles could be divided into four different groups according to their effect on OCT1 activity: alleles leading to complete substrate-wide loss of activity, alleles leading to strong but not complete substrate-wide loss of activity, alleles causing substrate-specific loss of activity, and alleles causing gain of OCT1 activity.

Firstly, the four alleles *OCT1*5* (G465R/M420del), *OCT1*6* (C88R/M420del), *OCT1*12* (S29L), and *OCT1*15* (E284K) were characterized as complete substrate-wide loss-of-function variants. They did not show transport activity with any of the substrates tested (Figure 4.5). In line with our observations, the variant alleles *OCT1*5* and *OCT1*6* were previously reported as loss of function variants (Shu et al., 2003; Shu et al., 2007; Tzvetkov et al., 2009; Ahlin et al., 2011; Saadatmand et al., 2012; Tzvetkov et al., 2012). The variant alleles *OCT1*12* (S29L) and *OCT1*15* (E284K) were newly identified as very rare OCT1 variants and were predicted by several bioinformatic tools to cause loss of OCT1 function (Seitz et al., 2015). Hence, this work provides the first characterization of S29L and E284K as complete substrate-wide loss of function variants.

Secondly, the three allelic variants of OCT1 characterized by a strong reduction in transport activity for all substrates tested were: *OCT1*3* (R61C), *OCT1*4* (G401S), and *OCT1*14* (R206C/M420del). The allelic variants R61C and G401S were commonly observed in Caucasians and were functionally characterized in detail before as variants that strongly decrease OCT1 activity (Shu et al., 2003; Tzvetkov et al., 2009; Tzvetkov et al., 2011; Tzvetkov et al., 2012; Tzvetkov et al., 2013). The allele *OCT1*14* was recently identified in Asians and has been shown to significantly decrease the uptake of metformin, MPP⁺, and TEA⁺ (Chen et al., 2010). In this work the number of substrates analyzed was extended and R206C/M420del was confirmed as a variant with strong substrate-wide reduction in transport activity.

Thirdly, a substantial number of allelic variants tested revealed substrate-specific loss of activity: *OCT1*2* (M420del), *OCT1*7* (S14F), *OCT1*10* (S189L), *OCT1*11* (I449T), and *OCT1*13* (T245M) (Figure 4.5). Substrate-specific effects for the allelic variants M420del, S14F, and S189L have been reported before (Shu et al., 2003; Shu et al., 2007; Tzvetkov et al., 2009; Ahlin et al., 2011; Tzvetkov et al., 2011; Saadatmand et al., 2012; Tzvetkov et al., 2012). The allelic variants I449T and T245M have been previously identified and were predicted by several bioinformatics tools to cause loss of OCT1 activity (Seitz et al., 2015). However, detailed functional characterization revealed that the alleles *OCT1*11* and *OCT1*13* (characterized by the variants I449T and T245M, respectively) caused substrate-specific loss of activity. The allele *OCT1*11* strongly reduced the uptake of metformin and almost abolished tropisetron uptake, but the uptake of MPP⁺, ASP⁺, and O-desmethyltramadol was not altered compared to the wild type. The allele *OCT1*13*

strongly decreased the uptake for most of the substances tested, but decreased MPP⁺ uptake only by 44 % and no differences were observed in the uptake of debrisoquine (Figure 4.5). Hence, the bioinformatic prediction of loss of function of the variants I449T and T245M could not be confirmed. This finding emphasizes the need for functional testing of newly identified variants.

Finally, the last group identified contained the two variants *OCT1*8* (R488M) and *OCT1*9* (P117L) that caused gain of activity for some of the substrates tested. They caused a more than 50 % increase in the uptake of at least one substrate tested (Figure 4.5). Previously, the variant R488M was reported not to affect the uptake of metformin (Shu et al., 2007; Chen et al., 2014). Here it could be shown that allele *OCT1*8* (containing the R488M variant) increased metformin uptake by 68 %. Moreover the uptake was also increased by more than 50 % for TEA⁺ and morphine (Figure 4.5). For all the other substances tested, R488M showed at least 74 % of wild type transport activity. The sub-allele *OCT1*8B* was characterized by combination of R488M and M408V. In line with previous findings, the presence of M408V did not affect the transport activity of the R488M variant (Figure 4.5) (Shu et al., 2003).

In contrast to our findings, in the study of Chen *et al.*, the allele *OCT1*9* (P117L) was shown to significantly decrease the uptake of metformin, MPP⁺, and TEA⁺ (Chen et al., 2010). In this work P117L increased the uptake of metformin and MPP⁺ by 39 % and 30 %, respectively, and no significant differences were observed in the uptake of TEA⁺ (92 % of wild type transport activity) (Figure 4.5). Uptake activity for a broader range of substrates than previously investigated by Chen *et al* was analyzed in the work. *OCT1*9* was shown not to decrease the uptake of any of the substrates tested, except for tropisetron and debrisoquine. And for these substrates, *OCT1*9* decreased the uptake by 49 % and 14 %, respectively. Additionally, the coding region of the *OCT1* clone used was re-sequenced and confirmed that the leucine₁₁₇, but not any other unwanted mutation was present.

Several differences between these measurements and those seen in Chen *et al.* should be noted. In contrast to Chen *et al.*, in which the uptake measurements were performed with 10 μM of [¹⁴C] metformin and [¹⁴C] TEA⁺ as well as with 1 μM of [³H] MPP⁺ for 5 min, the measurements of the uptake of [¹⁴C] metformin and [¹⁴C] TEA⁺ in this work were made using 5 μM of the substrates as well as 10 μM of [³H] MPP⁺ and were performed for 2 minutes. However, the differences in the observed uptake activity of *OCT1*9* cannot be

due to differences in the concentrations used as they were both far below the apparent K_m values for the respective substrate that were previously reported or determined in this thesis (K_m of 2.42 mM, 109 μ M, and 590 μ M for wild type OCT1 for metformin MPP^+ and TEA^+ , respectively; see Table 4.3) (Shu et al., 2007). If the substrate concentration used is far below the K_m of the substance, effects on transport kinetics might remain undetected if K_m or v_{max} are affected by the polymorphism to the same extent. Chen *et al.* analyzed the uptake kinetics for metformin of the P117L variant compared to wild type OCT1 (P117L: $K_m = 1.51$ mM and $v_{max} = 2.02$ nmol/mg protein/min; wild type: $K_m = 1.18$ mM and $v_{max} = 3.96$ nmol/mg protein/min) (Chen et al., 2010). Based on the Michaelis Menten equation we would have expected a 60 % decrease in metformin uptake at the concentration we used in our study. However, in our uptake experiments P117L showed an increase in metformin uptake by 39 % (Figure 4.5), which is contradictory to the results of Chen *et al.*

Moreover, Chen *et al.* used OCT1 with a C-terminal GFP-tag (Chen et al., 2010). The OCT1 used in this work did not contain a GFP-tag and therefore better represents the conditions found *in vivo*. Other than Chen *et al.*, no other studies have analyzed the effect of P117L on transport activity so far. More detailed analyses of the uptake kinetics for substrates like MPP^+ and morphine, which showed a strong increase in uptake, would be needed in order to verify the impact of P117L on transport activity.

Another example of contradictory observations is the S14F variant, which was reported to cause an increase of function. Shu *et al.* was the first group to characterize S14F transport activity. In their study, S14F was characterized as a variant with increased function showing an almost 2-fold increase in the uptake of MPP^+ compared to wild type (Shu et al., 2003). This observation is contradictory to observations in this work, as analysis found a 27 % decrease of MPP^+ uptake (Figure 4.5). Based on previous and current findings, the variant S14F can be characterized as a substrate-specific loss of function variant whereby making artifacts from the cloning strategies or transport assays unlikely (Shu et al., 2003; Shu et al., 2007; Chen et al., 2014; Seitz et al., 2015).

Taken together, neither in this work nor in previous studies, an *OCT1* allelic variant could be identified as a gain of function allele, in which the uptake of all substrates was increased. Data regarding the effect on transport activity is still contradictory. Hence, it is necessary to validate the observed effects of an increased uptake activity by determining the uptake kinetics of different substrates. Moreover, one should compare at least two

different clones of wild type, R488M, and P117L variants in order to exclude that the observed effects were caused by the expression system used.

My analyses were performed using stable transfected HEK293 cell lines generated by targeted chromosomal integration, which were validated in order to verify constant and equal overexpression of OCT1 variants used in this work. However, some discrepancies were observed in the generated constructs.

According to haplotype inferring analysis, P117L occurs in combination with F160L (Figure 1.2; (Seitz et al., 2015)). The construct that was used for transfection in this work contained phenylalanine₁₆₀. However, the F160L variant was shown not to affect OCT1 transport activity (Kerb et al., 2002; Sakata et al., 2004; Shu et al., 2007; Chen et al., 2014). Hence, it can be expected that the transport activity of P117L is not affected by the presence of phenylalanine₁₆₀.

The substrate-specific loss-of-function variants S14F and T245M exist in combination with M408V according to haplotype inferring analyses (Figure 1.2). In this thesis the plasmid constructs used for stable transfection contained a methionine₄₀₈ instead of a valine₄₀₈. However, it was shown that the variant M408V does not affect the impact of other polymorphisms (Shu et al., 2003; Tzvetkov et al., 2014). Additionally, cells overexpressing T245M were shown to have at least a double tandem integration of the respective expression plasmid (Figure 4.2). As the variant showed clear substrate-specific effects (Figure 4.5) it can be assumed that multiple tandem integration did not affect functional characteristics of T245M. So far no studies analyzing the effect of multiple tandem integrations into HEK293 cells after stable transfection are available. However, it needs to be considered that the allelic variants were selected based on equal overexpression of OCT1 (Figure 4.3).

According to haplotype inferring analyses the complete loss-of-function variants S29L and E284K exist in combination with P341L and M408V, respectively (Seitz et al., 2015) (Figure 1.2). The constructs that were used in this work contained proline₃₄₁ and methionine₄₀₈ instead. However, the amino acid substitutions in P341L and M408V were shown not to affect OCT1 transport activity *in vitro* or *in vivo* (Shu et al., 2003; Takeuchi et al., 2003; Sakata et al., 2004; Shu et al., 2007; Yoon et al., 2013; Chen et al., 2014). As the S29L and E284K variants showed complete lack of activity it is unlikely that proline₃₄₁

or methionine₄₀₈ could restore transport activity. This assumption is supported by the previous finding that M408V does not alter the impaired transport activity of M420del (Shu et al., 2003). Therefore, it can be concluded that it is unlikely that the complete loss of activity for the allelic variant S29L could be restored in combination with P341L.

Cells overexpressing C88R/M420del were previously generated and characterized in our lab (Tzvetkov et al., 2012). In this work a refined validation strategy was used in order to characterize the generated cell line in detail and tested for multiple tandem integration of the expression plasmid. This method has been previously established in the lab of Clinical Pharmacology (Pojar, 2015). It could be shown that the allelic variant C88R/M420del has at least a double tandem integration with the respective expression plasmid (Figure 4.2). However, despite the multiple-integration, the cells did not show transport for any of the substrates tested. Therefore it could be concluded that the multiple tandem integration does not affect the functional characteristics of C88R/M420del.

In summary, this work provides a detailed, functional characterization of global OCT1 genetic variants using a broad spectrum of structurally diverse substrates including both, typical model substrates as well as clinically relevant drugs. With this, a substantial number of substrate-specific variants could be identified. As a broad range of structurally diverse OCT1 substrates were tested, it could be shown that it is not sufficient to test single OCT1 substrates in order to predict the effect of identified OCT1 variants. This is especially true concerning the high number of variants showing substrate-specific loss of activity.

5.1.1 Complete loss of transport activity is caused by improper membrane localization

Analysis was performed on the 15 major alleles regarding their subcellular localization of OCT1 using immunofluorescent staining and confocal microscopy. It could be shown that the allelic variants *OCT1**5 (G465R/M420del), *OCT1**6 (C88R/M420del), *OCT1**12 (S29L), and *OCT1**15 (E284K) were not located in the plasma membrane, but rather seemed to be retained in the endoplasmic reticulum (Figure 4.6 A). Therefore, this data clearly shows that the reason for the complete lack of transport activity observed for these

variants is improper membrane localization and that complete loss of function of the polyspecific transporter OCT1 can only be achieved by lack of membrane localization.

Additionally, the allelic variants that lack correct membrane localization showed a different glycosylation pattern of the OCT1 protein (Figure 4.7). The mouse monoclonal anti-human OCT1 specific antibody (2C5) used in the western blot analysis of whole cell protein lysates revealed two bands for OCT1 at approximately 50 kDa and 70 kDa. As suggested earlier, the bands represent different glycosylation forms of OCT1 as shown by deglycosylation using *PNGaseF* (Denk et al., 2004). The glycosylated form of OCT1 at 50 kDa could be specified as being *EndoH* and *PNGaseF* sensitive and the 70 kDa form could be specified as being *EndoH* resistant and *PNGaseF* sensitive (Figure 4.7). *EndoH* only cleaves within the chitobiose core of high mannose and some hybrid oligosaccharides from *N*-linked glycoproteins (Capell et al., 2000; Hagglund et al., 2004). These sugar residues are formed at the beginning of the glycosylation process of the protein in the endoplasmic reticulum, when the active dolichol transfers sugar residues on asparagine (Hart, 1992). Higher glycans can only be cleaved by *PNGaseF* (Plummer et al., 1984) and appear after removal of mannose residues and the addition of sugar residues in the Golgi-apparatus (Hart, 1992; Helenius, 1994; Harding et al., 1999). The allelic variants C88R/M420del, G465R/M420del, S29L, and E294K showing complete loss of activity only revealed the *EndoH* sensitive form at approximately 50 kDa in western blot analysis suggesting abortion of protein maturation (Figure 5.1). In contrast, all other variants tested showed a glycosylation pattern similar to wild type OCT1.

Western blot analysis of human liver samples revealed only one band for OCT1 at approximately 70 kDa (Nies et al., 2009). Accordingly it can be interpreted that this band represents the *EndoH* resistant and *PNGaseF* sensitive glycosylated form of the protein, whereas the *EndoH* and *PNGaseF* sensitive form at 50 kDa is missing. As transfected HEK293 cells were used to overexpress *OCT1* for western blot analysis, this observation underlines the assumption that the observed glycosylated form at 50 kDa represents an immature form of the protein due to the *in vitro* system used.

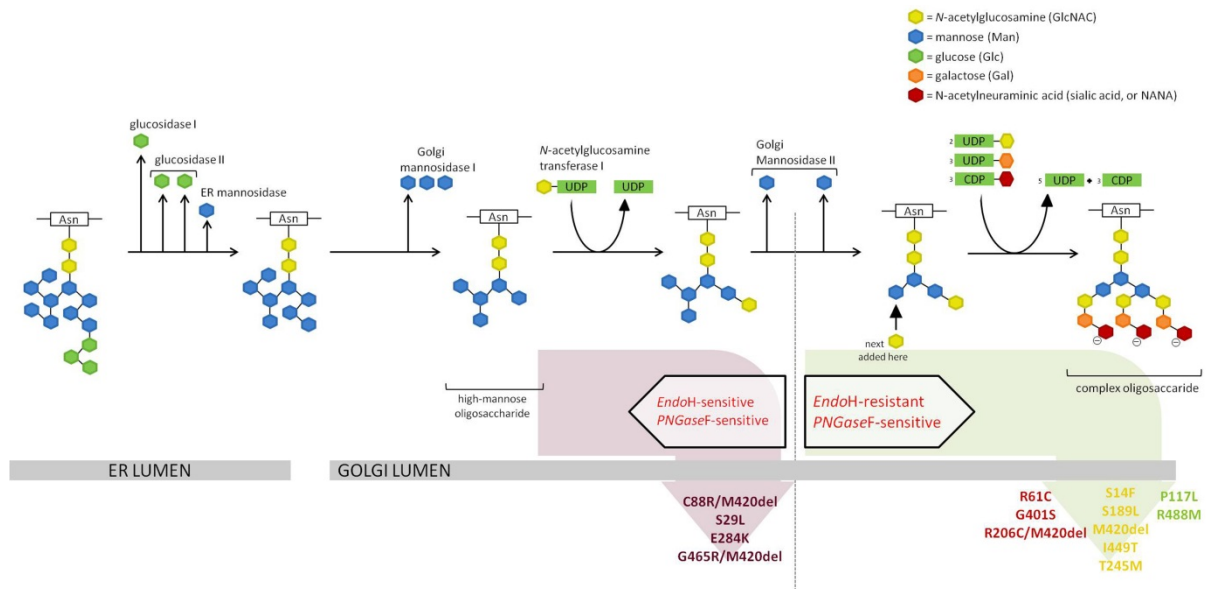


Figure 5.1 Processing of *N*-linked oligosaccharides of the glycosylated protein in the endoplasmic reticulum (ER) and in the Golgi apparatus. Shown is the processing pathway of *N*-linked oligosaccharides starting in the lumen of the endoplasmic reticulum. During the highly ordered processing sugar residues are removed or added by specific enzymes as indicated in order to finally generate highly complex oligosaccharides. The *EndoH* resistant oligosaccharide consists of a core of three mannoses that is present in all complex oligosaccharide. The resulting complex oligosaccharides are *EndoH*-resistant but remain *PNGaseF*-sensitive. As suggested by immunostaining the allelic variants S29L, C88R/M420del, E284K, and G465R/M420del are retained in the endoplasmic reticulum and revealed a glycosylated form of 50 kDa in western blot analysis, which is sensitiv to *EndoH*. This result indicates oligosaccharide processing of the glycosylated protein in these variants is terminated in the endoplasmic reticulum. All other variants were shown to be located in the plasma membrane and revealed a high glycosylated form at 70 kDa in western blot analysis, which in *EndoH*-resistant and *PNGaseF*-sensitive.

The G465R variant was reported to strongly decrease plasma membrane localization of OCT1 in MDCK and HEK293 transfected cells (Shu et al., 2003; Ahlin et al., 2011). The studies analyzed the membrane localization by confocal microscopy of cells transfected with GFP-tagged OCT1 constructs. Additionally, Ahlin *et al.* performed western blot analysis of membrane fractions. As a control they showed staining of Na⁺/K⁺ ATPase as a plasma membrane marker. However, contamination with cytosolic protein could not be excluded as an appropriate marker such as GAPDH (as a cytosolic protein) or calnexin (as a marker for the endoplasmic reticulum) was not included in their study. It needs to be pointed out that in the present thesis, both, immunofluorescence and western blot analysis of whole cell lysates, only allow qualitative statements about OCT1 membrane

localization. So far, it is not possible to obtain pure membrane fractions using different protocols, which included membrane isolation via ultracentrifugation or biotinylation of plasma membrane proteins and subsequent isolation via streptavidin coated columns (data not shown). But although qualitative analysis was performed, the observations of a lack of membrane localization using immunofluorescence were in line with western blot analysis. Assuming that the different glycosylation pattern of the allelic variants with complete lack of transport activity represent differences in protein maturation that further affects membrane trafficking, the different glycosylation patterns support the idea of improper membrane localization. In order to clarify the obtained observation of a lack of membrane localization it should be noted that the establishment of a protocol for membrane isolation and the verification of the purity of membrane fractions with appropriate controls is required.

The allelic variants with a strong substrate-wide decrease, but not complete loss, in transport activity *OCT1*3* (R61C), *OCT1*4* (G401S), and *OCT1*14* (R206C/M420del) were shown to be located on the plasma membrane (Figure 4.6 A). In comparison to staining of wild type, R61C and R206C, but not G401S, there seems to be less expressed in the plasma membrane. This observation is in line with previous studies that analyzed membrane localization of R61C and R206C in membrane fractions of stable transfected HEK293 cells and showed strong reduction of membrane localization for these variants (Chen et al., 2010; Ahlin et al., 2011). However, as the protein was not totally absent in the plasma membrane (Figure 4.6 A), one may conclude that the substrate-wide decrease in uptake activity is due to the reduced membrane localization. This would be in line with the observation that R206C decreased the uptake of metformin and R61C decreased the uptake of debrisoquine due to reduced v_{max} whereas the K_m was not affected for either variants (Chen et al., 2010; Saadatmand et al., 2012).

All variants showing substrate-specific loss of activity or no changes in the activity compared to wild type showed no aberrant plasma membrane localization (Figure 4.6 B, C). For the variants P117L, R488M and M420del correct membrane localization was shown before (Shu et al., 2003; Chen et al., 2010) whereas subcellular localization of the variants S14F, S189L, I449T, and T245M was characterized in this work for the first time.

5.1.2 Evolutionary conservation as a predictor of loss of function

The amino acid scoring systems Grantham and BLOSUM62 were previously used in order to predict the effect of identified OCT1 allelic variants on transport activity (Leabman et al., 2003). Lower Grantham values indicate chemical similarity, whereas higher values indicate radical chemical changes (Grantham, 1974). A more negative BLOSUM62 value indicates an evolutionary unfavorable change (Cargill et al., 1999; Shu et al., 2003).

Changes of evolutionarily conserved amino acids in OCT1 were predicted to cause OCT1 loss of function as evolutionarily conserved amino acids were suggested to be important for the structure of the transporter and hence its function (Shu et al., 2003).

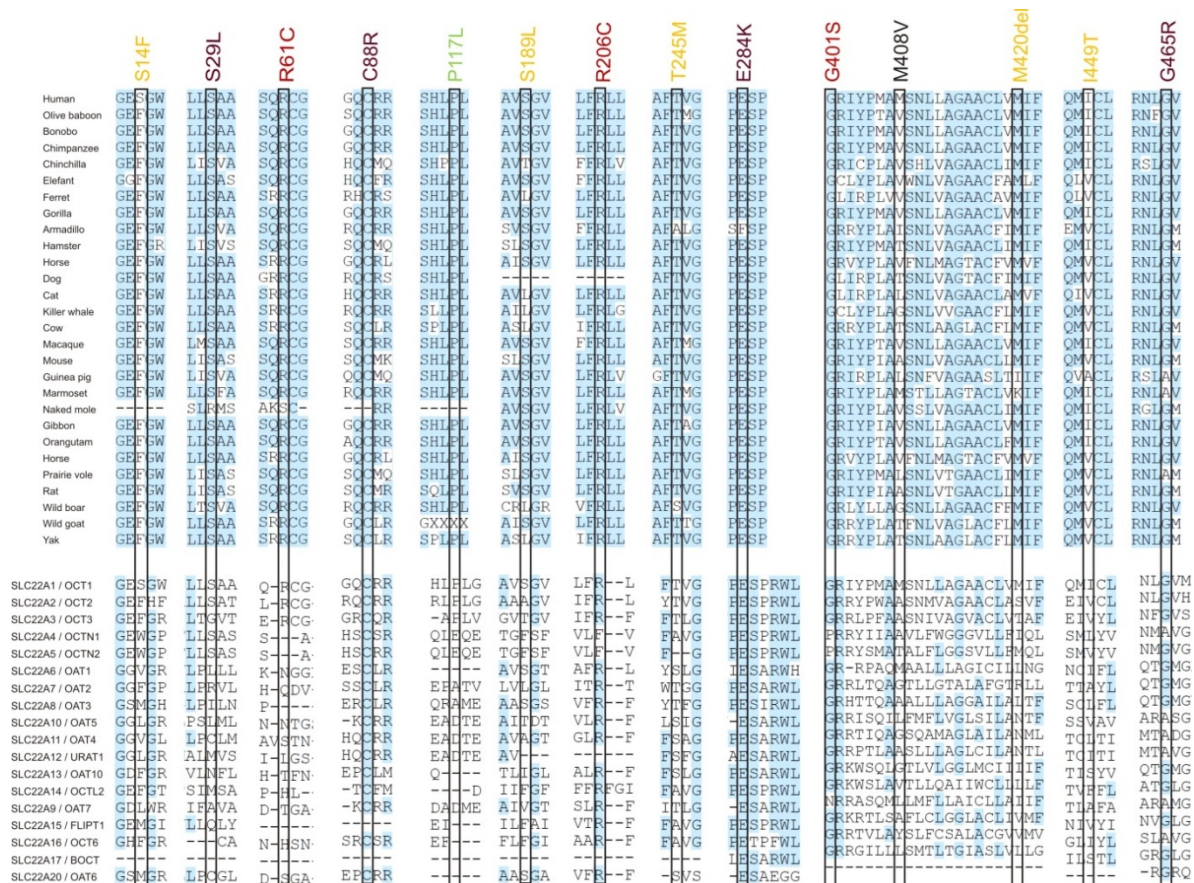


Figure 5.2 Evolutionary conservation of amino acids in OCT1 orthologs (upper part) and paralogs (lower part). Substitutions in OCT1 that caused complete loss of function are shown in dark red, substitutions causing substrate-wide strong decrease in transport activity are shown in light red, substitutions causing substrate-specific loss of function are shown in yellow and substitutions that cause gain of OCT1 function are shown in green. This figure was presented in a slightly modified form in Seitz et al. 2015 (Seitz et al., 2015)

In this study, complete loss of function was observed for the allelic variants C88R/M420del, G465R/M420del, S29L, and E284K as these variants lack plasma membrane localization (Figure 4.6). One might speculate that the affected amino acids are important for OCT1 structure and that changes of these amino acids prevent correct membrane localization. The affected amino acids are highly conserved among mammalian OCT1 orthologs (Figure 5.2). Moreover, serine₂₉ is conserved in organic cation members of the SLC22 family OCT2 and OCTN1-2, but not in OCT3. Serine₂₉ is located in the first transmembrane domain of the OCT1 protein (Figure 5.3). One may speculate about the involvement of the 1st transmembrane domain in trafficking of OCT1 to the plasma membrane as it was shown that the big extracellular loop between the 1st and the 2nd transmembrane domain is important for oligomerization and membrane localization of OCT1 (Keller et al., 2011). The exchange of the hydrophilic, polar serine₂₉ to the hydrophobic, non-polar leucine may affect amino acids interactions in the 1st transmembrane domain and hence impair correct protein folding that disable correct membrane localization.

Cysteine₈₈ and glutamic acid₂₈₄ are strongly conserved both in mammalian OCT1 orthologs and in the other members of the SLC22 family (Figure 5.2). The affected cysteine₈₈ is located in the big extracellular loop between the 1st and the 2nd transmembrane domain (Figure 5.3). Cysteines in the big extracellular loop were shown to be important for homo-oligomerization of OCT1 by formation of disulfide bonds (Keller et al., 2011). The homo-oligomerization is important for plasma membrane localization (Keller et al., 2011). The importance of extracellular cysteines for protein folding and oligomerization by formation of disulfide bonds and correct membrane localization has been shown for OCT2 (Brast et al., 2012). Therefore, substitution of cysteine₈₈ to arginine in OCT1 may prevent formation of disulfide bonds, which impairs plasma membrane localization.

Glutamic acid₂₈₄ is located at the beginning of the big intracellular loop between the 6th and the 7th transmembrane domain (Figure 5.3). The substitution of the negatively charged glutamic acid against the positively charged lysine represents a radical chemical change. The adjacent amino acid serine₂₈₅ is one of the proposed phosphorylation sites of protein kinase C and would possess a negative charge when phosphorylated (Zhang et al., 1997). Therefore, the exchange to a positively charged lysine₂₈₄ may strongly disturb theoretically possible charge interactions. This may impair protein folding and thus membrane

trafficking. However, according to prediction software analyzing potential serine phosphorylation sites, the potential serine₂₈₅ phosphorylation site is not altered by the E284K variant (using NetPhos 2.0; <http://www.cbs.dtu.dk/services/NetPhos>).

The conservation of glycine₄₆₅ was previously analyzed in detail. Glycine₄₆₅ is highly conserved among OCT1 orthologs, OCT2 and OCT3, and even in OAT1-3 (Figure 5.2) (Shu et al., 2003). The variant G465R was predicted as a loss of function variant due to its high Grantham value of 125, indicating radical chemical changes, and a negative BLOSUM62 value of -2, indicating evolutionarily unfavorable changes (Shu et al., 2003). One reason for the extreme effect of the G465R variant may be the radical chemical change from uncharged glycine to positively charged arginine. Alanine is the only other amino acid observed at codon 465 among OCT1 orthologs and paralogs (Figure 5.2). When glycine₄₆₅ was substituted against alanine, this artificial variant exhibited normal transport activity (Shu et al., 2003).

Additionally, the affected amino acids of variants showing a substrate-wide decrease of transport activity (R61C, G401S, and R206C/M420del) are highly conserved among OCT1 orthologs, and also in OCT2 and OCT3. The affected glycine₄₀₁ and arginine₂₀₆ are also conserved in OAT1-5 and some other members of the SLC22 family (Figure 5.2).

For R206C it is suggested that a decrease in transport activity is caused by reduced membrane localization (Chen et al., 2010). Using confocal microscopy analysis also in this work a decrease in membrane localization for the R206C variant could be suggested as the immunofluorescence staining intensity was decreased compared to wild type OCT1 (Figure 4.6). Chen *et al.* suggested that reduced membrane localization was due to the possible involvement of arginine₂₀₆ in the arginine-based endoplasmic reticulum localization signal (Chen et al., 2010). Another possibility is that substitution of arginine₂₀₆ in the extracellular loop between the 3rd and the 4th transmembrane domain against cysteine may lead to interactions with other extracellular cysteines. Formation of additional disulfide bonds may change protein structure and impair structural changes necessary for membrane trafficking. In order to emphasize the importance of the conserved arginine₂₀₆ for OCT1 membrane localization, Chen *et al.* mutated the respective amino acid in OCT3 (R212C) and OAT2 (R202C). Both mutants revealed strong reduction in membrane localization similar to R206C in OCT1 (Chen et al., 2010).

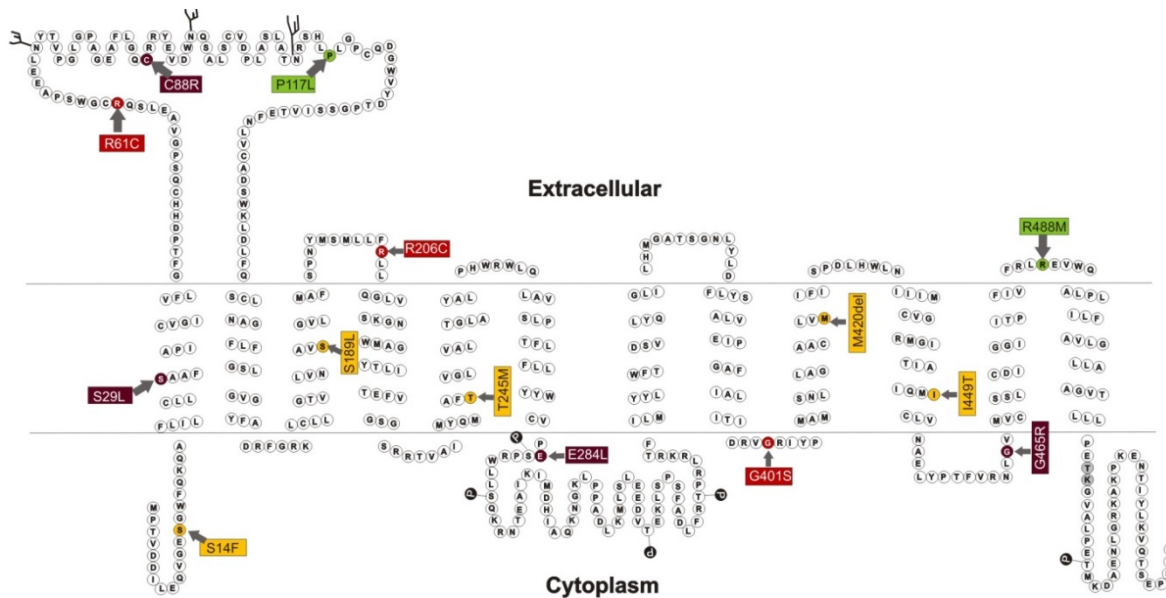


Figure 5.3 Localization of functional *OCT1* polymorphisms within the secondary structure of the *OCT1* protein. Substitutions that caused complete loss of function are shown in dark red, substitutions causing substrate-wide strong decrease in transport activity are shown in light red, substitutions causing substrate-specific loss of function are shown in yellow and substitutions that cause gain of *OCT1* function are shown in green. The amino acids threonine₅₁₆ and lysine₅₁₇ are suggested to interact with serine₄₀₁ (see below) and are shown in gray. This figure was presented in a slightly modified form in Seitz et al. 2015 (Seitz et al., 2015)

The conservation of glycine₄₀₁ has been previously noted (Shu et al., 2003). In line with the observations in this work and previous studies in our lab, Shu *et al.* observed strong decrease in transport activity for G401S and also a strong decrease in the v_{\max} for the uptake of metformin and debrisoquine whereas, the K_m of these substrates was not affected (Figure 4.5) (Shu et al., 2007; Saadatmand et al., 2012). It can be inferred that the strong decrease in transport activity was not due to decreased membrane localization (Figure 4.6 A). However, so far structural reasons for the strong decrease of the G401S variant are not known. Shu *et al.* suggested that the conserved glycine residue may be of high importance for *OCT1* structure and therefore substitution of glycine₄₀₁ may strongly affect *OCT1* function (Shu et al., 2003). But so far, the structural mechanism underlying the observed effect of G401S on transport activity is not known.

A first approach to explain the effect of the G401S variant was made together with Ralf Krätzner from Department of Pediatrics and Adolescent Medicine, University Medical Center Göttingen, using an inward open homology model of *OCT1* (Model-ID Q9NQD4,

<http://modbase.compbio.ucsf.edu>), that was derived from the crystal structure of LacY from *E.coli* (PDB number 1pv6) (Figure 5.4) (Seitz et al., 2015). The 3D model suggested close contact of serine₄₀₁, which is located in the intracellular loop between the 8th and the 9th transmembrane domain, with threonine₅₁₆ or lysine₅₁₇ at the C-terminal end of the 12th transmembrane domain. This close contact could lead to formation of a hydrogen bond between the hydroxyl group of serine₄₀₁ and the carbonyl oxygen of threonine₅₁₆ or the amino group of the lysine₅₁₇ side chain, respectively (Figure 5.4). Due to the hydrogen in the side chain of glycine₄₀₁ there is much more conformational flexibility than all the other amino acids. Due to the formation of a hydrogen bond when an exchange to serine₄₀₁ is performed there may be a reduction in protein plasticity, which is suggested to be important for the general structural changes within the OCT1 protein during the translocation process.

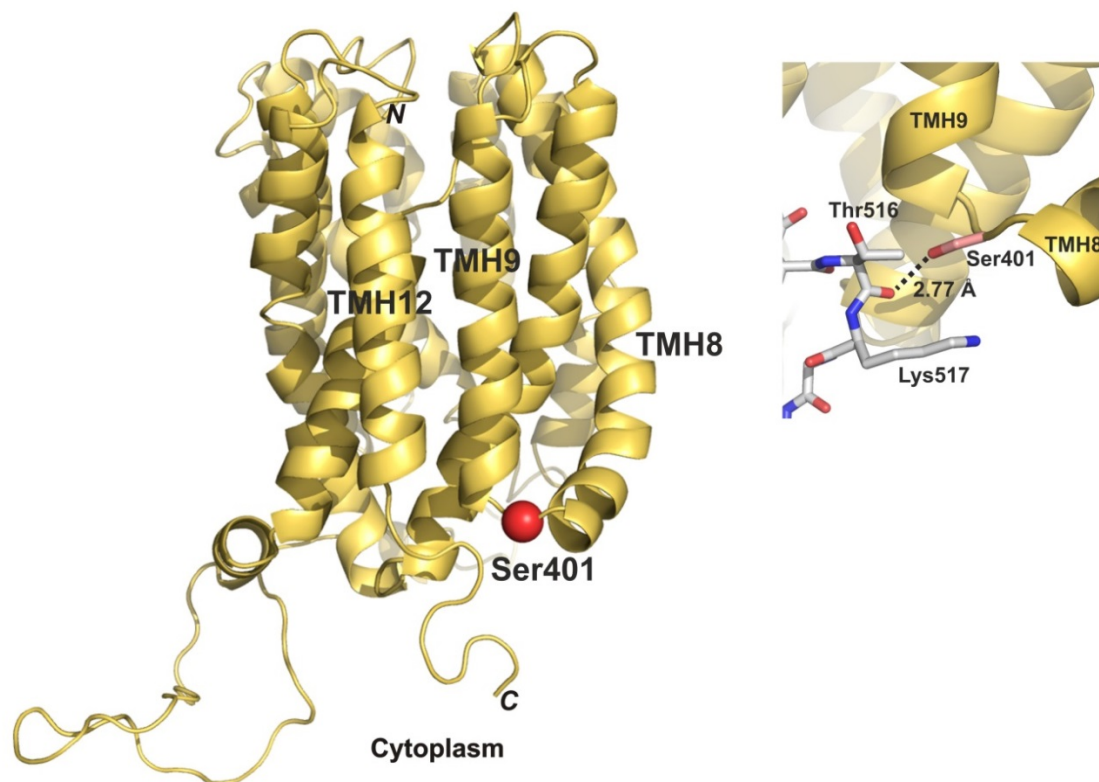


Figure 5.4 (previous page) Predicted 3D model of the OCT1 protein showing the position and possible interactions of serine₄₀₁. The homology model of the inward facing conformation of OCT1 (Model-ID Q9NQD4, ModBase) based on homology with lactose permease LacY of *E.coli* (PDB number: 1pv6). The model was visualized using the PyMol software version 1.3 (Schrödinger, LLC, München, Germany). The red sphere represents the G401S amino acid substitution between the 8th and the 9th transmembrane domain (left). The detailed representation on the right shows the predicted interaction via formation of a hydrogen bond between the hydroxyl oxygen of serine₄₀₁ and carbonyl oxygen threonine₅₁₆ or the side chain amino group of lysine₅₁₇, respectively. Oxygen atoms are represented in red and nitrogen atoms in blue. Figure taken from (Seitz et al., 2015)

The allelic variants I449T and T245M were newly identified and predicted by several bioinformatics tools to cause loss of OCT1 function (Seitz et al., 2015). However, these variants were shown to cause substrate-specific loss of activity (Figure 4.5). This finding emphasizes that bioinformatic prediction is not sufficient and a functional characterization of newly identified variants is essential. In case of threonine₂₄₅, which is highly conserved among OCT1 orthologs, OCT2 and OCT3, this strong evolutionary conservation is not sufficient to predict the effect of an amino acid exchange at position 245. Moreover the substitution of threonine₂₄₅ to methionine is a radical chemical change from a hydrophilic to a hydrophobic amino acid. Radical chemical changes of amino acids were predicted to strongly affect OCT1 activity (Shu et al., 2003). However, the variant T245M did not caused a complete loss of OCT1 activity, but a substrate-dependent loss of activity.

Similar observations were made for the variant P117L, which was shown not to affect OCT1 activity (Figure 4.5). Proline₁₁₇ is highly conserved among OCT1 orthologs, OCT2 and OCT3 (Figure 5.2). Proline residues are known to be important for protein structure. However, substitution of proline₁₁₇ to leucine did not affect transport activity.

Taken together, the evaluation of evolutionary conservation can be used as an indicator for the effects of newly identified variants on OCT1 function, but does not replace the need for functional characterization.

5.2 Strong worldwide variations in the frequency of loss of OCT1 activity

Together with the results from the global analyses of OCT1 genetic variability, previously performed by Robert Stalman and Nawar Dalila, and the functional data of OCT1 allelic variants presented in this thesis a world map is able to be created illustrating the global distribution of loss-of function variants in OCT1 (Figure 5.5; (Seitz et al., 2015)). With this in mind it was possible to analyze the frequency of the identified OCT1 variants in a sample set of 1079 DNA probes as well as the available data from the 1000 Genomes project (Seitz et al., 2015).

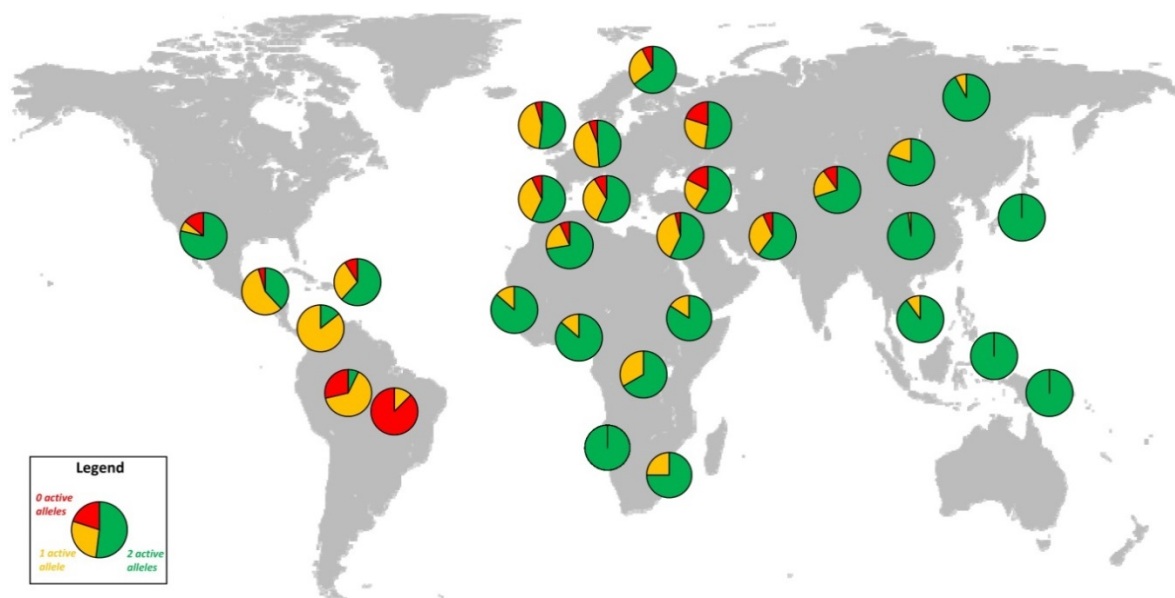


Figure 5.5 Map illustrating the global distribution of loss of function of OCT1 activity. According to the functional analyses the OCT1 allelic variants *OCT1*1*, *OCT1*8*, and *OCT1*9* were regarded as active, whereas the remaining major alleles *OCT1*2*, *OCT1*3*, *OCT1*4*, *OCT1*5*, *OCT1*6*, *OCT1*7*, *OCT1*10*, *OCT1*11*, *OCT1*12*, *OCT1*13*, *OCT1*14*, and *OCT1*15* were regarded as loss of function variants as they decreased the uptake by more than 65 % for at least one of the substrates tested (Figure 4.5). Frequencies of carriers with two (green), one (orange), and zero (red) active OCT1 alleles are shown for different regions worldwide. Figure taken from (Seitz et al., 2015)

In European populations, on average, 53 % carried two, 38 % one and 8 % carried zero active *OCT1* alleles (Figure 5.5). Similar frequencies to the European population have been reported before (Kerb et al., 2002; Shu et al., 2003; Tzvetkov et al., 2012). However, outside of Europe a strong variability in the frequency of loss-of-function *OCT1* variants was observed (Figure 5.5). In populations of Japan and Oceania all individuals carried two active *OCT1* allelic variants. In Han Chinese peoples, the major population in China, more than 98 % of the individuals carried two fully active *OCT1* alleles and the remaining 2 % carried only one active allele (Seitz et al., 2015). In contrast, 87 % of the Surui Indians, a Native American tribe in the Amazon, carried two loss-of-function *OCT1* alleles. The *OCT1* variant *OCT1*2* (M420del) was the most frequent loss-of-function variant observed in this population.

Surui Indians are a small tribe in the Amazon of South America. Only eight DNA samples from this Native American population were available for this study suggesting possible overestimation of the number of carriers of loss-of-function *OCT1* alleles in this population. However, the probability that the observation of 7 out of 8 Surui Indians are carriers of two loss-of-function alleles is made by chance and that the frequency of loss of *OCT1* function would be similar to Europe is 6.3×10^{-8} according χ^2 testing (chi-squared test) (Seitz et al., 2015). Other populations in South America were also found to have high frequencies of loss of function variants in *OCT1*. From the Karitina Indians, 29 % carried two and 64 % carried one loss-of-function *OCT1* variant. Only 7 % of the Karitina Indians carried two fully active *OCT1* alleles (Seitz et al., 2015).

The examples of East Asian populations in which almost all individuals carry two active *OCT1* alleles and the native populations in South America with very high frequency of loss of function *OCT1* activity illustrate the big difference in the frequencies of *OCT1* loss of function globally (Figure 5.5). This observation was further supported by analyzing the pairwise fixation index (FST value) that represents the divergence of loss of *OCT1* activity among different world regions. The highest FST value was observed between populations of East Asia and South America indicating strong divergence between these two world regions (Seitz et al., 2015). As the populations in South America and East Asia shared a common ancestor, one reason for the observed high genetic variability could be due to a

selection pressure for either keeping or losing OCT1 activity (Li et al., 2008; Seitz et al., 2015). A previous study from Raghavan *et al.* indicated that the ancestor of Native Americans is more likely found in the Siberian Upper Palaeolithic population indicating that the separation from East Asians and Japanese may have occurred earlier than expected (Raghavan et al., 2014). However, in this region two active *OCT1* alleles were observed with extreme frequency in the individuals that have been analyzed (Figure 5.5).

So far, the reason for the strong variation in loss of function of OCT1 activity between East Asian and South American populations is not known. One might speculate about a selection pressure that either favored keeping OCT1 activity in East Asia or losing it in South America. Population genetic analyses were performed to test for neutrality of the observed loss of OCT1 function. Based on the results from the functional analyses of OCT1 allelic variants, it is possible to analyze separately the nucleotide diversity for the amino acid substitutions causing loss of OCT1 function (LOF) and the ones not causing loss of function (non-LOF) (Seitz et al., 2015) (Table 5.1). The latter should represent the neutral effects on the distribution. The nucleotide diversity is used as a quantification parameter for the observed genetic variability. When comparing the observed (π) and expected nucleotide diversity of the OCT1 LOF variants (θ Teta), the observed loss-of-function nucleotide diversity in East Asia and Oceania was significantly lower than the expected value as shown by the significant negative values in the Tajima's D test (Tajima's $D = -1.64$, $P < 0.01$). This analysis delivered the strongest support for the existence of a selection pressure for maintaining OCT1 activity in East Asia rather than losing it in South America.

Table 5.1 Population genetic statistics for the OCT1 gene in different world regions. Table was taken with modifications from (Seitz et al., 2015)

World region	π ($\times 10^{-4}$)			Loss-of-function only (LOF)		
	LOF	non-LOF	$\pi_{LOF} / \pi_{non-LOF}$	π ($\times 10^{-4}$)	θ ($\times 10^{-4}$)	Tajima's D
Subsaharan Africa	0.85	4.06	0.21	0.85	1.73	-0.60
North Africa and Middle East	2.59	3.15	0.82	2.59	5.67	-1.04
Europe	3.06	4.87	0.63	3.06	4.65	-0.57
Central Asia	2.36	5.24	0.45	2.36	5.42	-1.04
East Asia and Oceania	0.16	5.32	0.03	0.16	4.79	-1.64**
America	2.76	0.87	3.18	2.76	1.06	1.68

The selective agent for keeping OCT1 activity has not yet been identified. For other polymorphic genes that are involved in the uptake and metabolism of drugs, exogenous toxins were suggested as a selective agent (Nebert, 1997; Ingelman-Sundberg, 2001). One may speculate that in the case of OCT1, organic cations or hydrophilicly weak organic bases as components of nutrition could act as selective agents. For example, monocrotaline is a pyrrolizidine alkaloid derived from the *Crotalaria* genus, which undergoes hepatic biotransformation resulting in toxic pyrrole derivatives (Adams and Rogers, 1939; Petry et al., 1984). Monocrotaline is a known substrate of OCT1 and genetic variants of OCT1 allelic variants were shown to affect uptake of monocrotaline (Tu et al., 2013; Seitz et al., 2015). Except for the gain of function allelic variants *OCT1**8 and *OCT1**9 all allelic variants analyzed in this work strongly decreased monocrotaline uptake by at least more than 67 % (Seitz et al., 2015). Individuals with reduced hepatic uptake of monocrotaline due to loss of function OCT1 allelic variants may be protected from monocrotaline induced hepatotoxicity. However, monocrotaline-containing plants are used in the traditional Chinese herbal medicine and in food supplements, but as unwanted contaminations *Crotalaria* is also found in beverages (Huxtable, 1980; Fu et al., 2002). Although the global occurrence of monocrotaline and the distribution of loss of function

OCT1 variants do not overlap, this example may illustrate how a certain natural toxin may act as a selective agent.

Another selection pressure may be the potential role of OCT1 in the development of Beriberi, a disease caused by deficiency of thiamine (vitamin B1). The clinical picture of beriberi is very complex: with common symptoms being loss of weight, emotional disturbance, impairment of sensory perception, weakness and pain in the limbs, periods of irregular heart rate, and edema (Williams et al., 1940; Whitfield, 1947; Minicucci et al., 2004). The first clear reports about the clinical picture of beriberi were found in the 10th century in China. But in the 18th century it became a serious problem in Japan (Carpenter, 2012). Good sources of thiamine are milk and milk products, pork, grain products, and eggs (Batcher and Nichols, 1984). Possibly due to their diet, high in consumption of polished rice, Asian populations have a thiamine undersupply which can lead to beriberi (Strong and Crowell, 1912). Thiamine was recently shown to be a substrate of OCT1 and loss-of-function genetic variants of OCT1 were shown to affect thiamine transport (Chen et al., 2014). Oct1 deficient mice have increased triglyceride levels in the liver caused by reduced hepatic uptake of thiamine (Chen et al., 2014). This loss of OCT1 activity may increase sensitivity towards thiamine malnutrition. Therefore, one may speculate that it is an advantage to keep OCT1 activity especially in East Asia, where polished rice is a dietary staple. However, retaining OCT1 activity seems to not be sufficient considering the high incidence of beriberi in China and Japan due to severe thiamine undersupply. Most importantly, as cultivation of rice started about 11 000 – 12 000 BC or later and the production of white rice is suggested to be begun around 1700 in Japan, polished rice may not be considered as a selective agent (Carpenter, 2000; Sweeney and McCouch, 2007). However, it is not known if the reported individuals that died of beriberi were carriers of loss-of function *OCT1* alleles and hence more susceptible to vitamin B1 malnutrition.

Although the examples of monocrotaline toxicity and the beriberi disease can theoretically explain the advantage for either losing or keeping OCT1 activity, respectively, they cannot explain the observed differences in the frequency of loss of OCT1 activity between East Asia and South America. The selective agent for keeping OCT1 activity in East Asia remains unknown.

Besides a certain selection pressure for keeping OCT1 activity in East Asia, also a genetic drift could be taken into consideration trying to explain the strong global variability in loss of OCT1 function. A genetic bottleneck may have caused the high frequency of loss of OCT1 activity in South America. In accordance to the Out of Africa hypothesis, the South American Indians have traveled the longest migration distance among the modern *Homo sapiens* (Nei and Roychoudhury, 1993; Goebel et al., 2008). Population genetic analysis revealed positive correlation of loss of OCT1 activity and the migration distance of the modern *Homo sapiens* from Addis Ababa, which is assumed as the starting point according to the Out of Africa model (Liu et al., 2006; Seitz et al., 2015). Moreover, genetic diversity decreased between North to South America (Hunley and Healy, 2011). The genetic bottleneck may have occurred when the Surui Indians came in contact with diseases of civilization like measles, influenza, and chicken pox to which they were not resistant to, e.g. the Surui Indians of Rondonia suffered mortality rates up to 50 % following colonialization in the first decades of the 20th century (Moran, 1996).

Although we can speculate only about probable causes, we can draw certain conclusions from the observed variability in loss of OCT1 function globally. Inter-individual differences in response to commonly used drugs like morphine, metformin, tropisetron, debrisoquine, and O-desmethyltramadol were observed due to loss-of function polymorphisms in *OCT1* (Tzvetkov et al., 2009; Tzvetkov et al., 2011; Saadatmand et al., 2012; Tzvetkov et al., 2012; Tzvetkov et al., 2013). Hence, one might speculate that in East Asia, the inter-individual differences in plasma concentrations of drugs that are substrates of OCT1 are smaller than in Europe. Indeed, Zouh *et al.* found higher renal clearance of morphine in Chinese individuals than in Caucasian individuals due to increased glucuronidation of morphine to its metabolites morphine-3-glucuronide and morphine-6-glucuronide (Zhou et al., 1993). Based on the current knowledge one might speculate that the high frequency of carriers of two active *OCT1* alleles in East Asia can be taken into consideration to describe the observed effect in the study of Zhou *et al.* Morphine is a substrate of OCT1 and needs to be taken up into hepatocytes in order to be metabolized prior to excretion (Sadhasivam et al., 2012; Fukuda et al., 2013; Tzvetkov et al., 2013). As in the Chinese population almost all individuals have two active *OCT1* alleles, the OCT1-mediated morphine uptake might be higher in the studied individuals of Zhou *et al.* and

hence more of its metabolites could be produced leading to generally lower plasma concentrations of morphine. Moreover, the Chinese individuals were less sensitive to the adverse effects of morphine such as respiratory depressant or the hemodynamic effects of morphine like vasodepression. Contradictory, Chinese individuals were more sensitive to nausea (Zhou et al., 1993). Next to East Asia, the majority of individuals from African populations carried two active *OCT1* alleles (Seitz et al., 2015). Fukuda *et al.* analyzed the higher incidence of morphine adverse effects in children from Caucasian population in comparison to children from African-American populations. They found that in homozygous carriers of loss of function *OCT1* allelic variants morphine clearance was significantly lower than in heterozygous carriers or carriers of two active *OCT1* alleles (Fukuda et al., 2013). This is in line with recent findings that in African populations the majority of individuals have two active *OCT1* alleles (Seitz et al., 2015).

In contrast to Chinese, Cepeda *et al.* reported that Native Americans were more susceptible to morphine induced respiratory suppression (Cepeda et al., 2001). One possible explanation could be the reduced OCT1-mediated uptake due to higher frequency of loss of function *OCT1* polymorphism in this ethnic group (Figure 5.5, Table 5.1). Unfortunately, the study does not specify the affiliation of the Native Americans studied. However, in the Karitiana tribe, a native Indian tribe of Brazil, the frequency of OCT1 loss of function was high with 29 % and 64 % of the individuals carrying two and one loss of function alleles, respectively (Seitz et al., 2015).

In conclusion, we observed strong global variation in the frequency of loss of OCT1 activity. The reason for the observed variability remains unknown. However, the genetic variability might account for the observed inter-individual differences in drug response for drugs that are substrates of OCT1. Inter-individual differences in drug response due to inter-ethnic genetic variability were also described for other enzymes responsible for drug uptake and metabolism (Xie et al., 2001; Burroughs et al., 2002). Hence, the knowledge of the individual genotype might help to improve adjustment of drug medication in order to achieve the best therapeutic efficacy while reducing adverse effects at the same time.

5.3 Model substrates are not sufficiently to predict allele-specific effects on morphine and metformin uptake

The substrate-specific loss-of-function allelic variants *M420del*, *S14F*, *S189L*, *I449T*, and *T245M* were analyzed for their ability to predict their effect on the uptake of morphine and metformin by measuring the uptake of model substrates (MPP⁺, TEA⁺, ASP⁺). None of the model substrates analyzed was able to predict the effect of both drugs (Figure 4.8). Whereas, the uptake of morphine correlated better with the uptake of ASP⁺, the uptake of metformin correlated better with the uptake of TEA⁺. Hence, using model substrates for the prediction of the functionality of new identified genetic variants for uptake of divers drugs cannot lead to reliable conclusions.

Similar observations were recently made in a study by Hacker *et al.* in which they screened for inhibitors of OCT2 and analyzed if the inhibition of the uptake of the model substrates MPP⁺ and ASP⁺ could be used to predict the effect of the inhibitors on the uptake of clinically relevant drugs that are substrates of OCT2 such as metformin. They found a moderate correlation between the inhibition of the OCT2-mediated uptake of MPP⁺, ASP⁺, and metformin (Hacker et al., 2015). According to their analyses, the inhibition of ASP⁺ mediated uptake correlated better with the metformin-mediated inhibition than MPP⁺. However, inhibition of ASP⁺-mediated uptake could only partially predict the effect of the inhibitor on metformin mediated uptake. Hacker *et al.* concluded that the inhibition of clinically relevant drugs is strongly substrate-dependent and that *in vitro* inhibition assays for the respective substrate are necessary to predict possible drug-drug interactions *in vivo* (Hacker et al., 2015).

Taken together, it is not sufficient enough to characterize the functionality of newly identified genetic variants by measuring the uptake of model substrates in order to predict their effects on the uptake of diverse drugs. As a crystal structure of OCT1 is not yet available and the structural mechanism behind OCT1-mediated transport is not fully understood, it is indispensable to evaluate the effects of substrate-specific loss-of-function variants on OCT1 activity for each single substrate.

5.4 Prediction of multiple binding sites in OCT1

Five out of 19 variants tested (26 %) showed substrate-specific loss of activity, which supported the analyses of Urban *et al.*, in which they reported that 17 % of non-synonymous variants in drug transporter causing substrate-specific effects (Urban *et al.*, 2006). As their study only analyzed the effect on two substrates, the percentage of substrate specific loss-of-function variants may be even higher. Interestingly, most of the variants showing substrate-specific loss of activity, except S14F, are located in the transmembrane domains of the protein (3rd, 5th, 9th, and 10th, Figure 5.3). Of these transmembrane domains the 5th and the 10th are known to be involved in formation of the substrate binding cleft (Gorboulev *et al.*, 2005; Popp *et al.*, 2005; Koepsell, 2011), but so far none of the variants located in these domains (S14F, S189L, I449T, T245M) are known to be involved in substrate binding. The fifth substrate-specific variant characterized in this thesis, M420del, is located at the end of 9th transmembrane. Up until now, it has not been reported that the 9th transmembrane is involved in the formation of the substrate binding cleft.

These five allelic variants showed up to 100 % loss of transport activity for some substrates tested and no difference to the wild type for others (Figure 4.5). Substrate-specific effects are another manifestation of the polyspecificity of OCT1. Therefore, detailed analyses of polymorphisms causing substrate-specific loss of function could give an insight into the mechanisms enabling the polyspecificity of OCT1 and its transport mechanisms in general.

The correlation between different effects of *OCT1* allelic variants and different structural properties of the substrates was tested. For this purpose, two-dimensional hierarchical clustering analyses were performed by the biostatistician Prof. Beißbarth from the department of Statistical Bioinformatics, University Medical Center Göttingen (Figure 5.6). The analyses were based on the functional data of the genetic variants and their effect on uptake activity of several substrates and the structural differences between these substrates. A majority of this functional data was generated for this thesis. One dimension was the substrates and the other the genetic variants analyzed. The variants showing substrate-specific effects: S14F, M420del, S189L, I449T, and T245M are clustered together. These variants showed a decrease in the uptake of O-desmethyltramadol, tyramine, monocrotaline, TEA⁺, metformin, and tropisetron (Figure 4.5). These substrates are clustered as substrate group B according to their chemical and molecular properties

(Figure 5.6). In contrast, the uptake of ranitidine, MPP⁺, morphine, sumatriptan, ASP⁺, and debrisoquine (substrate group A) was not affected by these variants.

As OCT1 is polyspecific, there is no single binding site but rather several binding sites that are forming a binding cleft. This makes it difficult to define distinct structural properties of a potential substrate. The substrate clustering in group A and B in this analysis is just a first approach to classify different substrates according to their different properties. So far it was not possible to define specific molecular or chemical determinants for classification. However, the more substrates are tested, the more this analysis could be refined. This presentation might help to identify structural properties of different substrates that could be affected by specific amino acids exchanges. With this one might identify possible multiple binding sites in OCT1.

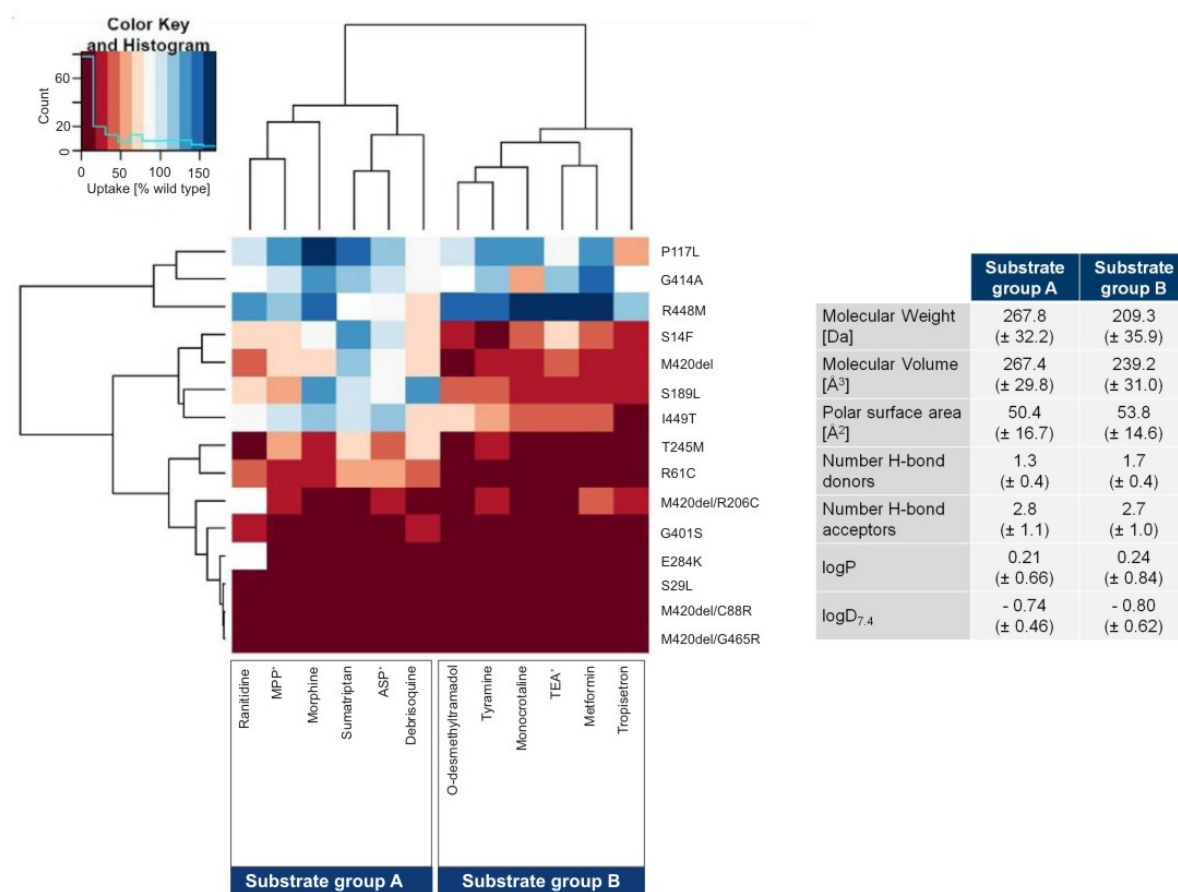


Figure 5.6 (previous page) Two-dimensional hierarchical clustering analysis. On the right are the different OCT1 variants clustered according to their effect on transport activity. On the bottom are the substrates tested, which are clustered according to their structural properties into substrate group A and B (table on the right). The different colors of the analysis represent the effect of the variants on OCT1 uptake activity ranging from dark red, which means complete loss of activity, to white and light blue, which means uptake activity like OCT1 wild type, up to dark blue, which means gain of activity. The analysis was performed with kind support of Prof. Beißbarth from the department of Statistical Bioinformatics, University Medical Center Göttingen.

5.5 M420del caused highly substrate specific effects in OCT1 loss of function

The *M420del* polymorphism is the most common and the only ubiquitously observed loss-of-function OCT1 variant showing highly substrate specific-effects (Figure 1.3, Figure 4.5). Characterization of the substrate specificity of M420del was performed in detail by determining the kinetic parameters K_m and v_{max} for the uptake of TEA^+ , MPP^+ , ASP^+ , metformin, sumatriptan, and proguanil (Figure 4.12, Figure 4.13).

In order to ensure that inter-day differences, like different cell passages, did not affect the extent of the observed substrate-specific loss of activity of the M420del variant uptake measurements with HEK293 cells overexpressing M420del and wild type were performed in parallel and were used for determination of the variation of K_m and v_{max} of M420del from wild type OCT1 in each single experiment. Therefore, simultaneous uptake measurements with fenoterol and sumatriptan with three different concentrations (below K_m , close to K_m , and close to v_{max}) on the same day using identical cell passages was performed. The effect of M420del on the uptake of fenoterol and sumatriptan did not differ in three independent experiments (Figure 4.14).

Highly substrate-specific effects of M420del were observed on the uptake kinetics of TEA^+ , MPP^+ , ASP^+ , metformin, sumatriptan, and proguanil (Figure 4.12, Figure 4.13). M420del decreased v_{max} for all substances tested except for metformin. The decrease varied from 30 % for TEA^+ up to 85 % for fenoterol. Also substrate-specific of M420del on the K_m were observed. M420del decreased the K_m of MPP^+ , ASP^+ , sumatriptan, and

proguanil (Figure 4.13) in a range from 20 % for MPP⁺ to 65 % for proguanil. In contrast, the K_m of TEA⁺ and metformin increased by 200 % and 400 %, respectively.

Previously, the effect of M420del on the uptake kinetics of metformin, ASP⁺, and sumatriptan was analyzed by different groups (Shu *et al.*, 2007; Ahlin *et al.*, 2011; Matthaiei *et al.*, 2015).

In the study of Shu *et al.*, M420del increased the K_m nearly 2-fold ($K_m = 2.42 \pm 0.52$ mM and 4.56 ± 1.08 mM for wild type and M420del, respectively), whereas in a study of Ahlin *et al.* no effect of M420del on the K_m ($K_m = 5.45 \pm 0.29$ mM and 5.19 ± 11.6 mM for wild type and M420del, respectively) was observed (Shu *et al.*, 2007; Ahlin *et al.*, 2011). In this work it could be shown that M420del increased the K_m of metformin by 400 % (Figure 4.13) demonstrating a strong decrease in metformin affinity. In both studies M420del significantly decreased the v_{max} by at least 2-fold (Shu *et al.*: $v_{max} = 6.74 \pm 0.88$ nmol/min/mg protein and 3.31 ± 0.56 nmol/min/mg protein for wild type and M420del, respectively; Ahlin *et al.*: ($v_{max} = 31.9 \pm 0.72$ nmol/min/mg protein and 11.6 ± 0.16 nmol/min/mg protein for wild type and M420del, respectively) (Shu *et al.*, 2007; Ahlin *et al.*, 2011). Contradictory to these findings, no differences in v_{max} for metformin between wild type and M420del could be observed in this work (Figure 4.12, Figure 4.13).

In a study from Ahlin *et al.* it is reported that M420del did not affect uptake kinetics of ASP⁺ and hence the transport efficacy, determined as the quotient K_m/v_{max} (Ahlin *et al.*, 2011). In this work, M420del insignificantly decreased the K_m of ASP⁺ by 50 % (Figure 4.13). However, it was observed that M420del affected the v_{max} to the same extent as K_m showing a decrease by 50 %. Hence, in line with Ahlin *et al.* the resulting transport efficacy did not differ between wild type and M420del (v_{max}/K_m of 4271.8 and 4154.2, respectively). It needs to be pointed out that at single concentration measurements, M420del showed 92 % of wild type activity (Figure 4.5). For these uptake measurements a substrate concentration of 5 μ M was used, which is far below the K_m determined in this study (Table 4.3). Hence, the effect of M420del on ASP⁺ uptake was not detected at single concentration measurements as M420del decreased the v_{max} and K_m to the same extent (by 50 %).

Recently, sumatriptan has been shown to be a substrate of OCT1 and that sumatriptan uptake was not affected by M420del (Matthaiei *et al.*, 2015). In line with Matthaiei *et al.* no

difference in the K_m between wild type and M420del were observed in this work (Table 4.3). Contradictory to the findings of Matthaei *et al.* a 44% decrease in v_{max} was observed. However, in line with the observations of Matthaei *et al.* the intrinsic clearance did not differ between wild type and M420del in this work (37×10^{-3} ml/min/mg protein and 26×10^{-3} ml/min/mg protein for wild type and M420del, respectively). *In vivo* analyses of sumatriptan kinetics revealed that the sumatriptan plasma concentration was not affected in carriers of the M420del variant (Matthaei *et al.*, 2015). However, also different *in vivo* data point to substrate-specific effects of M420del. Whereas the kinetics of sumatriptan were not affected, carriers of the M420del variant showed significantly higher plasma concentrations of morphine and O-desmethyltramadol (Tzvetkov *et al.*, 2011; Tzvetkov *et al.*, 2013; Matthaei *et al.*, 2015). The increased plasma concentrations were associated with increased risk of adverse effects of morphine (e.g. nausea, dizziness, headache) or prolonged miosis, which was used as a surrogate parameter for the effect of O-desmethyltramadol at the μ -opioid receptor (Tzvetkov *et al.*, 2011; Tzvetkov *et al.*, 2013).

Taken together, analyzing several previous studies, which observed an effect of M420del on the uptake of a distinct substrate, highly substrate-specific effects of M420del were found. Whereas M420del impaired the uptake of metformin, no effects were observed on the uptake of ASP^+ and sumatriptan (Shu *et al.*, 2007; Ahlin *et al.*, 2011; Matthaei *et al.*, 2015). However, so far a comparative analysis showing the effect of M420del on the uptake of different substrates is missing. In this work a detailed comparative analysis has been provided by determining the impact of M420del on a broad spectrum of substrates and the substrate-specific effect of M420del has been demonstrated. It needs to be pointed out, that in line with the previous studies, ASP^+ and sumatriptan are two substrates that were not strongly affected by M420del. However, as a broad spectrum of substrates, was used it could be shown that the uptake of such as TEA^+ and proguanil were strongly decreased by M420del due to reduced affinity or transport rate, respectively. Hence, these data demonstrate the highly substrate-specific effect of M420del.

The deletion of methionine₄₂₀ resulted in the decrease of v_{max} between 25 % and 85 % for all substrates tested, except for metformin (Figure 4.13). The v_{max} of metformin was not changed compared to wild type. In line with previous studies a reduced membrane localization of the M420del could not be observed (Figure 4.6 B) (Ahlin *et al.*, 2011). Hence, the decrease in v_{max} was not due to aberrant membrane localization but rather an effect of

M420del on transporter turnover. However, the observation regarding membrane localization of M420del is still controversial (Giannoudis et al., 2013). So far pure membrane fractions of protein lysates using different protocols for membrane isolation have not been successful. Therefore, the next aim is to improve protocols for membrane isolation for western blot analysis in order to verify the obtained results.

The effects of the M420del variant on K_m were highly variable among the substrates tested. For the majority of the substrates tested, M420del decreased the K_m and the extent of decrease was substrate-dependent. Furthermore, the extent of decrease correlated with the two-dimensional hierarchical clustering analysis (Figure 5.6), which was used to analyze the effects of OCT1 variants in correlation with structural properties of different substrates. M420del only slightly decreased the K_m of ranitidine, MPP^+ , and sumatriptan by on average of 20 %. According to the clustering analysis these substrates were found to be similarly affected. The K_m of ASP^+ was more affected by M420del causing a decrease by 50 %. Similar effects were observed for fenoterol and proguanil showing a decrease by 58 % and 64 %, respectively. It would be interesting to include these substrates in the clustering analysis, measuring the effects of different variants on the uptake of fenoterol and proguanil. On assumption that the uptake of these substrates would be similarly affected like the uptake of ASP^+ this would verify that the M420del effects correlate with the effects of other genetic variants analyzed in the clustering analysis.

A strong increase in K_m by 200 % and 400 % was observed in the M420del variant for TEA^+ and metformin, respectively (Figure 4.13). Hence, the affinity for TEA^+ and metformin was decreased by deletion of M420. A decrease in affinity might be caused by indirect effects on amino acids that are involved in substrate binding (Koepsell and Keller, 2016). TEA^+ and metformin have similar chemical structures that strongly differ from those of the other OCT1 substrates tested. TEA^+ and metformin are both aliphatic acyclic compounds, whereas the remaining substrates are aromatic compounds. TEA^+ and metformin were also found to be similarly affected by other OCT1 variants as suggested by clustering analysis (Figure 5.6). Hence, M420del might have specific effects on OCT1 substrates with similar chemical structures as TEA^+ and metformin e.g. choline. Like TEA^+ , choline is an aliphatic acyclic, quaternary ammonium compound. Choline was shown to be transported by rOct1 (Gorboulev et al., 1999). It might be interesting to analyze the effect of M420del on choline uptake kinetics and to compare them with the

obtained data for TEA⁺ and metformin. This could reveal insight in how M420del changes OCT1 affinity in a substrate-dependent manner. In conclusion, the highly substrate-specific effects of M420del on OCT1 affinity were observed with cationic substrates with an aliphatic structure showing a strong decrease in affinity whereas more aromatic substrates showed either no change or a slight increase in affinity.

5.5.1 Effects of M420del are caused by the specific loss of the methionine side chain

Methionine₄₂₀ is located in the 9th transmembrane domain of OCT1. So far, no amino acids of the 9th transmembrane have been reported to be involved in substrate binding or in transport mechanism of OCT1. Hence, one might speculate that indirect effects of a M420del are responsible for the observed substrate-specific effects. According to the homology model of rat Oct1, methionine₄₂₁ is located at the end of the 9th transmembrane domain and may stabilize the arrangement of the 9th and the 10th transmembrane domain within the three dimensional structure of the protein (Figure 4.18). Methionine is very flexible due to its low energy barrier between the different rotamer forms at the C-S bond (Gellman, 1991). Thus it was suggested that the flexibility is more due to the sulfur atom than to the lack of branching (Gellman, 1991). The sulfur atom of methionine is highly polarizable which makes the hydrophobic environment of methionine malleable (Gellman, 1991; Yuan et al., 2000). Hence, methionine₄₂₀ in human OCT1 might be important for the structural integrity and plasticity.

In order to reveal insights into the mechanism underlying the observed M420del specific effect, together with Prof. Hermann Koepsell and Prof. Thomas Mueller from the University of Würzburg two hypotheses were generated based on the structural homology model of the inward and outward conformation of rat Oct1 (Popp et al., 2005; Gorbunov et al., 2008). The first hypothesis analyzed, if M420del specific effects are caused by an unspecific deletion of an amino acid at codon 420 (in this case methionine) that could lead to reduction in size of the protein chain between the 9th and the 10th transmembrane domain. A reduction in the size of the protein chain could change the position of amino acids or the flexibility of the 10th transmembrane domain, which is known to be involved in the translocation process (Gorboulev et al., 2005).

Data from several experimental tests resulted in the rejection of this hypothesis. Firstly, leucine₄₂₇ or histidin₄₂₈ were deleted in the wild type in order to simulate the shortening of the protein chain between the 9th and the 10th transmembrane domain caused by M420del (Figure 4.15). These mutants were expected to lead to substrate-specific loss of activity as observed in the M420del variant. However, the mutants L247del and H428del did not affect OCT1 activity for the uptake of TEA⁺ (Figure 4.20). The uptake was performed with 5 μM TEA⁺, which is below the reported K_m of TEA⁺ (Table 5.2). As discussed earlier, when measuring the uptake of a single concentration that is far below the respective K_m of the substance, an impact on K_m and v_{max} might be undetected if both parameters are affected to the same extent. Therefore, it might be interesting to analyze the effect of L427del and H428del on TEA⁺ uptake kinetics in order to analyze their effect on OCT1 transport.

Secondly, a mutant A426ins on M420del background was generated. The insertion of alanine after proline₄₂₅ was expected to restore transport activity in M420del cells as the insertion should avoid the reduction in size of the protein chain between the 9th and the 10th transmembrane domain. However, the A426ins mutant could not restore transport activity in M420del cells for the uptake of TEA⁺ (Figure 4.17).

Finally and most importantly, a mutant in which methionine₄₂₀ was exchanged by alanine was generated in an attempt to avoid possible structural changes caused by deletion of methionine₄₂₀. Alanine is a hydrophobic amino acid with the second shortest side chain with minimal functional role among amino acid. The mutant was tested with regards to its uptake activity for single concentrations of MPP⁺, TEA⁺, ASP⁺, morphine, metformin, tyramine, and proguanil. No differences in the uptake between M420A and M420del were observed (Figure 4.22). Kinetic studies for the uptake of TEA⁺, MPP⁺, metformin, and sumatriptan did not reveal differences in transport efficacy between M420del and M420A for all substances tested (Figure 4.23, Table 4.4). These results confirmed the assumption that the observed effects of M420del are caused by the specific loss of the methionine side chain.

Taken together, the substrate-specific loss of function activity of M420del could not be explained by reduction of the protein chain and future work should be focused on the specific loss of the methionine amino acid side chain.

Methionine is a hydrophobic, aliphatic amino acid containing sulfur, which is not highly nucleophilic due to the methyl substituent. Due to its hydrophobicity methionine is more likely to be located in the protein core. The methionine side chain is non-reactive and it was difficult to suggest a direct role of methionine₄₂₀ in substrate binding and translocation of OCT1.

To experimentally clarify the potential role of the methionine₄₂₀ side chain, M420 was substituted with different amino acids. The amino acids were chosen according to their side chain length or their chemical properties being similar or totally different to methionine (Figure 5.7). Methionine₄₂₀ was exchanged against threonine, isoleucine or cysteine. Isoleucine is an uncharged hydrophobic amino acid with a non-reactive side chain having a similar length to methionine. However, in contrast to methionine it is more bulky close to the amino acid backbone due to its two substituents at the C-beta carbon. Thus, isoleucine is more conformational restricted. Therefore, it is more difficult for isoleucine to adopt in alpha helical conformations. Similar to isoleucine, threonine has two substituents at the C-beta carbon making threonine more bulky than methionine. However, in contrast to isoleucine, threonine is a polar although uncharged amino acid and has a reactive hydroxyl group. Cysteine was tested as it is the only amino acid other amino acid besides methionine that contains sulfur in its thiol group.

		Amino acid																							
		A	R	N	D	C	Q	E	G	H	I	L	K	M	F	P	S	T	W	Y	V	B	Z	X	*
Amino acid	A	4	-1	-2	-2	0	-1	-1	0	-2	-1	-1	-1	-2	-1	1	0	-3	-2	0	-2	-1	0	-4	
	R	-1	5	0	-2	-3	1	0	-2	0	-3	-2	2	-1	-3	-2	-1	-1	-3	-2	-3	-1	0	-1	-4
	N	-2	0	6	1	-3	0	0	0	1	-3	-3	0	-2	-3	-2	1	0	-4	-2	-3	3	0	-1	-4
	D	-2	-2	1	6	-3	0	2	-1	-1	-3	-4	-1	-3	-3	-1	0	-1	-4	-3	-3	4	1	-1	-4
	C	0	-3	-3	-3	9	-3	-4	-3	-3	-1	-1	-3	-1	-2	-3	-1	-1	-2	-2	-1	-3	-3	-2	-4
	Q	-1	1	0	0	-3	5	2	-2	0	-3	-2	1	0	-3	-1	0	-1	-2	-1	-2	0	3	-1	-4
	E	-1	0	0	2	-4	2	5	-2	0	-3	-3	1	-2	-3	-1	0	-1	-3	-2	-2	1	4	-1	-4
	G	0	-2	0	-1	-3	-2	-2	6	-2	-4	-4	-2	-3	-3	-2	0	-2	-2	-3	-3	-1	-2	-1	-4
	H	-2	0	1	-1	-3	0	0	-2	8	-3	-3	-1	-2	-1	-2	-1	-2	-2	2	-3	0	0	-1	-4
	I	-1	-3	-3	-3	-1	-3	-3	-4	-3	4	2	-3	1	0	-3	-2	-1	-3	-1	3	-3	-3	-1	-4
	L	-1	-2	-3	-4	-1	-2	-3	-4	-3	2	4	-2	2	0	-3	-2	-1	-2	-1	1	-4	-3	-1	-4
	K	-1	2	0	-1	-3	1	1	-2	-1	-3	-2	5	-1	-3	-1	0	-1	-3	-2	-2	0	1	-1	-4
	M	-1	-1	-2	-3	-1	0	-2	-3	-2	1	2	-1	5	0	-2	-1	-1	-1	1	-3	-1	-1	-1	-4
	F	-2	-3	-3	-3	-2	-3	-3	-3	-1	0	0	-3	0	6	-4	-2	-2	1	3	-1	-3	-3	-1	-4
	P	-1	-2	-2	-1	-3	-1	-1	-2	-2	-3	-3	-1	-2	-4	7	-1	-1	-4	-3	-2	-2	-1	-2	-4
	S	-1	-1	1	0	-1	0	0	0	-1	-2	-2	0	-1	-2	-1	4	1	-3	-2	-2	0	0	0	-4
	T	0	-1	0	-1	-1	-1	-1	-2	-2	-1	-1	-1	-1	-2	-1	1	5	-2	-2	0	-1	0	-1	-4
	W	-3	-3	-4	-4	-2	-2	-3	-2	-2	-3	-2	-3	-1	1	-4	-3	-2	11	2	-3	-4	-3	-2	-4
	Y	-2	-2	-2	-3	-2	-1	-2	-3	2	-1	-1	-2	-1	3	-3	-2	-2	2	7	-1	-3	-2	-1	-4
	V	0	-3	-3	-3	-1	-2	-2	-3	-3	3	1	-2	1	-1	-2	-2	0	-3	-1	4	-3	-2	-1	-4
	B	-2	-1	3	4	-3	0	1	-1	0	-3	-4	0	-3	-3	-2	0	-1	-4	-3	-3	4	1	-1	-4
	Z	-1	0	0	1	-3	3	4	-2	0	-3	-3	1	-1	-3	-1	0	-1	-3	-2	-2	1	4	-1	-4
	X	0	-1	-1	-1	-2	-1	-1	-1	-1	-1	-1	-1	-1	-1	-2	0	0	-2	-1	-1	-1	-1	-1	-4
	*	-4	-4	-4	-4	-4	-4	-4	-4	-4	-4	-4	-4	-4	-4	-4	-4	-4	-4	-4	-4	-4	-4	-4	1

Figure 5.7 BLOSUM62 matrix. The substitution matrix illustrates evolutionary divergence between methionine and alanine, cysteine, threonine or isoleucine, respectively. A negative BLOSUM value indicates evolutionary unfavorable changes. BLOSUM62 matrix was obtained from <http://www.ncbi.nlm.nih.gov>

The effect of the mutants M420T, M420I, and M420C on the uptake of MPP^+ , TEA^+ , ASP^+ , morphine, and metformin was investigated. None of the mutants tested could restore wild type activity (Figure 4.24). Moreover, none of the mutants showed significant difference in substrate uptake compared to M420del. Analysis of K_m and v_{max} for the uptake of TEA^+ showed no difference to M420del (Figure 4.25). Taken together none of these amino acids was functionally suitable to substitute methionine at position 420.

Interestingly, the mutant M420C was suggested to lead to miss-folding of the protein due to assumed formation of disulfide bonds with adjacent cysteines e.g. cysteine₄₁₉. This could have resulted in aberrant plasma membrane localization of the protein. However, M420C did not change subcellular localization of OCT1 (Figure 4.21). One explanation is that the cysteine residue was not exposed outside of the cell membrane and therefore was not in the highly oxidative milieu outside of the cell. This is an indirect indication that the methionine₄₂₀ residue is localized within the 9th transmembrane domain and not on the loop border of OCT1.

Wild type activity was unable to be restored by substituting methionine₄₂₀ against threonine, isoleucine, or cysteine. However, it could be possible that other amino acids than the ones tested could substitute for methionine. Therefore, it is interesting to analyze the conservation of methionine₄₂₀ among other OCTs or other members of the SLC22A family. Methionine₄₂₀ is highly conserved among OCT1 orthologs, but not in OCT2 and OCT3 or other paralogs (Figure 5.2). Evolutionary conservation was suggested to determinate the importance of an amino acid for transporter function (Shu et al., 2003). Methionine₄₂₀ is not highly conserved among different OCT1 paralogs. However, one cannot exclude an essential role in OCT1 function. Several examples are known. However, as discussed earlier threonine₂₄₅ is highly conserved among OCT1 orthologs and in OCT2 and OCT3. However, the allelic variant *T245M* was shown to cause substrate-specific effects comparable to M420del (Figure 4.5). Hence, substitution of threonine₂₄₅ did not cause a complete lack of transport activity. Moreover, although proline₁₁₇ is highly conserved among OCT1 homologs, OCT2, and OCT3, substitution against leucine did not affect OCT1 activity in these analyses. Nevertheless, the knowledge about the homology between different members of the SLC22A family especially between the OCTs might help to understand the effects of M420del.

At the position 420 in OCT2 and OCT3 are the amino acid serine and threonine, respectively. One of the mutants tested in this thesis was M420T. It is interesting to speculate if this mutant would behave as OCT3 concerning transport activity and substrate binding. Previous studies analyzed the uptake kinetics of morphine and metformin for OCT1 and OCT3 (Nies et al., 2009; Tzvetkov et al., 2013). Morphine is a substrate of OCT1, but it is not transported by OCT3 (Tzvetkov et al., 2013). In contrast, OCT3 had a 2-fold higher transport capacity for metformin than OCT1, whereas the affinity for metformin did not differ between the two paralogs (Nies et al., 2009). However, the mutant M420T transported both, morphine and metformin (Figure 4.24). Additionally, whereas TEA⁺ is not a substrate of OCT3, it is transported by M420T (Grundemann et al., 1998). These examples demonstrate that the mutant M420T and OCT3 differ in their substrate specificity. Furthermore, it was recently shown that OCT1 has a 10-fold higher transport capacity for sumatriptan uptake and that OCT1 wild type and M420del did not differ in their uptake kinetics (Matthaei et al., 2015). As it could be shown that the mutant M420T did not significantly differ from M420del in the uptake of several substrates (Figure 4.24),

one might speculate that similar results would be obtained for the uptake of sumatriptan. Hence, the mutant M420T is also suggested to have a different uptake rate than OCT3.

One has to consider that OCT1 and OCT3 only share 48 % identical amino acids. Hence, the amino acids that differ between OCT1 and OCT3 may have an impact on transporter structure and subsequently on its function. OCT1 and OCT2 share 68 % identical amino acids. As OCT2 has a serine at the respective position of methionine₄₂₀ in OCT1 it may be interesting to test the effect of a M420S mutation in OCT1 on substrate uptake.

In a previous study similar mutagenesis analyses were performed in order to analyze and characterize the importance of OCT1 function. Chen *et al.* analyzed the importance of arginine₂₀₆. R206C is a polymorphism found in Asians that strongly decreased metformin uptake and impaired membrane localization (Chen et al., 2010) (Figure 4.6 A). They generated two mutants with either similar (R206K) or different (R206E) chemical properties to arginine₂₀₆. Lysine is a positively charged amino acid like arginine and has a similar side chain length, whereas glutamic acid is negatively charged. The strong decrease of R206C in transport activity was suggested to be due to decrease membrane localization of the variant (Chen et al., 2010). The mutant R206K increased the amount of OCT1 in the plasma membrane and was shown to increase substrate uptake. However, R206K was not able to fully restore transport activity. In contrast, the substitution against the negatively charged glutamic acid caused a stronger decrease in substrate uptake than R206C and no appreciable membrane localization was detected for R206E (Chen et al., 2010).

Another example is the study of Popp *et al.* in which the group generated mutants using structurally different amino acids in order to characterize the involvement of tryptophan₂₁₈ in the transport mechanism of rat Oct1 (Popp et al., 2005). In order to characterize tryptophan₂₁₈, the amino acid was exchanged against phenylalanine (W218F), tyrosine (W218Y) or leucine (W217L). Phenylalanine and tyrosine are structurally similar to tryptophan, whereas substitution with leucine is a more radical chemical change. The mutant W218L decreased v_{\max} for both, MPP^+ and TEA^+ , in a similar range. The affinity for TEA^+ was decreased, but the affinity for MPP^+ was not affected. The mutant W218F did not change the K_m or v_{\max} for MPP^+ . In contrast, although the K_m for TEA^+ was not changed, the v_{\max} was decreased by 50 %. Popp *et al.* concluded that the K_m independent changes of v_{\max} in the mutants W218L and W218F might suggest involvement of tryptophan₂₁₈ in structural changes during the translocation process (Popp et al., 2005). In

contrast to W218F, the mutant W218Y showed significant decreases in K_m and v_{max} for MPP^+ and TEA^+ . The higher affinity for both substrates compared to the W218F mutant was suggested to be due to the hydroxyl group of tyrosine₂₁₈ (Popp et al., 2005). Based on their data Popp *et al.* concluded that tryptophan₂₁₈ is involved in binding of both, TEA^+ and MPP^+ , and in translocation TEA^+ .

Taken together, it could be shown that the substrate-specific effect of M420del is caused by the specific loss of the methionine side chain, but the structural mechanism underlying the effect of loss of the methionine side chain remains elusive.

An alternative approach to reveal the role of the methionine₄₂₀ side chain was to take an advantage from the existing homology models of OCT1 and try to validate potential interactions of methionine₄₂₀ with distal amino acids. Possible interactions between methionine₄₂₀ and amino acids of transmembrane domains, which are known to be involved in substrate binding, were analyzed. According to the homology model of rat Oct1 it was suggested that by deletion of methionine₄₂₀ the more bulky amino acid isoleucine₄₂₁ could be roped into the membrane and could interact with leucine₃₆₄ and histidine₃₆₇ in the 7th transmembrane domain, which could affect substrate uptake. The 7th transmembrane domain is known to be involved in formation of the substrate binding cleft (Popp et al., 2005). However, until now no amino acids in the 7th transmembrane domain were identified to be involved in substrate binding or in transport mechanism.

The mutants L364A and H367A on M420del background were generated. Due to exchange of leucine₃₆₄ and histidine₃₆₇ against alanine the supposed interaction with the “roped” isoleucine₄₂₁ should be avoided (Figure 4.18). Therefore, it was expected that these mutants will restore OCT1 wild type activity. However, it was observed that there was a significant decrease in the uptake of MPP^+ and ASP^+ in these mutants, although the uptake of MPP^+ and ASP^+ was not affected by M420del (Figure 4.20 A). The subcellular localization in these mutants was analyzed to ensure that the observed decrease was not caused by a decrease in membrane localization of the transporter. According to microscopy analysis the mutants L364A and H367A did not change the subcellular localization of OCT1 on M420del background (Figure 4.19). Hence, it is suggested that L364 and H367 might be important for substrate uptake independently from M420del. To test this assumption, the mutants L364A and H367A on wild type and M420del backgrounds were

generated, respectively, and the uptake of TEA⁺ was measured. L364A and H367A strongly decreased TEA⁺ uptake independent from the background tested (Figure 4.20 B).

Taken together, this data shows that an experimental validation for potential interaction of the “roped” isoleucine₄₂₁ or M420 with L364 and H367, respectively, could not be generated. However, the amino acids L364 and H367 themselves seem to be involved in binding or translocation of TEA⁺, MPP⁺, and ASP⁺. In order to reveal insights into the involvement of L364 and H367 in substrate binding or transport mechanism, analyses of uptake kinetics are needed to investigate their effect on substrate affinity and transport rate.

5.5.2 The D474E substitution in human OCT1 strongly affects substrate uptake

The amino acids D475, W218, and F160 are known to be located in the binding cleft and to be involved in transport mechanism of rat Oct1 (Gorboulev et al., 1999; Popp et al., 2005; Volk et al., 2009). This work aimed to analyze first, the impact of the respective amino acids in human OCT1 and second, to analyze possible interactions of these amino acids with M420.

In rat Oct1, D475 is suggested to be important for cation selectivity as D475E drastically decreases the v_{\max} for the uptake of TEA⁺, MPP⁺, and choline by 98 %, 87 %, and 97 %, respectively (Gorboulev et al., 1999). The K_m for TEA⁺ and choline was significantly decreased by 88 % and 93 %, whereas the K_m of MPP⁺ was not affected showing only a slight decrease by 19 % (Gorboulev et al., 1999). Gorboulev *et al.* concluded that the turnover for MPP⁺ was decreased. Furthermore they suggested that the increased affinity for TEA⁺ and choline in the D475E mutant may lead to impaired intracellular release of TEA⁺ resulting in a decreased transport rate (Gorboulev et al., 1999). Western blot analysis revealed an increase of protein of D475E mutants in plasma membrane fractions. However, according to visual inspections no differences in membrane localization between wild type Oct1 and the D475E mutants were observed using immunofluorescence analysis (Gorboulev et al., 1999). Independent homology modeling suggested also human D474 as the essential amino acid involved in the interaction of the positive charge of the substrate with OCT1 (Pedersen et al., 2013).

The function of W218 in rat Oct1 was characterized in detail in a study of Popp *et al.* The mutant W218Y significantly reduced the K_m and v_{max} for TEA⁺ and MPP⁺. Based on their results Popp *et al.* suggested that W218 interacts with both, TEA⁺ and MPP⁺ (Popp *et al.*, 2005).

Until now, the mutation F160Y has not been analyzed in rat Oct1. A study from Volk *et al.* analyzed the exchange of phenylalanine₁₆₀ to alanine. Their data indicates that phenylalanine₁₆₀ interacts with corticosterone and tetrabutylammonium (TBuA) (Volk *et al.*, 2009).

These studies demonstrate the important role of D475, W218, and F160 in the function of rat Oct1.

For this work the mutants D474E, W217Y, and F159Y were generated. The mutations were chosen according to the chemical similarity to the exchanged amino acid in order to avoid differences in uptake activity caused by radical chemical changes. Analysis of the mutants regarding their transport activity for the uptake of TEA⁺, MPP⁺, ASP⁺, morphine, proguanil, tyramine, and metformin at single concentrations was performed (Figure 4.27).

The mutants W217Y and F159Y did not affect the uptake of any of the substrates tested (Figure 4.27). It needs to be pointed out that the substrate concentrations used for MPP⁺, TEA⁺, ASP⁺, tyramine, and metformin were far below the determined or previously reported K_m of these substrates (see Table 4.3 and Table 5.2 for MPP⁺, TEA⁺, ASP⁺ and metformin; for tyramine: $K_m = 94.7 \mu\text{M}$ and $v_{max} = 380.9 \text{ pmol/mg protein/min}$ (Seitz *et al.*, 2015)). As Popp *et al.* showed that W218Y in rat Oct1 affects K_m and v_{max} of MPP⁺ and TEA⁺ transport to the same extent, we would expect no effect on the uptake MPP⁺ and TEA⁺ at single concentration measurements when using substrate concentrations far below the K_m . Hence, in order to clarify the effect of W217Y and F159Y in human OCT1 uptake kinetics for these substrates needs to be determined.

The substrate concentrations for morphine and proguanil (1 μM and 80 μM , respectively) were similar to the reported K_m value for morphine ($K_m = 3.4 \mu\text{M}$, (Tzvetkov *et al.*, 2013)) and to the K_m of proguanil determined in this thesis ($K_m = 21.7 \mu\text{M}$, Table 4.3). As W217Y and F159Y did not affect the uptake of morphine and proguanil, it is assumed that these amino acids are not critically involved in the transport of morphine and proguanil.

In contrast, the mutant D474E strongly decreased the uptake of all substrates tested (Figure 4.27). Immunofluorescence staining and confocal microscopy analysis revealed that the observed decrease in transport activity was not due to aberrant membrane localization of the mutants (Figure 4.26). D474E decreased the v_{\max} of TEA⁺ and MPP⁺ uptake by 82 % and 67 %, respectively (Figure 4.29), showing a similar decrease in TEA⁺ uptake as previously reported for rat Oct1 (Gorboulev et al., 1999). In contrast, the effect of D474E on the v_{\max} of MPP⁺ was lower in humans than observed in rat Oct1 (67 % and 87 % respectively, Figure 4.29 and (Gorboulev et al., 1999)). D474E did not affect the K_m of sumatriptan and MPP⁺. The K_m of MPP⁺ was only slightly, but insignificantly, increased by 17 %. This result is in line with the observation that D475E in rat Oct1 did not affect the K_m of MPP⁺ (Gorboulev et al., 1999). In contrast, the K_m values of TEA⁺ and ASP⁺ were significantly decreased by 41 % and 81 %, respectively (Figure 4.29). For rat Oct1 it was reported that D475E affected the K_m of TEA⁺ much stronger showing a decrease by 88 % (Gorboulev et al., 1999). Hence, although D474 in human OCT1 seems to be involved in binding of TEA⁺, the effect of D474E is not as strong as observed in rat Oct1. As in human OCT1 both, the K_m and v_{\max} for ASP⁺ was strongly decreased in D474E mutants by 81 % and 77 %, respectively, one might speculate that according to Gorboulev et al., D474 is involved in binding of ASP⁺.

D474E caused an increase in the K_m by 679 % for metformin suggesting a strong decrease in the affinity for metformin. This result was unexpected as previous observations showed that e.g. for M420del affected the uptake kinetics of TEA⁺ and metformin to the same extent.

Taken together, D474E strongly impaired OCT1 activity. The functional data of D474E in human OCT1 obtained in this study were similar to the data for D475E in rat Oct1 in the study of Gorboulev *et al.* However, the decrease in affinity for TEA⁺ due to D474E mutation in humans was not as strong as observed in rat Oct1. Hence, the decrease of v_{\max} for TEA⁺ uptake of D474E mutants in human OCT1 might not be caused by impaired intracellular release of TEA⁺ due to the increased affinity as previously suggested for rat Oct1 (Gorboulev et al., 1999). This is another indication for species-specific differences and the exact role of D474 in humans needs further investigation. As choline is structurally similar to TEA⁺, it might be interesting, if similar effects of D474E in human OCT1 could be observed for choline uptake as previously reported for the rat ortholog. In contrast to the

strong effects of D474E in humans, no effect of W217Y and F159Y on OCT1 function was observed in this study. However, it is necessary to determine K_m and v_{max} of the substrates in order to evaluate the impact of W217Y and F159Y in human OCT1 on transport function.

Next, possible interactions of D474E, W217Y, and F159Y with M420 were analyzed. Therefore, the mutants D474E, W217Y, and F159Y were generated and overexpressed in combination with M420del and their transport activity for the uptake of TEA^+ , MPP^+ , ASP^+ , morphine, proguanil, tyramine, and metformin at single concentrations was analyzed (Figure 4.27). The mutants W217Y and F159Y in combination with M420del did not affect the uptake of any of the substrates tested. In contrast, D474E in combination with M420del strongly decreased the uptake of all substrates tested. As the results were similar to the effects observed on wild type background, it was concluded that W217Y and F159Y did not interact with M420del and that D474E independent from M420del strongly affects transport activity.

However, detailed analyses of uptake kinetics revealed possible interactions between D474 and M420. The effect of D474E in combination with M420del on the uptake kinetics of TEA^+ , MPP^+ , ASP^+ , metformin, and sumatriptan was analyzed (Figure 4.28, Figure 4.29). D474E in combination with M420del strongly decreased the v_{max} for all substrates tested by at least 68 %, except for metformin. The v_{max} for metformin was not affected by D474E. D474E in combination with M420del increased the K_m of metformin by 133 %. This increase was less strong when D474E was expressed on wild type background showing an increase in the K_m of metformin by 679 %. As M420del increased the K_m by 400 % (Figure 4.12) and D474E by 679 % one may assume that the observed effect of D474E in combination with M420del on K_m of metformin is not an additive one. More likely, the effect of D474E on K_m of metformin is stronger than the effect of M420del. Similar effects were observed for the K_m of TEA^+ : M420del increased the K_m by 200 % (Figure 4.12), whereas D474E decreased the K_m by 41 %. D474E in combination with M420del increased the K_m of TEA^+ only by 34 % (Figure 4.29). This suggested that the effect of M420del on K_m of TEA^+ was abolished in combination with D474E. These data indicate that impact of D474E for the transport of TEA^+ and metformin is stronger than the effect of M420del.

One might also speculate about complex interactions between M420del and D474E when analyzing the effect on the K_m of MPP^+ and sumatriptan. In wild type, D474E did not

affect the K_m of MPP^+ and sumatriptan. In contrast, when D474E was expressed in combination with M420del the K_m for MPP^+ and sumatriptan increased by 102 % and 105 %, respectively. These results suggested that both mutations in combination decreased the affinity for MPP^+ and sumatriptan. However, the exact interaction remains elusive.

Additional analyses on the effect of M420del on K_m and v_{max} in the presence of the D474E mutation were performed (Figure 4.29). According to the previous analyses in the presence of M420del, the v_{max} was decreased for all substrates tested. M420del did not affect the K_m of MPP^+ and ASP^+ in D474E mutants. For MPP^+ it could be suggested that D474E did not strongly affect the affinity for MPP^+ as the mutation also in wild type cells did not change the K_m . For ASP^+ it is difficult to interpret the obtained data, as both M420del and D474E on wild type and M420del background rather lead to an decrease of K_m for ASP^+ . In contrast, the K_m of sumatriptan and metformin increased in the presence of M420del on D474E background by 76 % and 125 %, respectively. This increase is similar to the increase caused by D474E in combination with M420del (Figure 4.29). This data suggests that D474E and M420del affected the K_m of sumatriptan and metformin to the same extent.

In conclusion, it was observed that strong effects of D474E on the affinity for different substrates were present. As D474E strongly decreased affinity for metformin, involvement of D474 in metformin uptake needs further investigations. Furthermore, complex interactions were suggested between D474E and M420del especially concerning the uptake of metformin, MPP^+ and sumatriptan. However, so far the structural mechanism and possible interactions are still unknown. A 3D model of human OCT1 might help to shed light on the structural mechanism of the observed effects of M420del on wild type OCT1 and D474E mutants.

Table 5.2 Uptake kinetic parameters of different substrates in different *in vitro* systems

Substrate	K_m	V_{max}	Expression system	Reference
MPP⁺				
Human	14.6 ± 4.39 μM	3.69 ± 0.409 pmol/oocyte/h	oocytes	(Zhang et al., 1997)
Rat	n.s.	97 ± 5 pmol/oocyte/hr	oocytes	(Grundemann et al., 1994)
	3-19 μM	n.s.	oocytes	(Arndt et al., 2001)
	2.7 ± 1.1 μM	41 ± 3 pmol/oocyte/h	oocytes	(Gorboulev et al., 1999)
	5.6 ± 1.0 μM	n.s.	oocytes	(Gorboulev et al., 2005)
	3.9 ± 1.1 μM	122 ± 30 pmol/oocyte/h	oocytes	(Gorbunov et al., 2008)
	37 μM ± 12	n.s.	oocytes	(Sturm et al., 2007)
	13 μM	40.1 ± 2.6 pmol/min/mg protein	HEK293, transiently transfected	(Martel et al., 1996)
	30 ± 17 μM	324 ± 68 nmol/mg protein/s	Proteoliposomes cell free expression	(Keller et al., 2005)
TEA⁺				
Human	229 ± 78.4 μM	2.89 ± 0.448 nmol/mg protein/30 min	HeLa	(Zhang et al., 1998)
	1.27 ± 0.09 mM	4.09 ± 0.29 nmol/mg protein/ min	HEK293, transiently transfected	(Takeuchi et al., 2003)
Rat	95 ± 10 μM	81 ± 5 pmol/oocyte/hr, 148 ± 4 pmol/oocyte/h	oocytes	(Grundemann et al., 1994)
	95-129 μM	n.s.	oocytes	(Arndt et al., 2001)
	129 ± 17 μM	569 ± 27 pmol/oocyte/h	oocytes	(Gorboulev et al., 1999)
	55-133 μM, 94 ± 27 μM	60-420 pmol/oocyte/h	oocytes	(Popp et al., 2005)
	75 ± 11 μM	n.s.	oocytes	(Gorboulev et al., 2005)
	52 ± 21 μM	503 ± 73 pmol/oocyte/h	oocytes	(Gorbunov et al., 2008)
	Mouse	38 μM	585 pmol/oocyte/h	oocytes
ASP⁺				
Human	2.32 ± 0.29 μM	696 ± 198 RFU/min/mg protein	HEK293, stably transfected	(Ahlin et al., 2008)
	9.21 ± 0.9 μM	23900 ± 708 RFU/min/mg protein	HEK293, stably transfected	(Ahlin et al., 2011)
Rat	1 μM	> 10 μM	HEK293, stably transfected	(Mehrens et al., 2000)
Mouse	9 ± 0.5 μM	24 ± 0.6 a.u.	HEK293, stably transfected	(Schlatter et al., 2014)

Metformin				
Human	2.42±0.52 mM	6.74± 0.88 nmol/min/mg protein	HEK293, stably transfected	(Shu et al., 2007)
	1.18 ±0.18mM	3.47 ± 0.12 nmol/min/mg protein	HEK293, stably transfected	(Chen et al., 2010)
	5.45 ± 0.29 mM	31.9 ± 0.72 nmol/min/mg protein	HEK293, stably transfected	(Ahlin et al., 2011)
	2.16 ± 0.36 mM	4.84 ± 1.15 nmol /mg protein/min	CHO K1, stably transfected	(Nies et al., 2009)
Thiamine				
Human	0.78 ± 0.064 mM	2.77 ± 0.14 mol /mg protein/min	HEK293, stably transfected	(Chen et al., 2014)
Mouse	0.49 ± 0.035 mM	5.80 ± 0.37 nmol/mg protein/min	HEK293, stably transfected	(Chen et al., 2014)

5.5.3 Species-specific differences in transport activity between human OCT1 and rodent orthologs for different substrates

Most of the studies that analyzed OCT1 structure-function relationship or OCT1-mediated drug transport were performed using rat or mouse Oct1 (Shu et al., 2007; Koepsell, 2011; Li et al., 2011; Chen et al., 2014). The data obtained in this thesis enables the identification of whether similar effects were observed in humans. In order to analyze species-specific differences in the transport activity of human OCT1 and rodent orthologs we measured and compared the uptake of MPP⁺, TEA⁺ ASP⁺, and morphine. We found substantial species-specific differences between human OCT1 and rodent orthologs. In contrast, mouse and rat Oct1 did not differ in their uptake activity (Figure 4.31). Compared to human OCT1, mouse and rat Oct1 increased the uptake of TEA⁺ 2.3-fold, whereas uptake of ASP⁺ decreased 2.7-fold and 3.6-fold, respectively (Figure 4.31). This observation was supported by Dresser *et al.* who showed that human OCT1 had a lower affinity for TEA⁺ than rodent Oct1 (Dresser et al., 2000).

Most of the studies have been performed analyzing the uptake kinetics of the model substrates MPP⁺, TEA⁺, ASP⁺ or individual drugs such as metformin and thiamine in human OCT1 or rat Oct1. Studies analyzing mOct1 are still rare (Table 5.2). Until now only a few comparative studies regarding differences in substrate affinities and transport rates between these OCT1 orthologs are available (Dresser et al., 2000; Chen et al., 2014): For example Chen *et al.* analyzed uptake differences of thiamine in human OCT1 and

mouse ortholog. In mouse Oct1 the K_m of thiamine significantly decreased, whereas v_{max} was significantly increased compared to human OCT1 (Chen et al., 2014) (Table 5.2).

Additionally, different studies were performed using different *in vitro* systems such as stably or transiently transfected HEK293 cells or injected oocytes from *Xenopus laevis* (Table 5.2). That makes it difficult to compare the obtained results as for example the lipid environment of the *in vitro* system may affect the binding site of the transporter (Koepsell and Keller, 2016). It is also suggested that differences in experimentally determined K_m values in either oocytes or HEK293 cells may be due to differences in intracellular concentrations of endogenous cations or differences in post-translational modifications (Gorboulev et al., 1999). Even within the same *in vitro* system (especially using injected oocytes) strong variations in the obtained kinetic parameters K_m and v_{max} were observed (Popp et al., 2005). However, the available studies already indicated species-specific differences between OCT1 orthologs. Species-specific differences are getting even more important when considering that some substances that are substrates for human OCT1 act as inhibitors on rat Oct1, e.g. tetrabutylammonium (TBuA) (Dresser et al., 2000; Koepsell et al., 2007; Sturm et al., 2007). The molecular and structural mechanisms underlying these species-specific differences are still unknown (Dresser et al., 2000).

Applying protein sequence alignment, human OCT1 shares 78 % amino acid identity with mouse and rat Oct1 (human: NP_003048, rat: NP_036829, mouse: NP_033228, protein alignment using <http://blast.ncbi.nlm.nih.gov>). Similar numbers were published by Dresser *et al.* who found that 80 % and 78 % of the amino acids are identical between human OCT1 and mouse and rat orthologs, respectively (Dresser et al., 2000). One might speculate that the unequal amino acids among OCT1 orthologs may lead to structural changes that furthermore affect substrate binding and translocation. This is even more likely as the amino acids that are different between the orthologs have different chemical properties (Dresser et al., 2000). However, the observed species-specific differences may also be due to the tissue specific expression of human OCT1 and rodent orthologs: human OCT1 is predominantly expressed in the basolateral membrane of hepatocytes, whereas rodent Oct1 is found to be expressed next to the liver also in kidney and the intestine (Gorboulev et al., 1997; Jonker et al., 2001; Nies et al., 2009). Hence, species-specific differences in substrate specificity and transport might be due to tissue specific requirements.

It was observed that species-specific differences exist between human OCT1 and the rat ortholog in the involvement of D474, W217, and F157 in substrate uptake, and analyses on the effect of these amino acids in mouse Oct1 were performed. The uptake of MPP⁺, TEA⁺, ASP⁺, and morphine at single concentrations in the mutants D475E, W218Y, and F160Y of mouse Oct1 and the respective mutations in humans was measured (Figure 4.32).

In mouse Oct1, the mutant D475E did not affect the uptake of TEA⁺ and MPP⁺, whereas the uptake of ASP⁺ and morphine was significantly decreased. In contrast, in human OCT1 the D474E mutant significantly reduced the uptake of all substrates tested. As discussed earlier one might suggest that D474 in humans could be involved in TEA⁺ binding, whereas in mouse D475E seems not.

In mouse Oct1, the mutant W218Y did not affect the uptake of TEA⁺ and MPP⁺. In contrast, the uptake of ASP⁺ was significantly decreased and the uptake of morphine was significantly increased. In human OCT1, W217Y did not affect the uptake of any of the substances tested.

In mouse Oct1 the mutant F160Y did not affect the uptake of TEA⁺ and MPP⁺. In contrast, the uptake of ASP⁺ and morphine was significantly decreased. In human OCT1, F159Y did not affect the uptake of any of the substances tested.

Taken together, strong differences in the effects of D474E, W217Y, and F159Y between human OCT1 and the mouse orthologs on substrate uptake were observed. One might speculate about species-specific differences in substrate specificity and involvement of amino acids participating in translocation mechanism. However, in order to reveal the role of these amino acids in mouse Oct1, uptake kinetic studies are necessary, because the effects in mouse Oct1 could have been undetected as substrate concentrations far below the K_m were used.

5.6 The M408V and G414A polymorphism do not alter the effect of M420del

Haplotype inferring analyses revealed that M420del exists in combination with several other OCT1 polymorphisms like M408V and G414A (Tzvetkov et al., 2014; Seitz et al., 2015).

Recently, the M420del variant was associated with increased risk of imatinib treatment failure in chronic myeloid leukemia (Giannoudis et al., 2013). This observation was confirmed by *in vitro* studies in which M420del expressing CML cell lines decreased imatinib uptake. Similar results were obtained for the uptake of TEA⁺ and ASP⁺. This decrease was not observed in combination of M420del with V408. Furthermore, lower protein expression of M420del in combination with M408 was observed in western blot analysis of membrane fractions, but not in combination with V408 (Giannoudis et al., 2013). However, analyses of 371 Caucasians regarding their M420del-M408V genotype made by our group could show that M420del exclusively existed in combination with V408 (Tzvetkov et al., 2014). Furthermore, in contrast to the study of Giannoudis *et al.* it was shown in this work that V408 did not affect the impact of M420del on the uptake of TEA⁺ and ASP⁺ but also MPP⁺, morphine, metformin, and debrisoquine (Figure 4.10). M420del with M408 or V408 did not affect membrane localization or protein amount in whole cell lysates (Figure 4.9). As Giannoudis *et al.* used plasma membrane fractions and this work analyzed whole protein lysates, protein analyses by western blotting might not be comparable. However, these results were in line with Ahlin *et al.*, who could also not show differences in subcellular localization or protein expression of the M420del variant using confocal microscopy analysis and western blot analysis of membrane fractions (Ahlin et al., 2011). Additionally, the lack to modulate the effect of M420del by V408, which were observed, is in line with previous studies of Shu *et al.* in which they could show that MPP⁺ uptake in M420del cells is not affected by the presence of V408 (Shu et al., 2003). Shu *et al.* also showed that the presence of V408 did not affect the impact of other non-synonymous amino acid exchanges like R61C and G401S that strongly decreased MPP⁺ uptake independently from M408 and V408 (Shu et al., 2003).

In line with the observations of Shu *et al.*, it could be shown that the effect of M420del is also not altered by another non-synonymous amino acid exchange: the G414A variant. Haplotype inferring analyses revealed that the G414A variant only exists in combination

with M420del (Seitz et al., 2015). However, uptake measurements using HEK293 stably transfected to overexpress all theoretically possible combination of M420del-G414A revealed that no differences were observed in the uptake of MPP⁺, TEA⁺, ASP⁺, metformin, morphine, and O-desmethyltramadol in M420del cells in combination with G414 or A414. In contrast, M420 in combination with A414 revealed uptake activity comparable to wild type reference cells (Figure 4.11). However, a slight increase in the uptake was observed in the presence of V408 independently of M420del or A414. But this increase was also present in combination with M420 or G414.

Taken together, functional data demonstrated highly substrate-specific effects of M420del that are only marginally affected by V408 and A414; another two variants that are commonly inherited with M420del next to C88R and G465R. Recently, haplotype inferring analyses revealed that the variants C88R and G465R exist in combination with M420del (Seitz et al., 2015). Both variants were characterized as complete loss-of-function variants in previous studies *in vitro* and *in vivo* (Shu et al., 2003; Shu et al., 2007; Ahlin et al., 2011; Tzvetkov et al., 2011; Saadatmand et al., 2012; Tzvetkov et al., 2012; Tzvetkov et al., 2013). The studies of Shu *et al.* and Ahlin *et al.* characterized G465R as complete loss-of-function variant, but it is not pointed out if these studies were performed considering that G465R exist in combination with M420del. In contrast, the studies of Tzvetkov *et al.* and Saadatmand *et al.* considered the actual haplotype of C88R and G465R in combination with M420del. However, as all studies showed complete loss of function for these variants, one might speculate that C88R and G465R strongly affect protein structure (see chapter 5.1.2), which lead to lack of membrane localization.

6 Summary and outlook

A major part of this thesis was the functional characterization of common and newly identified OCT1 genetic variants. Nineteen OCT1 variants were functionally characterized regarding their uptake activity of a broad range of known OCT1 substrates including model substrates (MPP⁺, TEA⁺, and ASP⁺) as well as clinically relevant drugs like morphine, O-desmethyltramadol, tropisetron and metformin. A substantial number of OCT1 variants, 5 out of 19 tested, showed substrate-specific loss of activity. This finding emphasizes the need to test each *OCT1* genetic variant on a broad range of substrates in order to characterize them correctly. Furthermore, the high number of substrate-specific variants reflects the polyspecificity of OCT1 and suggests different substrate binding sites and transport mechanisms for different substrates.

More substrates and further mutations in OCT1 should be characterized in the future. This is one alternative strategy to identify the multiple binding sites and to reveal the mechanisms conferring OCT1 polyspecificity. A first approach was made in this thesis by correlating the effect of OCT1 variants on substrate uptake to the structural properties of the different substrates tested using the two-dimensional hierarchical clustering analysis. These were, however, only preliminary prove-of-principle analyses and more data both regarding additional substrates and regarding additional mutations is needed.

The detailed functional analyses of worldwide existing OCT1 genetic variants revealed strong variation in loss of OCT1 activity among different populations. This knowledge could help to explain population-specific differences in the pharmacokinetics and efficacy of drugs like morphine, metformin, and O-desmethyltramadol and may lead to therapy optimization for specific populations in the future. The functional data obtained in this work suggest that Surui Indians, as a population with extremely frequent loss of OCT1 activity, have a higher risk of adverse effect when treated with morphine. Systematic analyze the pharmacokinetics of drugs like morphine in populations with frequent loss of OCT1 activity are needed in order to “translate” our *in vitro* data into therapeutic recommendations.

So far the reason for the strong worldwide differences in the loss of OCT1 activity is not known and the possible selective agent(s) remain unknown. Future studies may focus on

endogenous substances, e.g. vitamin B1, which was recently identified as an OCT1 substrate, or hormones and metabolites that could be tested as potential OCT1 substrates and may differ between the populations due to environmental or nutritional differences among world regions.

The second part of this thesis was the in-depth analysis of the highly substrate-specific M420del variant as the most frequent and ubiquitously observed loss-of-function variant. M420del showed highly substrate-specific effects on substrate affinity. By deletion of methionine₄₂₀ the affinity to TEA⁺ and metformin was strongly decreased, whereas the affinity to the majority for the substrates, including MPP⁺, ASP⁺ and morphine, was increased. As TEA⁺ and metformin have similar structures one might speculate that the effect of M420del on substrate affinity may be restricted to substrates with a similar structure, e.g. strong bases or quaternary amines with aliphatic and not aromatic residues.

It would be interesting to test in the future the effect of M420del on structurally similar substrates. These may include substrates that are structurally similar to TEA⁺ (tetramethylammonium, tetrabutylammonium, tetrapentylammonium, choline) and to metformin (debrisoquine, buformin, phenformin, agmatine) in order to specify the observed substrate-specific effects of M420del.

The deletion of methionine₄₂₀ caused a substrate-dependent decrease of v_{\max} for all substrates tested. As reduced membrane localization for the M420del could not be detected, the decrease in v_{\max} was not due to aberrant membrane localization. However, the observation regarding membrane localization of M420del is still controversial. One of the next aims will be to improve protocols for membrane isolation in order to validate the obtained results using more quantitative methods like LC-MS-based protein quantification.

So far mutagenesis analyses revealed that the substrates-specific effects of M420del were caused by loss of the methionine₄₂₀ side chain. The specific properties of the methionine side chain could not be explained by substituting methionine against threonine, isoleucine or cysteine. Further substitutions like M420S could be tested. Furthermore, a general involvement of L364 and H367 in the transport process was observed that was independent of M420del.

In order to investigate the importance of these two amino acids in OCT1 function, uptake kinetics using of structural different substrates should be performed. Further mutants could

be generated (e.g. L364I, L364V, H367Y) in order to ensure that the observed effect was not due to the radical chemical change caused by substitution of the native amino acids to alanine.

This work suggested also indirect interactions of M420 with D474, but not with W217 and F159. Kinetic studies of F159Y and W217Y mutants in combination or without the M420del are necessary to exclude that the lack of effects on single concentrations tested is not due to simultaneous effects of these mutations on K_m and v_{max} . Furthermore, the mutants D474N and D474R should be generated with or without M420del in order to characterize the effects of D474 in humans and potential interaction with M420 in more details. Together with the recent published homology model of human OCT1 from Pederson *et al.* these efforts shall confirm the importance of D474 as the amino acid that determines the substrate charge specificity of OCT1.

Strong species-specific differences were observed between human OCT1 and its rodent orthologs. Further kinetic studies using a broad range of substrates should be performed in order to analyze species-specific differences in detail. Furthermore, chimeric constructs of human and mouse OCT1 could be used to analyze the structural differences between these two orthologs and to map the important transmembrane domains responsible for the observed species-specific differences. All together this shall help to interpret data obtained from rodent Oct1 and to transfer these findings to humans.

7 References

- , Available at: www.cabi.org/isc/datasheet/87408. Worldwide distribution map of *Crotalaria retusa* (rattleweed).
- Abbud, W., Habinowski, S., Zhang, J.Z., Kendrew, J., Elkairi, F.S., Kemp, B.E., Witters, L.A. and Ismail-Beigi, F., 2000. Stimulation of AMP-activated protein kinase (AMPK) is associated with enhancement of Glut1-mediated glucose transport. *Arch Biochem Biophys* 380, 347-52.
- Abramson, J., Smirnova, I., Kasho, V., Verner, G., Kaback, H.R. and Iwata, S., 2003. Structure and mechanism of the lactose permease of *Escherichia coli*. *Science* 301, 610-5.
- Adams, M., Soukop, M., Barley, V., Yosef, H., Anderson, H., Boesen, E., Trask, C.W., Rufenacht, E. and de Bruijn, K.M., 1995. Tropisetron alone or in combination with dexamethasone for the prevention and treatment of emesis induced by non-cisplatin chemotherapy: a randomized trial. *Anticancer Drugs* 6, 514-21.
- Adams, R. and Rogers, E.F., 1939. The Structure of Monocrotaline, the Alkaloid in *Crotalaria Spectabilis* and *Crotalaria Retusa*. I. *Journal of the American Chemical Society* 61, 2815-2819.
- Ahlin, G., Chen, L., Lazorova, L., Chen, Y., Ianculescu, A.G., Davis, R.L., Giacomini, K.M. and Artursson, P., 2011. Genotype-dependent effects of inhibitors of the organic cation transporter, OCT1: predictions of metformin interactions. *Pharmacogenomics J* 11, 400-11.
- Ahlin, G., Karlsson, J., Pedersen, J.M., Gustavsson, L., Larsson, R., Matsson, P., Norinder, U., Bergstrom, C.A. and Artursson, P., 2008. Structural requirements for drug inhibition of the liver specific human organic cation transport protein 1. *J Med Chem* 51, 5932-42.
- Amidon, G.L., Lennernas, H., Shah, V.P. and Crison, J.R., 1995. A theoretical basis for a biopharmaceutic drug classification: the correlation of in vitro drug product dissolution and in vivo bioavailability. *Pharm Res* 12, 413-20.
- An, H. and He, L., 2016. Current understanding of metformin effect on the control of hyperglycemia in diabetes. *J Endocrinol*.
- Arndt, P., Volk, C., Gorboulev, V., Budiman, T., Popp, C., Ulzheimer-Teuber, I., Akhoundova, A., Koppatz, S., Bamberg, E., Nagel, G. and Koepsell, H., 2001. Interaction of cations, anions, and weak base quinine with rat renal cation transporter rOCT2 compared with rOCT1. *Am J Physiol Renal Physiol* 281, F454-68.
- Batcher, O.M. and Nichols, J.M., 1984. Identifying important food sources of nutrients. *Journal of Nutrition Education* 16, 177-181.
- Bednarczyk, D., Ekins, S., Wikel, J.H. and Wright, S.H., 2003. Influence of molecular structure on substrate binding to the human organic cation transporter, hOCT1. *Mol Pharmacol* 63, 489-98.

- Bourdet, D.L., Pritchard, J.B. and Thakker, D.R., 2005. Differential substrate and inhibitory activities of ranitidine and famotidine toward human organic cation transporter 1 (hOCT1; SLC22A1), hOCT2 (SLC22A2), and hOCT3 (SLC22A3). *J Pharmacol Exp Ther* 315, 1288-97.
- Brast, S., Grabner, A., Sucic, S., Sitte, H.H., Hermann, E., Pavenstadt, H., Schlatter, E. and Ciarimboli, G., 2012. The cysteines of the extracellular loop are crucial for trafficking of human organic cation transporter 2 to the plasma membrane and are involved in oligomerization. *FASEB J* 26, 976-86.
- Breidert, T., Spitzenberger, F., Grundemann, D. and Schomig, E., 1998. Catecholamine transport by the organic cation transporter type 1 (OCT1). *Br J Pharmacol* 125, 218-24.
- Bruntsch, U., Rufenacht, E., Parker, I., Drechsler, S. and de Bruijn, K., 1993. Tropisetron in the prevention of chemotherapy-induced nausea and vomiting in patients responding poorly to previous conventional antiemetic therapy. *Ann Oncol* 4 Suppl 3, 25-9.
- Burroughs, V.J., Maxey, R.W. and Levy, R.A., 2002. Racial and ethnic differences in response to medicines: towards individualized pharmaceutical treatment. *J Natl Med Assoc* 94, 1-26.
- Capell, A., Steiner, H., Willem, M., Kaiser, H., Meyer, C., Walter, J., Lammich, S., Multhaup, G. and Haass, C., 2000. Maturation and pro-peptide cleavage of beta-secretase. *J Biol Chem* 275, 30849-54.
- Cargill, M., Altshuler, D., Ireland, J., Sklar, P., Ardlie, K., Patil, N., Shaw, N., Lane, C.R., Lim, E.P., Kalyanaraman, N., Nemesh, J., Ziaugra, L., Friedland, L., Rolfe, A., Warrington, J., Lipshutz, R., Daley, G.Q. and Lander, E.S., 1999. Characterization of single-nucleotide polymorphisms in coding regions of human genes. *Nat Genet* 22, 231-8.
- Carpenter, K.J., 2000. *Beriberi, White Rice, and Vitamin B*, University of California Press.
- Carpenter, K.J., 2012. The Discovery of Thiamin. *Annals of Nutrition and Metabolism* 61, 219-223.
- Cepeda, M.S., Farrar, J.T., Roa, J.H., Boston, R., Meng, Q.C., Ruiz, F., Carr, D.B. and Strom, B.L., 2001. Ethnicity influences morphine pharmacokinetics and pharmacodynamics. *Clin Pharmacol Ther* 70, 351-61.
- Chen, L., Shu, Y., Liang, X., Chen, E.C., Yee, S.W., Zur, A.A., Li, S., Xu, L., Keshari, K.R., Lin, M.J., Chien, H.C., Zhang, Y., Morrissey, K.M., Liu, J., Ostrem, J., Younger, N.S., Kurhanewicz, J., Shokat, K.M., Ashrafi, K. and Giacomini, K.M., 2014. OCT1 is a high-capacity thiamine transporter that regulates hepatic steatosis and is a target of metformin. *Proc Natl Acad Sci U S A*.
- Chen, L., Takizawa, M., Chen, E., Schlessinger, A., Segenthelar, J., Choi, J.H., Sali, A., Kubo, M., Nakamura, S., Iwamoto, Y., Iwasaki, N. and Giacomini, K.M., 2010. Genetic polymorphisms in organic cation transporter 1 (OCT1) in Chinese and Japanese populations exhibit altered function. *J Pharmacol Exp Ther* 335, 42-50.
- Ciarimboli, G., 2016. Introduction to the Cellular Transport of Organic Cations, in: Ciarimboli, G., Gautron, S. and Schlatter, E. (Eds.), *Organic Cation Transporters:*

- Integration of Physiology, Pathology, and Pharmacology. Springer International Publishing, Cham, pp. 1-47.
- Crews, K.R., Gaedigk, A., Dunnenberger, H.M., Klein, T.E., Shen, D.D., Callaghan, J.T., Kharasch, E.D., Skaar, T.C. and Clinical Pharmacogenetics Implementation, C., 2012. Clinical Pharmacogenetics Implementation Consortium (CPIC) guidelines for codeine therapy in the context of cytochrome P450 2D6 (CYP2D6) genotype. *Clin Pharmacol Ther* 91, 321-6.
- de Boer, A.G., van der Sandt, I.C. and Gaillard, P.J., 2003. The role of drug transporters at the blood-brain barrier. *Annu Rev Pharmacol Toxicol* 43, 629-56.
- Denk, G.U., Soroka, C.J., Mennone, A., Koepsell, H., Beuers, U. and Boyer, J.L., 2004. Down-regulation of the organic cation transporter 1 of rat liver in obstructive cholestasis. *Hepatology* 39, 1382-9.
- Dresser, M.J., Gray, A.T. and Giacomini, K.M., 2000. Kinetic and selectivity differences between rodent, rabbit, and human organic cation transporters (OCT1). *J Pharmacol Exp Ther* 292, 1146-52.
- Egenberger, B., Gorboulev, V., Keller, T., Gorbunov, D., Gottlieb, N., Geiger, D., Mueller, T.D. and Koepsell, H., 2012. A substrate binding hinge domain is critical for transport-related structural changes of organic cation transporter 1. *J Biol Chem* 287, 31561-73.
- Foretz, M., Hebrard, S., Leclerc, J., Zarrinpashneh, E., Soty, M., Mithieux, G., Sakamoto, K., Andreelli, F. and Viollet, B., 2010. Metformin inhibits hepatic gluconeogenesis in mice independently of the LKB1/AMPK pathway via a decrease in hepatic energy state. *J Clin Invest* 120, 2355-69.
- Fu, P.P., Yang, Y.-C., Xia, Q., Chou, M.W., Cui, Y.Y. and Lin, G., 2002. Pyrrolizidine alkaloids-tumorigenic components in Chinese herbal medicines and dietary supplements. *Journal of Food and Drug Analysis* 10, 198-211.
- Fukuda, T., Chidambaram, V., Mizuno, T., Venkatasubramanian, R., Ngamprasertwong, P., Olbrecht, V., Esslinger, H.R., Vinks, A.A. and Sadhasivam, S., 2013. OCT1 genetic variants influence the pharmacokinetics of morphine in children. *Pharmacogenomics* 14, 1141-51.
- Gasche, Y., Daali, Y., Fathi, M., Chiappe, A., Cottini, S., Dayer, P. and Desmeules, J., 2004. Codeine intoxication associated with ultrarapid CYP2D6 metabolism. *N Engl J Med* 351, 2827-31.
- Gellman, S.H., 1991. On the role of methionine residues in the sequence-independent recognition of nonpolar protein surfaces. *Biochemistry* 30, 6633-6.
- Giannoudis, A., Wang, L., Jorgensen, A.L., Xinarianos, G., Davies, A., Pushpakom, S., Liloglou, T., Zhang, J.E., Austin, G., Holyoake, T.L., Foroni, L., Kottaridis, P.D., Muller, M.C., Pirmohamed, M. and Clark, R.E., 2013. The hOCT1 SNPs M420del and M408V alter imatinib uptake and M420del modifies clinical outcome in imatinib-treated chronic myeloid leukemia. *Blood* 121, 628-37.
- Goebel, T., Waters, M.R. and O'Rourke, D.H., 2008. The late Pleistocene dispersal of modern humans in the Americas. *Science* 319, 1497-502.
- Gong, I.Y. and Kim, R.B., 2013. Impact of genetic variation in OATP transporters to drug disposition and response. *Drug Metab Pharmacokinet* 28, 4-18.

- Gorboulev, V., Shatskaya, N., Volk, C. and Koepsell, H., 2005. Subtype-specific affinity for corticosterone of rat organic cation transporters rOCT1 and rOCT2 depends on three amino acids within the substrate binding region. *Mol Pharmacol* 67, 1612-9.
- Gorboulev, V., Ulzheimer, J.C., Akhoundova, A., Ulzheimer-Teuber, I., Karbach, U., Quester, S., Baumann, C., Lang, F., Busch, A.E. and Koepsell, H., 1997. Cloning and characterization of two human polyspecific organic cation transporters. *DNA Cell Biol* 16, 871-81.
- Gorboulev, V., Volk, C., Arndt, P., Akhoundova, A. and Koepsell, H., 1999. Selectivity of the polyspecific cation transporter rOCT1 is changed by mutation of aspartate 475 to glutamate. *Mol Pharmacol* 56, 1254-61.
- Gorbunov, D., Gorboulev, V., Shatskaya, N., Mueller, T., Bamberg, E., Friedrich, T. and Koepsell, H., 2008. High-affinity cation binding to organic cation transporter 1 induces movement of helix 11 and blocks transport after mutations in a modeled interaction domain between two helices. *Mol Pharmacol* 73, 50-61.
- Grantham, R., 1974. Amino acid difference formula to help explain protein evolution. *Science* 185, 862-4.
- Green, R.M., Lo, K., Sterritt, C. and Beier, D.R., 1999. Cloning and functional expression of a mouse liver organic cation transporter. *Hepatology* 29, 1556-62.
- Grundemann, D., Gorboulev, V., Gambaryan, S., Veyhl, M. and Koepsell, H., 1994. Drug excretion mediated by a new prototype of polyspecific transporter. *Nature* 372, 549-52.
- Grundemann, D., Schechinger, B., Rappold, G.A. and Schomig, E., 1998. Molecular identification of the corticosterone-sensitive extraneuronal catecholamine transporter. *Nat Neurosci* 1, 349-51.
- Hacker, K., Maas, R., Kornhuber, J., Fromm, M.F. and Zolk, O., 2015. Substrate-Dependent Inhibition of the Human Organic Cation Transporter OCT2: A Comparison of Metformin with Experimental Substrates. *PLoS One* 10, e0136451.
- Hagglund, P., Bunkenborg, J., Elortza, F., Jensen, O.N. and Roepstorff, P., 2004. A new strategy for identification of N-glycosylated proteins and unambiguous assignment of their glycosylation sites using HILIC enrichment and partial deglycosylation. *J Proteome Res* 3, 556-66.
- Hanks, G.W., Conno, F., Cherny, N., Hanna, M., Kalso, E., McQuay, H.J., Mercadante, S., Meynadier, J., Poulain, P., Ripamonti, C., Radbruch, L., Casas, J.R., Sawe, J., Twycross, R.G., Ventafridda, V. and Expert Working Group of the Research Network of the European Association for Palliative, C., 2001. Morphine and alternative opioids in cancer pain: the EAPC recommendations. *Br J Cancer* 84, 587-93.
- Harding, H.P., Zhang, Y. and Ron, D., 1999. Protein translation and folding are coupled by an endoplasmic-reticulum-resident kinase. *Nature* 397, 271-4.
- Hart, G.W., 1992. Glycosylation. *Curr Opin Cell Biol* 4, 1017-23.
- Hayer-Zillgen, M., Bruss, M. and Bonisch, H., 2002. Expression and pharmacological profile of the human organic cation transporters hOCT1, hOCT2 and hOCT3. *Br J Pharmacol* 136, 829-36.

- Helenius, A., 1994. How N-linked oligosaccharides affect glycoprotein folding in the endoplasmic reticulum. *Mol Biol Cell* 5, 253-65.
- Hendrickx, R., Johansson, J.G., Lohmann, C., Jenvert, R.M., Blomgren, A., Borjesson, L. and Gustavsson, L., 2013. Identification of novel substrates and structure-activity relationship of cellular uptake mediated by human organic cation transporters 1 and 2. *J Med Chem* 56, 7232-42.
- Hunley, K. and Healy, M., 2011. The impact of founder effects, gene flow, and European admixture on native American genetic diversity. *Am J Phys Anthropol* 146, 530-8.
- Huxtable, R.J., 1980. Herbal teas and toxins: novel aspects of pyrrolizidine poisoning in the United States. *Perspect Biol Med* 24, 1-14.
- Ikeda, T., Iwata, K. and Murakami, H., 2000. Inhibitory effect of metformin on intestinal glucose absorption in the perfused rat intestine. *Biochem Pharmacol* 59, 887-90.
- Ingelman-Sundberg, M., 2001. Genetic susceptibility to adverse effects of drugs and environmental toxicants. The role of the CYP family of enzymes. *Mutat Res* 482, 11-9.
- Itoda, M., Saito, Y., Maekawa, K., Hichiya, H., Komamura, K., Kamakura, S., Kitakaze, M., Tomoike, H., Ueno, K., Ozawa, S. and Sawada, J., 2004. Seven novel single nucleotide polymorphisms in the human SLC22A1 gene encoding organic cation transporter 1 (OCT1). *Drug Metab Pharmacokinet* 19, 308-12.
- Jonker, J.W., Wagenaar, E., Mol, C.A., Buitelaar, M., Koepsell, H., Smit, J.W. and Schinkel, A.H., 2001. Reduced hepatic uptake and intestinal excretion of organic cations in mice with a targeted disruption of the organic cation transporter 1 (OCT1 [Slc22a1]) gene. *Mol Cell Biol* 21, 5471-7.
- Kaiser, R., Sezer, O., Papies, A., Bauer, S., Schelenz, C., Tremblay, P.B., Possinger, K., Roots, I. and Brockmoller, J., 2002. Patient-tailored antiemetic treatment with 5-hydroxytryptamine type 3 receptor antagonists according to cytochrome P-450 2D6 genotypes. *J Clin Oncol* 20, 2805-11.
- Kees, F., Farber, L., Bucher, M., Mair, G., Morike, K. and Grobecker, H., 2001. Pharmacokinetics of therapeutic doses of tropisetron in healthy volunteers. *Br J Clin Pharmacol* 52, 705-7.
- Keller, T., Egenberger, B., Gorboulev, V., Bernhard, F., Uzelac, Z., Gorbunov, D., Wirth, C., Koppatz, S., Dotsch, V., Hunte, C., Sitte, H.H. and Koepsell, H., 2011. The large extracellular loop of organic cation transporter 1 influences substrate affinity and is pivotal for oligomerization. *J Biol Chem* 286, 37874-86.
- Keller, T., Elfeber, M., Gorboulev, V., Reilander, H. and Koepsell, H., 2005. Purification and functional reconstitution of the rat organic cation transporter OCT1. *Biochemistry* 44, 12253-63.
- Kerb, R., Brinkmann, U., Chatskaia, N., Gorbunov, D., Gorboulev, V., Mornhinweg, E., Keil, A., Eichelbaum, M. and Koepsell, H., 2002. Identification of genetic variations of the human organic cation transporter hOCT1 and their functional consequences. *Pharmacogenetics* 12, 591-5.
- Kim, M.K., Cho, J.Y., Lim, H.S., Hong, K.S., Chung, J.Y., Bae, K.S., Oh, D.S., Shin, S.G., Lee, S.H., Lee, D.H., Min, B. and Jang, I.J., 2003. Effect of the CYP2D6 genotype on the pharmacokinetics of tropisetron in healthy Korean subjects. *Eur J Clin Pharmacol* 59, 111-6.

- Kim, R.B., Fromm, M.F., Wandel, C., Leake, B., Wood, A.J., Roden, D.M. and Wilkinson, G.R., 1998. The drug transporter P-glycoprotein limits oral absorption and brain entry of HIV-1 protease inhibitors. *J Clin Invest* 101, 289-94.
- Kim, Y.D., Park, K.G., Lee, Y.S., Park, Y.Y., Kim, D.K., Nedumaran, B., Jang, W.G., Cho, W.J., Ha, J., Lee, I.K., Lee, C.H. and Choi, H.S., 2008. Metformin inhibits hepatic gluconeogenesis through AMP-activated protein kinase-dependent regulation of the orphan nuclear receptor SHP. *Diabetes* 57, 306-14.
- Kimura, H., Takeda, M., Narikawa, S., Enomoto, A., Ichida, K. and Endou, H., 2002. Human organic anion transporters and human organic cation transporters mediate renal transport of prostaglandins. *J Pharmacol Exp Ther* 301, 293-8.
- Kirchheiner, J., Keulen, J.T., Bauer, S., Roots, I. and Brockmoller, J., 2008. Effects of the CYP2D6 gene duplication on the pharmacokinetics and pharmacodynamics of tramadol. *J Clin Psychopharmacol* 28, 78-83.
- Kirchheiner, J., Schmidt, H., Tzvetkov, M., Keulen, J.T., Lotsch, J., Roots, I. and Brockmoller, J., 2007. Pharmacokinetics of codeine and its metabolite morphine in ultra-rapid metabolizers due to CYP2D6 duplication. *Pharmacogenomics J* 7, 257-65.
- Koepsell, H., 2011. Substrate recognition and translocation by polyspecific organic cation transporters. *Biol Chem* 392, 95-101.
- Koepsell, H., 2013. The SLC22 family with transporters of organic cations, anions and zwitterions. *Mol Aspects Med* 34, 413-35.
- Koepsell, H. and Endou, H., 2004. The SLC22 drug transporter family. *Pflugers Arch* 447, 666-76.
- Koepsell, H. and Keller, T., 2016. Functional Properties of Organic Cation Transporter OCT1, Binding of Substrates and Inhibitors, and Presumed Transport Mechanism, in: Ciarimboli, G., Gautron, S. and Schlatter, E. (Eds.), *Organic Cation Transporters*. Springer International Publishing, pp. 49-72.
- Koepsell, H., Lips, K. and Volk, C., 2007. Polyspecific Organic Cation Transporters: Structure, Function, Physiological Roles, and Biopharmaceutical Implications. *Pharmaceutical Research* 24, 1227-1251.
- Leabman, M.K., Huang, C.C., DeYoung, J., Carlson, E.J., Taylor, T.R., de la Cruz, M., Johns, S.J., Stryke, D., Kawamoto, M., Urban, T.J., Kroetz, D.L., Ferrin, T.E., Clark, A.G., Risch, N., Herskowitz, I., Giacomini, K.M. and Pharmacogenetics Of Membrane Transporters, I., 2003. Natural variation in human membrane transporter genes reveals evolutionary and functional constraints. *Proc Natl Acad Sci U S A* 100, 5896-901.
- Lehtonen, P., Sten, T., Aitio, O., Kurkela, M., Vuorensola, K., Finel, M. and Kostianen, R., 2010. Glucuronidation of racemic O-desmethyltramadol, the active metabolite of tramadol. *Eur J Pharm Sci* 41, 523-30.
- Li, J.Z., Absher, D.M., Tang, H., Southwick, A.M., Casto, A.M., Ramachandran, S., Cann, H.M., Barsh, G.S., Feldman, M., Cavalli-Sforza, L.L. and Myers, R.M., 2008. Worldwide human relationships inferred from genome-wide patterns of variation. *Science* 319, 1100-4.
- Li, S., Chen, Y., Zhang, S., More, S.S., Huang, X. and Giacomini, K.M., 2011. Role of organic cation transporter 1, OCT1 in the pharmacokinetics and toxicity of cis-

- diammine(pyridine)chloroplatinum(II) and oxaliplatin in mice. *Pharm Res* 28, 610-25.
- Lips, K.S., Volk, C., Schmitt, B.M., Pfeil, U., Arndt, P., Miska, D., Ermert, L., Kummer, W. and Koepsell, H., 2005. Polyspecific cation transporters mediate luminal release of acetylcholine from bronchial epithelium. *Am J Respir Cell Mol Biol* 33, 79-88.
- Liu, H., Prugnolle, F., Manica, A. and Balloux, F., 2006. A geographically explicit genetic model of worldwide human-settlement history. *Am J Hum Genet* 79, 230-7.
- Livak, K.J. and Schmittgen, T.D., 2001. Analysis of relative gene expression data using real-time quantitative PCR and the 2(-Delta Delta C(T)) Method. *Methods* 25, 402-8.
- Lotsch, J., Rohrbacher, M., Schmidt, H., Doehring, A., Brockmoller, J. and Geisslinger, G., 2009. Can extremely low or high morphine formation from codeine be predicted prior to therapy initiation? *Pain* 144, 119-24.
- Maley, F., Trimble, R.B., Tarentino, A.L. and Plummer, T.H., Jr., 1989. Characterization of glycoproteins and their associated oligosaccharides through the use of endoglycosidases. *Anal Biochem* 180, 195-204.
- Martel, F., Vetter, T., Russ, H., Grundemann, D., Azevedo, I., Koepsell, H. and Schomig, E., 1996. Transport of small organic cations in the rat liver. The role of the organic cation transporter OCT1. *Naunyn Schmiedebergs Arch Pharmacol* 354, 320-6.
- Matthaei, J., Kuron, D., Faltraco, F., Knoch, T., Dos Santos Pereira, J.N., Abu Abed, M., Prukop, T., Brockmoller, J. and Tzvetkov, M.V., 2015. OCT1 mediates hepatic uptake of sumatriptan and loss-of-function OCT1 polymorphisms affect sumatriptan pharmacokinetics. *Clin Pharmacol Ther*.
- Mayer, D.J. and Price, D.D., 1976. Central nervous system mechanisms of analgesia. *Pain* 2, 379-404.
- Mehrens, T., Lelleck, S., Cetinkaya, I., Knollmann, M., Hohage, H., Gorboulev, V., Boknik, P., Koepsell, H. and Schlatter, E., 2000. The affinity of the organic cation transporter rOCT1 is increased by protein kinase C-dependent phosphorylation. *J Am Soc Nephrol* 11, 1216-24.
- Minicucci, M.F., Zornoff, L.A., Matsue, M., Inoue, R.M., Matsubara, L.S., Okoshi, M.P., Okoshi, K., Campana, A.O. and Paiva, S.A., 2004. Generalized edema and hyperdynamic circulation. A possible case of beriberi. *Arq Bras Cardiol* 83, 176-8; 173-5.
- Molsa, M., Heikkinen, T., Hakkola, J., Hakala, K., Wallerman, O., Wadelius, M., Wadelius, C. and Laine, K., 2005. Functional role of P-glycoprotein in the human blood-placental barrier. *Clin Pharmacol Ther* 78, 123-31.
- Moran, E.F.F.-M., M., 1996. Global environmental change: The health and environmental implications in Brazil and the Amazon basin. *Environmental Sciences* 4, S025-033.
- Motohashi, H. and Inui, K.-i., 2016. Pharmacological and Toxicological Significance of the Organic Cation Transporters OCT and MATE: Drug Disposition, Interaction and Toxicity, in: Ciarimboli, G., Gautron, S. and Schlatter, E. (Eds.), *Organic Cation Transporters: Integration of Physiology, Pathology, and Pharmacology*. Springer International Publishing, Cham, pp. 73-92.

- Motohashi, H., Sakurai, Y., Saito, H., Masuda, S., Urakami, Y., Goto, M., Fukatsu, A., Ogawa, O. and Inui, K., 2002. Gene expression levels and immunolocalization of organic ion transporters in the human kidney. *J Am Soc Nephrol* 13, 866-74.
- Mystakidou, K., Befon, S., Liozzi, C. and Vlachos, L., 1998. Comparison of tropisetron and chlorpromazine combinations in the control of nausea and vomiting of patients with advanced cancer. *J Pain Symptom Manage* 15, 176-84.
- Nagel, G., Volk, C., Friedrich, T., Ulzheimer, J.C., Bamberg, E. and Koepsell, H., 1997. A Reevaluation of Substrate Specificity of the Rat Cation Transporter rOCT1. *Journal of Biological Chemistry* 272, 31953-31956.
- Nebert, D.W., 1997. Polymorphisms in drug-metabolizing enzymes: what is their clinical relevance and why do they exist? *Am J Hum Genet* 60, 265-71.
- Nei, M. and Roychoudhury, A.K., 1993. Evolutionary relationships of human populations on a global scale. *Mol Biol Evol* 10, 927-43.
- Nies, A.T., Herrmann, E., Brom, M. and Keppler, D., 2008. Vectorial transport of the plant alkaloid berberine by double-transfected cells expressing the human organic cation transporter 1 (OCT1, SLC22A1) and the efflux pump MDR1 P-glycoprotein (ABCB1). *Naunyn Schmiedebergs Arch Pharmacol* 376, 449-61.
- Nies, A.T., Koepsell, H., Damme, K. and Schwab, M., 2011. Organic Cation Transporters (OCTs, MATEs), In Vitro and In Vivo Evidence for the Importance in Drug Therapy, in: Fromm, F.M. and Kim, B.R. (Eds.), *Drug Transporters*. Springer Berlin Heidelberg, Berlin, Heidelberg, pp. 105-167.
- Nies, A.T., Koepsell, H., Winter, S., Burk, O., Klein, K., Kerb, R., Zanger, U.M., Keppler, D., Schwab, M. and Schaeffeler, E., 2009. Expression of organic cation transporters OCT1 (SLC22A1) and OCT3 (SLC22A3) is affected by genetic factors and cholestasis in human liver. *Hepatology* 50, 1227-40.
- Paar, W.D., Poche, S., Gerloff, J. and Dengler, H.J., 1997. Polymorphic CYP2D6 mediates O-demethylation of the opioid analgesic tramadol. *Eur J Clin Pharmacol* 53, 235-9.
- Pao, S.S., Paulsen, I.T. and Saier, M.H., Jr., 1998. Major facilitator superfamily. *Microbiol Mol Biol Rev* 62, 1-34.
- Pedersen, B.P., Kumar, H., Waight, A.B., Risenmay, A.J., Roe-Zurz, Z., Chau, B.H., Schlessinger, A., Bonomi, M., Harries, W., Sali, A., Johri, A.K. and Stroud, R.M., 2013. Crystal structure of a eukaryotic phosphate transporter. *Nature* 496, 533-6.
- Pentikainen, P.J., Neuvonen, P.J. and Penttila, A., 1979. Pharmacokinetics of metformin after intravenous and oral administration to man. *Eur J Clin Pharmacol* 16, 195-202.
- Petry, T.W., Bowden, G.T., Huxtable, R.J. and Sipes, I.G., 1984. Characterization of hepatic DNA damage induced in rats by the pyrrolizidine alkaloid monocrotaline. *Cancer Res* 44, 1505-9.
- Pickering, G., Faure, M., Commun, F., de Boissy, E.C., Roche, G., Mom, T., Simen, E., Dubray, C., Eschalier, A. and Gilain, L., 2012. Tropisetron and paracetamol association in post-operative patients. *Fundam Clin Pharmacol* 26, 432-7.
- Plummer, T.H., Jr., Elder, J.H., Alexander, S., Phelan, A.W. and Tarentino, A.L., 1984. Demonstration of peptide:N-glycosidase F activity in endo-beta-N-acetylglucosaminidase F preparations. *J Biol Chem* 259, 10700-4.

- Pojar, S., 2015. Characterization of the β 2-adrenoreceptor agonist fenoterol as a substrate of the highly polymorphic human organic cation transporter OCT1, *Clinical Pharmacology*. Georg-August-Universität Göttingen, pp. 74.
- Popp, C., Gorboulev, V., Muller, T.D., Gorbunov, D., Shatskaya, N. and Koepsell, H., 2005. Amino acids critical for substrate affinity of rat organic cation transporter 1 line the substrate binding region in a model derived from the tertiary structure of lactose permease. *Mol Pharmacol* 67, 1600-11.
- Raghavan, M., Skoglund, P., Graf, K.E., Metspalu, M., Albrechtsen, A., Moltke, I., Rasmussen, S., Stafford, T.W., Jr., Orlando, L., Metspalu, E., Karmin, M., Tambets, K., Rootsi, S., Magi, R., Campos, P.F., Balanovska, E., Balanovsky, O., Khusnutdinova, E., Litvinov, S., Osipova, L.P., Fedorova, S.A., Voevoda, M.I., DeGiorgio, M., Sicheritz-Ponten, T., Brunak, S., Demeshchenko, S., Kivisild, T., Villemes, R., Nielsen, R., Jakobsson, M. and Willerslev, E., 2014. Upper Palaeolithic Siberian genome reveals dual ancestry of Native Americans. *Nature* 505, 87-91.
- Reddy, V.S., Shlykov, M.A., Castillo, R., Sun, E.I. and Saier, M.H., Jr., 2012. The major facilitator superfamily (MFS) revisited. *FEBS J* 279, 2022-35.
- Saadatmand, A.R., Tadjerpisheh, S., Brockmoller, J. and Tzvetkov, M.V., 2012. The prototypic pharmacogenetic drug debrisoquine is a substrate of the genetically polymorphic organic cation transporter OCT1. *Biochem Pharmacol* 83, 1427-34.
- Sadhasivam, S., Krekels, E.H., Chidambaran, V., Esslinger, H.R., Ngamprasertwong, P., Zhang, K., Fukuda, T. and Vinks, A.A., 2012. Morphine clearance in children: does race or genetics matter? *J Opioid Manag* 8, 217-26.
- Saito, S., Iida, A., Sekine, A., Ogawa, C., Kawauchi, S., Higuchi, S. and Nakamura, Y., 2002. Catalog of 238 variations among six human genes encoding solute carriers (hSLCs) in the Japanese population. *J Hum Genet* 47, 576-84.
- Sakata, T., Anzai, N., Shin, H.J., Noshiro, R., Hirata, T., Yokoyama, H., Kanai, Y. and Endou, H., 2004. Novel single nucleotide polymorphisms of organic cation transporter 1 (SLC22A1) affecting transport functions. *Biochem Biophys Res Commun* 313, 789-93.
- Sala-Rabanal, M., Li, D.C., Dake, G.R., Kurata, H.T., Inyushin, M., Skatchkov, S.N. and Nichols, C.G., 2013. Polyamine transport by the polyspecific organic cation transporters OCT1, OCT2, and OCT3. *Mol Pharm* 10, 1450-8.
- Sanger, F., Nicklen, S. and Coulson, A.R., 1977. DNA sequencing with chain-terminating inhibitors. *Proc Natl Acad Sci U S A* 74, 5463-7.
- Sarabia, V., Lam, L., Burdett, E., Leiter, L.A. and Klip, A., 1992. Glucose transport in human skeletal muscle cells in culture. Stimulation by insulin and metformin. *J Clin Invest* 90, 1386-95.
- Schlatter, E., Klassen, P., Massmann, V., Holle, S.K., Guckel, D., Edemir, B., Pavenstadt, H. and Ciarimboli, G., 2014. Mouse organic cation transporter 1 determines properties and regulation of basolateral organic cation transport in renal proximal tubules. *Pflugers Arch* 466, 1581-9.
- Seitz, T., Stalmann, R., Dalila, N., Chen, J., Pojar, S., Dos Santos Pereira, J.N., Kratzner, R., Brockmoller, J. and Tzvetkov, M.V., 2015. Global genetic analyses reveal

- strong inter-ethnic variability in the loss of activity of the organic cation transporter OCT1. *Genome Med* 7, 56.
- Sevcik, J., Nieber, K., Driessen, B. and Illes, P., 1993. Effects of the central analgesic tramadol and its main metabolite, O-desmethyltramadol, on rat locus coeruleus neurones. *Br J Pharmacol* 110, 169-76.
- Shitara, Y., Itoh, T., Sato, H., Li, A.P. and Sugiyama, Y., 2003. Inhibition of transporter-mediated hepatic uptake as a mechanism for drug-drug interaction between cerivastatin and cyclosporin A. *J Pharmacol Exp Ther* 304, 610-6.
- Shu, Y., Leabman, M.K., Feng, B., Mangravite, L.M., Huang, C.C., Stryke, D., Kawamoto, M., Johns, S.J., DeYoung, J., Carlson, E., Ferrin, T.E., Herskowitz, I., Giacomini, K.M. and Pharmacogenetics Of Membrane Transporters, I., 2003. Evolutionary conservation predicts function of variants of the human organic cation transporter, OCT1. *Proc Natl Acad Sci U S A* 100, 5902-7.
- Shu, Y., Sheardown, S.A., Brown, C., Owen, R.P., Zhang, S., Castro, R.A., Ianculescu, A.G., Yue, L., Lo, J.C., Burchard, E.G., Brett, C.M. and Giacomini, K.M., 2007. Effect of genetic variation in the organic cation transporter 1 (OCT1) on metformin action. *J Clin Invest* 117, 1422-31.
- Simpson, K., Spencer, C. and McClellan, K., 2000. Tropisetron. *Drugs* 59, 1297-1315.
- Sistonen, J., Madadi, P., Ross, C.J., Yazdanpanah, M., Lee, J.W., Landsmeer, M.L., Nauta, M., Carleton, B.C., Koren, G. and Hayden, M.R., 2012. Prediction of codeine toxicity in infants and their mothers using a novel combination of maternal genetic markers. *Clin Pharmacol Ther* 91, 692-9.
- Smith, P.K., Krohn, R.I., Hermanson, G.T., Mallia, A.K., Gartner, F.H., Provenzano, M.D., Fujimoto, E.K., Goeke, N.M., Olson, B.J. and Klenk, D.C., 1985. Measurement of protein using bicinchoninic acid. *Anal Biochem* 150, 76-85.
- Sparreboom, A., van Asperen, J., Mayer, U., Schinkel, A.H., Smit, J.W., Meijer, D.K., Borst, P., Nooijen, W.J., Beijnen, J.H. and van Tellingen, O., 1997. Limited oral bioavailability and active epithelial excretion of paclitaxel (Taxol) caused by P-glycoprotein in the intestine. *Proc Natl Acad Sci U S A* 94, 2031-5.
- Stamer, U.M., Lehnen, K., Hothker, F., Bayerer, B., Wolf, S., Hoeft, A. and Stuber, F., 2003. Impact of CYP2D6 genotype on postoperative tramadol analgesia. *Pain* 105, 231-8.
- Strong, R.P. and Crowell, B., 1912. The Etiology of Beriberi. *Philippine Journal of Science* 7, 271-411.
- Sturm, A., Gorboulev, V., Gorbunov, D., Keller, T., Volk, C., Schmitt, B.M., Schlachtbauer, P., Ciarimboli, G. and Koepsell, H., 2007. Identification of cysteines in rat organic cation transporters rOCT1 (C322, C451) and rOCT2 (C451) critical for transport activity and substrate affinity. *Am J Physiol Renal Physiol* 293, F767-79.
- Sweeney, M. and McCouch, S., 2007. The complex history of the domestication of rice. *Ann Bot* 100, 951-7.
- Tahrani, A.A., Bailey, C.J., Del Prato, S. and Barnett, A.H., 2011. Management of type 2 diabetes: new and future developments in treatment. *Lancet* 378, 182-97.

- Takeda, M., Khamdang, S., Narikawa, S., Kimura, H., Kobayashi, Y., Yamamoto, T., Cha, S.H., Sekine, T. and Endou, H., 2002. Human organic anion transporters and human organic cation transporters mediate renal antiviral transport. *J Pharmacol Exp Ther* 300, 918-24.
- Takeuchi, A., Motohashi, H., Okuda, M. and Inui, K., 2003. Decreased function of genetic variants, Pro283Leu and Arg287Gly, in human organic cation transporter hOCT1. *Drug Metab Pharmacokinet* 18, 409-12.
- Tu, M., Sun, S., Wang, K., Peng, X., Wang, R., Li, L., Zeng, S., Zhou, H. and Jiang, H., 2013. Organic cation transporter 1 mediates the uptake of monocrotaline and plays an important role in its hepatotoxicity. *Toxicology* 311, 225-30.
- Tzvetkov, M.V., Dalila, N. and Faltraco, F., 2016. Genetic Variability in Organic Cation Transporters: Pathophysiological Manifestations and Consequences for Drug Pharmacokinetics and Efficacy, in: Ciarimboli, G., Gautron, S. and Schlatter, E. (Eds.), *Organic Cation Transporters: Integration of Physiology, Pathology, and Pharmacology*. Springer International Publishing, Cham, pp. 93-137.
- Tzvetkov, M.V., dos Santos Pereira, J.N., Meineke, I., Saadatmand, A.R., Stingl, J.C. and Brockmoller, J., 2013. Morphine is a substrate of the organic cation transporter OCT1 and polymorphisms in OCT1 gene affect morphine pharmacokinetics after codeine administration. *Biochem Pharmacol* 86, 666-78.
- Tzvetkov, M.V., Saadatmand, A.R., Bokelmann, K., Meineke, I., Kaiser, R. and Brockmoller, J., 2012. Effects of OCT1 polymorphisms on the cellular uptake, plasma concentrations and efficacy of the 5-HT(3) antagonists tropisetron and ondansetron. *Pharmacogenomics J* 12, 22-9.
- Tzvetkov, M.V., Saadatmand, A.R., Lotsch, J., Tegeder, I., Stingl, J.C. and Brockmoller, J., 2011. Genetically polymorphic OCT1: another piece in the puzzle of the variable pharmacokinetics and pharmacodynamics of the opioidergic drug tramadol. *Clin Pharmacol Ther* 90, 143-50.
- Tzvetkov, M.V., Seitz, T., Bokelmann, K., Mueller, T., Brockmoller, J. and Koepsell, H., 2014. Does the haplotype Met408-Del420, which was apparently predictive for imatinib efficacy, really exist and how strongly may it affect OCT1 activity? *Blood* 123, 1427-9.
- Tzvetkov, M.V., Vormfelde, S.V., Balen, D., Meineke, I., Schmidt, T., Sehr, D., Sabolic, I., Koepsell, H. and Brockmoller, J., 2009. The effects of genetic polymorphisms in the organic cation transporters OCT1, OCT2, and OCT3 on the renal clearance of metformin. *Clin Pharmacol Ther* 86, 299-306.
- Urban, T.J., Sebro, R., Hurowitz, E.H., Leabman, M.K., Badagnani, I., Lagpacan, L.L., Risch, N. and Giacomini, K.M., 2006. Functional genomics of membrane transporters in human populations. *Genome Res* 16, 223-30.
- Vahakangas, K. and Myllynen, P., 2009. Drug transporters in the human blood-placental barrier. *Br J Pharmacol* 158, 665-78.
- van Montfoort, J.E., Muller, M., Groothuis, G.M., Meijer, D.K., Koepsell, H. and Meier, P.J., 2001. Comparison of "type I" and "type II" organic cation transport by organic cation transporters and organic anion-transporting polypeptides. *J Pharmacol Exp Ther* 298, 110-5.

- Volk, C., Gorboulev, V., Kotsch, A., Muller, T.D. and Koepsell, H., 2009. Five amino acids in the innermost cavity of the substrate binding cleft of organic cation transporter 1 interact with extracellular and intracellular corticosterone. *Mol Pharmacol* 76, 275-89.
- Whitfield, R.G.S., 1947. Malnutrition in Japanese Prison Camps. *British Medical Journal* 2, 164-168.
- Williams, R.D., Mason, H.L., Wilder, R.M. and Smith, B.F., 1940. Observations on induced thiamine (vitamin b1) deficiency in man. *Archives of internal medicine (Chicago, Ill. : 1908)* 66, 785-99.
- Wu, C.Y. and Benet, L.Z., 2005. Predicting drug disposition via application of BCS: transport/absorption/ elimination interplay and development of a biopharmaceutics drug disposition classification system. *Pharm Res* 22, 11-23.
- Wu, X., Huang, W., Ganapathy, M.E., Wang, H., Kekuda, R., Conway, S.J., Leibach, F.H. and Ganapathy, V., 2000. Structure, function, and regional distribution of the organic cation transporter OCT3 in the kidney. *Am J Physiol Renal Physiol* 279, F449-58.
- Xie, H.G., Kim, R.B., Wood, A.J. and Stein, C.M., 2001. Molecular basis of ethnic differences in drug disposition and response. *Annu Rev Pharmacol Toxicol* 41, 815-50.
- Yasujima, T., Ohta, K., Inoue, K. and Yuasa, H., 2011. Characterization of human OCT1-mediated transport of DAPI as a fluorescent probe substrate. *J Pharm Sci* 100, 4006-12.
- Yoon, H., Cho, H.Y., Yoo, H.D., Kim, S.M. and Lee, Y.B., 2013. Influences of organic cation transporter polymorphisms on the population pharmacokinetics of metformin in healthy subjects. *AAPS J* 15, 571-80.
- Yuan, T., Yap, K. and Ikura, M., 2000. Calmodulin Target Recognition: Common Mechanism and Structural Diversity, in: Carafoli, E. and Krebs, J. (Eds.), *Calcium Homeostasis*. Springer Berlin Heidelberg, pp. 59-81.
- Zhang, B.B., Zhou, G. and Li, C., 2009. AMPK: an emerging drug target for diabetes and the metabolic syndrome. *Cell Metab* 9, 407-16.
- Zhang, L., Dresser, M.J., Gray, A.T., Yost, S.C., Terashita, S. and Giacomini, K.M., 1997. Cloning and functional expression of a human liver organic cation transporter. *Mol Pharmacol* 51, 913-21.
- Zhang, L., Schaner, M.E. and Giacomini, K.M., 1998. Functional characterization of an organic cation transporter (hOCT1) in a transiently transfected human cell line (HeLa). *J Pharmacol Exp Ther* 286, 354-61.
- Zhou, G., Myers, R., Li, Y., Chen, Y., Shen, X., Fenyk-Melody, J., Wu, M., Ventre, J., Doebber, T., Fujii, N., Musi, N., Hirshman, M.F., Goodyear, L.J. and Moller, D.E., 2001. Role of AMP-activated protein kinase in mechanism of metformin action. *J Clin Invest* 108, 1167-74.
- Zhou, H.H., Sheller, J.R., Nu, H., Wood, M. and Wood, A.J., 1993. Ethnic differences in response to morphine. *Clin Pharmacol Ther* 54, 507-13.

8 Curriculum Vitae

Personal Information

Name: Tina Seitz
Address: Stettiner Str. 52, 37083 Göttingen
Date of birth: May 17th, 1989
Place of birth: Hoyerswerda

Education

1995 – 1999: Primary School, Hoyerswerda (“Grundschule am Park”)

1999 – 2007: Academic High School, Hoyerswerda (“Lessing-Gymnasium”)
University entrance diploma

2007 – 2012: University, Greifswald (“Ernst-Moritz-Arndt”)
Field of study: Human Biology
Major subject: Immunology
Minor subjects: Biochemistry
Human ecology and Environmental toxicology
University qualification: Diploma in Human biology

Since 2012: **PhD student** in the study program “Molecular Medicine” at the Georg-August University of Göttingen in the department of Clinical Pharmacology of the University Medical Center Göttingen

Honors and Awards

- 2012 – 2014:** Scholarship from the German Research Foundation (DFG) within the Research Training Group “GRK 1034”
- 2014:** Poster Award from “Deutsche Gesellschaft für Experimentelle und Klinische Pharmakologie e.V.” (DGPT) for the poster entitled “Functional characterization of rare and population specific genetic variants in the organic cation transporter OCT1“ on the occasion of the 80th Annual Meeting of the DGPT in Hannover 2014
- 2015:** Travel Award from the Drug Transport Focus Group on the occasion of the 2015 AAPS/ITC Joint Workshop on Drug Transporters in ADME in Baltimore (poster podium presentation)

Additional Qualifications

- 2010:** Certificate in laboratory animal science (FELASA – B)
(In fulfillment of the qualifications guidelines of the Federation of European Laboratory Animal Science Associations category B)
- 2014:** Certificate “ICH/GCP-Good Clinical Practice“ from IFS GmbH, Institut für anwendungsorientierte Forschung und klinische Studien

Publications

Seitz T, Stalman R, Dalila N, Chen J, Pojar S, Dos Santos Pereira JN, Krätzner R, Brockmüller J, Tzvetkov MV, 2015 Global genetic analyses reveal strong inter-ethnic variability in the loss of activity of the organic cation transporter OCT1. *Genome Medicine*, 7(1):56

Tzvetkov MV, **Seitz T**, Bokelmann K, Mueller T, Brockmüller J, Koepsell H, 2014, Does the haplotype Met408-Del420, which was apparently predictive for imatinib efficacy, really exist and how strongly may it affect OCT1 activity? *Blood*, 123(9):1427-9

Fluhr H, **Seitz T**, Zygmunt M, 2013 Heparins modulate the IFN- γ -induced production of chemokines in human breast cancer cells. *Breast Cancer Research and Treatment*, 137(1):109-18